Support interference in oscillatory dynamic tunnel testing

Taylor, Gordon Stuart

Award date:
2003

Awarding institution:
University of Bath

SUPPORT INTERFERENCE IN OSCILLATORY DYNAMIC TUNNEL TESTING

Submitted by Gordon Stuart Taylor

for the degree of Ph.D.

of the University of Bath

2003

COPYRIGHT

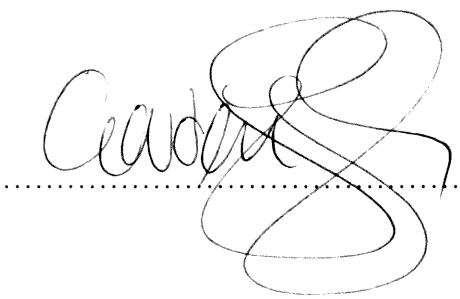

.....

ProQuest LLC
789 East Eisenhower Parkway
P.O. Box 1346
Ann Arbor, MI 48106-1346

ABSTRACT

An investigation was undertaken to understand support interference in high angle of attack testing with particular emphasis on premature vortex breakdown induced by support structures. Simple delta wing models were used to generate a vortical flow field suitable for studying, and dummy support structures were placed downstream in order to simulate the presence of a c-strut type support structure.

In static experiments efforts concentrated on a parametric study of the geometry and location of the support, and the wing geometry (sweep) and orientation (incidence and sideslip). Extensive flow visualisation studies and PIV measurements allowed the identification of specific conditions under which support interference of this form may be of particular concern. Of particular interest was the observation of static hysteresis of vortex breakdown location as the lateral distance between the vortex core and the support was varied. Although similar results have been presented in the literature for cases of varying vortex strength, such as changing incidence, this is the first indication of hysteresis in the absence of changes in vortex strength. The results indicate that support interference may be minimized by placing the support at least one chord length downstream of the trailing edge of the model.

In order to remove the effects of time-dependent vortex strength in dynamic testing, the model remained stationary while the dummy support was oscillated in its wake. Large amplitude fluctuations of vortex breakdown location were observed at low frequencies that were shown by spectral analysis to be a result of the support motion. At high frequencies, this correlation reduced significantly, indicating a frequency response similar to that of a low-pass filter. Variation of phase-averaged breakdown location showed hysteresis loops and timelags that were larger for a thin flat plate than a circular cylinder. In transient tests, a time-parameter was derived that correlated well with severity of the breakdown response.

Finally the more complex moving wing case was considered, with the dummy support remaining static. In this case a jumping of the vortex breakdown location was observed at high forcing frequencies, and subsequent analysis have suggested a possible mechanism for this behaviour.

For Philip and Polly.

ACKNOWLEDGEMENTS

First and foremost, I would like to thank to my supervisor, Ismet, for guiding me through three and a half years experimental testing and analysis. Also thanks to Doug Greenwell and the former DERA (Bedford) for funding this research. Thanks to all the technicians, with special thanks to Les for his mocking, Dave for skiving more than me, and Roland for his witticisms. Also to Steve and Rob from instrumentation for consistently not telling me where to go when they had every right to do so. Thanks to Martin Hyde of TSI for answering all my PIV and LDV questions as if he had nothing better to do.

Very special thanks to all those who have been around me for the last three years. The diving lot: American Steve, Hazelyburstlbry, Lord Jim, Uncle Tom, Old Man Fingers, Scary, Rach, Queeny, and not forgetting Sausage and Sweets. The office who have distracted me with (almost) endless games of table pool and "Office Ball": James and James, Steve, Caroline, Martin, Colin, Sam, and the others. To Matt for keeping me company in the pub when Forest are on the box. To Julie for being a mate for as long as I can remember. And to the family, particularly Lyn, Steve, and Amy.

But mostly, thanks to Emma. It cant have been easy putting up with my research related grumbles over the last three years, but you have always been more than supportive. I promise I will never again try to discuss the flow physics of delta wings with you! And remember: "If you're not in the car ..." !

Thank you all.

CONTENTS

LIST OF FIGURES

NOMENCLATURE

b	Wing span	[m]
c	Wing root chord	[m]
C_L	Lift coefficient	[-]
d_p	Stream-wise length of flat-plate support	[m]
d_r	Diameter of cylindrical support	[m]
f	Frequency	[Hz]
F	Force	[N]
f_e	Excitation frequency	[Hz]
f_s	Sampling frequency	[Hz]
h	Half side length of integration square	[m]
K	Gain	[-]
L	Lift Force	[N]
Re_c	Reynolds number based on root chord	[-]
S	Wing surface area	[m^2]
t	Time	[s]
t	Thickness of plate	[m]
T	Period of motion ($1/f_e$)	[s]
U_∞	Free stream velocity	[m/s]
x	Streamwise dimension	[m]
x'_{BD}	Breakdown location in plane of wing	[m]
x_{LE}	Streamwise location of dummy support	[m]
y	lateral dimension	[m]
z	vertical dimension	[m]
α	Angle of attack	[°]
β	Sideslip angle	[°]
ε	Distance between vortex core and support	[m]
ϕ	Phase lag or Swirl angle	[°]
γ	Leading edge bevel angle	[°]
Γ	Circulation	[m^2/s]
φ	Vortex core radius	[m]

λ	A parameter that affects the flow	[-]
Λ	Wing sweep angle	[°]
τ	Time constant	[s]
ξ	Vorticity	[rad/s]
ω	Angular velocity	[rad/s]
ω_n	Natural Frequency	[rad/s]
ψ	A parameter that defines the flow	[-]
ζ	Damping Ratio	[-]

Subscripts

α_{TE}	α at which breakdown occurs at the trailing edge	[°]
ε_0, ε_1	Mean and amplitude of sinusoidal motion	[m]
$(\varepsilon/b)_0$	Value of ε/b at which breakdown is first observed aft of the trailing edge when increasing ε	[-]
$(\varepsilon/b)_{CRIT}$	Value of ε/b at which breakdown is first observed forward of the trailing edge when decreasing ε	[-]
$(\varepsilon/b)_{min}$	Smallest value of (ε/b) during support/wing motion	[-]
$(x'_{BD}/c)_{min}$	Most forward breakdown location	[-]

TERMINOLOGY AND ABBREVIATIONS

PIV	Particle Image Velocimetry
Forced case	Case including dummy support
Natural case	Case in the absence of dummy support
RMS	Root-Mean-Square value of a parameter
FFT	Fast Fourier Transform
CSD	Cross-Spectral Density
Windward	That side of the model facing the mean flow
Leeward	The side of the model in the lee of the flow
CFD	Computational Fluid Dynamics

Chapter 1 Introduction

1.1 Background

The wind-tunnel is a popular and reliable tool for conducting aeronautical research, and are used in industry and academia for testing of current aircraft configurations, for exploratory investigations of novel plan-forms, and for more basic research of simplified aircraft shapes. Further, wind-tunnel use is not restricted to aeronautical research; testing of cars, ships and buildings all use experimental testing to validate designs prior to production.

However, for full and proper consideration of wind-tunnel test data, it is necessary to consider the dissimilarities between wind-tunnel testing and free-flight. These differences are collectively known as *wind-tunnel interference*, but there are actually a number of sources of error that can be considered and accounted for individually. One of these sources of error is *support interference*, which refers to the effect of the model support structure on the measured flow.

Many types of model support structure have been designed over the years to accommodate a range of models and wind-tunnel configurations. In static testing at least, careful arrangement of the support structure relative to the model can all but eliminate the effects of support interference. The most significant form of support interference, however, is encountered while performing dynamic (transient or oscillatory) testing. In this case, a larger support is required than in static testing to ensure a smooth motion whilst eliminating unwanted vibrations.

Of particular interest is the effect of support structures on the vortices formed on models at high angles of attack. Premature vortex breakdown resulting from vortex interactions with support structures can significantly affect wing loading, and it is therefore imperative that such interactions be understood so that they may be accounted for when analysing test results. However, as will be shown in the subsequent sections of this chapter, there is little quantitative data available in the literature that describe the combined effects of support geometry and location on the breakdown of vortices shed from models in static high angle of attack testing. Neither have the effects of frequency and amplitude of relative support/wing motion been studied in dynamic (oscillatory or transient) testing. It is therefore the aim of this investigation to investigate the problem of support interference in static, oscillatory and transient testing, with particular emphasis on the effect of support structures on the breakdown of vortices shed from models in high angle of attack testing.

The thesis begins with a discussion of literature relevant to support interference and delta wing aerodynamics, following which is a statement of the objectives of the research program. The following two chapters discuss the experimental apparatus and procedures adopted in pursuit of these objectives. The results of the investigation are divided into three chapters which tackle the effect of support interference in static, oscillatory and transient testing separately. Finally, the thesis concludes with a synopsis of the principal conclusions, and recommendations for future research.

1.2 Literature Review

This chapter reviews literature relevant to this investigation, and begins with a discussion of literature pertaining to support interference. As will be shown, there has been surprisingly little consideration of the vortex-support interaction problem that was the focus of the current investigation. As a result it has been necessary to look to alternative fields of aerodynamics for parallel problems that may aid understanding of the problem, such as vortex body interactions, and rotor dynamics. Significant emphasis in this chapter has been placed on reviewing and explaining the structure of leading edge vortices generated over delta wings, and their effect on the aerodynamic

properties of delta wings. This is because delta wings were used in this investigation to generate vortices with which support interactions were then studied. Further to this, a detailed discussion of the vortex breakdown phenomenon, its causes, prediction, and explanation is then presented, for reasons that, it is hoped, will become clear as the reader progresses.

Next is an outline of the principal objectives of the research programme, as identified prior to undertaking the investigation.

1.2.1 Wind Tunnel Interference

As an introduction to support interference, the topic of tunnel interference effects in general is first introduced. There are many interference effects that the experimentalist must contend with, and the following discussion is by no means intended to be exhaustive. A review of tunnel interference effects in general may be found in Pankhurst and Holder (1965). Factors that lead to discrepancies between tunnel test and free flight data include: boundary constraints imposed by the tunnel walls, tunnel blockage effects, and interference of the studied flow with the support structures.

1.2.1.1 Wall Interference and Tunnel Blockage

The boundary condition imposed by the presence of the tunnel walls affects the formation of the streamlines around a test model, since the streamlines at the wall must be parallel. Where there is vortical flow present in the working section, wall effects can induce artificial variations of camber and twist along the working section. A number of studies into the specific effects of wall interference on delta wing flows have been conducted. Frink (1987) studied the variations of longitudinal and lateral variations in the flow caused by the proximity of tunnel walls to a delta wing model, and found that an increase in the suction peak beneath the leading edge vortices exists compared to the free-flight case. This increase in suction was attributed to an increase in the up-wash experienced by the model due to the presence of the tunnel walls, which increases the effective incidence of the model, and subsequently promotes the onset of vortex breakdown. Similar results have been presented by other investigators, both in computational (Thomas and Lan, 1991; Hsing and Lan, 1997) and experimental

(Thompson and Nelson, 1992) studies. However, conflicting evidence is given by Weinburg (1992), who used a theoretical approach to show that the up-wash increased in the streamwise direction, resulting in an effectively cambered wing, so delaying the onset of breakdown. These results were subsequently confirmed by experimental results presented in the same paper.

More recent computational studies by Allan (2002) indicate that the effect of wall interference is to: increase the magnitude of the up-wash at the wing; increase the magnitude of the up-wash with streamwise distance along the wing; and to increase the strength of the vortices. All of these effects lead to an effective increase in the incidence of the wing, and the occurrence of breakdown will be promoted. Allan shows that although there is an effective camber induced by the variation of up-wash along the chord of the wing similar to that predicted by Weinburg (1992), the magnitude of this effect is small in comparison with the magnitude of the up-wash, and breakdown will therefore tend to be promoted in the presence of tunnel walls. Allan (2002) also shows that the magnitude of the wall interference is a function of the model span to tunnel width ratio, and the strength of the vortices generated.

Blockage effects are concerned with the conservation of mass flow rate along the test section, a requirement which induces an increased velocity at the working section due to the constriction caused by the presence of the test model. However, for swept wings tunnel interference effects can usually be considered to be negligible for blockage ratios of less than 0.08 (ESDU, 1980), and so careful design of experiments can almost eliminate these effects.

1.2.1.2 Support Interference

It is more difficult, though, to remove entirely the effects of support interference, since a model must necessarily be supported in the tunnel to allow testing to take place. Figure 1.1 shows a number of simple structures that have been used to support models. The wire support is impractical for anything other than low speed static tests, but the strut and sting supports have been used both individually and in combination for high and low speed, static and dynamic tests. An important feature of dynamic test rigs is that they are necessarily much bulkier than their static counterparts due to the high stiffness

needed to avoid excessive deflections and vibrations that would otherwise result from high speed dynamic tests. However, a more bulky support implies a greater effect on the flow that is being studied, and so support interference is much more of a problem for dynamic testing than for static. The most common arrangement for dynamic testing is the strut-sting support as it allows control of the model in both pitch and roll simultaneously. Figure 1.2 shows such a support in use at the DERA test facility at Bedford.

Aircraft in flight commonly form vortices over the leading edges of delta wings, canards and strakes, forebodies at incidence, and many other types of surface discontinuity. These vortices become stronger with incidence, so it follows that almost all aircraft that operate at high angles of attack, such as fighter configurations, will generate a wake that is highly vortical in nature. Such vortical wakes are prone to a naturally occurring event known as vortex breakdown, which sees the nature of the vortex rapidly change. The nature of vortices and vortex breakdown will be discussed in detail in the following sections of this chapter, but it is important to realise at this point that the existence of vortex breakdown over a lifting surface will significantly reduce the lift generated by that surface. Whilst the delay of vortex breakdown over a wing is difficult, premature breakdown is easily achieved and is clearly detrimental to aircraft performance. An often cited example of premature vortex breakdown is the case of the McDonnell-Douglas F/A-18 'Hornet' aircraft. Research commissioned by the United States Air Force (USAF) following a number of problems have indicated that the fins of the aircraft lie in the path of vortices generated from its leading edge extensions. The resulting impingement of the vortices on the fin structure causes premature breakdown. Not only does this cause a loss of lift, it has also resulted in fatigue failure of the fin structures as a result of buffeting induced by the highly turbulent wake that exists downstream of a vortex breakdown.

With respect to support interference, the ability of an obstruction to promote breakdown was first demonstrated by Hummel (1965). In his famous experiment, Hummel demonstrated that the breakdown location of a leading edge vortex was moved by 40% of the chord length by placing an obstacle one chord length downstream of a 75° delta (see Figure 1.3). This experiment showed that one must therefore be careful in the

design of tunnel testing of aircraft with vortical wakes as a carelessly placed support structure may induce premature breakdown, which would in turn significantly affect the results obtained from the test. Whilst Hummel's experiments were not representative of support interference due to the large cross-flow area of the obstacle, they do show the potential of support structures for affecting vortical wakes in particular.

Early work in the field of support interference was conducted by Perkins (1951). Further work followed by Ericsson and Reding (1983; 1986) among others, although these articles are restricted to the testing of bodies of revolution rather than aircraft configurations. A significant contribution to the field was made by Johnson *et al* (1980), who studied the effect of different support structures on the lift generated by a generic aircraft model in static wind-tunnel testing. Figure 1.4 shows how the lift and moment characteristics of the model differ when supports of different types are used; in this case a c-strut, similar to that shown in Figure 1.2, and a vertical strut. In particular a reduction in lift is noted at high incidences. A discussion by Ericsson and Reding (1986) suggested that this observation was a direct result of the premature breakdown of leading edge vortices due to their interaction with the support. Further studies by Johnson *et al* (1980) considered the effect of placing a 'dummy' support structure in line with the model centreline instead of the curved strut used previously, and supporting the model by another method. The aim of this approach was to attempt to duplicate the effect of a c-strut support. Figure 1.5 shows that the lift generated by a generic fighter is altered only slightly by the dummy support approach, indicating that it is a useful approach in studying support interference effects.

Dynamic support interference relating to aircraft configurations has been the subject of many investigations, including the ones by Ericsson and Reding (1983; 1986), Ericsson (1991), Beyers (1992) and Beyers and Ericsson (1993; 2000). However, none of these articles provide quantitative data relating to the effect of support location on the breakdown of vortices, either statically or dynamically. The most recent relevant investigation in this specific area is that by Ericsson and Beyers (2000), which reviews literature relating to the factors affecting the breakdown of leading edge vortices generated by a 70° delta. In particular the effects of model size, test facility, camber, and Reynolds number scaling are discussed, with the rather inadequate conclusion that

attention must be paid to all of these factors when designing experiments. No specific methods for reducing these effects are proposed.

It has been shown, then, that there exists a gap in our knowledge of wind-tunnel interference effects. It is important that the effect of bulky support structures, such as those found in dynamic wind-tunnel testing, on vortical wakes generated by aircraft configurations at incidence be investigated in full. The methodology of this investigation will involve the use of various delta wing configurations to generate vortices suitable for investigation. As such, this literature review will not be complete without a discussion of delta wing aerodynamics and, in particular, vortex breakdown.

1.2.2 Delta Wing Aerodynamics

It is the ability of a delta wing to maintain lift at high angles of attack that has made it of primary importance to modern fighter aircraft configurations. A typical slender delta wing may stall at an incidence of around 40°, more than twice that at which a conventional aerofoil will stall. This section reviews the flow topology over highly swept delta wings at medium to high angles of attack.

A delta wing set at incidence to the free stream will generate a pair of leading edge vortices, the size and strength of which are dependant on the angles of incidence and sweep. Figure 1.6 shows how these vortices are formed. Flow approaching the wing forces the boundary layer on the windward surface to flow outboard toward the leading edges. The boundary layer separates from the surface as it leaves the leading edge of the wing, forming a free shear layer which curves inboard and wraps around itself to form the leading edge vortices that characterise delta wing flow. Viscous dissipation is rapid so that individual strands of the shear layer are not observed in the vortex core. Continuous feeding of vorticity from the shear layer along the leading edge of the wing imparts a near linear expansion to the vortex core in the axial direction, with an associated increase in circulation.

Investigators often refer to the vortex 'core', but this term is ill defined and largely open to interpretation. Different definitions have been proposed: Hall (1961) suggests that it is the region within which the axial velocity and pressure distributions are

axisymmetric; Leibovich (1984) suggests that it is the region containing most of the vorticity. Other definitions are based on the extent of that region, nearest the centreline of the vortex, in which viscosity dominates the flow. Based on the definition of axial symmetry, the centre of a leading edge vortex typically lies of the order of one core diameter above the lifting surface of the wing (Leibovich, 1984). This proximity of the leading edge vortices to the wing surface imparts an outboard motion to the flow on the surface of the wing directly beneath the vortex core. The pressure field approaching the leading edge from this location is such that the flow once again separates from the surface forming a secondary vortex. The secondary vortex differs from the primary vortex in that it is much smaller, and rotates in the opposite sense. Studies by Nelson and Visser (1990) indicated that the strength of the secondary vortices are not affected by changes in incidence or sweep. Further separations have been also reported in the region proximal to the leading edge (Délery, 1992).

A number of investigators have shown the existence of instabilities in the shear layer that rolls up to form the leading edge vortices. Gad-el-Hak and Blackwelder (1985) detailed the pairing of discrete vortices in the shear layer of a highly swept delta wing, similar to the Kelvin-Helmholtz instability observed in a mixing layer. Further investigations of this phenomenon were made by Payne *et al* (1988) and separately by Lowson (1988), in detailed laser-sheet and smoke visualisation experiments. Computational studies have also been performed by Gordnier and Visbal (1994), amongst others. In addition to this unsteady vortex pairing mechanism, more recent studies have identified the existence of vortical sub-structures in the mean flow shear layer. These sub-vortices have been examined by Mitchell *et al* (2001) and Mitchell and Molton (2002), who showed both that their rotation is in the same sense as, and that they follow a helical path around, the primary vortices.

An interesting feature of leading edge vortices over slender delta wings is that the axial velocity in the vortex core may increase to as much as 4 to 5 times the free stream velocity (Hall, 1966). The high velocities associated with the leading edge vortices are responsible for the presence of suction 'peaks' on the suction surface (Greenwell and Wood, 1982). A trough of low pressure exists directly beneath each of the vortices, which provides a major contribution to the lift force generated by the wing.

The trailing edge region of the delta wing is characterised by a pressure recovery region, a result of the deflection of the streamlines as they re-align themselves with the free stream. As the leading edge vortices leave the trailing edge they too are deflected to align with the free stream. Once downstream of the trailing edge the strength of the vortices no longer increases in the axial direction since there is no longer a feeding of vorticity from the leading edges. As the vortex progresses downstream the vortex core gradually expands while its azimuthal velocity reduces due to the effects of viscous dissipation.

As the incidence of a delta wing is increased, the vortices generated over its leading edges increase in strength. Clearly, this relationship cannot hold indefinitely, and when the strength of the vortices increases to a certain level they can no longer hold their form and vortex breakdown is observed, a phenomenon that will be discussed at length in the subsequent section. The location of the breakdown is a relation of the strength of the vortices, and therefore of the incidence of the wing, so that at high angles of attack the breakdown moves forward until it occurs at the apex, at which point no coherent leading edge vortex structure is generated. A further increase in incidence will result in vortex shedding of a form similar to that observed over two-dimensional bluff bodies (Rediniotis *et al*, 1993).

1.2.3 Vortex Breakdown

Normally the strength of a vortex along its length is constant and any variation of the vortex in the axial direction is slow and predictable. However, one of the most fascinating features of vortical flow is that there exists a condition where the vortex may be seen to burst or breakdown. There have been many investigations of vortex breakdown since the phenomenon was first discovered by Peckham and Atkinson (1957). Significant early articles are those by Elle (1958, 1960), Lambourne and Bryer (1961), Lowson (1964), Sarpkaya (1971a, 1971b, 1974) and Faler and Leibovich (1977). Comprehensive review articles have also been published by Hall (1972), Leibovich (1978, 1984), Escudier (1988) and Délery (1994).

1.2.3.1 Description of vortex breakdown

Vortex breakdown is characterised by the rapid transition of a vortex core from a slender and roughly axisymmetric flow system, to a region of reversed flow and instability, following which the flow is invariably turbulent.

Figure 1.7 shows that the breakdown of a vortex may commonly assume one of two forms. Although other forms of breakdown have been discovered (Faler and Leibovich, 1977), it is only the bubble (or axisymmetric) and the spiral (or asymmetric) forms that are observed over delta wings, with the spiral form being most prevalent. Despite the visual differences between these forms of breakdown, they develop in a similar manner. Far upstream of the breakdown region, the vortex core is axisymmetric and any changes velocity and pressure gradient in the axial direction are small compared with those in the radial. As the flow approaches breakdown the high axial velocities associated with the vortex core undergo rapid deceleration to form a stagnation point. This deceleration may occur within an axial distance of just one or two core diameters (Leibovich, 1984). Flow in the wake of the breakdown differs according to the form of breakdown.

In the bubble form of breakdown, the stagnation point is followed by a region of roughly axisymmetric flow reversal, around which oncoming streamlines are obliged to deflect giving the impression that a bubble has formed in the flow. A similar flow may be achieved by placing a body of revolution on the axis of the unbroken vortex (Garg and Leibovich, 1979). Flow downstream of the region of flow reversal soon becomes turbulent. In the spiral breakdown, stagnation is followed by the deflection of the vortex filament outwards and subsequent development of a spiral motion that soon deteriorates into turbulence. Differences in the flow pre- and post-breakdown are illustrated in Figure 1.8, which shows the developmental stages of the axisymmetric form of breakdown, and the velocity profiles through the vortex core up- and downstream of breakdown. Jet-like flow is observed upstream of the breakdown but is transformed into a wake-like profile downstream, a feature common to both forms of breakdown.

As mentioned previously, further forms of breakdown to those discussed here have been identified. Vortex tube experiments performed by Sarpkaya (1971b) and by Faler and

Leibovich (1977) documented the existence of up to 6 forms of breakdown. However, only the spiral and bubble forms have been observed over delta wings. Vortex tube experiments differ from flow over delta wings in that the vortices they produce are axisymmetric to a high degree. A significant feature of a leading edge vortex is that, due to the continuous feeding of vorticity from the shear layer, the vortex is not axisymmetric. This may explain why only two forms of breakdown have been observed occurring over delta wings. For these reasons this review is limited to discussion of only the axisymmetric and spiral forms of vortex breakdown.

There is much controversy regarding the existence of individual forms of breakdown as separate cases or as different aspects of the same phenomenon. Leibovich (1984) believes that bubble and spiral forms are indeed separate cases, a conclusion drawn from observations regarding differences in expansion ratio and mean location of the two forms. Escudier (1988) on the other hand relates his belief that the axisymmetric breakdown is the fundamental form, and that other forms are a consequence only of instabilities in the bubble form. This belief is supported by carefully controlled vortex tube experiments in which a pure axisymmetric rotation was achieved, the results of which being that only the bubble form of breakdown was observed. If the spiral form results from an instability in the bubble form, consideration of the asymmetry of leading edge vortices, and indeed the instabilities associated with the shear layer, may help explain why the spiral form of breakdown is more commonly observed over delta wings than is the bubble. Whichever standpoint is ultimately proved, it is a curious feature of vortex breakdown that the breakdown of one leading edge vortex need not necessarily take the same form as its opposing vortex. The famous photograph of Lambourne and Bryer (1961) is reproduced in Figure 1.9 to illustrate this point.

1.2.3.2 Vortex breakdown over delta wings

The significance of vortex breakdown to the field of aeronautics was first identified by Peckham and Atkinson (1957), who noted its occurrence over highly swept delta wings at high angles of attack. The first detailed study followed by Lambourne and Bryer (1961) who used flow visualisation to identify factors affecting vortex breakdown location over various delta wing configurations. Further investigations by other authors

(as listed above) have identified the following primary factors. First, breakdown is only observed in highly swirling flows. The measure of swirl is generally the swirl angle, which has been defined in a number of ways, but is most commonly described as $\phi = \tan^{-1}(v/u)$, where v and u are the swirl (or tangential) and axial components of velocity respectively. It has been found that vortex breakdown only occurs in flows where the maximum swirl angle is greater than about 40° (Hall, 1972). This explains the propensity of the breakdown of leading edge vortices to move forward with increasing effective angle of attack or decreasing effective sweep angle (Gursul, 1995). In fact, not only is high swirl a necessary condition for breakdown, but the amount of swirl is also a factor in determining the type of breakdown that occurs. Sarpkaya (1971b) noted that lower swirl angles result in the spiral form, whereas a higher swirl is required for the breakdown to assume the bubble form. More important than swirl angle though is the presence, or otherwise, of a positive (adverse) pressure gradient. It has long been recognised that vortex breakdown is promoted in the presence of an adverse pressure gradient (Lambourne and Bryer, 1961; Lowson, 1964). Although Hall (1972) demonstrated how small external pressure gradients can be amplified along a vortex core leading to a breakdown of the vortex, it was not until Sarpkaya (1974) that the first quantitative study into the effects of pressure gradient was made. Figure 1.10, reproduced from Sarpkaya (1974), shows both forms of breakdown existing in a divergent vortex tube experiment. By varying the divergence angle of the tubes, Sarpkaya was able to quantify the effect of the adverse pressure gradient.

The occurrence of vortex breakdown over a wing significantly alters the flow over the wing aft of the breakdown. Most significantly the flow is decelerated, reducing the magnitude of the suction peaks and resulting in a loss of lift. The location of vortex breakdown under varying conditions is therefore of prime interest. The influence of wing geometry and orientation on the location of vortex breakdown has been the subject of numerous investigations, including those by Lambourne and Bryer (1961), Earnshaw and Lawford (1964), Wéntz and Kohlman (1971), and Gursul (1995). The dependence of breakdown on swirl angle dictates that as incidence is increased, breakdown over the wing will be promoted, moving upstream towards the apex. It should be noted that breakdown over the surface of the wing only occurs at moderate to high angles of

attack; the exact angle of attack at which breakdown moves across the trailing edge depends on the sweep angle. At lower incidences breakdown, if it is present, will occur downstream of the trailing edge. Wéntz and Kohlman (1971) noted that the relationship between breakdown location and incidence is not linear, and that on increasing the angle of attack breakdown first moved rapidly forward, and then slowed as it approached the apex, behaviour described as "approximately parabolic" by Huang and Hanff (2000). This characteristic is another indication of the pressure distribution over the wing. The adverse pressure gradient in the trailing edge region makes the breakdown more susceptible to changes in incidence, while at higher angles of attack the breakdown moves away from the trailing edge region and thus becomes more stable. The effect of increasing sweep angle is to delay breakdown for a given angle of attack. The effect of yaw is to promote breakdown on the advancing side, and delay breakdown on the retreating side.

An extensive review of vortex breakdown locations over delta wings under static conditions for varying sweep and incidence was conducted by Gursul (1995). This reference provides a comprehensive database of past research in the field. As Figure 1.11 shows, there is some scatter in the data. One of the reasons for the difficulty in predicting vortex breakdown locations under different conditions was first identified by Lowson (1964). In static tests of an 80° delta over a range of angles of attack, hysteresis was noted with regard to the breakdown location. With the delta wing set at an incidence of 34° vortex breakdown was initially observed aft of the trailing edge. On statically increasing the incidence to 41° the breakdown was then observed to move onto the wing surface. However, on subsequently reducing the angle of incidence back to the original 34°, the breakdown remained on the surface of the wing rather than returning to its original position downstream of the trailing edge. This hysteresis of vortex breakdown location has since become well known. Hysteresis due to yaw (Elle, 1958) and Reynolds number changes (Traub *et al,* 1998) have also been noted. The significance of hysteresis of this form is widespread, and complicates experimental examination of the breakdown location over delta wings.

Further complexities in determining the breakdown location were identified by Lowson (1964), who studied the breakdown of both leading edge vortices over a slender delta

wing. At a given angle of attack, breakdown did not occur at the same location in each vortex. Neither was there any perceptible pattern relating to which vortex would break down upstream of the other. A further observation was that breakdown location was not static for either vortex, and exhibited streamwise fluctuations of the order of 10% of the chord length. There is an anti-symmetry between the breakdown location oscillations observed in each of the leading edge vortices, as observed by Menke *et al* (1999). As the breakdown on one side of the wing advances, the breakdown of the opposite vortex retreats.

Figure 1.12, reproduced from Menke *et al* (1999), which summarises the previous work of Gursul (1994), Gursul and Yang (1995), Gad-el-Hak and Blackwelder (1985) and Gordnier and Visbal (1994), shows the spectrum of unsteady flow phenomena over slender delta wings as a function of reduced frequency. The figure shows how the frequency of the breakdown location oscillations is of the order of 10^{-1}, adjacent to the range of frequencies at which aircraft manoeuvres are performed. It was pointed out by Menke *et al* that the proximity of these characteristic frequencies may lead to possible coupling between wing motion and the breakdown location – a phenomenon known as 'wing rock'. The flow oscillations directly in the wake of the spiral breakdown (referred to as the helical mode instability) are observed in the frequency range of the order of unity. Gad-el-Hak and Blackwelder (1985) documented the shedding of small scale vortex pairs from the leading edge. This instability was observed at the higher end of the spectrum, at frequencies of the order 10^{1}.

1.2.3.3 Prediction of vortex breakdown location over a delta wing

There have been many investigations of the parameters affecting vortex breakdown over delta wings, and the subject is controversial. It is widely agreed though that there are two principal factors affecting the location of the breakdown, being the amount of swirl and the presence or otherwise of an adverse pressure gradient (see §1.2.3.2). However, although a knowledge of the swirl angles in vortex flows over delta wings of various configurations exists, the same is not true for the pressure field and it is unlikely that that this knowledge will exist in the near future due to the complexity of the problem.

Therefore, although it is known that these are the principal factors affecting the breakdown location, they cannot be used as a tool to predict the breakdown location.

The attention of published literature has therefore been primarily focussed on the identification of alternative parameters that may allow the prediction of breakdown without requiring a knowledge of the pressure field. One criterion was suggested by Lambourne and Bryer (1961), who proposed that the angle between the leading edge and the free stream was related to the location of burst. This angle is given by:

$$\gamma = \cos^{-1}(\cos\alpha \cdot \sin\Lambda)$$

Where α is the incidence to the free stream, and Λ is the leading edge sweep angle. It was suggested that by plotting this parameter against breakdown location, the data would collapse onto a curve, hence allowing the simple prediction of breakdown location.

Lee and Ho (1990) suggested a swirl angle derived from the geometry of the wing:

$$\phi = \tan^{-1}\left(\frac{\sin\alpha}{\cos\alpha \cdot \sin\Lambda}\right)$$

Jumper *et al* (1993) suggested that vortex breakdown was observed when the normalised circulation of the leading edge vortices reached a critical value:

$$\frac{\Gamma_{bd}}{U_\infty c} = 0.132$$

Gursul (1994) suggested that the circulation normalised by the free-stream and streamwise distance from the apex, $\Gamma/U_\infty x$, would provide a more suitable correlation.

Gursul (1995) tested these criteria against a large database of previous tests, the results of which are reproduced in Figure 1.13. Whilst on a limited dataset these criteria may have appeared to be suitable to the individual investigator, when rigorously tested on a

much larger dataset, none has provided the single criterion for breakdown that has long been desired.

Robinson *et al* (1994) used a Rossby number criterion as the basis for their numerical prediction technique. The Rossby number is defined as the ratio of the maximum axial to swirl velocities in a vortex, and was found to have a critical value of between 0.9 and 1.4; a vortex with a Rossby number below this was found to indicate a burst vortex. Although this technique is simple to apply to numerical codes, it does not provide the simple parameter that can predict breakdown without the need for numerical calculations.

Traub (1996) managed to find a reasonable correlation for breakdown location, also by considering the circulation of the leading edge vortices. The analysis is based on the assumption that the circulation of the vortex at the point of breakdown is equal to the value when breakdown is observed at the trailing edge. Thus, given the distribution of circulation along the wing, the predicted breakdown location is that at which the circulation reaches this value. Firstly, the value of circulation at the trailing edge of the wing is recorded at an incidence at which breakdown is first observed there. This is labelled $\Gamma_{BD@TE}$. At any greater incidence (at which breakdown will occur forward of the trailing edge) the circulation of a hypothetical unbroken vortex at the trailing edge is predicted using the relation derived by Hemsch and Luckring (1990) for determining the value of circulation at the trailing edge of a simple delta:

$$\frac{\Gamma_{TE}}{U_\infty c} = 4.83 \tan^{0.8}(90 - \Lambda) \tan^{1.2} \alpha \cos \alpha$$

The location of the breakdown at this higher incidence is then predicted by interpolating to find the location on the wing at which the circulation is equal to $\Gamma_{BD@TE}$, thus:

$$\left(\frac{x}{c}\right)_{BD} = \left(\frac{\Gamma_{BD@TE}}{\Gamma_{TE}}\right)^3$$

This method was shown to provide a good estimation of the breakdown location over wings with a range of sweep angles, but is limited by its requirement for a knowledge of the circulation of a vortex at the point of breakdown proximal to the trailing edge.

1.2.3.4 Explanations of vortex breakdown

Many investigators have focused their attention on the physical explanation of the breakdown process, rather than studying its forms. The consideration of vortex breakdown has not resulted in any single consistent argument to explain the phenomenon. An exhaustive review of the various theories relating to the explanation of vortex breakdown is beyond the scope of this discussion. However, an overview of related literature is presented to give the reader an appreciation of the more popular theories. For critical discussions of the various theories the reader is directed to the review articles of Hall (1972), Leibovich (1978; 1984), Escudier (1988) and Délery (1994).

Quasi-cylindrical approximation of vortex flow

The starting point for many theoretical investigations of vortex breakdown has been the quasi-cylindrical approximation to vortex flow. The validity of this approximation is based on observations of the flow preceding breakdown, where axial velocity and pressure gradients are small compared to those in the radial direction. For a steady, incompressible flow with axially symmetric velocity and pressure fields, simplification of the full Navier-Stokes and Continuity equations yields:

$$\frac{\partial u}{\partial r}+\frac{u}{r}+\frac{\partial w}{\partial z}=0; \qquad \frac{v^2}{r}=\frac{1}{\rho}\frac{\partial p}{\partial r}$$

$$u\frac{\partial v}{\partial r}+\frac{uv}{r}+w\frac{\partial v}{\partial z}=\nu\left(\frac{\partial^2 v}{\partial r^2}+\frac{1}{r}\frac{\partial v}{\partial r}-\frac{v}{r}\right)$$

$$u\frac{\partial w}{\partial r}+w\frac{\partial w}{\partial z}=-\frac{1}{\rho}\frac{\partial p}{\partial z}+\nu\left(\frac{\partial^2 w}{\partial r^2}+\frac{1}{r}\frac{\partial w}{\partial r}\right)$$

Where r and z are cylindrical polar coordinates, u, v and z are the radial, azimuthal and axial components of velocity, p is the pressure, ρ is the density and ν the dynamic viscosity. The prediction of breakdown is assumed to occur when this approximation to the flow fails; that is, when the axial velocity and pressure gradients become large. The interpretation of this method is that breakdown is a similar phenomenon to that of the separation point of a boundary layer. Indeed, the similarities between the two flows provide a compelling argument. The structure of both flows are similar; a region of flow reversal is accompanied by deceleration of the approaching flow and dilation of the streamlines. Additionally, both are sensitive to axial pressure gradients, where an adverse pressure gradient promotes stagnation of the flow.

However, although experimental investigations of breakdown have produced comparable results to those predicted using this method, the method is limited in its ability to *explain* the occurrence of vortex breakdown.

Theory of critical state

Squire (1960) considered the existence of long standing waves on an axisymmetric cylindrical vortex, arguing that if such waves could exist then small disturbances originating downstream would be capable of propagating in the upstream direction, ultimately inducing the breakdown of the vortex. Squire went on to define two flow states: for *subcritical* flow small disturbances may propagate upstream; for *supercritical* flow they cannot. It was implied that the breakdown of the vortex would occur at the point of transition between the two states.

Benjamin (1962) criticised Squire's theory by pointing out that although the phase velocity of the standing waves was directed upstream at the point of criticality, the group velocity was directed downstream, so that waves could not propagate upstream from a disturbance. Hall (1972) also criticised the theory for its lack of explanatory power, as it does not define when and where the critical state is reached, nor how the propagation of such waves could lead to the dramatic change in the core structure observed in a breakdown. However, despite its limitations the critical state theory has proved a useful starting point for a number of other investigators.

Theory of conjugate states

Benjamin (1962; 1967) famously proposed the theory of conjugate states, where the breakdown is assumed to occur at the transition between two conjugate swirling flows. The theory is based on an analogy with hydraulic jump in open channel flow, the concept being that vortex breakdown is the swirling flow equivalent of hydraulic jump. Benjamin defined a pair of flow states and showed that if the upstream flow was supercritical, its conjugate flow downstream was subcritical. A fundamental element of Benjamin's theory is the explanation of the excess flow force or momentum flux that is found to occur in the subcritical flow compared to the supercritical flow. As no energy is applied to the flow, Benjamin postulated the existence of weak standing waves on the subcritical flow to account for the difference.

It is the assumption of small standing waves which provides Hall (1972) with his greatest criticism of Benjamin's theory. Observations made from experiments show that the perturbations in vortex breakdown are necessarily large. A further criticism was that the theory is no more powerful in its explanation of breakdown than is the previous explanation by Squire. Further, the theory does not specify where or when the 'jump' from supercritical to subcritical flow will occur. Finally, and in the view of Leibovich (1984) most seriously, the theory is much more difficult to examine experimentally on account of its mathematical complexity.

Wave propagation

A refinement of the theories of Squire and Benjamin is the wave propagation theory discussed by Leibovich (1984), amongst others. The concept is to consider an infinitesimal dispersive disturbing wave of the form $\exp i(\omega t + n\theta + kx)$, where n and k are the azimuthal and axial wave numbers respectively, propagating along a vortex core. Benjamin (1962) considered axisymmetric waves of azimuthal wave number $n = 0$ in the long axial wave limit of $k \rightarrow 0$. Once again referring to the concept of criticality, Benjamin defined a supercritical flow as one that could not support the upstream propagation of such disturbing waves, a situation which exists if the phase velocity of the wave, given by $c = \omega/k$, is directed downstream, i.e. the phase velocity is positive.

If the phase velocity is negative, the disturbing wave is directed upstream, and the flow is subcritical. Leibovich (1984) corrected this concept by pointing out that it is the group velocity, $C_g = \partial\omega/\partial k$, not the phase velocity, which defines the ability of a disturbing wave to propagate upstream. Nevertheless, Leibovich went on to demonstrate that a flow that is subcritical based on the phase velocity criterion is also subcritical based on the group velocity criterion in the long axial wave limit $k \rightarrow 0$, so that Benjamin's original assumption was correct.

Tsai and Widnall (1980) used linear wave propagation analysis to obtain the dispersion relation, which relates wave number to radial frequency in a dispersive wave, and the group velocity for the experimental data presented by Garg and Leibovich (1979). It was shown that the ability of a wave to propagate upstream decreases with increasing axial wave number; that is, the group velocity of the wave becomes less negative with increasing wave number.

Gursul and Xie (1999) used the results of Tsai and Widnall and others to explain their observations of the breakdown response to an oscillating fin, with application to that fin buffet problem. Figure 1.14 shows that the response observed was similar to that of a low-pass filter. Further analysis showed that this behaviour could be explained using wave propagation theory, although estimates of the cut-off frequency were only order of magnitude accurate.

Gursul (2000) observed that the breakdown response to dynamic changes in wing geometry and flow regime was universal regardless of the type of forcing motion applied. Figure 1.15 shows the forcing mechanisms considered, and their response to inputs of varying frequencies. Using the wave propagation theory described above in an attempt to explain these observations, Gursul produced a model which adequately, if not accurately, predicts the vortex breakdown response phase lag.

1.2.3.5 Breakdown response to dynamic perturbation

There have been many investigations of the vortex breakdown response to dynamic and transient disturbances. One popular area has focused on the breakdown response to a pitching wing, both transiently and dynamically. Greenwell and Wood (1994) and

Srinivas *et al* (1994) provide useful reviews of previous studies considering either sinusoidal or ramping pitching motions for a range of delta wing geometries and pitching rates. Srinivas *et al* (1994) indicates that the response of the breakdown to these motions gives a normalised time constant of the order of unity for the higher sweep angles (> 70°). Greenwell and Wood (1994) continued the analysis of dynamic pitching data by consolidating results from previous studies and attempting to establish the order of the breakdown response. It was found that the overall breakdown response to a dynamic perturbation of this type might be modelled as a second order spring-damper system. An adequate approximation to the response was obtained using a damping ratio of $\zeta = 1.67$ and a reduced natural frequency of $\omega_n = 2.0$. However, for pitching motions representative of typical aircraft manoeuvring ($fc/U_\infty < 0.03$) it was shown that a first order analysis with a time-constant of 1.67 would suffice. For the transient pitching tests considered it was found that the breakdown response was slow, requiring of the order of 10 convective time units to reach a steady state position.

The effect of other dynamic disturbances on breakdown response have also been considered at various times, including the effect of an accelerating free-stream by Gursul and Ho (1994), variable leading edge sweep by Srinivas *et al* (1994), and oscillating leading edge flaps by Deng and Gursul (1997). Gursul (2000) observed that the overall breakdown response to an unsteady disturbance was similar regardless of the type of disturbance considered, and presented a mechanism for the response, as discussed in §1.2.3.4.

1.2.4 Vortex-Body Interactions

To this point literature in the fields of support interference, delta wing aerodynamics and vortex breakdown have been reviewed. Whilst it has been shown that no detailed studies of dynamic support interference currently exists in literature, there have been a number of investigations that can be applied to this field. Here, literature relating to fin buffet and vortex body interactions, two important fields which are closely related to the current research, are considered.

1.2.4.1 Static vortex-body interactions

The first investigation of the effect of the impingement of a leading edge vortex on a body was described by Lambourne and Bryer (1961). The results suggested that a thin body could be placed in the vortex without the precipitation of burst, but that a larger obstacle would induce a more significant response. It was noted that the distance of the burst upstream of the obstacle decreased with the progressive upstream movement of the body. Somewhat elusively, no mention was made of the type or dimensions of the bodies used in these experiments, other than that a ½ inch diameter rod would at some point induce breakdown over the wing surface. This investigation was followed by that of Hummel (1965), the results of which are described in §1.2.1.

There have been a number of more recent investigations of the breakdown response to a static disturbance as this particular problem has specific relevance to the field of fin buffeting. This area of research focuses on the buffeting effect of a vortex impinging on an aircraft fin structure. Once again the reader is referred to the case of the F/A-18 'Hornet' aircraft which has particularly suffered from this problem and has been the focus of much recent research. A number of investigators have studied in some detail the interaction of a vortex with a flat-plate – the significance being that the flat-plate may be used to approximate the fin in the fin buffet problem. Canbazoglu *et al* (1995) is one such study, which considers the interaction of an impinging broken vortex with a fin model. However, the aim of the current research is not to investigate the interaction process but the *effect* of the interaction on the breakdown location.

Gursul and Xie (1999) investigated the effect of a vortex impinging on a horizontal flat-plate placed one-quarter-chord length downstream of a 70° delta set at a range of angles of incidence. It was observed that the presence of the plate reduced the magnitude of the streamwise variations of breakdown location; the RMS value of breakdown location was reduced by around 50% compared to the non-impinging flow. It was also noted that the time-averaged breakdown location was moved upstream in the presence of the plate, although no quantitative data were presented so no conclusions can be drawn as to the extent of the interference. A further observation was that the dominant frequencies observed in the breakdown location spectrum in the absence of the plate were replaced

by much higher dominant frequencies of smaller amplitude in the impinging flow. This observation has particular significance in buffeting flows, and shows how the nature of vortical flow is altered in impinging flow. It should be noted that in contrast to this investigation, the mean flow was impinging on the horizontal plate at an angle, so that the effective thickness of the plate in the plane of interest was larger than its actual thickness.

Earlier studies by Mayori and Rockwell (1994) and Wolfe *et al* (1995) used PIV, and in the latter case surface pressure measurements, to investigate the structure of a vortex impinging on a horizontal thin flat-plate using a setup similar to that of Gursul and Xie (1999), though neither explicitly considers the effect of such impingement on the vortex breakdown location. A computational study of a similar nature was also performed by Gordnier and Visbal (1997), who considered a configuration identical to that of Wolfe *et al* (1995), being vortices generated by a 75° delta wing set at 30° incidence impinging on a horizontal thin flat plate placed $0.32c$ downstream of the trailing edge of the wing. In this case it was shown that the mean breakdown location exhibited low frequency fluctuations with a magnitude of approximately $0.15c$. The time-averaged breakdown location was approximately $0.62c$, although no mention of the undisturbed breakdown location was given for comparison.

Although the field of fin buffeting provides an insight into the ability of an obstacle to induce premature breakdown over a wing, the obstacle in question (the fin) is necessarily much further upstream than in the case of support interference, so the analogy is limited in its use. The result of this is that fin-buffeting problems consider only the breakdown of vortices above the wing, where breakdown can occur either over the wing or in the wake in the case of support interference.

1.2.4.2 Dynamic vortex-body interactions

Gursul and Xie (2001) studied the effect of a vortex impinging on an oscillating fin. Observations of breakdown location for different forcing frequencies showed that the breakdown response was similar to that of a low-pass filter, with only lower frequencies of forcing having an effect on the breakdown location; no response was observed at higher forcing frequencies. Figure 1.14 shows the variation of the amplitude ratio (AR)

with reduced frequency for this case. It is seen that the breakdown location becomes much less sensitive to fin oscillations as the frequency of the oscillations is increased. For this type of forcing the non-dimensional cut-off frequency was estimated to be approximately 0.40.

A further field of research that has relevance is that of vortex-body interactions. This area of research has many practical applications, such as vortex-blade interactions in helicopter rotor-dynamics and gas turbines, and vortex-fuselage interactions in low-speed helicopter flight. A simplification of this latter application is to consider the interaction of a vortex with a simple cylindrical body. However, although the interaction of these bodies has been analysed in some detail, the arrangement of the interaction does not allow a comparison with support interference. The vortex axis is in this case orthogonal to both the free stream velocity and the cylinder axis so that the free stream velocity drives the vortex into the cylinder. In addition the focus of the research has been on the details of the interaction rather than the effect of the presence of the body on the presence and location of vortex breakdown. A review of this subject area has been made by Rockwell (1998).

1.2.5 Lift and Moment Characteristics of Delta Wings

The lifting characteristics of delta wings give them a major advantage over conventional aerofoils. A slender delta wing exhibits a much higher stall angle than an aerofoil, a characteristic attributable to the existence of the leading edge vortices over delta wings. The high velocities associated with the leading edge vortices imply a more energetic flow regime, and lifting flow is therefore maintained to much higher angles of attack. At a sufficiently high angle of attack, the reattachment of the flow to the suction surface fails and vortex breakdown is observed, resulting in the stalling of the wing. Figure 1.16 shows the lift curve for a typical slender delta wing compared with that for a conventional aerofoil. An interesting feature is that the delta wing exhibits a much shallower lift-curve slope compared to the aerofoil, but continues to develop lift to much higher angles of attack so that C_{Lmax} for the two types of wing are comparable. It is important that the lifting characteristics of the delta wing be fully understood since the onset of breakdown will incur a loss of lift. It is therefore fundamental to the

consideration of support interference that the development and subsequent loss of lift be fully explored. A physical explanation and discussion of experimental observations relating to the lifting characteristics of delta wings follows.

Early investigations of the lift and moment characteristics of delta wings were carried out by Ernshaw and Lawford (1964) and Hummel and Srinivasan (1967). Ernshaw and Lawford considered wings with sweep angles in the range $45° < \Lambda < 76°$ and provided a comprehensive database of the lift and normal force characteristics of delta wings. Hummel and Srinivasan (1967) considered wings with 60° and 68.2° sweep, and studied the effect of vortex breakdown on the lift, drag and moment curves at higher incidences. It was observed that the appearance of vortex breakdown at the trailing edge of the wing corresponded with a marked reduction in the lift, drag and moment curve slopes.

While it is understood that it is the leading edge vortices produced by slender delta wings that allow lift to be generated to high angles of attack, according to the widely accepted theoretical analysis of Polhamus (1971), this is not the only component of lift acting on the wing. In his analysis the total lift acting on the wing is the sum of the Potential-flow Lift (L_p) and Vortex Lift (L_v). The potential flow lift component is defined as the attached flow lift developed in the absence of the leading edge vortices, and is given by:

$$C_{Lp} = k_p \sin\alpha \cos^2\alpha$$

Where the coefficient k_p is the lift curve slope of the wing at zero lift, and is estimated for a delta wing by Traub (1997):

$$k_p = 4\tan^{0.8}(90 - \Lambda)$$

The vortex lift component is the component of lift attributable entirely to the presence of the leading edge vortices, and is given by:

$$C_{Lv} = k_v \sin^2\alpha \cos\alpha$$

Where it may be assumed that $k_v = \pi$ for slender delta wings. This theory, termed the Polhamus Leading Edge Suction (LES) Theory due to its derivation, is a simple and accurate method for estimating the lift curve of slender delta wings. However there have been relatively few experimental investigations of the lifting characteristics of delta wings. Articles that exist in addition to those mentioned previously include those by Wéntz and Kohlman (1971) and Roos and Kegelman (1990).

Figure 1.17, reproduced from Wéntz and Kohlman (1971), compares the Polhamus theory with experimental data obtained in wind-tunnel experiments. It is seen that Polhamus' theory compares favourably with experimental data, and that the theory is particularly suited to predicting the lift over wings with leading edge sweep angles of 70° and 75°. However, there are some limitations to the method, as it tends to over-estimate lift at higher sweep angles. Polhamus (1971) suggested that this may be attributable to proximity of the vortices to each other over highly swept wings, which results in one vortex becoming displaced above the other, effectively removing the lift contribution from the displaced vortex. In addition the theory does not predict the onset of the stall in any way, and this must be accounted for when applying the theory in the absence of qualifying experimental data.

Figure 1.17 also shows the pitching moment (defined positive nose down) characteristics of the delta wing. In this figure it is the pitching moment about the quarter chord, normalised by the aerodynamic mean chord that is plotted. It is seen that the delta wing exhibits a nose up pitching moment through the entire range of incidences considered, and that the magnitude of the moment falls significantly during the stall. Polhamus' LES Theory that has been applied for approximating lift has not been extended to consider pitching moments. An earlier analysis reported by Bartlett and Vidal (1955) is a more complex one. In this analysis the pitching moment coefficient is given by:

$$C_M = -\left(\frac{dC_M}{dC_L}\right)_0 \cdot \left(\frac{dC_L}{d\alpha}\right)_0 \cdot \alpha + \left(\frac{\bar{x}}{c}\right) \cdot C_{Dc}\alpha^2$$

Where C_{Dc} is the cross-flow drag coefficient, which may be taken as equal to 2 for slender sharp edge thin delta wings, and $\bar{x}$ is the distance from the apex of the wing to the centroid of area. The limitation of this method is that it requires some knowledge of the aerodynamic properties of the wing before it can be applied. Further, Bartlett and Vidal do not state about which point on the wing the moment is taken, which somewhat limits its validity. Once again there are few published experimental data to justify this theory, although the authors perform an extensive comparison of experimental data of various planforms, which suggests that its application to the slender delta wing may be valid.

Figure 1.17 also shows how the occurrence of vortex breakdown over the wing affects lift and moment characteristics. It can be seen that the onset of breakdown at the trailing edge marks the onset of stall, and that by the time the breakdown has progressed to the apex the wing has fully stalled. A number of conclusions may be drawn from this. Firstly, it is apparent that the breakdown does not affect the lift generated by the wing until it has progressed to the trailing edge. A breakdown aft of the trailing edge does not affect lift. Secondly, as indicated above, it is the onset of breakdown that is the stalling mechanism for the delta wing. This has significant implications for this research since it implies that premature breakdown induced by a support structure may not simply induce a local reduction in lift, but trigger the stalling process.

1.3 Chapter Review and Objectives of the Research Program

The above survey has shown that little consideration of the support interference problem, and specifically of the vortex-support interaction problem, in testing has previously been made in the literature. A specific need given current military aircraft designs is the appreciation of support interference in high angle of attack testing. The wake of models at high incidences is highly vortical, and the occurrence of vortex breakdown over lifting surfaces may be considerably detrimental to test results. Little is known of the interaction of streamwise vortices formed over test models with the structures used to support them. While a number of research areas, such as fin buffet and vortex-body interactions, encompass some aspects of these interactions, a full

understanding is elusive in literature. An understanding of vortex-structure interactions is particularly important for high angle of attack, oscillatory dynamic testing, where the support structures used are by necessity much more bulky than their static counterparts, and more often than not placed in the wake of the test model.

It was the aim of this investigation to study the effects of support interference in high angle of attack testing under static, oscillatory and transient test conditions. The specific aim was to determine those conditions under which support interference may be a factor, so that future experimentalists may use this information when designing tests. The following aims were identified prior to commencement of the research.

(i) To study the effect of support interference in static, oscillatory and transient testing;

(ii) To place specific emphasis on the interaction between the vortices generated by test models and their supporting structures;

(iii) To establish a database of conditions under which support interference may become a problem;

(iv) To use experimental results to formulate a prediction tool that would enable future researchers to identify potential interference problems at an early stage in the design of testing programme.

Discussion of the success of this investigation in achieving these aims will be given in the penultimate chapter, Chapter 7.

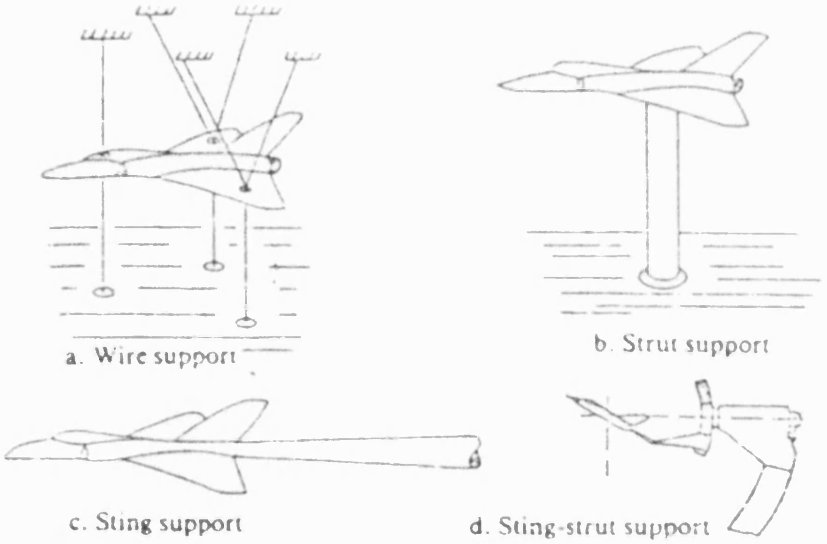

Figure 1.1: Commonly used support structures (Ericsson and Reding, 1983).

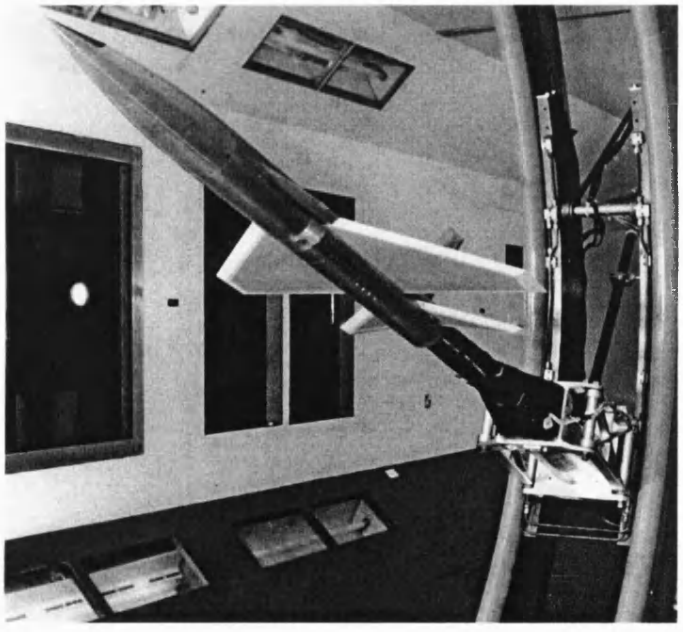

Figure 1.2: A typical dynamic support rig used by DERA (Bedford).

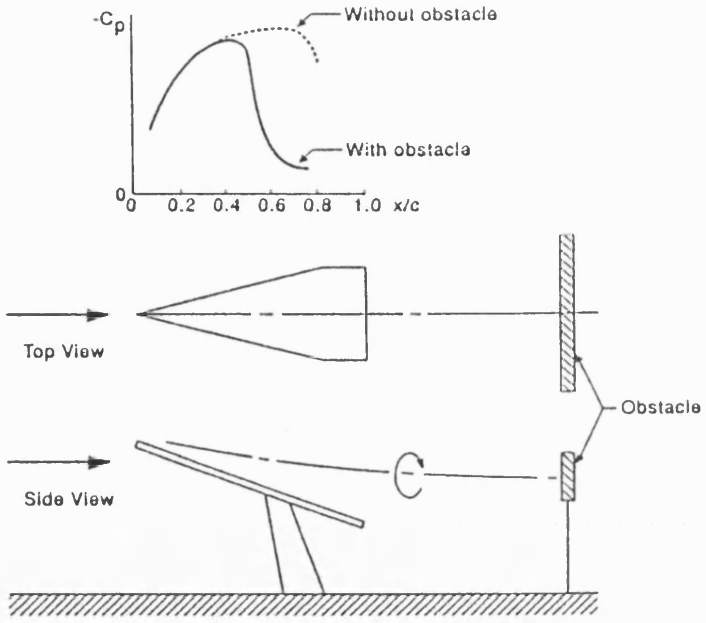

Figure 1.3: Effect of an obstacle on vortex breakdown location (Hummel, 1965).

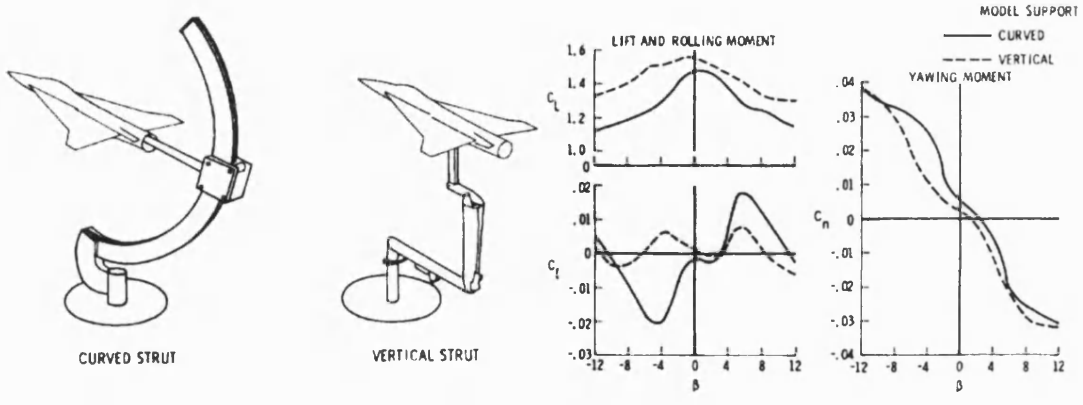

Figure 1.4: Effect of support type on aerodynamic coefficients (Johnson *et al*, 1980).

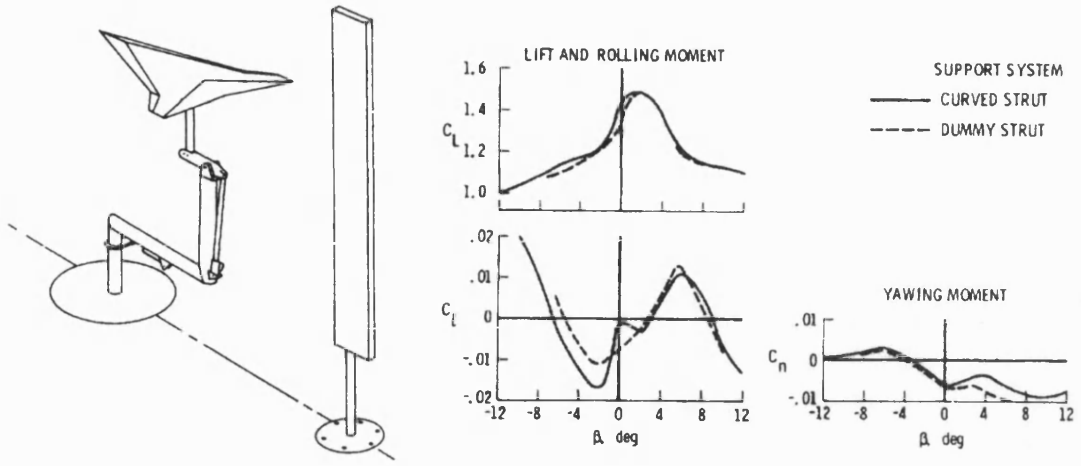

Figure 1.5: Comparison of curved strut with dummy strut (Johnson *et al* 1980).

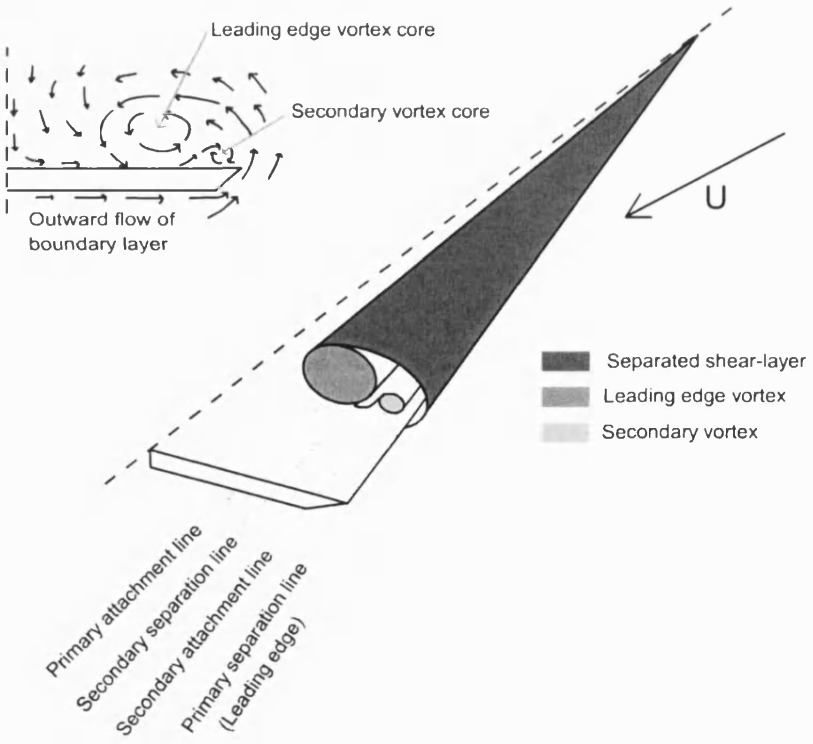

Figure 1.6: Delta wing flow topology.

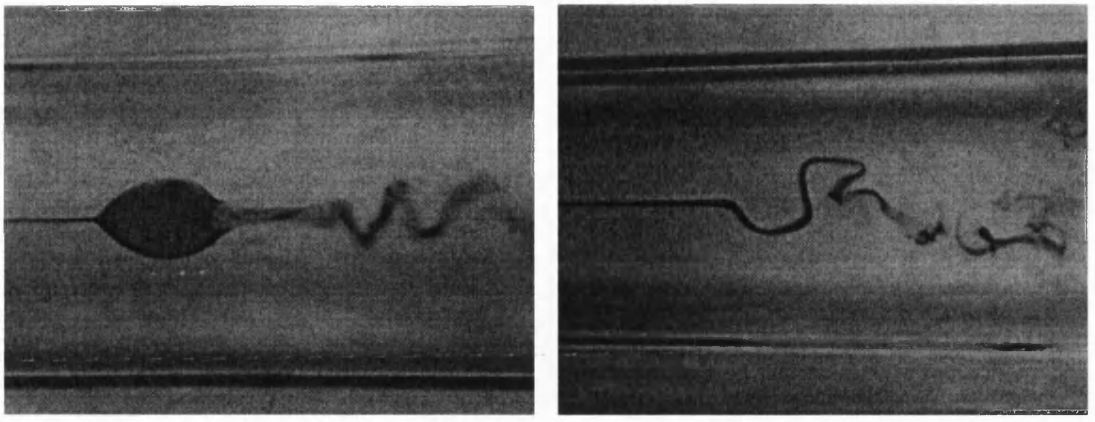

Figure 1.7: Bubble and spiral forms of vortex breakdown (Leibovich, 1978).

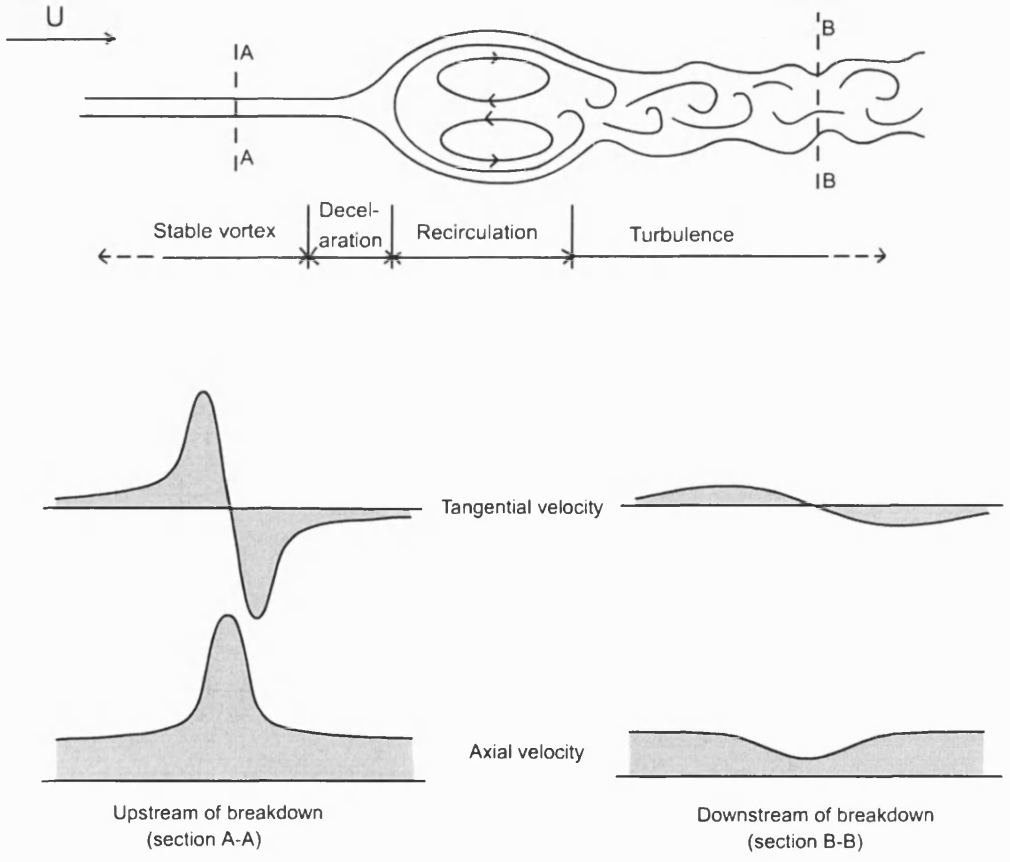

Figure 1.8: Stages of development of axisymmetric breakdown.

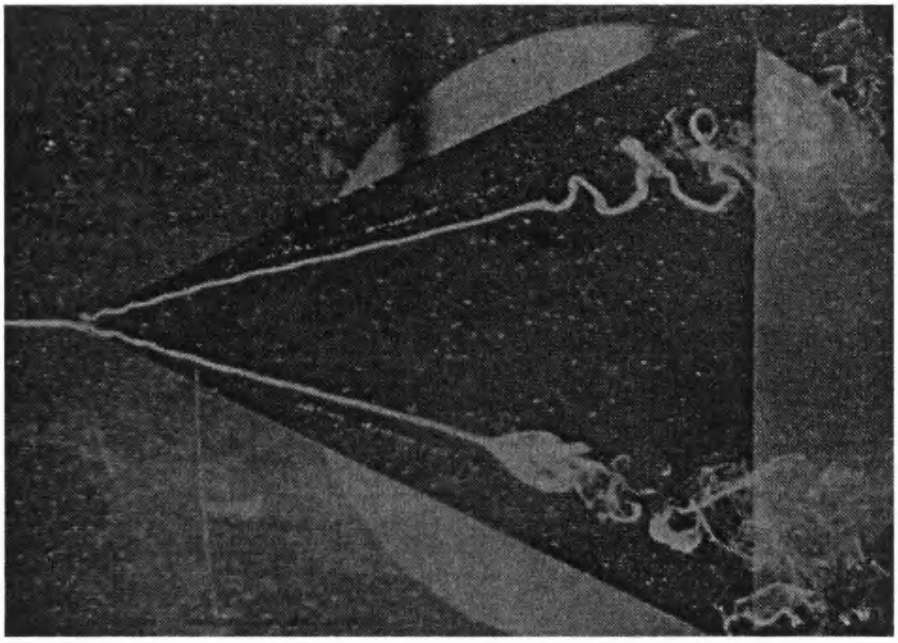

Figure 1.9: Vortex breakdown over a delta wing (Lambourne and Bryer, 1961).

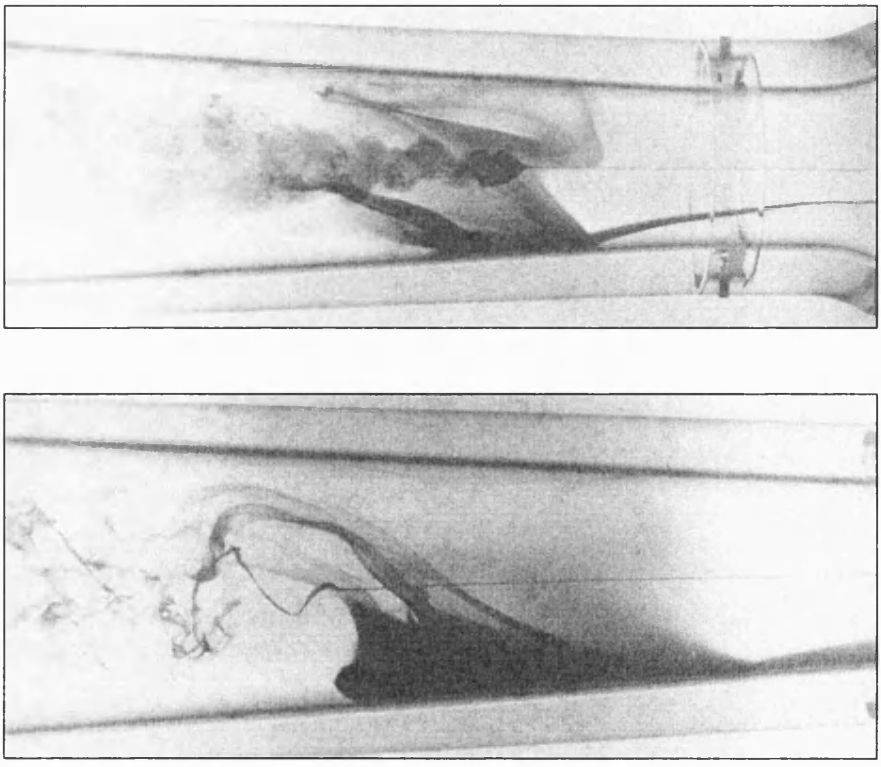

Figure 1.10: Vortex breakdown in a diverging tube (Sarpkaya, 1974).

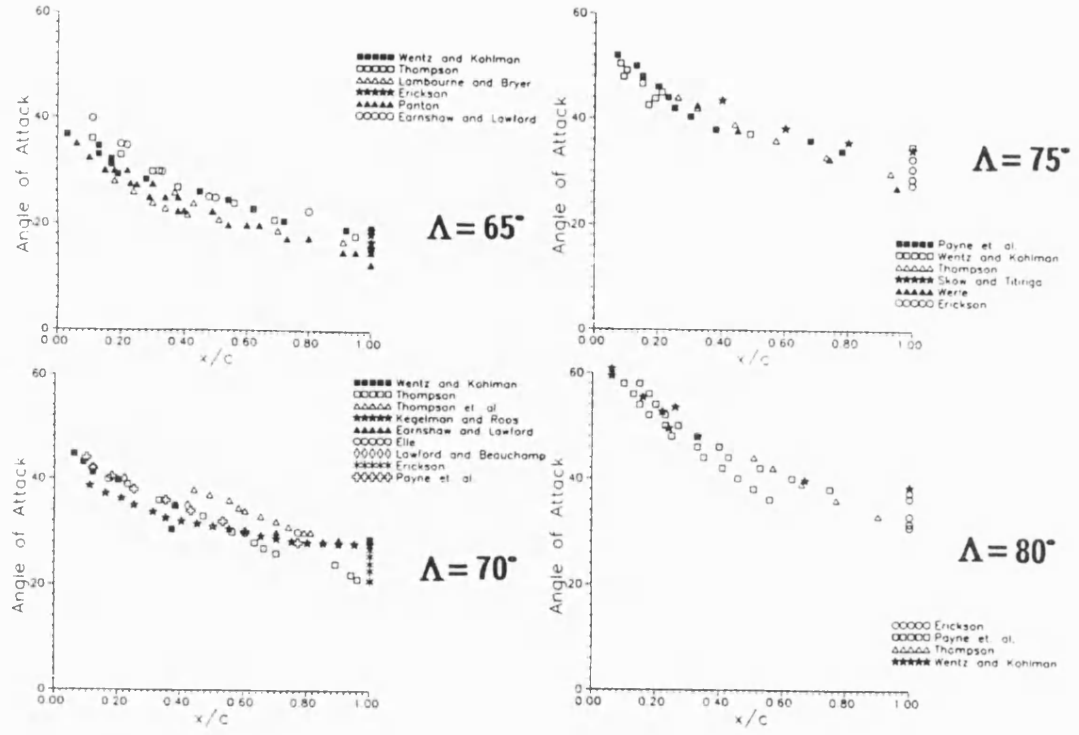

Figure 1.11: Variation of breakdown location with incidence (Gursul, 1995).

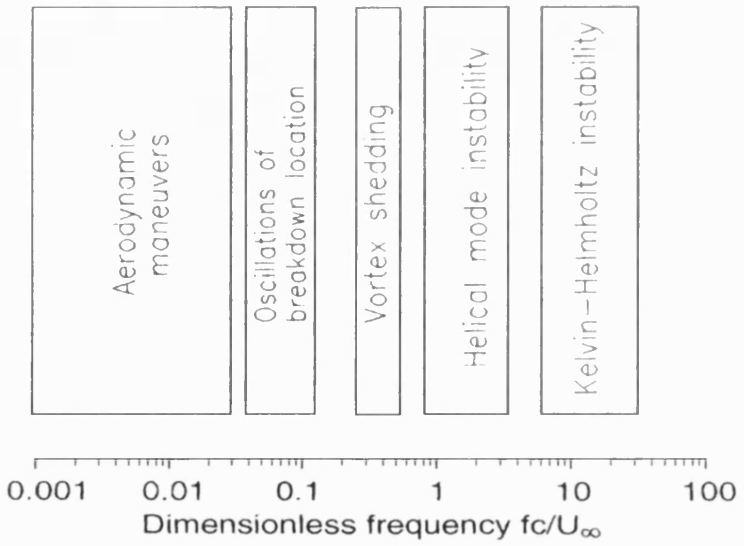

Figure 1.12: Spectrum of unsteady flow phenomena (Menke *et al*, 1999).

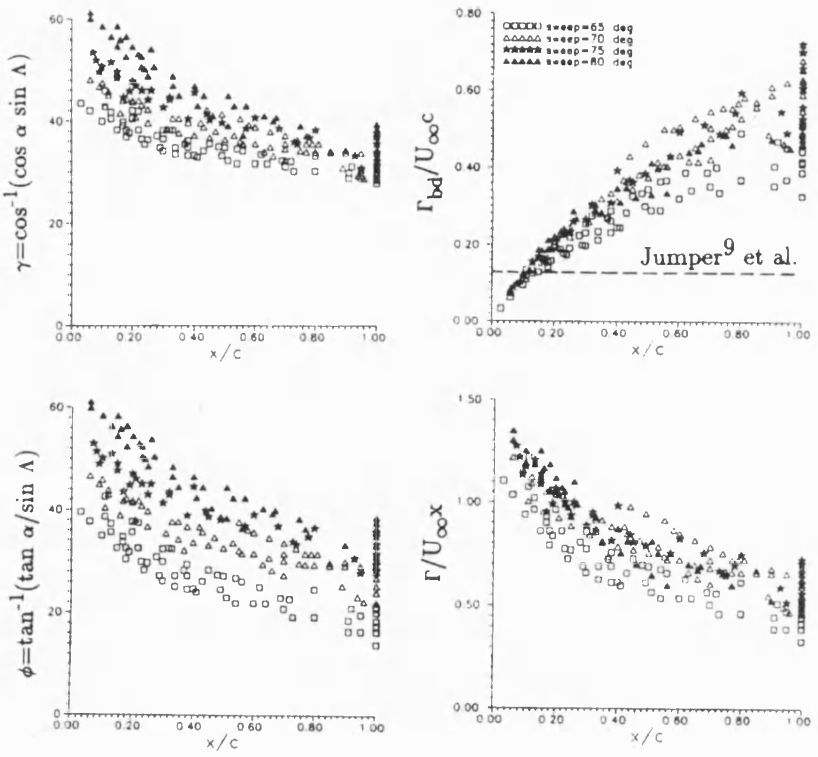

Figure 1.13: Inadequacy of proposed breakdown criteria (Gursul, 1995).

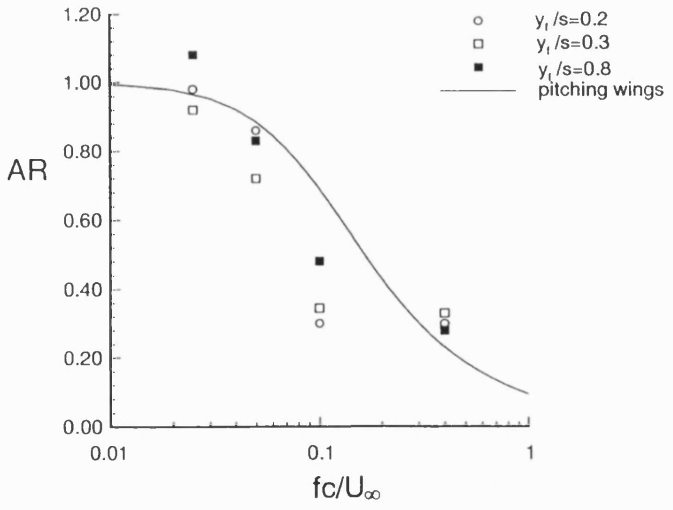

Figure 1.14: Frequency response to oscillating fin (Gursul and Xie, 1999).

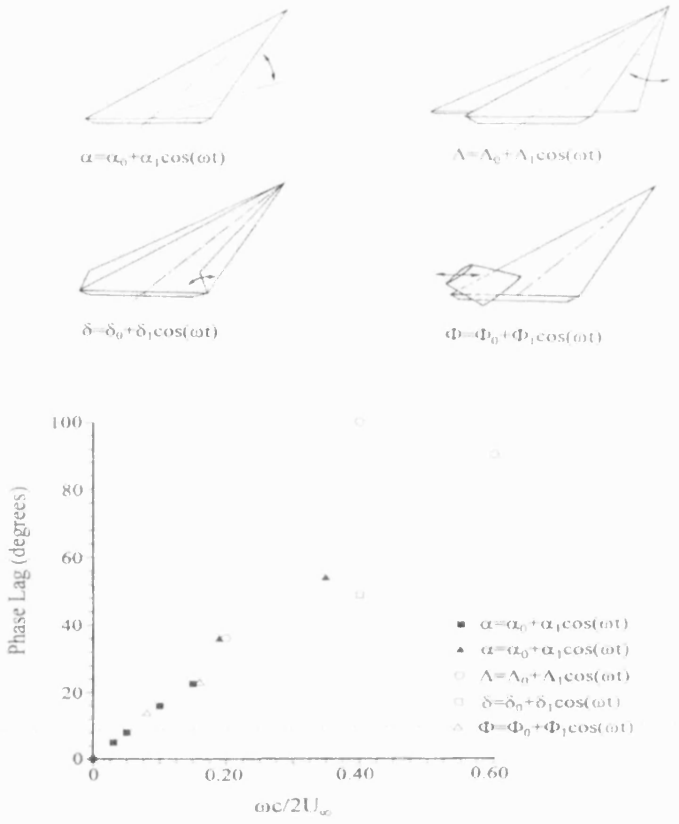

Figure 1.15: Universal response of vortex breakdown (Gursul, 2000).

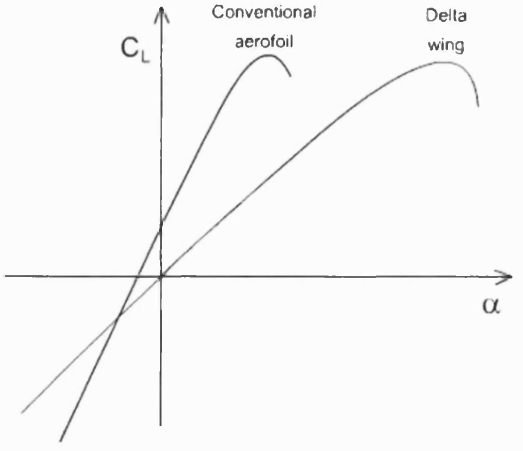

Figure 1.16: Comparison of lift-curves of delta wing and conventional aerofoil.

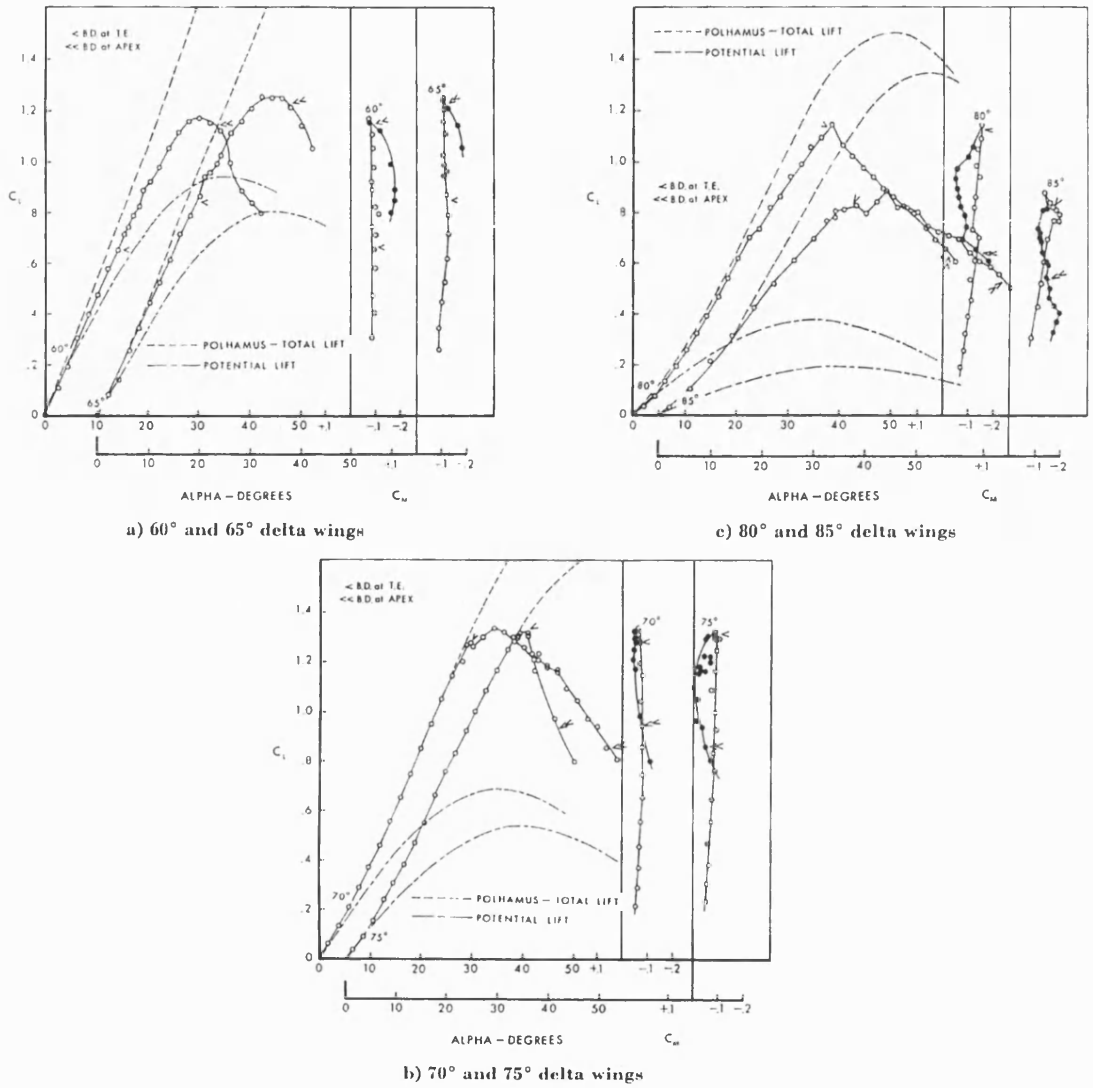

Figure 1.17: Lift and pitching moment characteristics of delta wings (Wéntz and Kohlman, 1971).

Chapter 2 Experimental Apparatus

2.1 Introduction

This chapter concerns itself with the description of the apparatus employed through the course of this investigation. Firstly, the test facility and models are discussed, following which is a description of the instrumentation used to measure the relevant quantities presented in the subsequent chapters.

2.2 Water-tunnel Facility

All experimental testing was conducted in the water-tunnel facility at the University of Bath. The tunnel is an Eidetics Model 1520 Water-tunnel of 0.38 x 0.51 x 1.52 m working section, which can provide velocities in the range 0 to 0.45 m/s with a turbulence intensity of less than 1% RMS (from water-tunnel reference material), through a horizontal, closed circuit continuous flow system. The tunnel has four viewing windows: three surrounding the test section, and one downstream allowing axial viewing. The height of the test section above the floor means that flow visualisation may easily be achieved from below as well as from the sides. A schematic of the water-tunnel facility is shown in Figure 2.1. The tunnel is complete with 6 pressurised dye canisters to facilitate dye flow visualisation. Metering of the dye was achieved using gate valves placed in-line between the dye canisters and the model. The dye used was food colouring diluted 1:4 with tap water.

The water-tunnel was chosen as the tool for this research as careful experimentation can yield strikingly vivid flow visualisation results, as will be demonstrated in Chapter 3.

Similar visualisations performed in a wind-tunnel are difficult due to the higher Reynolds numbers involved. A full discussion of the ability to compare wind and water-tunnel results may also be found in Chapter 3.

2.3 Water-tunnel Models

Vortical flows are of prime interest to the field of aeronautics. Vortices are shed from many aircraft configurations, and their interaction with each other, the airframe, and other aircraft is a major concern, and the study of these interactions requires a tool for generating suitable vortices. Historically there have been two methods of generating vortices under experimental conditions. The vortex tube is popular with many investigators as it provides an axisymmetric vortex under very controllable conditions. However, vortex flows generated in vortex tubes are not representative of typical external aerodynamic conditions. Thus, the alternative to a vortex tube is to use a simple delta wing to generate a suitable vortex. Whilst the vortices generated in this manner are unavoidably asymmetric, they do provide a 'real' flow, and the strength of the vortices may be altered by changing the free-stream velocity, or the incidence or sideslip of the model. The use of simple delta wings to generate a vortical flow is a common method, and one that was adopted in this investigation.

Λ [°]	c [mm]	b [mm]	d [mm]
70	137	100	30
75	187	100	30
80	250	88	32
85	285	50	84

Table 2.1: Model dimensions.

Four models were tested, having sweep angles of 70°, 75°, 80° and 85°. The principal dimensions of the models used are defined in Figure 2.2, and are listed in Table 2.1, above. All models were bevelled on the pressure surface by $\gamma = 30°$ to produce a sharp

leading edge, and had a thickness, t, of 5mm. The blockage ratio was approximately 3.7% in the worst case, which was for the $\Lambda = 80°$ wing at $\alpha = 40°$.

Two separate sets of models were used, one for flow visualisation and Particle Image Velocimetry (PIV) measurements, the other for force balance measurements. Flow visualisation models were fabricated from aluminium, and incorporated dye tubes with an internal and external diameter of 0.81mm and 1.02mm embedded in the pressure surface, exiting just aft of the wing apex (see Figure 2.2). The dye tubes were connected to pressurised dye canisters using plastic tubing of a similar diameter. Embedding the tubes in this manner allowed precise injection of the dye into the vortex core. It was noted that the closer the point of dye injection was to the apex of the delta, the better the quality of the visualisations, as this allows the dye to be injected directly into the vortex core. This dimension, labelled d in Figure 2.2, was therefore minimised where possible, although for highly swept wings d increases as the model size constrains the design. The distance between the wing apex and the dye injection point for each of the wings is given in Table 2.1. The models were spray-painted to protect them from corrosion while in contact with the water. For flow visualisation tests the models were painted white for contrast with the dye; for PIV measurements the models were painted black to reduce unwanted reflections from the wing surface. Force balance measurements were undertaken with models constructed from PVC to reduce weight and pre-loading of the load cells. These models did not incorporate dye tubes, and were not painted.

To consider the effect of support interference on the vortices developed by the test models, a number of 'dummy' supports were used. By supporting the delta models by a strut attached to the pressure surface, interference between the leading edge vortex structure and the support was minimised. A dummy support was then placed at a distance x_{LE} downstream of the test model to simulate the effect of a support structure placed in the wake of a vortical flow. Dummy supports of various configurations were considered, being cylindrical rods of circular cross section with diameters, d_r = 12 and 24mm and three flat-plates of thickness t = 2mm and streamwise length of d_p = 24, 48 and 96mm. The supports were spray-painted black for corrosion protection, and are illustrated in Figure 2.3.

2.4 Model Installation

The water-tunnel has a free surface allowing mounting of models from above. The models were mounted using a strut attached to the pressure surface in such a way that the leading edge vortices generated by the wing were not affected by the supporting strut. This was achieved by mounting the models upside down, therefore keeping the support away from the region of interest. For static testing, mounting of the delta models and dummy supports was achieved using a simple arrangement of crossbeams. For dynamic testing, oscillatory motions were achieved by mounting a hydraulic actuator above the water-tunnel. The actuator piston was rigidly connected to a square-sectioned beam, through which a vertical slot was machined; the wing or dummy support was bolted through this slot. The actuator piston and crossbeam ran through two guides fixed rigidly to the base plate to ensure motion was along a single axis only. The set-up is illustrated in Figure 2.4. Both the dummy supports and wing models could be mounted on the oscillating mechanism as required.

Motion of the mechanism was controlled via a desktop PC using a Data Translation DT21EZ 12 bit D/A and A/D data acquisition card; output from the card was to a valve drive amplifier utilising feedback control to position the support correctly. A feedback loop was created using a linear potentiometer connected at one end to the base plate, and at the other to the actuator piston. Output from the potentiometer was downloaded to another desktop PC so that motion of the rig could be studied as part of the post-processing procedure.

2.5 Instrumentation

2.5.1 Flow Visualisation

All flow visualisation pictures were taken using a Panasonic NV-DS99B digital video camera with a capture rate of 25 frames per second and a resolution of 570,000 pixels, which was mounted on a Velbon D700 tripod. The camera was interfaced to a desktop

PC with an integrated Pinnacle Systems DV Studio video capture board and software, which allows real time viewing and capture of video images.

2.5.2 Force Balance

Forces were measured using two load cells mounted on an external frame positioned above the water-tunnel. Forces from the wing were transmitted to the load cells using the cross beam and sting arrangement illustrated in Figure 2.5. The sting was arranged so that the longest dimension of the cross section was parallel to the free stream in order to reduce off axis loading of the cells. To keep component weight to a minimum, and therefore reduce pre-loading of the load cells, the cross beam and sting were manufactured from a carbon fibre composite, and the test models were manufactured from PVC.

The cells were model 31/1435-03 load cells supplied by RDP Electronics Ltd, each having a capacity of 250g. The minimum measurable lift force was approximately 0.0012N; the maximum approximately 2.5N. The cells were interfaced to a desktop PC via a Data Translation DT3001 12 bit A/D and D/A data acquisition card, and the data recorded using a program written using HP-VEE software (Hewlett-Packard). The card was used to record signals from 3 channels simultaneously: one channel for each of the load cells, and one for the linear potentiometer recording the actuator piston movement.

2.5.3 Particle Image Velocimetry (PIV)

Measurements of the cross-flow velocity field were performed using a Particle Image Velocimetry (PIV) system. Variations of PIV have been around for many years, and original techniques involved the use of conventional film cameras; analysis of images was performed manually and was a laborious task. However, the emergence of Digital PIV (DPIV) techniques have transformed PIV into a much more user-friendly method. There follows a brief introduction to DPIV theory, followed by an outline of the equipment used for this investigation.

Particle Image Velocimetry is a measurement technique that allows the velocities in a plane of a fluid to be quantified instantaneously and non-intrusively. This is achieved by seeding the flow with particles selected for their ability to trace the flow. A plane of

interest is interrogated using a light source (usually a laser) to illuminate the particles passing through the plane. By capturing two images with a finite, known separation in time, Δt, the distance each particle has travelled in that time interval, Δx and Δy, can be measured. As the time interval tends to zero ($\Delta t \rightarrow 0$), so $\Delta x/\Delta t \rightarrow dx/dt$ and $\Delta y/\Delta t \rightarrow dy/dt$, and the velocities of the particles can be calculated. Since the particles are assumed to trace the motion of the flow exactly, the flow velocity is therefore known. Compared to the more established technique of Laser Doppler Anemometry (LDA), PIV is an instantaneous multi-point method, rather than a single point method. The disadvantage of PIV over LDV is that the time resolution is limited to the rate at which the camera can capture and download images to the computer, and this currently limits PIV to a maximum frequency of around 15 measurements per second. Care must therefore be taken in analysing time-averaged results to ensure aliasing of the features of an unsteady flow is avoided. However, PIV has the capability of calculating many thousands of velocity vectors at an instant in time, and is therefore a very powerful tool. The spatial resolution of the method depends on the quality of seeding, and relies on the optimisation of the camera and light sheet optics.

Once images have been captured and downloaded to the computer, they must be analysed to determine Δx and Δy for each particle. There are a number of methods which are used to perform these calculations, which include cross-correlation, auto-correlation and particle tracking. A detailed explanation of each of these methods is beyond the scope of this discussion although a brief discussion of the benefits of cross correlation over auto-correlation and particle tracking is included in Chapter 3. An excellent review of DPIV theory and application is provided by Willert and Gharib (1991).

A schematic of the PIV setup is shown in Figure 2.6. Illumination of the cross-flow plane was achieved using a pair of pulsed mini Nd:YAG lasers with a maximum energy of 120mJ per pulse situated beneath the water-tunnel. For the majority of tests the lasers were run at approximately 80mJ per pulse. A combination of spherical and cylindrical lenses were used to produce a light sheet of sufficient divergence and focus for the experiments. Digital images were captured with an 8bit TSI PowerView 4M CCD camera with a resolution of 2048^2 pixels and a maximum capture rate of 7.5

frames per second, giving 3.75 measurements per second in cross-correlation. Synchronisation of the laser pulses with the camera captures was achieved using a TSI LaserPulse computer controlled synchronizer. Best results were achieved by seeding the flow with hollow glass spheres of mean diameter 4μm, again from TSI, although a number of different particle types were used in the course of the investigation. Coagulation of the particles was prevented where necessary by thoroughly mixing the particles with water and a drop of surfactant (a detergent) prior to incorporation with the flow. The particles were allowed to mix thoroughly with the flow to ensure uniform seeding prior to beginning the experiments. Post processing and data reduction was performed using INSIGHT (TSI), MATLAB (The Mathworks Inc.) and TecPlot (AMTEC) software packages.

To achieve phase averaging, a system was set up whereby the PIV system could be triggered to capture at specific points in the oscillating cycle of the wing or dummy support. The trigger was in the form of a positive TTL pulse (a voltage of approximately 5V) sent from the software controlling the oscillating mechanism at the beginning of each cycle. The PIV software was then instructed to capture a set number of frames for each trigger, and then to wait until the next trigger.

2.5.4 Laser Sheet Visualisation

Preliminary cross-flow visualisation tests prior to development of the PIV system used a continuous emission laser to illuminate a plane of the seeded flow. The laser was a water cooled Coherent Innova70 12W Argon-Ion continuous emission unit. Light was transmitted to an optical head via a fibre-optic cable, and spherical and cylindrical lenses were used in combination to spread the beam into a suitable sheet. The optical head was placed under the tunnel, and directed upwards to illuminate a plane of the cross-flow. The digital video camera was placed in the downstream viewing window and focused on the particles passing through the light sheet. The particles used for these experiments were Polyamide seeding particles of 50μm mean diameter.

2.6 Chapter Review

This chapter has introduced and discussed the apparatus employed in this investigation, which is summarised for convenience here.

The water-tunnel facility at the University of Bath was used as the test bed for this research, as it enables vivid visualisations of the flows being studied. Simple delta wing models were used to generate vortices suitable for study in this environment, which were mounted upside-down to prevent unwanted interference between the mounting sting and the suction surface flow. Two sets of models were used, one set for flow visualisations that incorporated embedded dye tubes to transport the dye to the point of injection, and one set for force balance measurements that were designed to reduce pre-loading of the load cells. Vortex-support interactions were studied using a number of 'dummy' support structures, the positions of which were varied relative to the vortex trajectory. Five dummy supports were used, being cylindrical supports of diameter, d_r = 12 and 24mm, and flat-plates with stream-wise dimensions, d_p = 24, 48 and 96mm, and thickness, t = 2mm. The detailed apparatus involved in flow visualisation, force balance and PIV measurements, image capturing and laser sheet visualisation has also been discussed.

Having discussed the apparatus used in this investigation, the following chapter discusses the methodology employed in the use of this equipment. Also discussed is the manner in which data were processed and flow and analytical quantities derived.

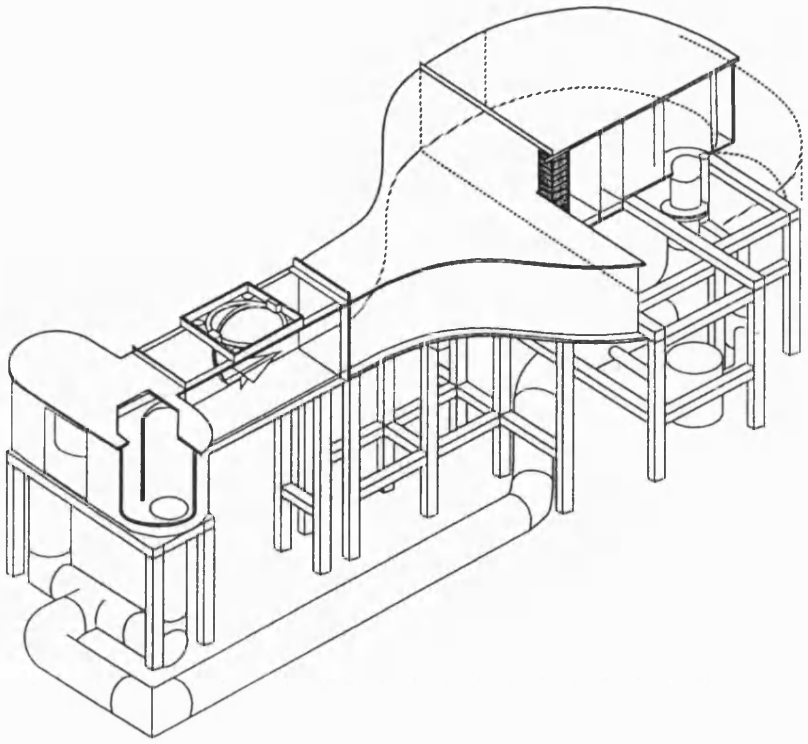

Figure 2.1: Eidetics model 1520 water-tunnel (Courtesy Eidetics Corporation).

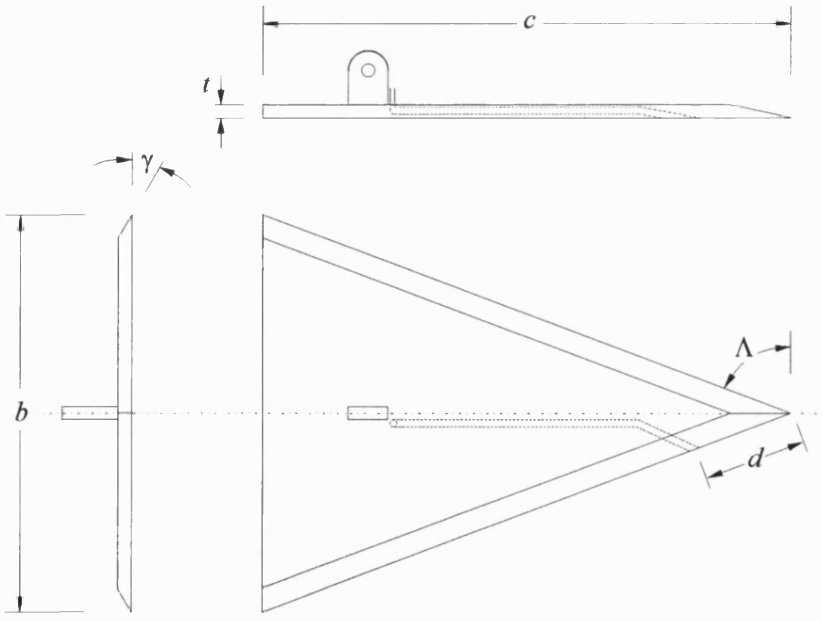

Figure 2.2: Simple delta wing model geometry and principal dimensions.

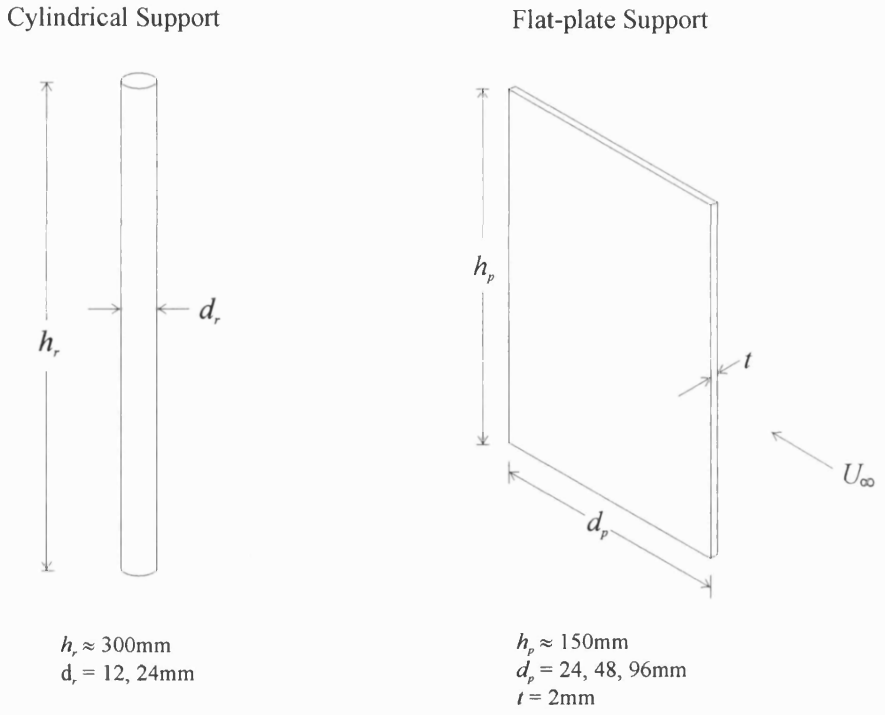

Figure 2.3: Dummy support principal dimensions (not to scale).

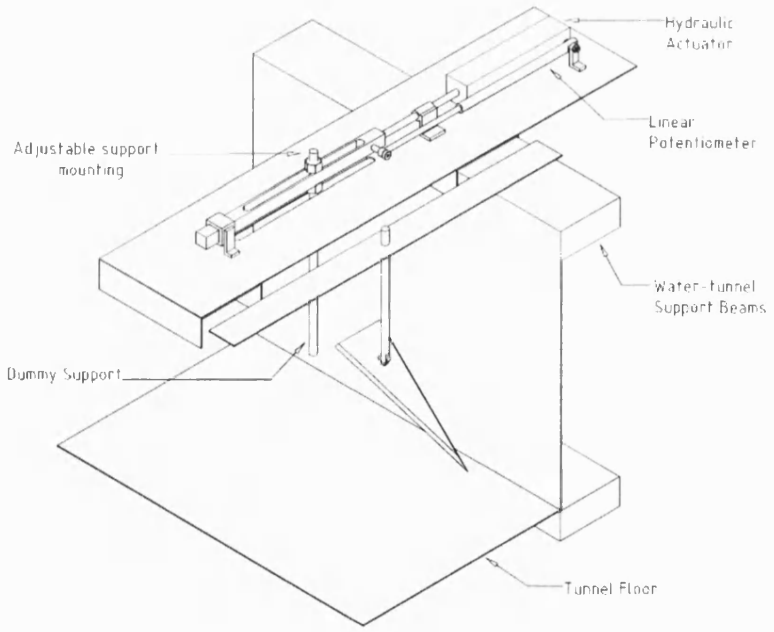

Figure 2.4: Schematic of oscillating mechanism used for dynamic testing.

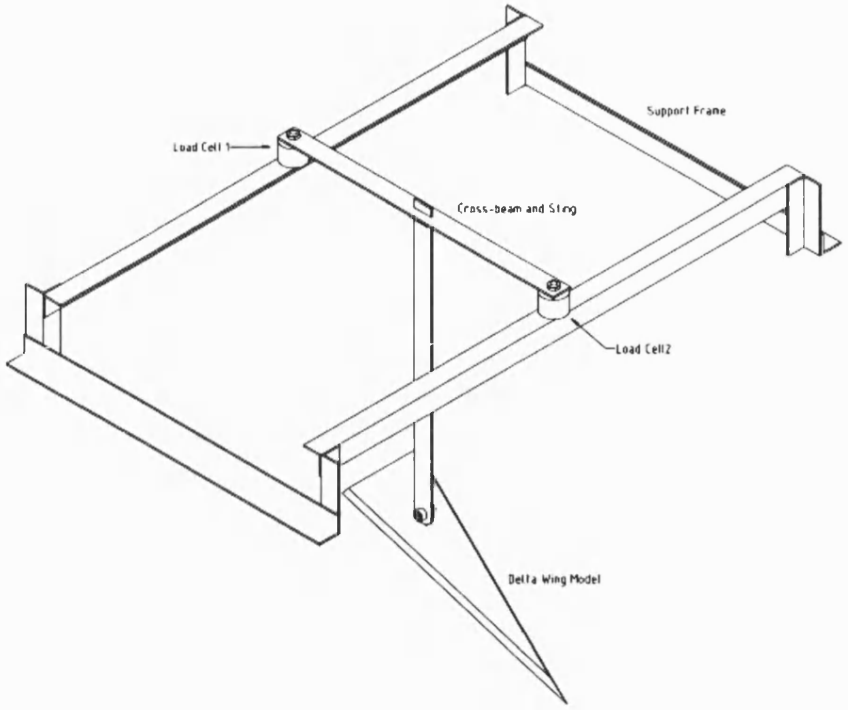

Figure 2.5: Force balance schematic.

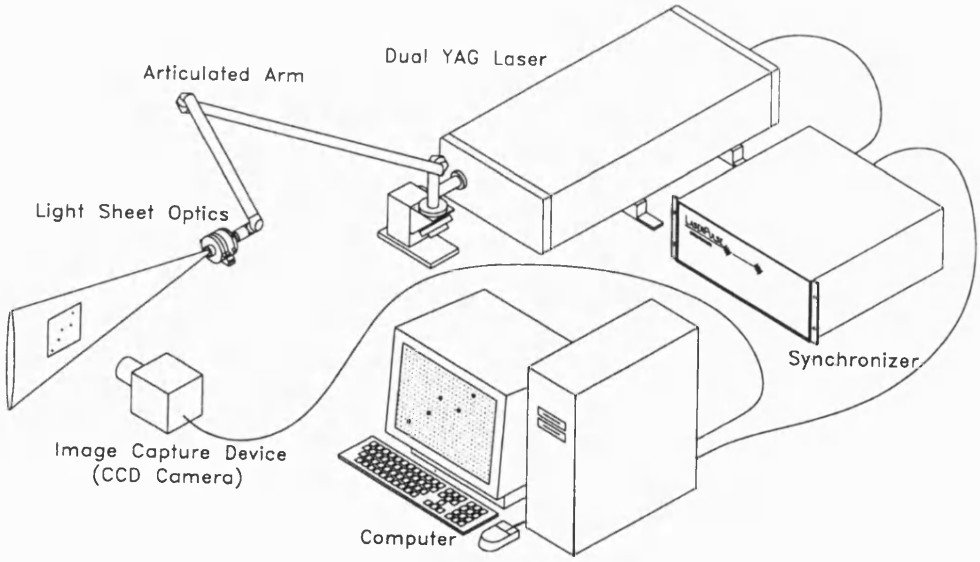

Figure 2.6: Schematic of PIV system and methodology (Courtesy BIRAL).

Chapter 3 Experimental Procedures

3.1 Introduction

This chapter introduces and discusses the methodology employed during the course of the investigation. Discussion begins with a brief summary of the experimental procedure undertaken, which is necessary in order to acquaint the reader with the general approach taken in tackling the support interference problem prior to discussion of the detailed experimental methodology employed that follows. A discussion of the validity of the data and quantification of the errors associated with the apparatus and methodology are then discussed, following which is a summary of the principal items covered in this chapter for the convenience of the reader.

3.2 Overview of Experimental Procedure

The methodology employed in static testing involved the use of a range of dummy support structures to simulate the effect of a strut-sting or 'c-strut' support placed downstream of a test model. Simple delta wing models were used to generate a vortical flow, and were mounted up-side down using a simple strut to avoid interference with the leading edge vortices. The effect of a number of parameters on the location of breakdown of the leading edge vortices was measured so that regions of particular sensitivity could be identified.

In dynamic testing (which includes both oscillatory and transient testing), the methodology was complicated by the realisation that dynamic motion of the wing

would result in vortices with a time-dependent vortex strength. Taking an oscillatory lateral wing motion as an example, the strength of the leading edge vortices is a function of the velocity of the wing at any point through its cycle. The windward leading edge experiences an increased effective sweep angle and the strength of the leading edge vortex is increased; the opposite is true of the leeward vortex. Thus, in such an experiment, breakdown of the leading edge vortices would be a function of both the state of the vortex and the degree of support interference. Two approaches to the investigation were therefore taken. Initially, to remove time-dependent vortex strength effects, the wing remained static while the dummy support oscillated in its wake. This approach was designed to separate vortex/support interactions from unsteady vortex flow effects, enabling a clearer picture of the interaction to be formed. To complete the study, the full moving wing case with a static support structure was investigated. By comparing data from the two approaches, the effects of vortex/support interactions and time-dependent vortex strength could be individually quantified.

Figure 3.1 shows the principal dimensions of interest in this investigation. The dimension x'_{BD} was defined as the distance between the apex of the wing and the location of the breakdown, measured in the plane of the wing rather than the horizontal. The principal variables in terms of support location were the lateral and streamwise coordinates of the dummy support. The lateral location of the support, defined as the spanwise distance between the undisturbed vortex core and the centreline of the dummy support, is labelled ε. The streamwise location, defined as the streamwise distance between the wing trailing edge and the leading edge of the dummy support, is labelled x_{LE}.

3.3 Data Acquisition and Analysis

3.3.1 Flow Visualisation and Vortex Breakdown Location

Food colouring diluted 1:4 with water was used to visualise the trajectory of the leading edge vortices. Since the water-tunnel is a closed loop flow system, build up of dye in the free stream was a problem as contrast between the visualised flow and the free stream was lost. Swimming pool chlorine was used to neutralise the dye to prevent significant build up of background dye, although the tunnel was emptied and refilled

with fresh water at intervals to prevent excessive build up of chlorine. It was found that although the best visualisations were achieved at very low speeds ($U_\infty < 15$ cm/s), it was possible to apply the technique throughout the range of water-tunnel velocities. Figure 3.2 shows the quality of the flow visualisations achieved at low speeds, and it was for this reason that all visualisation experiments were conducted at a free-stream velocity of U_∞ = 10cm/s. Light from a flood lamp placed behind the water-tunnel was diffused using a large sheet of plain white paper. By careful arrangement of the light source and camera, the model may be silhouetted while the vortex visualisation remains very clear. The technique of dye injection ensured that dye was entrained into the vortex, but the exit of the dye was perpendicular to the flow itself due to the size of the models constraining their design. To ensure the dye injection process did not affect the formation of the vortices over the leading edges, the exit velocity was carefully controlled (Goldstein, 1983). The location of the breakdown is defined as the location at which the vortex core undergoes a rapid expansion. It was often possible to identify the front of the flow reversal region inside the breakdown, and this proved a useful reference point in determining the breakdown location.

For each case the visualisation image was recorded for a period of time and either stored on camera or simultaneously downloaded to a desktop PC. Examination of the video files at a later date allowed individual frames to be identified, which were then captured as still images and saved using the Pinnacle Studio software. For dynamic tests where a series of captures was required at constant time intervals, MATLAB .m-files were written to automate the capturing process. Vortex visualisations were recorded either from the side or from below the model, depending on the type of test. For dynamic tests where it was important to capture the movement of either the wing or support in addition to the breakdown location, the camera was placed below the tunnel. For most static tests the camera was mounted beside the tunnel, as the overall quality of the images produced was better.

In the majority of cases the visualised vortex was on the port side of the model as it sits in the water-tunnel. For dynamic testing, the visualised vortex was on the windward side of the wing as it began its motion. In cross-flow visualisation and PIV

measurements, reference will be made to the 'left' and 'right' vortices, these being the vortices on the left and right of the inverted model as viewed from the rear.

3.3.2 Control of Wing or Dummy Support in Dynamic Testing

In dynamic testing the distance between the undisturbed vortex core location and the dummy support, ε, was varied in a sinusoidal manner using the oscillating mechanism illustrated in Figure 2.4. Figure 3.3 shows the form of, and principal dimensions relevant to, the dynamic testing. The motion of the support or wing may be described by the equation:

$$\frac{\varepsilon}{b} = \frac{\varepsilon_0}{b} + \frac{\varepsilon_1}{b}\cos\omega t = \frac{\varepsilon_0}{b} + \frac{\varepsilon_1}{b}\cos 2\pi f_e t$$

It was possible to control the amplitude, ε_1/b, the mean location, ε_0/b, and the frequency, f_e, of the oscillating motion remotely from the PC. The offsets and amplitudes of the motions were chosen based on results from static experiments defining the regions in which the vortices were particularly sensitive to the location of the dummy support structures, and will be discussed fully in subsequent chapters. The forcing frequencies of the motions were chosen to represent the actual testing regimes of aircraft configurations undertaken in air where possible. Testing undertaken at the wind-tunnel facility at the former DERA (Bedford) used reduced pitching frequencies of the order of $f_e c/U_\infty = 0.1$ (Greenwell, 1998). Therefore, frequencies in the range $0.015 < f_e c/U_\infty < 0.5$ were studied to give a full appreciation of the breakdown response over a wide range of frequencies.

3.3.3 Force Balance Measurements

Force balance tests were conducted at a higher free stream velocity (U_∞ = 30cm/s) than flow visualisation tests (U_∞ = 10cm/s) to provide sufficient measurable force. The length of the data record was dependent on the type of test. Typically for static tests, data were sampled at 50Hz for a period of 10s, giving 500 data points. Dynamically the sample frequency, f_s, was adjusted to give at least 40 samples per cycle. Each force balance measurement required a recalibration of the load cells to remove the effects of

pre-loading of the cells due to the weight of the components. Calibration of the cells was performed by recording the signal from the cells with zero free-stream velocity. It was often necessary to wait 10-15 minutes before transients in the tunnel had died down sufficiently following switching off the tunnel to record the calibration data. During tests the force acting on each cell was found by first subtracting the calibration result from the voltage signal from the cell, and then dividing by the cell sensitivity as provided by the manufacturer, thus:

$$F_{celli} = \frac{(S_{celli} - S_{calib})}{K_i}$$

Where, for cells i = 1 or 2, F_{celli} is the force measured by cell i, S_{celli} is an array containing the signal (in volts) from cell i, S_{calib} is the calibration result and K_i is the calibration factor. From manufacturer's data: $K_1 = 0.077$, and $K_2 = 0.08$. The lift force coefficient could then be found by summing the forces measured by each cell:

$$C_L = \sum_{i=1}^{2} \frac{F_{celli}}{\frac{1}{2}\rho U_\infty^2 S}$$

During post-processing it was found that the signal recorded from the cells, S_{celli}, contained a significant proportion of noise. The source, it was discovered, was RF noise generated by the operation of the water-tunnel pump, which made it impossible to remove the noise at its source. Although the amount of noise could be reduced by careful arrangement of the electronic components comprising the data acquisition system, it was not possible to eliminate the noise entirely. The presence of noise in the signals meant that static and dynamic tests required different post-processing. In static tests only one time-averaged value of force was required for each test. The simplest method of removing the noise was therefore to average it out. Since the noise was intermittent and generally resulted in peaks above the apparent average, the most suitable averaging method was to take the median of the data.

In dynamic testing the required end result was a time-history of lift force which could be compared with the dummy support location. Averaging of the data was therefore not

a suitable method for removing the noise. Since the noise was at a higher frequency to the excitation frequencies to be studied, it was possible to apply a low-pass filter to the signal from each of the load cells to remove the noise. Filtering of the lift force under dynamic conditions was necessary only to yield a visual indication of the lift force response, i.e. no quantitative data were taken from the filtered force data. The unfiltered lift force was used in calculating the cross-spectra and phase lags. Filtering was implemented where necessary by applying a fifth-order elliptical low-pass filter with a pass frequency of twice the frequency of the support oscillations. Filtering was applied in both directions to ensure that the phase of the signal was not affected. This was achieved using the `FILTFILT` command in MATLAB. The mean values of the signals were found to be unaffected by the filtering process; RMS lift force magnitude was reduced while maintaining trends observed prior to filtering.

3.3.4 PIV Data

All PIV data were gathered using INSIGHT (TSI) software, which not only controlled the setup of the system and allowed capture of the PIV images, it also performed analysis of the images. Analysis of the images was performed using the Hart cross-correlation algorithm provided with the software. The cross-correlation (CC) technique is the most popular method for determining particle displacements in PIV, as it removes the directional ambiguity inherent in auto-correlation (AC) and particle-tracking (PT). Traditionally, FFT CC algorithms have been used, which compare the locations of particles in image pairs in a single pass to yield a correlation map with the dominant peak relating to the most likely mean displacement of the particles in the interrogation window. However, background noise can be large due to particles which enter or leave the window between the two images. The Hart technique improves on the conventional FFT algorithms by reducing the interrogation spot size to improve spatial resolution by a factor of two. In addition, a dual pass scheme allows the second pass to take account of particles moving out of the frame of interest by shifting the interrogation window by the average displacement calculated in the first pass. A detailed account of the Hart technique is given by Hart (1998). In the current investigation the algorithm was used with a 32 by 32 pixel grid, and an equally sized sub-grid. Approximately 2500 vectors were calculated for each field. Spurious velocity vectors were removed using a

validation macro, and removed vectors were replaced with vectors interpolated from the surrounding field.

For the majority of the PIV tests, phase averaging was performed over ten cycles using the triggering system described above. Where time averaging is used, averaging was performed over 30 frames at a capture rate of 15 frames/sec, giving 7.5 measurements per second in CC. The cross-flow plane measured was in all cases orthogonal to the free stream.

3.3.5 Calculation of Flow Quantities

Circulation and vorticity are closely related quantities that have great significance in aeronautics, and are commonly used in the analysis of rotating flows such as vortices. Vorticity, denoted by ξ in most text books, is a measure of the angular velocity of an element of the fluid and is simply twice the angular velocity of the element:

$$\xi = 2\omega$$

Where ω is the angular velocity of the fluid. Vorticity is a useful measure of the amount of rotation undertaken by a fluid. In an *irrotational* flow, one where vorticity is zero, the motion of elements of the flow are purely translational, i.e. the elements undergo no rotation. However, in a *rotational* flow, the motion of the elements contain a proportion of rotation, and it is the rate of this rotation that defines the vorticity. While vorticity is certainly a useful measure, its evaluation from PIV data requires the differentiation of the velocity field, since the angular velocity is given by:

$$\omega = \frac{1}{2}\left[\left(\frac{\partial w}{\partial y} - \frac{\partial v}{\partial z}\right)\mathbf{i} + \left(\frac{\partial u}{\partial z} - \frac{\partial w}{\partial x}\right)\mathbf{j} + \left(\frac{\partial v}{\partial x} - \frac{\partial u}{\partial y}\right)\mathbf{k}\right]$$

Where **i**, **j** and **k** are unit vectors in the x, y, and z directions respectively. It is often difficult to obtain 'perfect' PIV data, and the velocity field is rarely devoid of a random element. This makes calculation of vorticity problematic as the noise contained by the vector field is magnified by the differentiation. A better quantity, therefore, is the

circulation, which is simply the integral of the vorticity contained by a closed loop. However, although related to vorticity, the measurement of circulation may be performed without using vorticity in the calculation, which removes the noise problem. Circulation, denoted by Γ, is given by:

$$\Gamma = -\oint_C v_t ds$$

Which may be described as the integral around the closed curve C of the velocity tangential to the curve, v_t. Circulation is therefore the more useful quantity as it relies entirely on the velocity field, not derivatives thereof, and the selection of the closed curve, C. When discussing the strength of a vortex one is most commonly referring to its circulation, although both quantities may be accurately used.

In this investigation both circulation and vorticity are discussed. Vorticity in a flow was calculated using a Tecplot macro provided by TSI. The circulation was evaluated using a MATLAB macro written by the author for the purpose. The tangential component of velocity around a square path centred on the vortex core was integrated for different sizes of integration square. Inputs to the macro were the velocity field of the cross-flow plane, the centre of the integration square (the centre of the vortex) and the half length of the side of the integration square, *h*. Given this information, the macro calculated the circulation within the square, which was then non-dimensionalised by (cU_∞). The errors associated with the evaluation of circulation are discussed below.

3.3.6 Statistical Methods

The Root-Mean-Square (RMS) value of a variable is a useful parameter as it gives an indication of the magnitude of fluctuations of a variable about its mean. The RMS values of C_L and x'_{BD}/c have been calculated at various points in this thesis using the following equation:

$$p_{RMS} = \sqrt{\frac{\sum_{n=1}^{N}(p_n - \bar{p})^2}{N}}$$

Where p is the parameter under scrutiny, and N is the number of values of p.

While the RMS value gives an indication of the variance of a quantity, some knowledge of the frequency components of the fluctuations is often required, and this information is not contained in the RMS value. For this, the Power Spectral Density (PSD) of a parameter history is often used. The PSD is defined as the Fourier Transform of the auto-correlation sequence of the time series, the units of which are power per unit frequency. However, the PSD parameter was not evaluated in this investigation as it gives an indication of the frequency component of only a single parameter. Rather, it was the Cross-Spectral Density (CSD) which was of more use, since it compares the frequency components of two separate signals, giving a spectral peak at those frequencies which are contained in both signals. The CSD, $S_{xy}(\omega)$, is the Fourier Transform of the cross-correlation function, and was evaluated using the following expression:

$$S_{xy}(\omega) = \int_{-\infty}^{+\infty} R_{xy}(\tau) e^{-j\omega\tau} d\tau$$

Where $R_{xy}(\tau)$ is the cross-correlation function, which may itself be evaluated using:

$$R_{xy}(\tau) = \lim_{T\to\infty} \frac{1}{2T} \int_{-T}^{+T} x(t-\tau) y(t) dt$$

One advantage of the CSD function is that it also yields the phase delay between the two signals at a given frequency. Thus, given a dominant spectral peak, the phase delay between the two signals at this dominant frequency can be evaluated. Determination of the phase delay involves a simple manipulation of the real and imaginary components of the CSD function at a given frequency. All CSD calculations, including estimations of the phase delay, were performed using MATLAB software.

3.4 Data Quality and Validation

3.4.1 Delta wing models

All the wing models, regardless of the type of test being undertaken, were mounted upside-down in the tunnel using a strut attached to the pressure surface. While mounting the models in this manner allows the undisturbed formation of the leading edge vortices on the suction surface, any support structure has an interference effect. In this case vortex shedding aft of the supporting structure will interfere with the wake of the model along its centre-line. In force balance measurements, the effect was reduced because a streamlined support was used, but in all other tests the strut was of circular cross-section. These effects are expected to be small and have not been accounted for.

It was necessary to replace the test models at intervals due to wear and tear. Although every care was taken to ensure consistency between the successive models, Lowson and Riley (1995) showed that the detailed geometry of the wing, particularly near the apex, is of particular importance in determining the breakdown location over a delta wing. Minute changes in wing geometries may explain the spread in published data relating to breakdown locations on wings of similar sweep.

The models used for lift force measurements differed from those used in flow visualisation experiments. The force balance models were fabricated from PVC to reduce the pre-load of the balance, but this material was difficult to machine into a consistent sharp leading edge, which may lead to inconsistencies between the flow visualisation and force balance results.

The greatest error in this investigation was undoubtedly the measurement of the angle of attack of the test model. The accuracy of the angle of attack measurements is estimated to be of the order of $\pm$ 1° at best.

3.4.2 Vortex Breakdown Location

When testing in water it is important to consider whether or not the data obtained may be readily extrapolated to air. In the case of water-tunnel flow, Reynolds numbers are significantly lower than in air, so for similarity with air the flow must be insensitive to

Reynolds number changes. Providing the leading edges are sharp, the formation of leading edge vortices over a delta wing may be considered Reynolds number insensitive (Erickson, 1982; Lowson, 1991; Lowson and Riley, 1995). Lambourne and Bryer (1961) first identified the insensitivity of vortex breakdown location to Reynolds number changes. A more recent study by Traub *et al* (1998) has extended this survey to include the Reynolds number insensitivity of lift and pressure coefficients, span-wise vortex trajectories, and surface flow patterns over 60° and 70° delta wings. Figure 3.4 shows a comparison between wind and water-tunnel visualisations of vortices developed by the wings of a generic delta wing fighter. The two images show very good agreement in terms of the breakdown locations of the leading edge vortices. It is therefore reasonable to expect water-tunnel investigations of a simple flat-plate delta wing configuration to be representative of air, provided the leading edges are kept sharp.

The measurement uncertainty of the breakdown location from a single image was approximately 0.01c. The time averaged breakdown location, in the static tests, was estimated from long records of the breakdown location. In some cases the breakdown locations were analysed frame by frame to obtain the time-history, allowing the RMS value of the breakdown fluctuations to be determined. A typical value of RMS breakdown location was $(x'_{BD}/c)_{RMS} \approx 0.035$ which is in close agreement with previous studies (Xie, 1998; Menke *et al*, 1999).

The natural breakdown location over each of the wings was validated by undertaking a comparison with published data. The review of Gursul (1995) shows that there is a large scatter in the natural breakdown location recorded by different investigators, and that the greatest scatter is in the region of the trailing edge. In this study, the data for $\Lambda = 70°$ and 75° are near the lower end of the reported range, whereas the data for $\Lambda = 80°$ and 85° are near the middle of the range.

3.4.3 Force Balance Measurements

Uncertainty in the force balance measurements was calculated using the Kline-McClintock method for analysing error propagation (Kline and McClintock, 1953).

Using this method, the effects of a number of sources of error may be combined to give the uncertainty in the result. If the output variable, R is a linear function of n independent variables: v_1, v_2, ..., v_n, then the total uncertainty in W, W_r may be expressed as:

$$W_r = \sqrt{\left(\frac{\partial R}{\partial v_1} w_1\right)^2 + \left(\frac{\partial R}{\partial v_2} w_2\right)^2 + \ldots + \left(\frac{\partial R}{\partial v_n} w_n\right)^2}$$

In order to analyse the lift force uncertainty properly, the individual sources of error must be identified and quantified. The forces measured in this investigation will be expressed non-dimensionally in terms of C_L, and the individual sources of uncertainty therefore include: the quantisation error associated with the data acquisition process; the linearity of the load cells; and the uncertainty in the free stream velocity. Applying the above equation yields:

$$W_r = \sqrt{\left(\frac{\partial C_L}{\partial L}\Delta L_{Q1}\right)^2 + \left(\frac{\partial C_L}{\partial L}\Delta L_{Q2}\right)^2 + \left(\frac{\partial C_L}{\partial L}\Delta L_{NR1}\right)^2 + \left(\frac{\partial C_L}{\partial L}\Delta L_{NR2}\right)^2 + \left(\frac{\partial C_L}{\partial U_\infty}\Delta U_\infty\right)^2}$$

Where ΔL_{Qi} is the uncertainty in load due to the quantisation error from cell *i*, ΔL_{NRi} is the uncertainty due to the non-repeatability of load cell *i*, and ΔU_∞ is the uncertainty of the freestream velocity.

Output from the load cells was in the form of a voltage proportional to the applied load. The signal from the cells was processed by a desktop PC via a Data Translation DT3001 data acquisition card, and HP-VEE software. The acquisition card was capable of descretising the input voltage into 4096 bits. The voltage range, set by the software was ±10V, and it was therefore possible to resolve the voltage from the load cells to an accuracy of $\pm$ 4.8828 x 10^{-3} V. Converting this into a lift force for each of the load cells (recalling that each cell has a different calibration factor, and the quantisation error will therefore not be the same), yields: ΔL_{Q1} = 6.2208 x 10^{-4} N; ΔL_{Q2} = 5.9875 x 10^{-4} N. Non-repeatability of the load cells is given by the manufacturer as $\pm$ 0.1% of the full scale deflection, which relates to an error of ΔL_{NR} = 2.453 x 10^{-3} N. The free stream

velocity can be controlled to an accuracy of approximately $\Delta U_\infty = 0.088$ cm/s, based on a prior calibration of the tunnel.

Figure 3.5 shows the uncertainty of the lift force measurement as a function of the lift coefficient based on the individual errors evaluated above. It can be seen that the error tends to a value of 0.59% as the lift force increases, but that the lower the lift the greater the percentage error, as is to be expected. For the range of lift forces considered in this investigation, $W_R \approx 1.0\%$.

To further validate the force balance, the lift-curve slope of a $\Lambda = 70°$ wing was measured using the current apparatus and the results were compared to existing data in literature. The results, shown in Figure 3.6, show that the force balance captures the lift curve slope and stall angle well. Additionally, the data lies in the middle of the spread of data presented in literature. It may therefore be concluded that the overall accuracy of the force balance is good.

Lift force measurements undertaken in oscillatory testing were subjected to a further form of error. Due to the sampling of high frequency noise originating from the water-tunnel pump some filtering of the lift force data was necessary. The filter took the form of a fifth-order elliptical low-pass filter using a cut-off frequency of twice the frequency of the support oscillations. While it was recognised that it is usual to implement a cut-off frequency of around 5 to 10 times the frequency of interest, in this case the filtering was only performed to give a visual indication of the response of the lift generated by the wing. All the quantities derived from the force measurements were calculated from the raw, unfiltered data on the basis that the noise was random and would therefore not bias the result significantly.

3.4.4 Oscillating Mechanism Control

The oscillating mechanism was positioned using a closed loop system controlled by a desktop PC. A potentiometer attached to the oscillating arm provided the feedback for the system, the output from which was downloaded to the PC via a Data Translation DT21EZ data acquisition card. Descretisation errors in the data acquisition card mean a

minimum measurable distance of 7.0 x 10^{-3}cm. Thus the error in the positioning of the oscillating arm may be considered to be negligible.

Experience with the oscillating mechanism showed that the maximum operating frequency of the mechanism was $f_{max} \approx 0.5$Hz, and was attributed to the hydraulic motor being undersized. At frequencies above this, the amplitude of the motion was significantly reduced. As such the maximum test frequency for this research was $f_{max} = 0.2$Hz.

3.4.5 PIV

There are many potential sources of error in PIV measurements, although the majority of these can be reduced or eliminated by optimising the experimental setup. Potential sources of uncertainty may include particle size, interrogation window size compared to the magnitude of local velocity gradients, number of particle pairs in the interrogation window, quantisation errors, and computational errors (i.e. rounding and truncation errors).

The spatial resolution of the technique is limited by the amount of seeding particles there are in the flow, as there is an optimum number of particles pairs per interrogation window (of the order of 3 pairs/window). Provided there are at least this number of particle pairs, window size does not directly affect accuracy where there are small velocity gradients (Willert and Gharib, 1991). Since the vector placed on a window is equal to the average velocity of the particles within the window, high velocity gradients can only be dealt with by improving spatial resolution.

In vortex flows it is often difficult to take measurements near the vortex core as high swirl velocities centrifugally displace particles, reducing the seeding density in the core. In regions where reflections from models interfere with the particle field it is also difficult to obtain reliable measurements. This occurs near the surface of wings and can be reduced by careful preparation and arrangement of the model and illumination. Areas like these often end up producing spurious velocity vectors which are ultimately eliminated by the validation algorithm. However, this leaves regions where no velocities have been calculated, and to complete the vector field interpolation of

surrounding velocity vectors is necessary. This leads to a further source of error as in any vector field there will be a certain amount of estimated vectors. In this investigation, light reflecting from the model surfaces were a particular problem, and velocities near the wing surface have therefore been interpolated. While this is obvious in some cases due to the velocity vectors apparently passing through solid boundaries (i.e. the wing surface), it does not affect the overall quality of these results as it is the location of the vortex cores and the peak velocities and vorticity that are of interest; the region near the wing is only of secondary interest.

Thorough analyses of errors involved in PIV measurements can be found in Willert and Gharib (1991) and Hart (1998), and the overall uncertainty of the method may be expected to be of the order of 1–5%.

3.4.6 Flow Quantities

As mentioned previously, there is an inherent error associated with the calculation of vorticity. Since its calculation relies on differentiating the velocity field, errors in the velocity field will propagate in the vorticity calculation, resulting in a field with a significant amount of noise. In these tests, this error was reduced by only calculating the vorticity for velocity fields averaged by at least 10 frames. However, it was felt that circulation could be calculated with more confidence, and little analysis of vorticity has therefore been used.

The calculation of circulation was performed using a macro written by the author. A significant factor in determining the error in the calculations is the size of the integration square. For a very small integration square, the value of the circulation will tend to zero. As the size of the square increases, the value of circulation increases rapidly at first, then reaches a plateau, following which further increasing the square size will result in no significant change in the value of circulation calculated. However, by increasing the size of the square too high, the integration square encroaches on the opposite vortex, and will include these velocities in its calculation. The result is that the value of circulation will then decrease. The size of the integration square is therefore critical in ensuring the circulation is evaluated accurately. In all of the cases presented

herein, circulation was calculated for a range of values of h, the half side length of the integration square, and the most suitable value of h was then selected.

In terms of the accuracy of the code in evaluating the circulation, the main error was in selecting those vectors associated with an integration square of a given size. Since velocity vectors were provided at discrete points, a given value of h is unlikely to correspond exactly to a row of vectors. In this case, the nearest row of vectors was taken. The maximum error in h in this case is estimated to be of the order of 6.7% at h/b = 0.227. However, the error in h does not affect the calculation of the circulation; merely the dimensions of the square around which it is calculated. A further error associated with the calculation of circulation itself comes from the use of the trapezoidal method of numerically integrating the velocities around the integration square. This method was used due to its simplicity and ease of application, although it is recognised that the error associated with this method may have been reduced by applying alternative numerical integration schemes, such as Simpson's rule.

3.5 Chapter Review

This chapter has discussed the procedures and methodology employed in the course of this investigation, has validated data where necessary, and has attempted to evaluate the principal errors associated with the methodology used herein.

In terms of the underlying methodology, it has been shown how a dummy support placed downstream of the model was used to simulate the effect of a c-strut or strut-sting support. In the static case, the location and geometry of the dummy support was varied in order to determine those regions in which support interference may or may not be a problem. In dynamic testing, time-dependent vortex strength effects were separated from the vortex support interaction by considering a moving support in addition to the more realistic moving wing case.

It was concluded that the most significant error is in the selection and measurement of the angle of attack, the accuracy of which was estimated to be $\pm 1°$. The accuracy of the

breakdown location calculations was estimated as approximately 0.01c. Other sources of error were considered to be small.

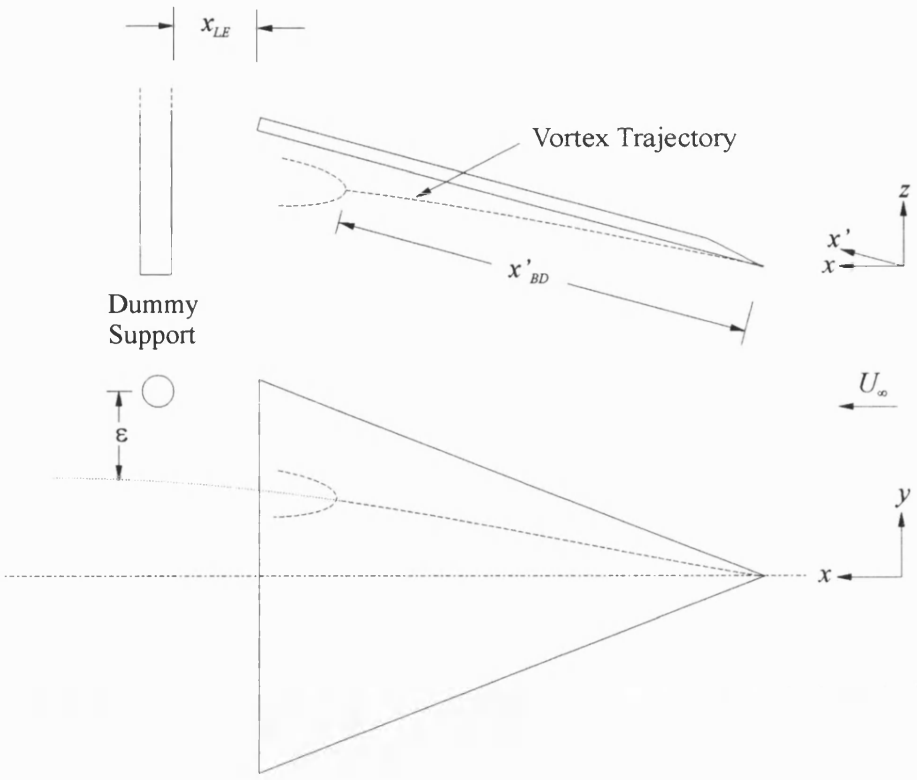

Figure 3.1: Experimental set-up and principal dimensions.

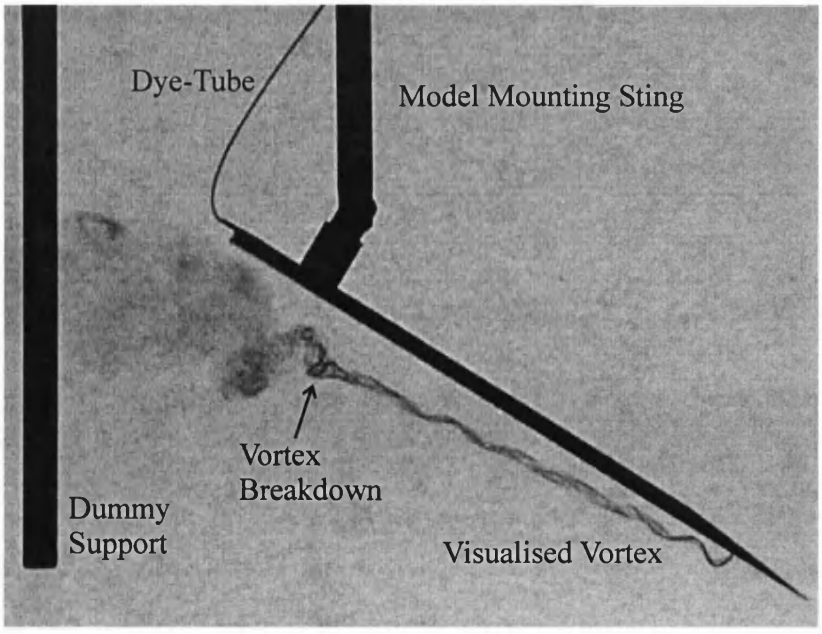

Figure 3.2: Example flow visualisation image.

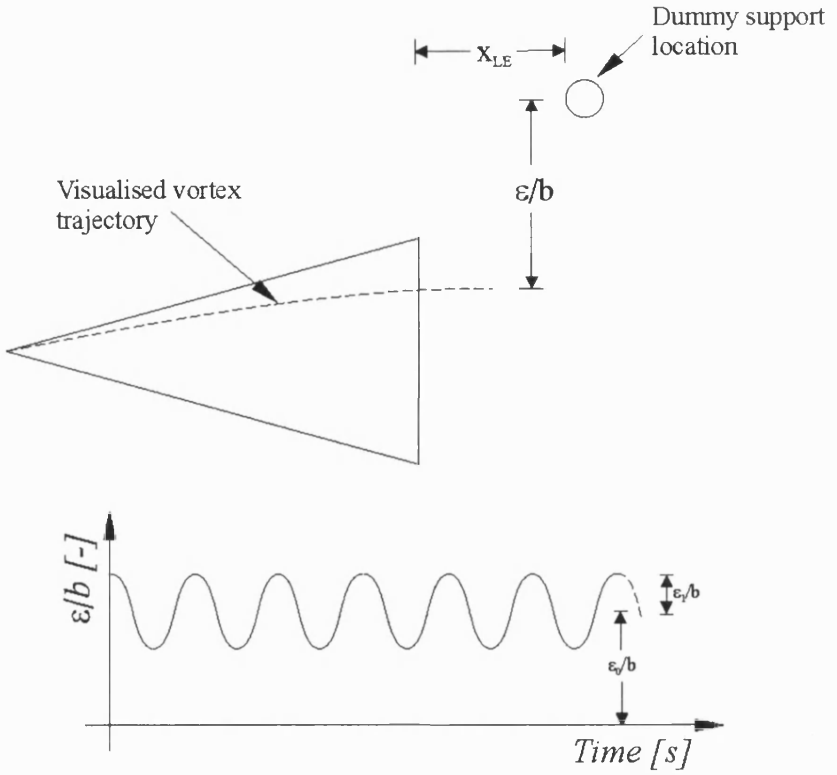

Figure 3.3: Definition of ε/b and its variation during dynamic testing.

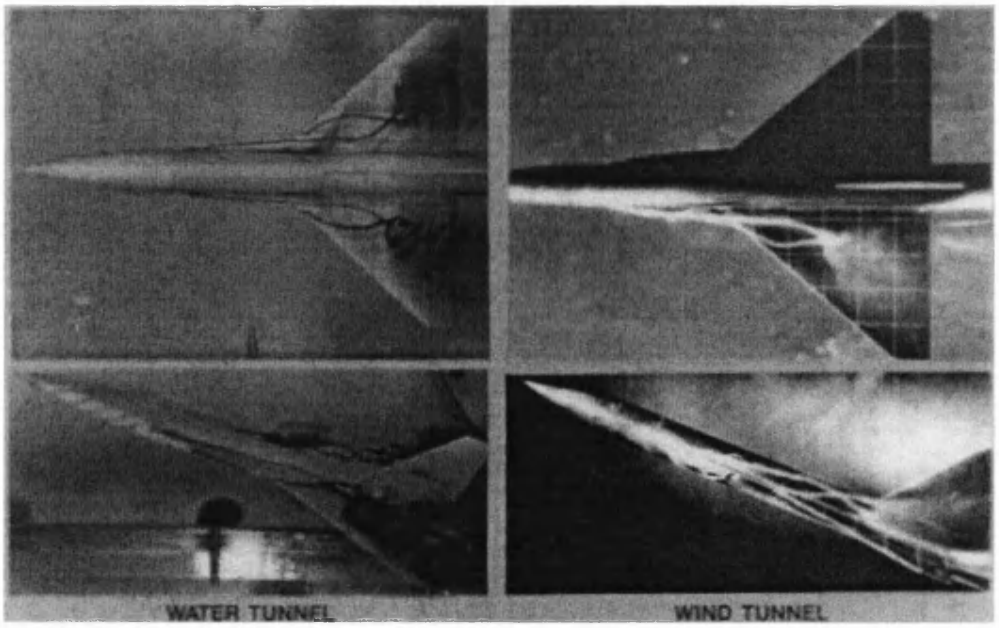

Figure 3.4: Comparison of visualisation studies (Goldstein, 1983).

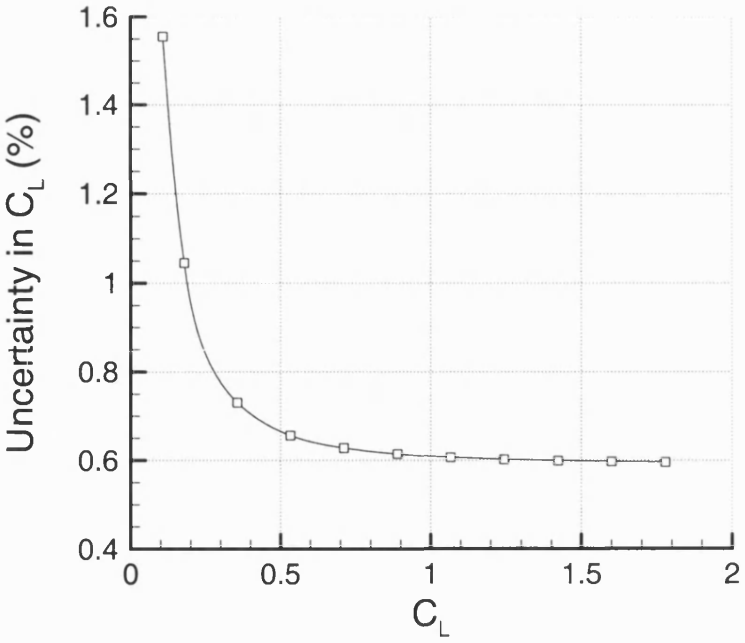

Figure 3.5: Uncertainty in lift force measurements.

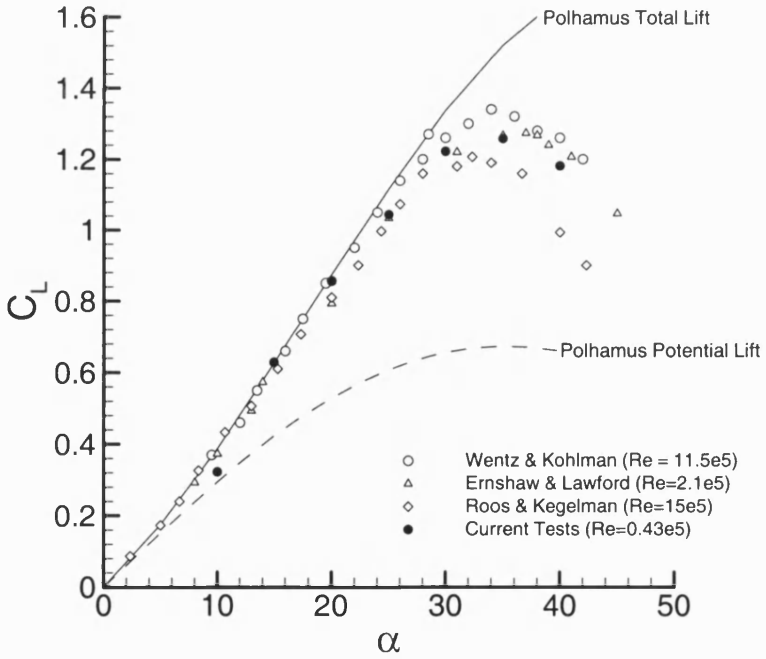

Figure 3.6: Comparison of C_L for $\Lambda = 70°$ delta with data from literature.

Chapter 4 Support Interference in Static Testing

4.1 Introduction

The aim of this chapter is to describe the effect of support interference in static testing. Following a definition of the terminology to be used herein, the chapter begins with an overview of the general breakdown response to acquaint the reader with the dominant characteristics of the flow. Focus is then moved to the documentation of the undisturbed flow for a specific case so that these data may be referred to at a later point in the chapter. Following this, the results of a parametric study into the effects of a range of parameters that affect the severity of the vortex-support interaction are presented. Finally the principal findings and conclusions are reviewed for convenience.

The parameters investigated in this study may be split into two groups and considered separately. First, there are those parameters that directly affect the formation of the leading edge vortices, which will be termed *flow parameters*. Flow parameters considered were the orientation (incidence and sideslip), and geometry (sweep) of the model wing. These parameters are important as they affect the strength of the leading edge vortices, which in turn has a significant effect on breakdown location. Secondly, there are those parameters that impose boundary conditions on the flow, which will be termed *boundary condition parameters*. Boundary condition parameters considered were the geometry (cross-section and dimensions) and location of the support structures. These parameters are important as they introduce an adverse pressure gradient. Although it is known that pressure gradients have a significant effect on the occurrence or otherwise of vortex breakdown (Lambourne and Bryer, 1961 and

Lowson, 1964), quantitative knowledge of the interactions between the pressure gradient and the vortex breakdown location do not exist in literature.

As discussed in Chapter 2, the procedure for this investigation involved the use of a range of 'dummy' support structures that were placed downstream of the wing models with a lateral offset, ε, from the vortex core. This approach, first used by Johnson *et al* (1980), is useful as it allows the study of many different types of support structure without the need for manufacturing full scale support rigs for each configuration. Five dummy support structures are used, being cylindrical supports of circular cross section and diameter d_r = 12 and 24mm, and flat-plate support with thickness, t = 2mm, and streamwise length, d_p = 24, 48 and 96mm.

Before presenting the detailed results, it is useful to demonstrate the overall form of the breakdown response. Figure 4.1 shows how a leading edge vortex responds to the presence of a dummy support of circular cross-section and diameter, d_r = 12mm, placed at x_{LE} = c/4, for angles of attack, α = 20°, 25° and 30°. The free-stream velocity was U_∞ = 0.1 m/s, corresponding to Re_c = 25,000, and the 80° wing was used. Figure 4.1 demonstrates that although the vortex was unbroken in the natural case in this range of incidences, the effect of the support structure was to promote breakdown in all cases. The figure also clearly demonstrates that the magnitude of the interference was dependent on the incidence of the wing, and therefore on the strength, or condition, of the vortices.

4.2 Documentation of the Flow

4.2.1 PIV Measurements

The properties of the undisturbed flow were documented using Particle Image Velocimetry (PIV). Documentation of the cross-flow velocity field was undertaken at four streamwise locations, corresponding to x_{LE} = c, c/2 and c/4, and a further location being at the trailing edge, x_{LE} = 0. Figure 4.2 shows the time-averaged cross-flow velocity field measured at each of these streamwise locations. The vortex pair were

symmetric about the centre-line at each stream-wise location, and were seen to expand and separate slightly with streamwise distance downstream of the trailing edge. No evidence of breakdown was observed for this configuration within one chord length of the trailing edge.

The variation of normalised horizontal component of velocity with vertical distance from the vortex core is shown in Figure 4.3, for the left and right vortices at each of the streamwise stations. Velocity profiles at the trailing edge exhibited asymmetries due to the presence of the wing surface, with velocities close to the wing having a larger magnitude than those on the opposite side of the vortex core. These asymmetries more or less disappeared at one-quarter chord length downstream of the trailing edge. The maximum swirl velocity reached $1.2U_\infty$ at the trailing edge near the wing surface, but decreased with increasing streamwise distance. By comparing the velocity profiles shown in Figure 4.3, it can be seen that in this experiment the radius of the left vortex was in fact larger than that of the right, based on the location of maximum swirl velocity. The core radius of both vortices increased with downstream distance as a result of viscous dissipation. Towards the wing surface (positive z/b), swirl velocities at the trailing edge ($x_{LE} = 0$) did not tend to zero, as the boundary condition imposed by the presence of the wing constrained the flow. Even at stations further downstream, the magnitude of the swirl velocities seemed to be greater on this side of the vortex. On the negative z/b side of the vortex, swirl velocities tended to zero quickly.

Figure 4.4 shows the variation of the normalised vertical component of velocity with horizontal distance from the vortex core. A reduction in peak velocities with downstream distance from the trailing edge was observed, with peak swirl velocities in this orientation as high as $1.6U_\infty$. The time-averaged separation of the vortices did not change with downstream distance aft of the trailing edge. At the trailing edge, peak velocities were significantly higher than at stations further downstream, with peak velocities at $x_{LE} \geq c/4$ being approximately equal. The velocities between the vortices were much higher than those on the outside of the vortices due to the combined effect of the two vortices on the flow in this region. At $x_{LE} = 0$, peak swirl velocities were as much as 3 times greater on the inside of the vortex compared to the outside.

The strength of left vortex at each of the test locations is shown in Figure 4.5, which shows the variation of the circulation measured around a square path centred on the vortex centre as a function of the size of the square. As the size of the square increased the circulation contained by the square increased, levelling off at a half side length of around h/b = 0.25; further increasing the square size had no effect on the measured circulation. Table 4.1 shows how the strength of the vortices varied during their progression downstream. The maximum value of circulation at the trailing edge, Γ/cU_∞ = 0.401, was approximately twice that observed at x/c = 0.5 on a similar wing by Visser and Nelson (1993), implying that at the trailing edge the measured circulations would be comparable due to the linear increase of circulation along the length of the wing. The strength of the vortex diminished significantly within the first quarter chord length downstream of the trailing edge, but at locations further downstream the measured circulation was comparable. This shows that viscous dissipation is large within the first quarter chord downstream of the trailing edge, but smaller thereafter. This may in part be due to the reorientation of the vortex as it leaves the trailing edge.

x/c	Γ/cU_∞
1	-0.401
1.25	-0.279
1.5	-0.294
2	-0.264

Table 4.1: Variation of maximum circulation of left vortex with downstream location.

4.2.2 Flow visualisation

Before continuing with the parametric study of static support interference, flow visualisation was used to study the magnitude of the fluctuations of breakdown location in the static case. The unsteady nature of the breakdown location is well known, and previous studies have observed values of RMS breakdown location of the order of $(x'_{BD}/c)_{RMS}$ = 0.03 (Gursul and Yang, 1995) for a Λ = 70° wing at α = 37°. RMS breakdown locations were calculated from time-histories of breakdown location lasting

for approximately 100 c/U_∞ with a resolution of 1 c/U_∞. Table 4.2 shows the effect of the two support structures placed in-line with the undisturbed vortex core location and at $x_{LE} = c/4$ on the RMS breakdown locations for the $\Lambda = 80°$ wing at $\alpha = 30$ and 40°. Also shown is the range of the fluctuations of breakdown locations, $(x'_{BD}/c)_{range} = (x'_{BD}/c)_{max} - (x'_{BD}/c)_{min}$, for the same cases.

α	Support	$(x'_{BD}/c)_{RMS}$	$(x'_{BD}/c)_{range}$
30	96mm Plate	0.0371	0.1917
30	12mm Cylinder	0.0326	0.1407
40	None	0.0270	0.1304
40	96mm Plate	0.0182	0.1069
40	12mm Cylinder	0.0165	0.0795

Table 4.2: Variation of the RMS and range of breakdown location.

In the absence of a support, at $\alpha = 30°$, no breakdown was observed. At $\alpha = 40°$ $(x'_{BD}/c)_{RMS}$ was reduced significantly by the presence of a dummy support structure. For a given incidence, the presence of the cylinder had a greater effect on the fluctuations of breakdown location than did the plate. Xie (1998) and Gursul and Xie (1999) showed that for a vortex generated by a 75° wing at 30° incidence impinging on a horizontal flat-plate, the RMS breakdown location was altered from 0.029 in the natural case by 50% to 0.015 in the impinging case. In the current configuration the RMS breakdown location was reduced by approximately 30% and 40% by the plate and cylindrical supports respectively.

Similar trends were observed regarding the maximum amplitude of the breakdown fluctuations. At $\alpha = 40°$ in the absence of a support a fluctuation magnitude of $(x'_{BD}/c)_{range} = 0.1304$ was observed, which is of the order of that expected from the results of Lowson (1964), who indicated a fluctuation amplitude of approximately 0.1c for a $\Lambda = 80°$ wing at $\alpha = 41°$. The effect of imposing a support structure on the flow is

to reduce the fluctuation magnitudes significantly, with the cylindrical support having the greater effect.

4.3 Effect of Boundary Condition Parameters

This section considers the results of a parametric study into the effect of boundary condition parameters on the location of breakdown in static testing. Reviewing some terminology, the parameters considered were ε, the lateral distance between the undisturbed vortex core location and the dummy support centre-line, x_{LE}, the distance between the trailing edge of the wing and leading edge of the dummy support, and the type and geometry of the dummy supports. All of the data presented in this section record the breakdown response over an 80° delta wing set at $\alpha = 30°$. To study the effect of varying ε, a dummy support was first positioned at a fixed streamwise location, x_{LE}, and laterally away from the model centreline where no effect on the vortex was observed, corresponding to large positive ε; the support was then stepped towards the vortex core, $\varepsilon = 0$. At each spanwise location, the vortex was allowed to settle so that the static response was measured and the time-averaged breakdown location was recorded for both increasing and decreasing values of ε.

The response of the breakdown to a dummy support of circular cross-section and diameter, d_r = 12mm, placed at one half chord length downstream of the trailing edge, $x_{LE} = c/2$, is shown in Figure 4.6. For decreasing ε, breakdown was first observed in the wake when $\varepsilon/b \approx 0.3$. As ε was decreased to around $\varepsilon/b \approx 0.2$, the breakdown moved over the wing ($x'_{BD}/c < 1.0$) and stayed around nearly the same location ($x'_{BD}/c \approx 0.82$) with further decreases in ε, until $\varepsilon/b \approx -0.2$. Stepping the support further away from the vortex from this point resulted in the downstream progression of the breakdown. The response was roughly symmetric about the vortex core ($\varepsilon/b = 0$). However, when the same experiment was repeated in the opposite direction (increasing ε), some asymmetry in the response of the breakdown was observed. As the support was stepped towards the vortex, the breakdown moved over the surface of the wing at $\varepsilon/b \approx -0.1$, twice as close to the vortex core as was observed previously, and remained over the wing until $\varepsilon/b \approx 0.35$. When over the wing, the breakdown was observed at roughly the same

streamwise location as previously. Despite these asymmetries the overall response was similar in both directions. In fact, this hysteresis of breakdown location was symmetric, albeit not about $\varepsilon/b = 0$. Since the main features of the breakdown response were similar regardless of the direction in which the data were taken, it was decided to simplify further investigation by studying only positive values of ε.

The results of a parametric study into the effect of ε, x_{LE}, and support geometry are shown in Figure 4.7 and Figure 4.8. Each dummy support was placed in turn at $x_{LE} = c$, c/2, c/4 and the effect of ε on the breakdown location studied. Figure 4.7 shows how the cylindrical supports affected the breakdown location. The figure clearly demonstrates that the existence of hysteresis of vortex breakdown location was not limited to the conditions considered in Figure 4.6. For example, for the 12mm cylinder placed at $x_{LE} = c/4$, for decreasing ε the breakdown was observed over the wing at $\varepsilon/b \approx 0.32$, but in the reverse case, when the support was moved away from the vortex core, breakdown remained over the wing until $\varepsilon/b \approx 0.65$. Breakdown occurred most forward when the support was coincident with the undisturbed vortex core location, $\varepsilon = 0$. When the support was located further downstream, at $x_{LE} = c/2$, breakdown occurred slightly further downstream when it was over the wing and the width of the hysteresis region was reduced. When placed at $x_{LE} = c$, the presence of the support no longer induced a breakdown over the surface of the wing and hysteresis was hardly noticeable.

Similar trends were observed for all the cases shown in Figure 4.7 and Figure 4.8, and may be summarised as follows. The effect of an obstacle placed in the vicinity of a vortex generated by a $\Lambda = 80°$ wing set at $\alpha = 30°$ was to promote the breakdown of the vortices where it would otherwise not occur. Breakdown was induced furthest upstream when the support was positioned laterally in line with the vortex core so that the unbroken vortex would impinge on the support. However, a lateral displacement away from the vortex core resulted in only a small movement of the breakdown downstream providing the breakdown remained over the surface of the wing. When the support was moved far enough away from the vortex for the breakdown to move to a position downstream of the trailing edge, a large displacement of the breakdown is observed for a small movement of the support structure. Moving the support downstream resulted in

a small movement of the breakdown downstream, but did not seem to reduce the width of the hysteresis region when the breakdown remained over the wing. Significantly different results were obtained depending on whether the breakdown location was measured by stepping the support towards or away from the vortex core.

The following sub-sections highlight and address specific areas of interest identified in the results presented to this point.

4.3.1 Hysteresis of Breakdown Location

Several investigators have made similar observations of vortex breakdown location hysteresis when the angle of attack is varied. For a $\Lambda = 80°$ delta wing, Lowson (1964) noted that when incidence was slowly increased, the breakdown was observed to broach the trailing edge and occur over the wing at $\alpha = 41°$, with further increases of incidence resulting in the breakdown moving further upstream. However, when the incidence was reduced the breakdown was observed to remain over the wing until $\alpha = 34°$. Whilst this was the first recorded observation of the effect due to changing incidence, Elle (1958) had previously found a similar result when the sideslip angle was varied. Non-uniqueness and hysteresis of vortex breakdown has also been noted in several theoretical and numerical studies (Beran and Culick, 1992 and Lopez, 1994) when the swirl level was varied in axisymmetric cases, and in delta wing flows when the angle of attack was varied (Visbal, 1995). However, in all of these investigations it was the variation of flow parameters (i.e., those that affect the strength of the vortices) that resulted in hysteresis of vortex breakdown location. In contrast, in the present study no flow parameters have been varied and yet similar hysteretic results have been observed.

Despite the differences in the conditions under which hysteresis has been observed, it is possible that the mechanisms responsible for these observations are similar. Returning to Figure 4.7 and Figure 4.8, it was noted that there are some conditions under which hysteresis was not observed. It would appear that the hysteresis region was *only* significant when breakdown was induced over the wing in the presence of the support. In all cases where breakdown was not observed over the wing, hysteresis was not observed. This is also true of cases observed in literature: hysteresis of breakdown

location has only been observed in static testing when breakdown is in the region of the trailing edge. It is therefore reasonable to infer that the presence of the trailing edge is a major contributor to the existence of hysteresis. Lambourne and Bryer (1961) identified the pressure recovery region at the trailing edge of delta wings as an influential factor in determining the breakdown location. When breakdown occurs downstream of the trailing edge, the adverse pressure gradient associated with the trailing edge region acts to encourage a forward movement of the breakdown to a position over the wing. Thus only a small encouragement in the form of an increased incidence or small movement of a downstream obstacle is enough to move the breakdown in this direction. However, in order to move from a position above the wing surface to one downstream of the trailing edge, the breakdown must re-negotiate the trailing edge pressure gradient, which this time is acting to impede its movement downstream. Thus a greater disturbance is required in order to delay the breakdown to a position aft of the trailing edge.

In considering the effect of hysteresis of vortex breakdown location, it is useful to invoke the concept of bifurcation. Figure 4.9, from Tobak and Peake (1982), illustrates the concept. Define λ as a parameter that *affects* the flow being studied (the freestream velocity, for example), and ψ as a parameter that *defines* the flow (the separation point over a body, for example). As the parameter λ is varied, the parameter ψ remains on a specified path up to a critical value of $\lambda = \lambda_c$. Once the point of criticality is reached, the flow cannot sustain itself in its current form. In a *supercritical bifurcation*, the flow bifurcates onto an alternative path, but the differences between the bifurcated and original flows are small. However, in a *subcritical bifurcation*, there are no adjacent paths along which the flow can deviate. Instead, the flow must jump from one path to another, representing a finite change from one flow regime to another quite different one. If the parameter λ is then reduced, the flow remains on the same path until the limit point $\lambda = \lambda_0$ is reached, at which point the flow rapidly returns to its original flow state.

The theory of subcritical bifurcation described above may be shown to compare well with the observations of vortex breakdown hysteresis presented in this investigation, as Figure 4.10 shows. Indeed, Tobak and Peake (1982) themselves use the example of

hysteresis of vortex breakdown due to a quasi-static pitching wing to demonstrate the application of subcritical bifurcation to flows of this type. In this case the parameter λ is the lateral location of the support structure, ε/b, and the parameter ψ is the breakdown location, x'_{BD}/c. As ε/b is reduced, breakdown is either not observed or is observed in the wake of the wing. At the point of criticality, $(\varepsilon/b)_{CRIT}$, the vortex cannot sustain its form and the breakdown is seen to find an alternative equilibrium location forward of the trailing edge, far upstream of its original position. Further reduction of ε/b results in only a gradual movement of breakdown upstream. In the opposite direction, as ε/b is increased, the critical point $(\varepsilon/b)_{CRIT}$ can be passed while breakdown maintains its equilibrium location over the wing. However, at some point, $(\varepsilon/b)_0$, the breakdown can no longer remain in such an upstream location, and it rapidly dissipates downstream. Thus the hysteresis loop is formed.

Both a physical explanation and an analogy in terms of subcritical bifurcation for the hysteretic behaviour observed in the vortex breakdown location in static testing have been presented here, which is useful in aiding our understanding of the phenomenon. As has been mentioned previously, it is suspected that the mechanism controlling breakdown location hysteresis in static testing is common regardless of the parameters varied, and it has been suggested that this mechanism is the existence of the trailing edge and the adverse pressure gradients associated with it. The hysteretic effects are an important aspect of the support interference characteristic, as they imply that while a small perturbation may lead to breakdown existing over the wing, a larger change is required for the vortex to return to its original state. It is therefore important in static testing to ensure that breakdown does not broach the trailing edge due to the effects of support interference, as not only will loading characteristics be significantly altered, but hysteresis may mean that the breakdown exists over the wing for longer than expected. For example, in quasi-static testing unfortunate positioning of the model relative to the support may induce breakdown over the wing, but the investigator may expect this given the results presented herein. However, given a further change in position where one might expect the breakdown to have dissipated, the breakdown may actually have persisted due to the effects of hysteresis.

4.3.2 The Effect of Support Location

Returning again to consider the data presented in Figure 4.7 and Figure 4.8, one curious result is the lateral distance away from the vortex core within which the dummy support can induce breakdown. The subscript $_{CRIT}$ will be used to denote the critical value of the parameter to which it is applied, where its critical value is that at which breakdown occurs at the trailing edge, unless otherwise stated. A useful measure in describing the effect of lateral support location is the parameter $(\varepsilon/b)_{CRIT}$, which was conveniently introduced in the previous section. For the purposes of analyses used in the remainder of this thesis, it is useful to explicitly define $(\varepsilon/b)_{CRIT}$ as the lateral distance from the undisturbed vortex core location at which breakdown is first observed over the wing when a dummy support is stepped *towards* the vortex. Results presented above have shown that for the flat-plate supports, $(\varepsilon/b)_{CRIT} = 0.2$ at $x_{LE} = c/4$, and that this value does not depend on the streamwise length of the plate. For the 12mm cylindrical support, $(\varepsilon/b)_{CRIT} = 0.32$, indicating that this support can affect the vortex from a greater lateral distance than can the support. The term "range of influence" will be used to describe the range that for a given support, $|\varepsilon/b| < (\varepsilon/b)_{CRIT}$, so for example, the range of influence of the 12mm cylindrical support is $|\varepsilon/b| < 0.32$.

PIV measurements presented above have been used to document the cross-flow velocity field at four streamwise stations. Figure 4.11, adapted from these data, shows the swirl velocity component along a horizontal line through the vortex core at $x_{LE} = c/4$. Also shown on this figure are the values of $(\varepsilon/b)_{CRIT}$ for the cylindrical and flat-plate support when placed at $x_{LE} = c/4$, and the relative widths of the support, d_p and t. If the extent of the vortex core is defined at the point of maximum swirl velocity, the core radius measures roughly $\varphi/b = 0.08$ at this station. The plate induced breakdown of the vortex at 2.5 core radii away from the vortex core, $(\varepsilon/\varphi)_{CRIT} = 2.5$, while the 12mm rod can induce breakdown from a distance of nearly four core radii, $(\varepsilon/\varphi)_{CRIT} = 4.0$. An alternative method of measuring this distance is in terms of the number of support widths. Given that $t = 2$mm, the plate supports can induce breakdown from a distance of $(\varepsilon/t)_{CRIT} = 9.68$. The 12mm cylindrical support can induce breakdown from a distance of $(\varepsilon/t)_{CRIT} = 2.2$. Whilst it is reasonable to expect that the cylindrical support

would influence the vortex from a greater lateral distance, it is surprising just how far away the plate support can affect the breakdown given the relative thickness of the supports. Considerations of the mechanism of this interaction is given in the following section.

Few instances of non-direct streamwise vortex impingement (i.e. $\varepsilon/b \neq 0$) investigations exist in literature that may be compared to the current results. Xie (1998) and Gursul and Xie (1999) conducted investigations into the impingement of vortices shed from the leading edges of a $\Lambda = 75°$ wing upon a horizontal flat-plate placed at $x_{LE} = c/4$. In these studies a relatively thick plate of t = 6mm was considered. It was found that breakdown of the vortices was influenced when the plate was placed at $\varepsilon/b = 0.15$ at $\alpha = 30°$, which is of the order of that found in this investigation. However, in terms of the thickness of the plate, $(\varepsilon/t)_{CRIT} = 2.71$, which is significantly lower than may be expected from the results presented herein, possibly due to the relative thickness of the plate considered, and its horizontal orientation.

The effect of streamwise location of the support structures is more clear. It was shown in the results presented above that the closer the support is to the trailing edge, the greater the effect on the vortex for a given ε/b. $(\varepsilon/b)_{CRIT}$ for a given support reduces with increasing x_{LE}, to the point where the parameter is meaningless in the limit $x_{LE} \rightarrow \infty$, i.e. breakdown does not occur over the wing even at $\varepsilon = 0$. For example, for none of the cases considered did breakdown occur forward of the trailing edge for $x_{LE} > c/2$. This is an exceptionally important result, as it indicates that the effect of support interference can be reduced significantly provided the supporting structure can be placed far enough downstream of the model. Further, the distance required is not very large, being of the order of one chord length aft of the trailing edge. Since the lift generated by a wing is only affected when breakdown occurs over the wing surface, it may be concluded that for the configuration considered in these tests ($\Lambda = 80°$ and $\alpha = 30°$), support interference effects are negligible in static testing for $x_{LE} = c$.

4.3.3 The Effect of Support Geometry

Increasing the diameter of the cylindrical support caused earlier breakdown and widened the region over which hysteresis was observed, as shown in Figure 4.7. When supports of rectangular cross section were considered, there was little to separate the results for those of d_p = 24mm and 48mm, as shown in Figure 4.8. Results for the 96mm plate support show that to be the worst configuration of all, as not only did it push the breakdown further forward than any of the other supports, but the hysteresis region is also wide. In addition, the 96mm plate is the only plate to induce breakdown over the wing at x_{LE} = c/2. These results show that a thin cross-section is not necessarily desirable if the length in the stream-wise direction is large, and based on this study one may define the critical length as lying in the region 48mm < d_p < 96mm. In other words streamlined supports may not be as good as those with a circular cross-section.

4.3.3.1 Discussion of the interaction of the vortex with the cylindrical support

The effect of placing bluff body, such as the cylindrical dummy support used in this investigation, in a flow is to deflect the oncoming streamlines away from their undisturbed path. Flow approaching the body is forced to decelerate resulting in an adverse axial pressure gradient. The physics of a cylinder placed in a two dimensional parallel flow is a common problem addressed by fluid mechanics textbooks (Anderson, 2001, for example). The pressure field around such a body is well documented and is shown in Figure 4.12 for potential flow, which predicts C_p = 1.0 at the stagnation point. However, the theory also predicts C_p = –3.0 at the sides of the cylinder, indicating a significant *favourable* pressure gradient along the side of the cylinder. This is interesting given $(\varepsilon/d_r)_{CRIT} \approx 2.2$ for the 12mm cylindrical support; at this point the vortex core should actually be experiencing the effects of the favourable pressure gradient which exists on the side of the cylinder, based on a two-dimensional idealised model of the flow. Adding to the complexity of the vortex-support interaction are the effects of viscosity; clearly the flow cannot be assumed to be inviscid. In the static case, the Reynolds number based on the diameter of the 12mm cylindrical support, Re_{dr} = 1200, which would, in a parallel viscous flow, tend to indicate the presence of laminar

separation over the rear of the cylinder and subsequent vortex shedding. However, it is a major simplification to assume a parallel flow-field in this case, since significant swirl velocities are associated with the vortex structure, even at relatively large lateral distances, as Figure 4.3 and Figure 4.4 show. The effect of this swirl velocity component is to change the effective angle at which the flow approaches the support, and clearly this angle will strongly depend on the location of the support relative to the axis of the vortex. While this effect significantly complicates analysis of the problem, it is expected that the laminar separation and vortex shedding characteristics of the interaction will remain unaffected; only the angle of the wake will be deflected somewhat to reflect the orientation of the oncoming flow.

It is noted that the dominant frequencies associated with the shedding of vortices in the rear of a cylinder lie at around $fd_r/U_\infty = 0.2$ (White, 1991), and that this lies just above the range of frequencies associated with the helical mode instability, $0.048 < fd_r/U_\infty < 0.144$ (see Figure 1.12, but note the change of scaling length). In addition, a relatively large wake is expected due to the laminar separation over the cylinder, and the forming of a von Karman vortex street in its wake. It is therefore possible that an interaction of the vortex with the wake of the cylinder drives the breakdown process at large ε/b, where the axial pressure gradient is perhaps too distant from the vortex core to induce breakdown of its own accord. A further instability that may result in premature breakdown at large ε/b is associated with the rotation of fluid past the support. Since the fluid continues to rotate around the vortex, any disturbance introduced by the presence of the support can only serve to destabilise the vortex, possibly resulting in premature breakdown.

A discussion of the vortex-support interaction has therefore been made. A mechanism for the premature breakdown of the vortex in the presence of a cylindrical type support has been suggested based on the interaction of the vortex with the wake of the support for large ε/b, and on the axial pressure gradients associated with stagnation as the support is placed closer to the vortex core. However, it is clear that further work is required to elucidate the interesting features of the vortex-support interaction process highlighted herein. Specifically, detailed study of the possible interaction with the support wake and the unbroken vortex would be beneficial.

4.3.3.2 Discussion of the interaction of the vortex with the flat-plate support

Many investigations have been published that consider the effect of vortex impingement on the surface pressure loading and spectral flow characteristics over a flat-plate (Canbazoglu *et al*, 1995, Mayori and Rockwell, 1994, Wolfe *et al*, 1995, for example), as this is of great interest to the field of fin buffeting. However, little work has focused on the effect of this interaction on vortex breakdown, and what factors affect the location of the breakdown. One exception is the work undertaken by Gordnier and Visbal (1999) who performed a numerical study of vortex plate interactions. The study investigated the impingement of a leading edge vortex pair on a horizontal flat-plate placed at $x_{LE} = 0.31c$, and noted large scale separations at the leading edge of the plate due to the varying effective angle of attack of the plate due to the vortical nature of the flow. This separation in turn promotes premature breakdown. It was shown that the breakdown location is very sensitive to the extent of the obstruction caused by the separation regions at the leading edge of the plate. However, because the study considered a horizontal rather than vertical plate, the separation region will be exaggerated compared to the current case due to the upwash induced by the delta wing at incidence. Lee and Tang (1994) investigated the surface pressure distribution over the inboard and outboard surfaces of an F/A-18 fin, and showed regions of large-scale separation on both surfaces under some conditions. Whilst the setup is considerably different to the much simplified support interference situation discussed herein, the results nevertheless detail the interaction of a streamwise vortex impinging on a vertical plate-like structure and comparisons with the current research may therefore be drawn.

As a vortex impinges on a vertical flat-plate, the cross-flow velocity varies along the leading edge of the plate due to the variation of tangential velocity through the vortex core (see Figure 1.8). Over large portions of the plate this cross-flow is sufficient to induce separation over the front portion of the plate, which effectively increases the frontal area of the obstruction. Although there would be no adverse pressure gradient in a parallel flow, the regions of stalled flow generate a significant obstruction to the flow. It has been hypothesised that local pressure gradients can affect the vortex core significantly to the point where breakdown is induced, and in the light of this it may be seen how separation over the leading edges of the plate may similarly induce

breakdown from such a lateral distance. This much may be inferred from the literature reviewed here, and may explain the mechanism by which a flat-plate can induce premature breakdown despite its apparently small cross-flow area. However, it does not sufficiently explain why the 96mm plate should induce such a severe response compared to the smaller plates and the 12mm rod, which has a greater projection area. It can only be inferred that the width of the separation region is much greater in this case, resulting in a larger projected area and a greater effect on the vortex. Alternatively it may be that instabilities in the breakdown process unique to the interaction with the plate are allowed to propagate further upstream.

4.4 Effect of Flow Parameters

The effects of angle of attack and sweep angle were investigated in detail for the cylindrical support with diameter, d_r = 12mm. In these experiments, the location of the dummy support was fixed at x_{LE} = c/4 and the direct impingement of the vortex was considered (ε = 0) as previous tests have shown that this configuration represented a condition where the breakdown location was particularly sensitive to the support location. The variation of breakdown location is shown as a function of angle of attack and sweep angle in Figure 4.13, both in the presence and absence of the dummy support. The effect of each parameter on the breakdown response will be considered separately.

4.4.1 The Effect of Incidence and Sweep

Considering first the effect of incidence, clearly shown is the upstream progression of the breakdown location in both the forced and unforced cases with increasing incidence. Also shown is that the effect of the dummy support was in all cases to promote the onset of breakdown. At low angles of attack, the effect of the dummy support was to induce breakdown just upstream of its leading edge ($x_{BD}/c \approx x_{LE}$). As the angle of attack was increased, the breakdown location moved forward, reaching the trailing edge at a higher incidence for increasing sweep angles. At large angles of attack, the data for the natural and induced breakdowns tended to converge as the breakdown approached the apex.

For the 80° wing, the forced breakdown location exhibited a region of increased sensitivity, either side of which were two plateaus of reduced gradient. These high gradients were also observed at the lower sweep angles, but the plateau at high incidences was not captured, perhaps because high enough incidences were not considered. In the limit $\alpha \rightarrow 90°$, x'_{BD}/c must be asymptotic to zero since it is known that the breakdown is observed at the apex at very high incidences. The high gradients of breakdown location with incidence were in all cases observed in the region of the trailing edge, as the adverse pressure gradient associated with the trailing edge promotes the breakdown in this region.

A useful parameter is the angle of attack at which the breakdown is observed at the trailing edge of the wing ($x'_{BD}/c = 1.0$), in both the natural ($\alpha_{TE,n}$) and forced ($\alpha_{TE,f}$) cases. These parameters are labelled in Figure 4.13 for the four sweep angles considered. Figure 4.14 plots the variation of these parameters as a function of sweep angle, and shows that the effect of sweep angle was to delay breakdown in both the natural and forced cases. Arguably, the low sweep cases represented the worst case, as breakdown occurred at the trailing edge at the lowest incidence. However, also plotted in Figure 4.14 is the parameter ($\alpha_{TE,f} - \alpha_{TE,n}$), the difference between α_{TE} in the forced and natural cases, which is a measure of the sensitivity of the breakdown at each sweep angle. It is interesting to note that the breakdown was most sensitive at $\Lambda = 80°$, as at this sweep there was greatest difference between the natural and forced breakdowns. As the sweep angle was increased, the strength of the vortices reduced, and the leading edge vortices became more stable, delaying breakdown to a higher angle of attack. Figure 4.14 shows how, up to $\Lambda = 80°$, α_{TE} for the natural breakdown increased more rapidly with sweep than it did in the forced case. At $\Lambda = 85°$, the natural breakdown was unaffected by the increase in sweep angle, but the forced breakdown moved to a higher incidence, resulting in the reduction of sensitivity. Similar insensitivity of the natural breakdown location at high sweep angles was also observed by Wéntz and Kohlman (1971).

These results have shown that both the incidence and sweep angles have a significant effect on the sensitivity of the breakdown to support interference. While it may be

expected that a linear relationship would exist between the strength of a vortex and the magnitude of its response to a disturbance in a vortex tube experiment, it has been shown that this is not the case for leading edge vortices shed from delta wings, as the geometry of the wing imposes a number of external influences on the vortex. Such external influences are the effect of the trailing edge pressure gradient, and the boundary conditions imposed by the wing surface itself. These influences are the reason why 'worse case' conditions have been observed in relation to both the angle of attack and sweep angle. It has been shown that the breakdown is most sensitive to support interference when it exists in the region of the trailing edge in the natural case, and for a wing of $\Lambda = 80°$ sweep.

4.4.2 Definition of Severity of Breakdown Response

By examining Figure 4.13 and Figure 4.14 it is possible to identify those regions in which the vortex is most sensitive to support interference. This is an important step, as a full discussion of support interference requires a knowledge of the severity of the interference so that comparisons may be made when analysing the above results. In order to measure the severity of the breakdown response, the effect of breakdown on the overall flow structure will be considered. The effect of premature breakdown on wing loading provides an insight as to the overall effect of the support on the model. For highly swept delta wings ($\Lambda \geq 75°$) breakdown occurring at the trailing edge marks a precipitous fall in the lift generated by the wing (Wéntz and Kohlman, 1971) with further increasing incidence, indicating the onset of stall. The more forward the breakdown location, the greater the reduction in lift compared to the natural case. The severity of the breakdown response may be measured by considering the following regions, each of which imply a different level of interference.

(i) At low angles of attack the vortex does not naturally break down, and even when forced to break down by the presence of a dummy support, breakdown only occurs downstream of the trailing edge. Although in this region the support is inducing vortex breakdown where it would not naturally occur, the effect on wing loading will be negligible, as the breakdown does not occur over the surface of the wing.

(ii) At medium angles of attack, breakdown is observed over the surface of the wing in the presence of a dummy support, when in the natural case breakdown is either not observed, or is observed aft of the trailing edge. In this region the support has a large effect, as wing loading will be significantly affected.

(iii) As the angle of attack is increased further, vortex breakdown occurs naturally over the wing. The effect of the support is to push the breakdown further towards the wing apex, but the effect reduces as the angle of attack increases. At very high angles of attack the locations of the forced and unforced breakdown tend to the same location.

These regions are illustrated in Figure 4.15, for $\Lambda = 85°$. Of the three, it would be expected that Region (i) represents the least significant breakdown response, since the breakdown at no point appears over the surface of the wing, and so no effect on wing loading will be observed. Region (ii) represents a severe response as breakdown is observed over the wing and therefore a significant reduction of lift will be observed in relation to the undisturbed case. The effect of Region (iii) is also likely to be severe. In fact, from consideration of Figure 4.13 it may be concluded that the worst case of all is on the boundary of regions (ii) and (iii). At this point the breakdown is at the trailing edge in the natural case, and the pressure distribution associated with the trailing edge means that the location of the breakdown is very sensitive to external disturbances. Thus, the disturbance resulting from the presence of a dummy support results in a large movement of the breakdown upstream. Considering the data for the 80° wing shown in Figure 4.13, it can be seen that at this point the breakdown occurs $0.33c$ further upstream in the forced case compared to the natural case, implying a significant reduction in the vortex lift contribution from the affected vortex. Although at lower incidences there is a bigger difference between the natural and forced breakdown location, the measure of severity should be the distance between the forced breakdown location and the trailing edge, since breakdown only affects the lift distribution when over the wing. At higher incidences the degree of interference may be measured simply as the difference between the breakdown locations in the two cases.

To verify these findings force balance measurements were undertaken. Due to the sensitivity of the force balance, it was necessary to conduct these experiments with a higher free stream velocity than was used for the flow visualisation tests. For these tests U_∞ = 0.31 m/s which corresponds to Re_c = 77,500 for the Λ = 80° wing (compared to Re_c = 25,000 for the flow visualisation experiments). As discussed in §3.4.2, literature suggests that the breakdown location is insensitive to changes in Reynolds number within this range, and it can therefore be assumed that, providing the leading edge geometries remain consistent between the tests, comparison between the force measurements and flow visualisation experiments is valid. It should be recalled, however, that the models used in force balance measurements differed from those used in flow visualisation in that they were fabricated from PVC rather than aluminium, and creating a consistent sharp leading edge was therefore difficult. As shown above, this was the greatest error associated with the force balance measurements, other than the uncertainty in the angle of attack.

Figure 4.16 compares the variation of lift coefficient measured for the Λ = 70, 75, and 80° delta wings both in the presence and absence of the cylindrical support. In all of these cases, the lift generated by the wing in the natural case (that is, in the absence of the dummy support), was comparable with that predicted by the Leading Edge Suction (LES) Theory of Polhamus (1971), and stall angles were similar to those observed by Wéntz and Kohlman (1971). At low incidences, the lift generated in the presence of the dummy support also compared well to that predicted by LES theory. However, above a certain incidence, a marked drop in lift was noted compared to the natural case. The incidence at which the dummy support began to affect the lift generated by the wing varied according to the wing studied, and was in all cases equal to the incidence at which breakdown broached the trailing edge in the forced case in the flow visualisation experiments. $\alpha_{TE,f}$ and $\alpha_{TE,n}$ for each wing are shown on Figure 4.16 for convenience, and it can be seen that $\alpha_{TE,f}$ corresponds to the break point in the lift curve in the presence of the dummy support for each wing, although this is most clearly seen for the Λ = 80° wing.

Figure 4.16 shows that $\alpha_{TE,n}$ did not necessarily correspond to the worst case in terms of lift detriment as reasoned from the flow visualisation results, particularly for the $\Lambda = 70$ and 75° wings. It is not clear why this might be, since the visualisation data plotted in Figure 4.13 indicates that at this point the breakdown is perturbed most by the presence of the dummy support. It is suggested, though, that the fact that the other vortex of the leading edge vortex pair is unperturbed by the presence of the support accounts for this anomaly. In fact, the incidence at which the greatest reduction in lift force was observed was much greater than expected, being $\alpha = 30°$ for the $\Lambda = 70$ and 75° wings, and $\alpha = 35°$ for the $\Lambda = 80°$ wing.

For the 80° wing at least, the lift curve was similar to that predicted from the results of the flow visualisation experiments. For this reason, the definition of severity of breakdown response will remain as outlined above. In fact, the bulk of subsequent analysis will consider the occurrence of breakdown forward of the trailing edge in the forced case as being a severe breakdown response. This is a fair analysis as in all the cases plotted in Figure 4.16, $\alpha_{TE,f}$ corresponds to the break-point in the lift-curve, and lift is therefore affected by the presence of the dummy support. The fact that the magnitude of the lift detriment is greater at higher incidences is interesting, but does not affect the classification of the severity of the support interference effect.

4.4.3 The Effect of Sideslip

It has been shown that the strength of the leading edge vortices is an important factor in determining the severity of the breakdown response to support interference, and that specific worst case conditions exist for both the angles of incidence and sweep. A further commonly considered parameter in wind-tunnel testing is the effect of sideslip. This orientation change also affects the strength of the leading edge vortices, but not symmetrically, with the leading (or windward) vortex strengthening due to an effective reduction in sweep, and the trailing (or leeward) vortex weakening due to an effective increase in sweep. Figure 4.17 shows the variation of breakdown location with sideslip angle at $\alpha = 30°$ for $\Lambda = 80°$. This configuration was considered as it has been shown to represent a particularly sensitive case. The sideslip angle, β, is defined as positive with the visualised vortex on the windward side of the model, corresponding to a reduced

effective sweep angle as shown in the inset of this figure. The effect of sideslip was similar in many respects to the effect of incidence, with increasing sideslip moving the breakdown (of the windward vortex) forward in both the natural and forced cases. The effect of the presence of the support on the windward vortex reduces with increasing sideslip angle.

It was also decided to test a similar case for the $\Lambda = 70°$ wing, and an angle of attack of $\alpha = 15°$ was chosen as it represented a similarly sensitive configuration; the results from these tests are shown in Figure 4.18. The breakdown location in this case was much less sensitive to sideslip than in the case of the $\Lambda = 80°$ wing at $\alpha = 15°$, a further indication of the reduced effect of support interference for less slender wings (see Figure 4.14). However, as observed in the previous case, the locations of the breakdowns converge as the sideslip angles become more positive, indicating a reduction in the magnitude of the interference effect.

These results indicate that support interference may be of concern when testing a wind-tunnel model in sideslip when testing models of greater sweep. A reduction in the magnitude of the interference effect on the windward vortex with increasing sideslip has been observed, and similarly the interference effect increases on the leeward vortex. Taking the case of a model supported by a strut-sting support, the reorientation of the model will tend to shift the trajectory of the leeward vortex in such a way that it impinges on the support structure thus inducing premature breakdown.

4.5 Chapter Review

This chapter has addressed the problem of support interference in static testing, and has considered the effects of a number of parameters on the severity of the interference. Simple delta wing models were used to generate a leading edge vortex and the effect of a number of dummy support structures on the breakdown of the vortex was studied. Following this brief review, the focus of the thesis shifts to understanding support interference in oscillatory testing.

It is useful to begin with a review of some of the terms and parameters that have been introduced in this chapter. The parameters studied have been the location (ε and x_{LE}), dimensions (d_r and d_p), and cross-sections (cylindrical or rectangular) of the supports, and the shape (Λ), and orientation (α and β) of the wing. The parameter $(\varepsilon/b)_{CRIT}$ has been used to describe the lateral offset from the vortex core at which breakdown is first observed when stepping the support in the direction of the vortex. As will be seen, this parameter is used frequently in the following chapters to explain observations relating to dynamic support interference. It is important to recall that $(\varepsilon/b)_{CRIT} = 0.32$ and 0.20 for the 12mm cylindrical and 96mm flat-plate supports respectively at $x_{LE} = c/4$, as these values will be relied upon heavily in subsequent analyses. Associated with this parameter is the term "range of influence", which is the lateral range within which a support may affect the vortex. $(\varepsilon/b)_0$ is the lateral offset from the vortex core at which the breakdown is seen to dissipate when stepping the support away from the vortex. The difference between $(\varepsilon/b)_0$ and $(\varepsilon/b)_{CRIT}$ is a measure of the extent of hysteresis.

The effect of support interference is to induce breakdown where it would not otherwise occur. If breakdown is already present in the flow, the effect is to induce breakdown further upstream than would otherwise be expected. This is clearly detrimental since, should breakdown occur over a lifting surface, a significant reduction in lift will be observed compared to the undisturbed case. Further, a reduction in the magnitude of the natural fluctuations of breakdown location is observed in an impinging flow, with RMS breakdown locations reducing by up to 40% compared to the natural case. Thus, not only lift but the spectral characteristics of lift force measurements will be detrimentally affected. It has been shown that a cylindrical support has a greater effect on the RMS breakdown location than does the plate support.

Support interference is most severe when a support structure is placed coincident with the vortex core, so that the undisturbed vortex would impinge directly, and close to the trailing edge. The effect of lateral offset of the support is to affect a slight downstream movement of the breakdown within the range $|\varepsilon/b| < (\varepsilon/b)_0$. Outside of this range, the breakdown is seen to rapidly approach its natural location with small movements of the support. This again is a result that will be relied upon in subsequent chapters. The

effect of moving the support downstream is to allow the breakdown to also move downstream. This investigation has shown that the effects of support interference may be constrained to the region downstream of the trailing edge provided the support is kept a distance of at least one chord length downstream of the trailing edge of the model. Should this not be possible due to constraints imposed by the wind-tunnel or model designs, the investigator should be aware of the importance of avoiding direct impingement of vortices on the support structure.

One of the major observations was that of hysteresis of breakdown location as the lateral position of the dummy support was varied. Although similar hysteresis of vortex breakdown location has been observed in cases where the vortex strength was varied, this is the first case of hysteresis due to an external influence, such as the location of a downstream obstacle. It has been shown that the theory of subcritical bifurcation allows a suitable analogy to be drawn with the theoretical approaches of other investigators. A mechanism for the behaviour has been advanced based on the presence of the trailing edge and the pressure gradients and non-linearities associated with it.

It has been shown that the extent of interference is dependent on the state, or condition, of the vortex. The effect of altering the sweep, incidence or sideslip is to alter the strength of the leading edge vortices, and it is only under certain configurations that severe vortex support interactions have been observed. Lift force measurements have been used to confirm that the lift generated by the wing may be severely reduced due to the effects of support interference, particularly for higher sweep wings. The results of the parametric study have given an indication of where this region lies for all the wings tested. Further, it was found that support interference was worst in the case of the 80° wing. These results are important as they give the experimentalist an indication of the regions under which support interference may be a potential problem. Operating at conditions away from these will result in the avoidance of interference effects.

Whilst it may be intuitively expected that a streamlined support would be beneficial in reducing the effects of support interference, the results of this investigation have shown this may not be true if the streamwise dimension is large. Although it has been shown that a cylindrical support may induce premature breakdown from a greater lateral offset

than a plate, a plate with a large streamwise dimension placed on the vortex centre-line induces breakdown further upstream than a cylinder. A discussion of the relative breakdown mechanisms of the two types of support has indicated that it is the separation region over the leading edges of the plate which result in the vortex breaking down in this case. It was hypothesised that the extent of this separation region is large in the case of the long plate, and this is the cause of the surprisingly large effect on the breakdown location. Clearly this speculation needs to tested to form a proper understanding of the flow before any firm conclusions can be drawn. For the cylindrical support, the mechanism thought to drive the breakdown process is the axial pressure gradient resulting from the stagnation of the flow upstream of the support, although an interaction between the vortex and cylinder wake for high ε/b has also been hypothesised.

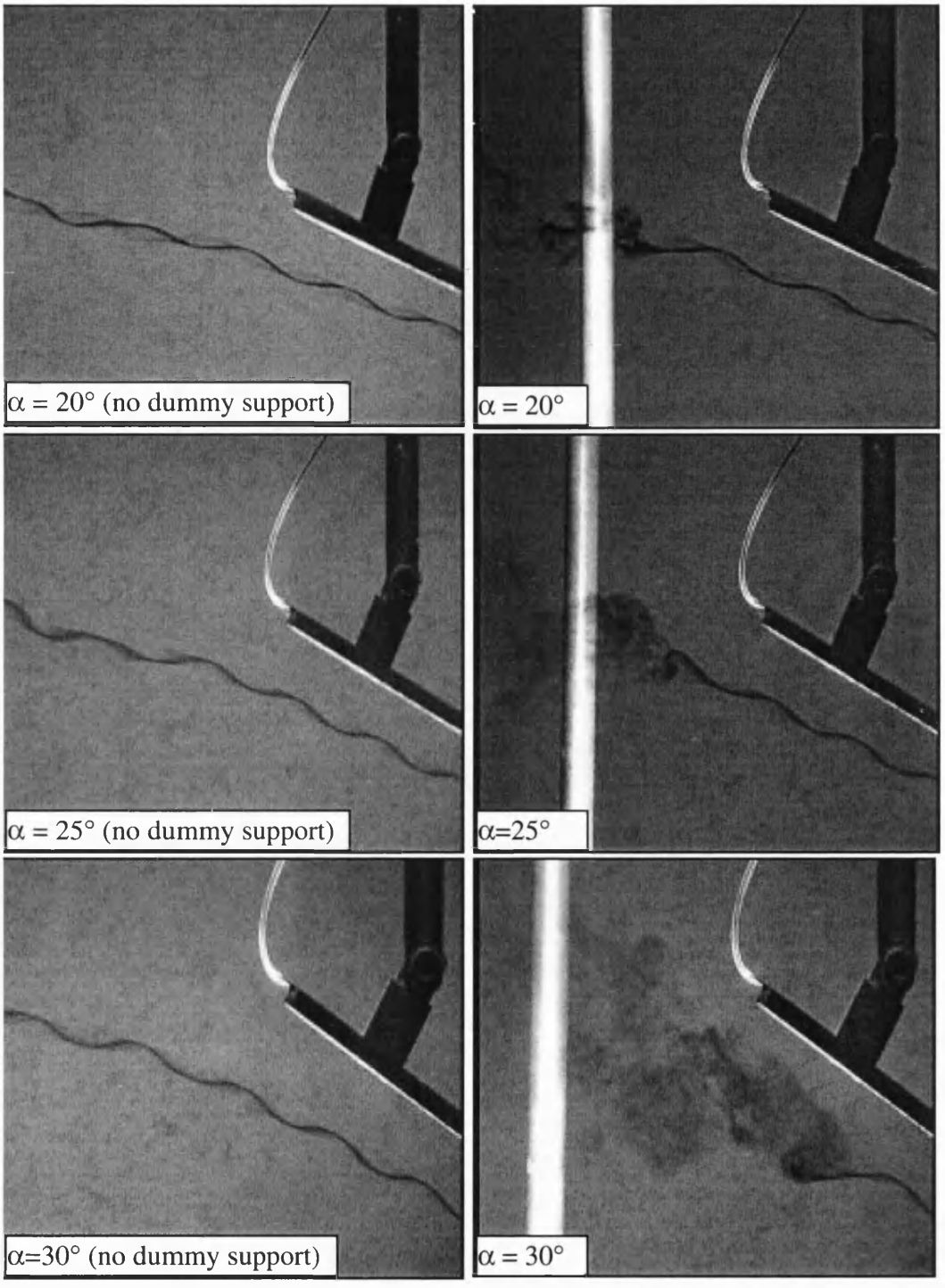

Figure 4.1: Effect of a dummy support on the breakdown of leading edge vortices.

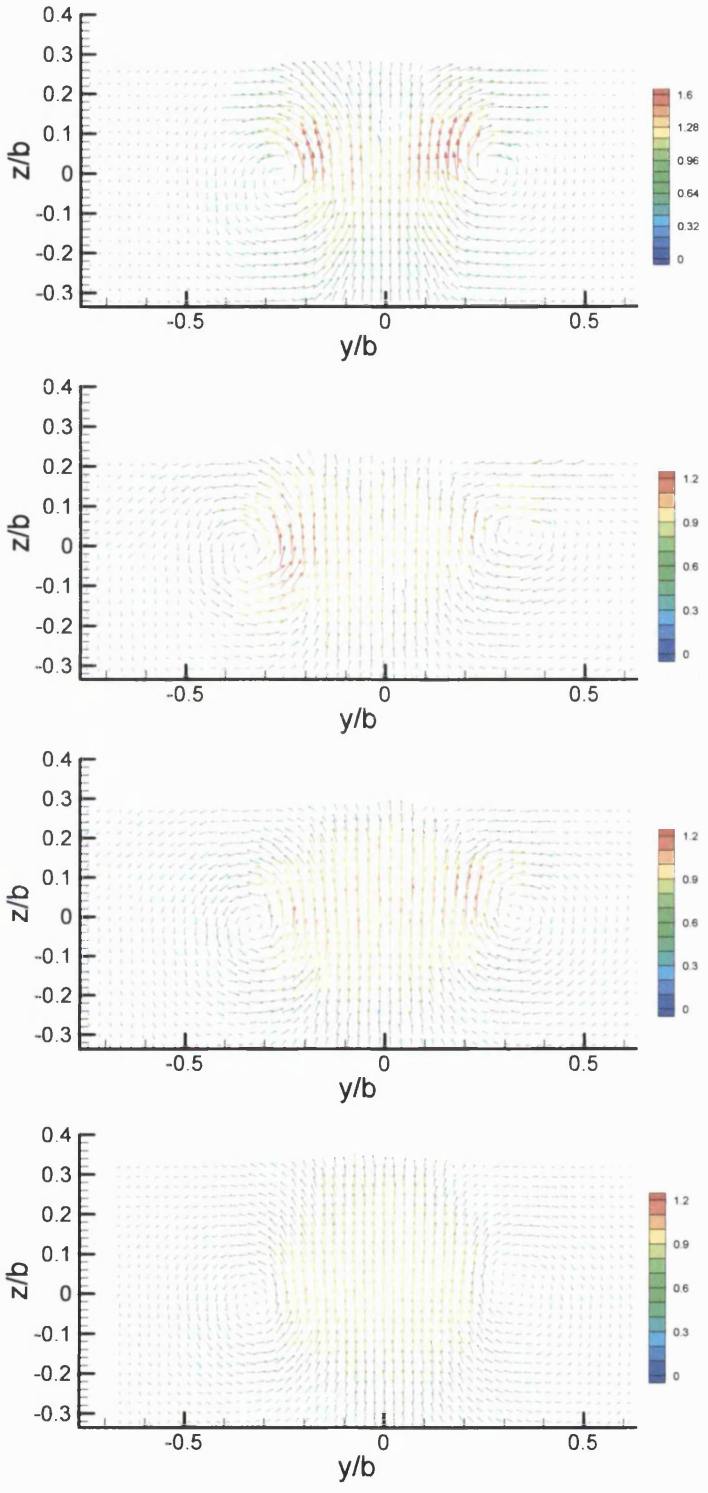

Figure 4.2: Cross-flow velocity fields at (from top) trailing edge and x_{LE} = c/4, c/2 and c. Note the change of color scales in some of the plots.

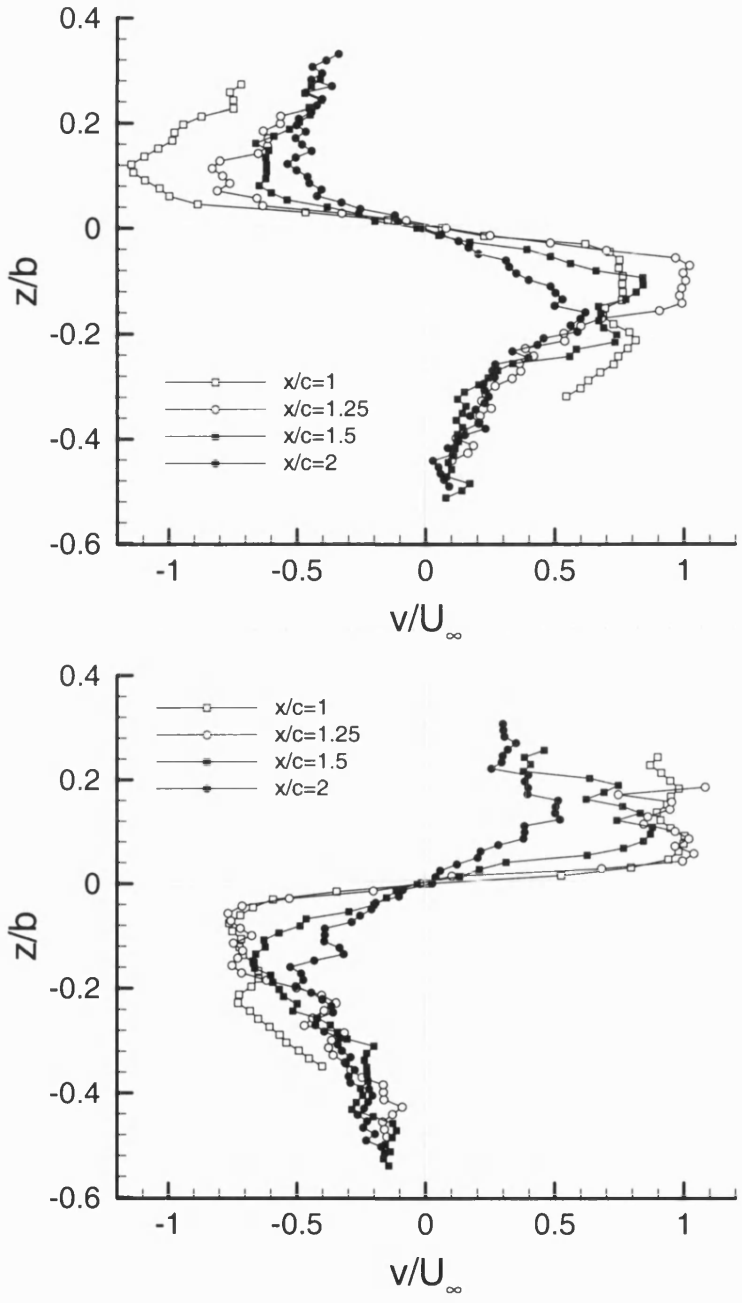

Figure 4.3: Variation of normalised horizontal component of velocity with vertical distance from the vortex core for left (top) and right (bottom) vortices.

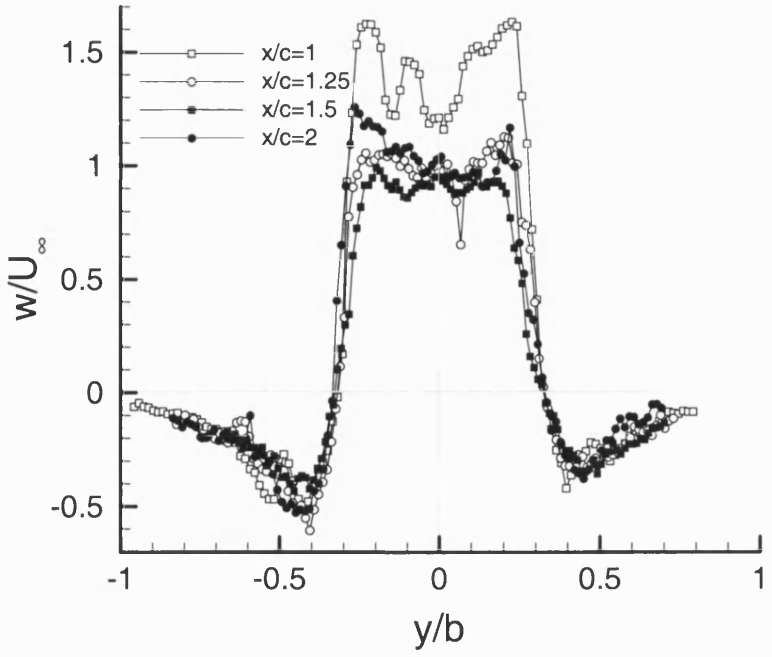

Figure 4.4: Variation of normalised vertical component of velocity with horizontal distance from the wing center-line for both vortices.

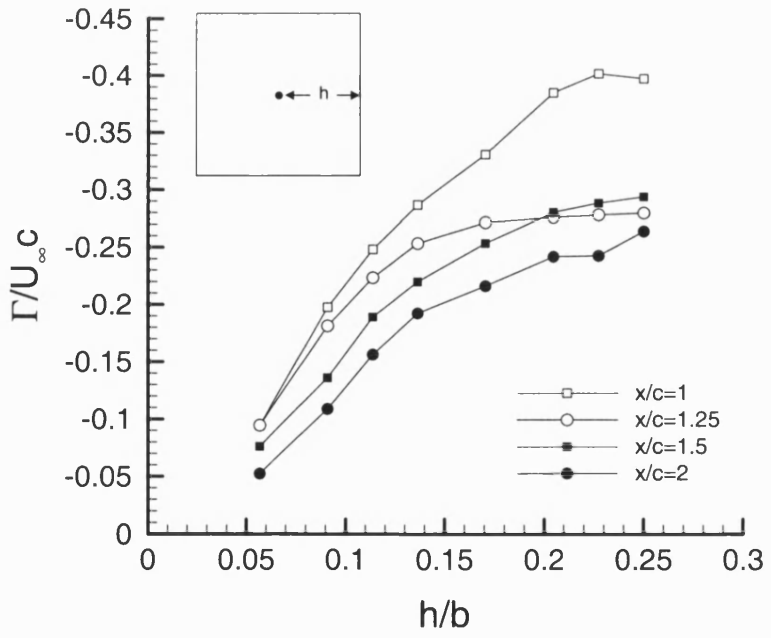

Figure 4.5: Variation of normalised circulation around a square path as a function of the size of the square.

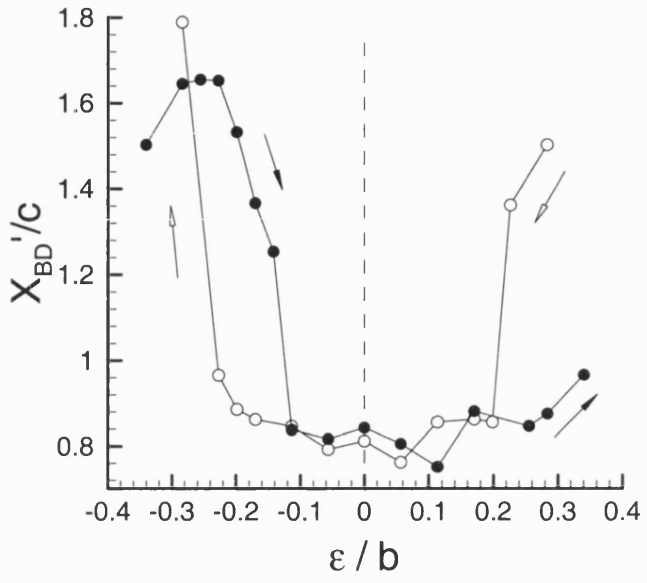

Figure 4.6: Variation of time-averaged breakdown location with ε: $\Lambda = 80°$, $\alpha = 30°$, $x_{LE} = c/4$, 12mm cylindrical support.

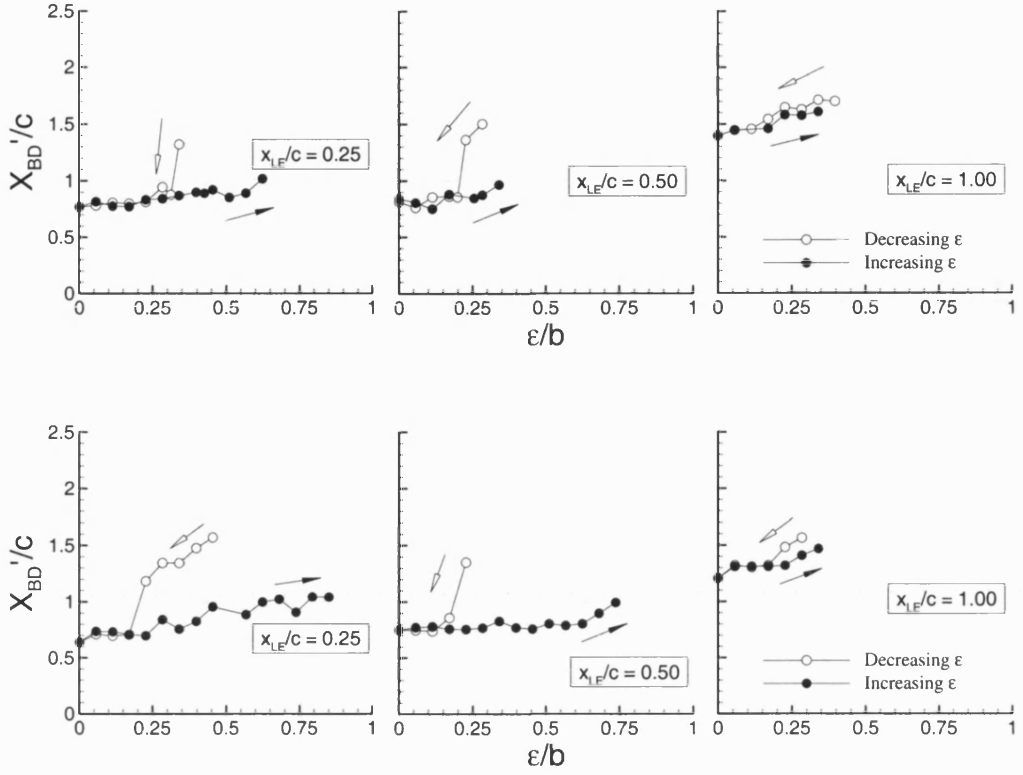

(top) $d_r = 12\text{mm}$ $(d_r / b = 0.136)$

(bottom) $d_r = 24\text{mm}$ $(d_r / b = 0.273)$

Figure 4.7: Variation of time-averaged breakdown location with lateral and streamwise support location for support of cylindrical cross-section.

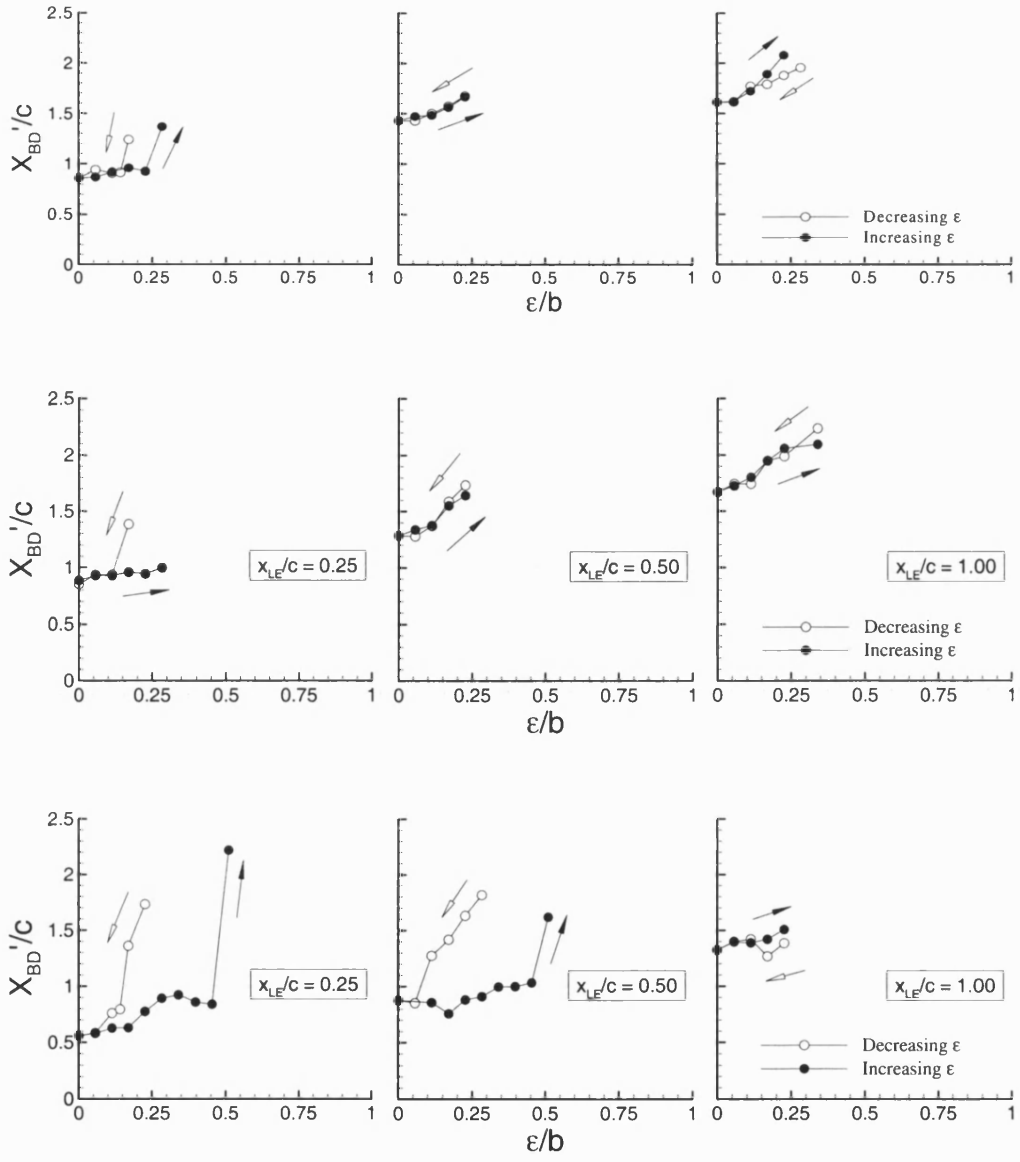

(top) d_p = 24mm (d_p / b = 0.273)

(middle) d_p = 48mm (d_p / b = 0.545)

(bottom) d_p = 96mm (d_p / b = 1.091)

Figure 4.8: Variation of time-averaged breakdown location with lateral and streamwise support location for flat-plate supports.

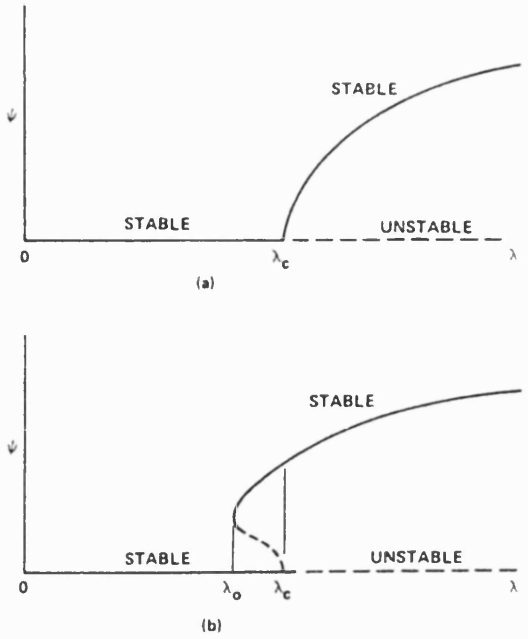

Figure 4.9: Examples of (a) supercritical and (b) subcritical bifurcation (Tobak and Peake, 1982).

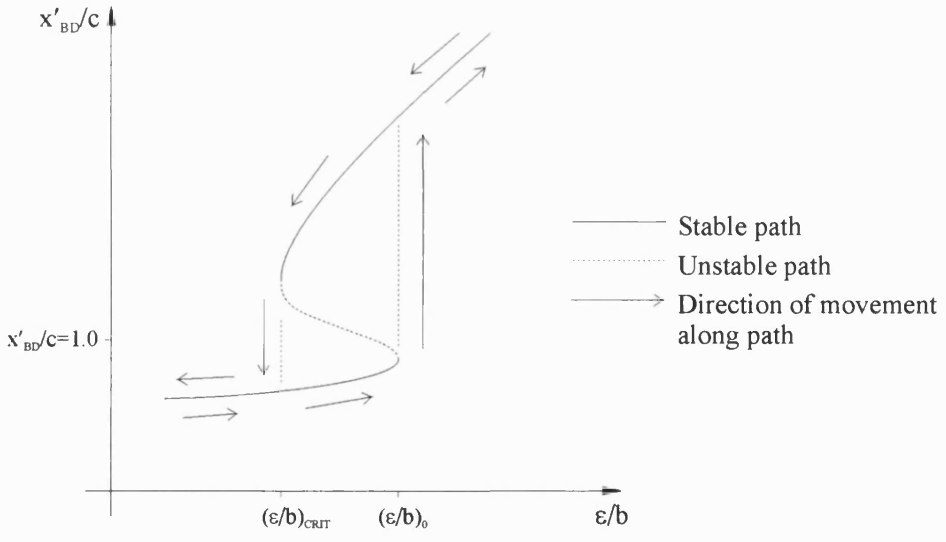

Figure 4.10: Bifurcation analysis applied to hysteresis of breakdown location due to support interference.

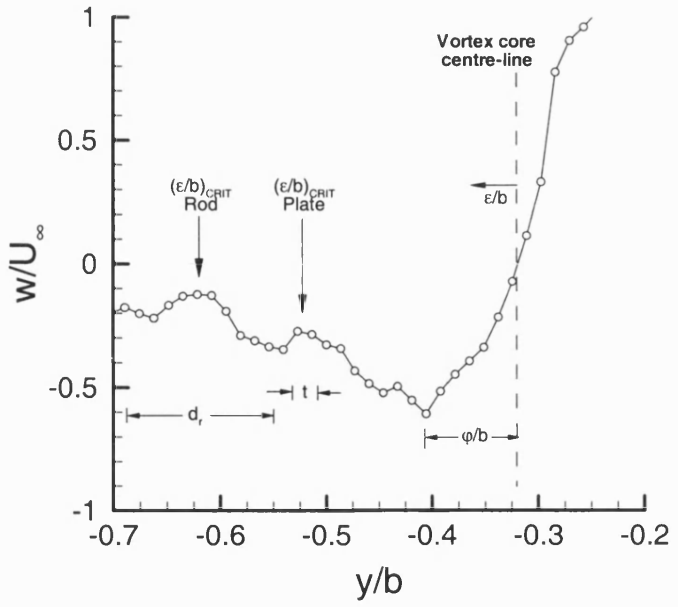

Figure 4.11: Swirl velocity profile of left vortex at x_{LE} = c/4, showing values of $(\varepsilon/b)_{CRIT}$ for the cylindrical and plate supports.

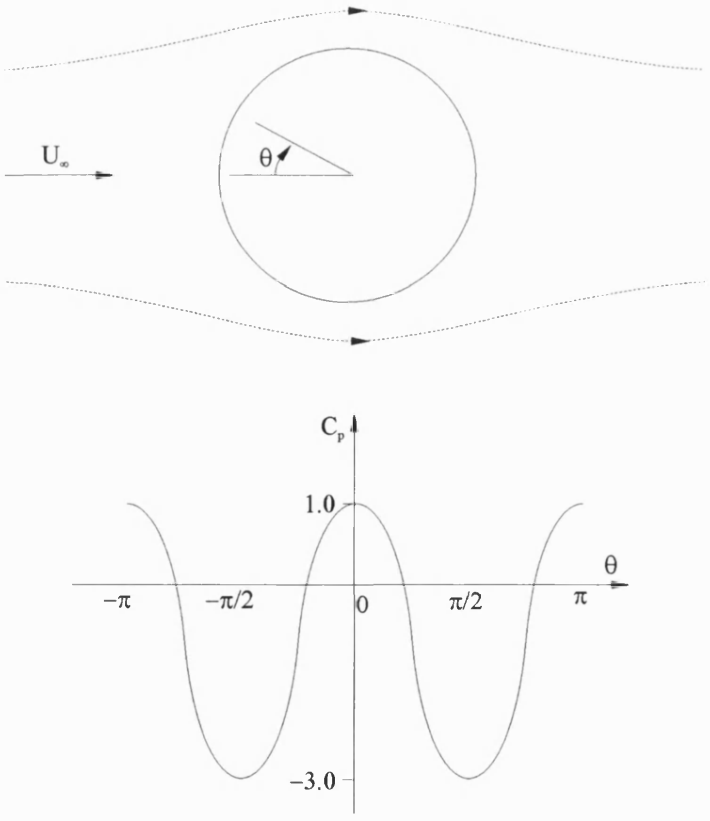

Figure 4.12: Variation of pressure coefficient around a cylinder in potential flow.

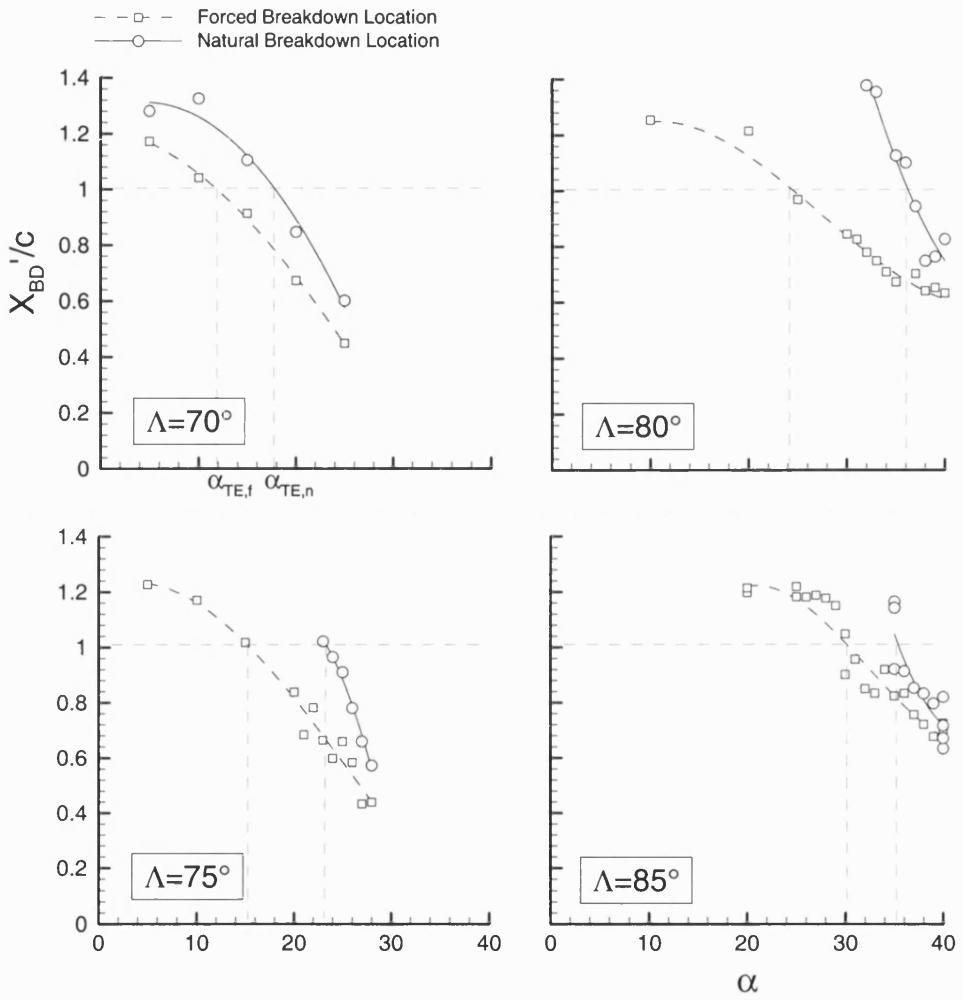

Figure 4.13: Variation of time-averaged breakdown location with angle of attack in the absence and presence of 12mm cylindrical support.

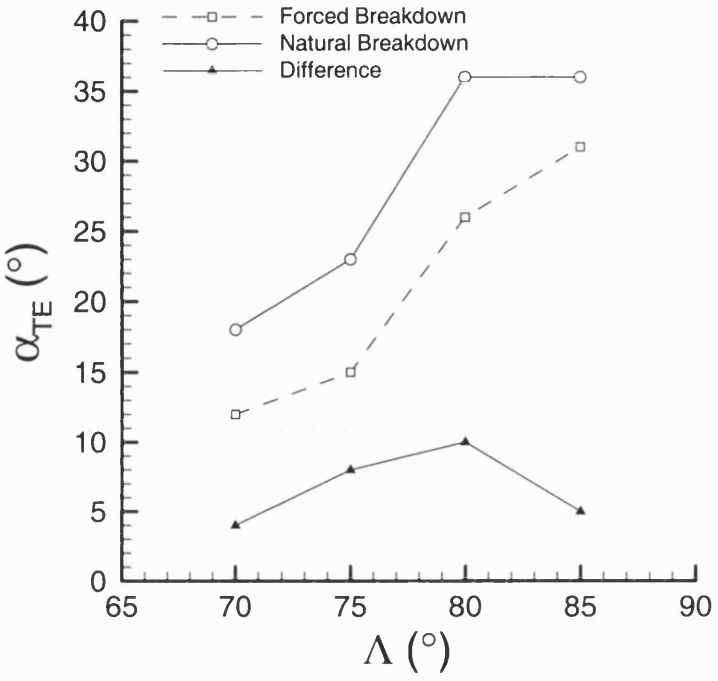

Figure 4.14: Variation of α_{TE} with sweep angle for forced and natural breakdown.

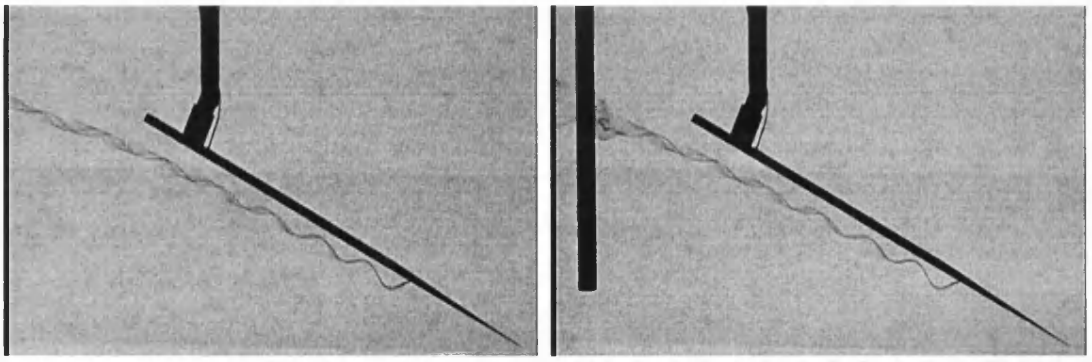

Region (i): $\alpha = 30°$; No natural breakdown; forced breakdown proximal to support.

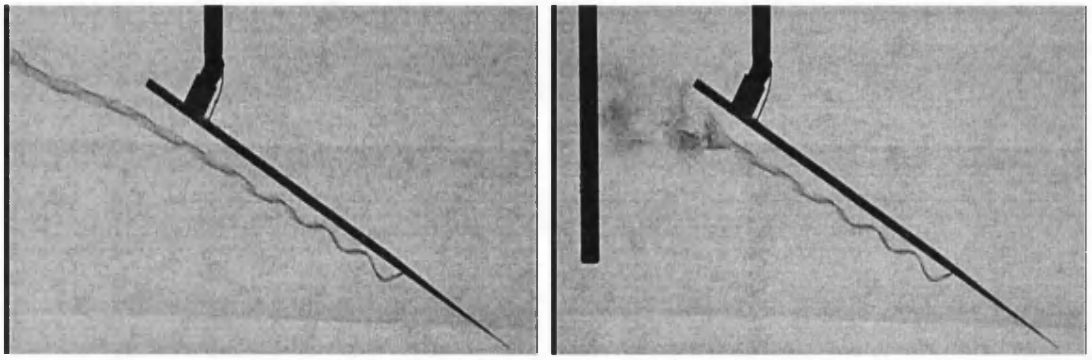

Region (ii): $\alpha = 35°$; No natural breakdown, forced breakdown over wing surface.

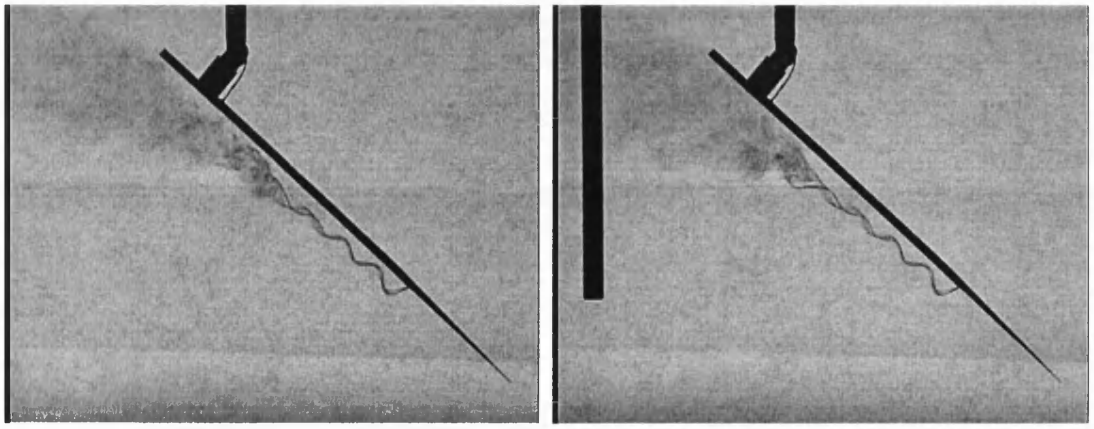

Region (iii): $\alpha = 40°$; Natural and forced breakdowns occur over wing surface.

Figure 4.15: Three regions defining the severity of influence of a dummy support on vortex breakdown location for $\Lambda = 85°$ wing.

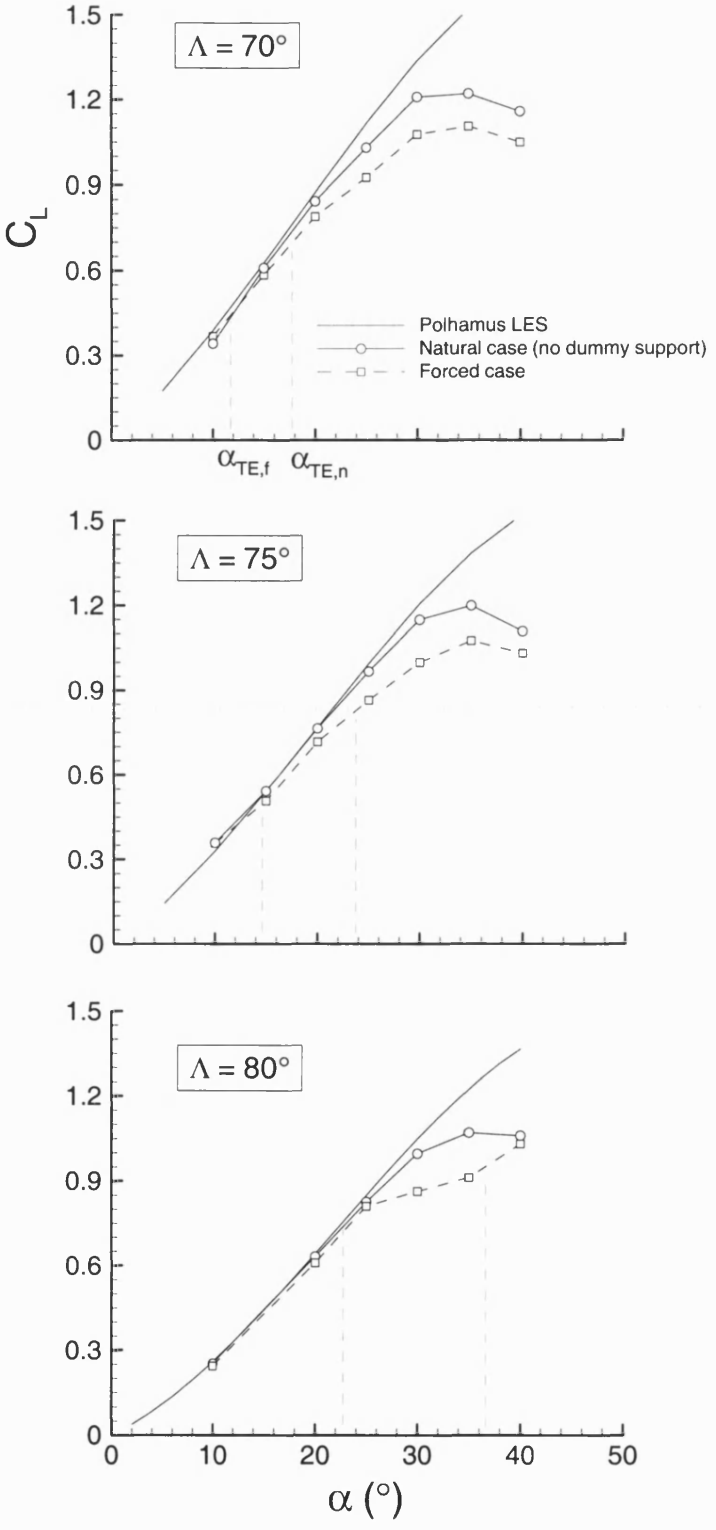

Figure 4.16 Variation of lift force with incidence for 70°, 75° and 80° delta wings in the absence and presence of 12mm cylindrical support.

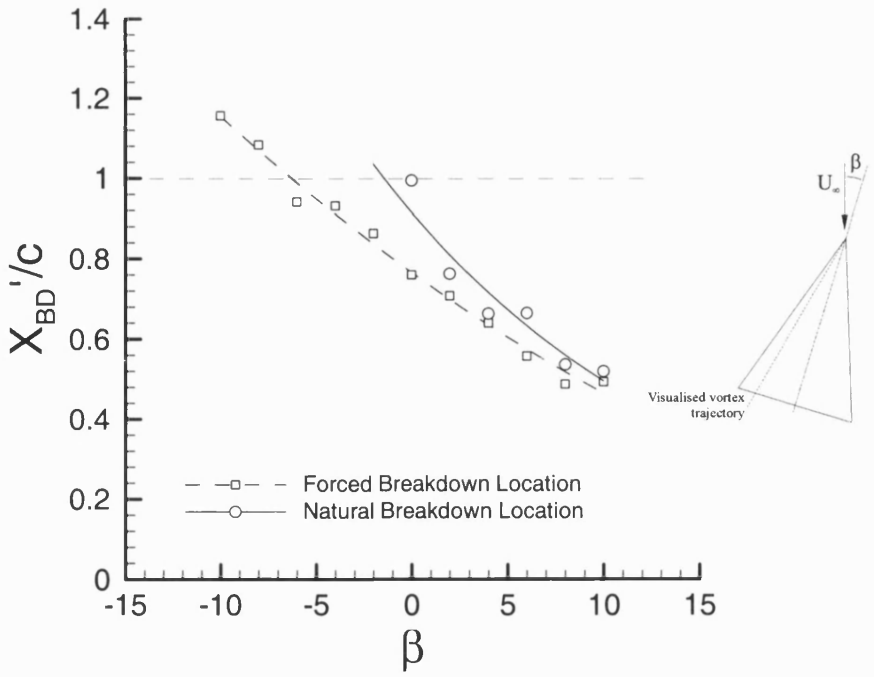

Figure 4.17: Variation of time-averaged breakdown location with sideslip angle for Λ = 80°, α = 30° and cylindrical support, d_r = 12mm, x_{LE} = c/4.

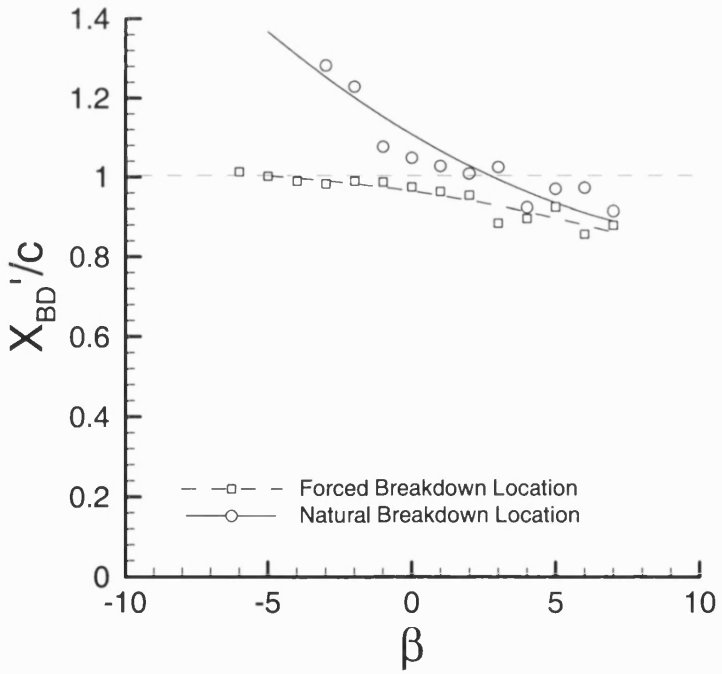

Figure 4.18: Variation of time-averaged breakdown location with sideslip angle for Λ = 70°, α =15° and cylindrical support, d_r = 12mm, x_{LE} = c/4.

Chapter 5 Support Interference in Oscillatory Testing

5.1 Introduction

The aim of this chapter is to extend the static results presented in the previous chapter to describe the effects of support interference in oscillatory testing. The chapter begins with a review of the terminology and methodology employed in dynamic testing, which was discussed in detail in Chapter 3, following which the results of this stage of the investigation are presented. A review of the principal conclusions completes the chapter.

The investigation of support interference in dynamic testing was complicated by the time-dependent nature of the leading edge vortices over an oscillating wing. For a given set of results, it would be difficult to identify those effects which were due to the vortex-support interaction, and those due purely to the changes in strength of the vortices. Thus, in order to simplify the problem, it was necessary to implement a testing methodology which would separate the effects of vortex strength time dependency and support interference while still allowing meaningful dynamic cases to be studied. Therefore, two approaches to the investigation were taken. Firstly, the effect of a dummy support oscillating in the wake of a static wing was considered. This allowed the effect of the support on the vortex to be directly considered, by removing time dependent vortex strength effects. To complete the study, these results were compared with the case of the more realistic oscillating wing case, with the dummy support being located statically in its wake.

Oscillatory motions for both the moving support and moving wing tests were similar, and were generated using the mechanism described in Chapter 2. The oscillating

waveform used in these experiments involved the lateral translation of the wing along the y-axis (see Figure 3.1). This motion was chosen as, although it is unlikely to be a form of motion that relates to real aircraft motion, it represents a simplified dynamic movement of the wing, and therefore a reasonable starting point for the investigation. It also represents a case where the time-dependent nature of the vortices may be inferred from the lateral velocity of the wing at any point in the cycle. The lateral distance between the undisturbed vortex core and the centre-line of the dummy support, ε, was varied in a sinusoidal manner according to:

$$\varepsilon/b = \varepsilon_0/b + (\varepsilon_1/b)\, cos(\omega t) = \varepsilon_0/b + (\varepsilon_1/b)\, cos(2\pi f_e t)$$

where ε_0/b is the mean about which the motion oscillates; ε_1/b is the amplitude; and f_e is the frequency of the motion. Reduced frequencies in the range $0.015 < f_e c/U_\infty < 0.5$ were considered, representing a large range of possible aircraft manoeuvring speeds. The dummy supports used for oscillatory testing were the 12mm cylindrical and 96mm flat-plate supports placed at $x_{LE} = c/4$. The waveforms considered are illustrated in Figure 5.1, and may be described as follows:

A) A large amplitude oscillation with $\varepsilon_0/b = 0.285$; $\varepsilon_1/b = 0.285$, representing a motion that moves a considerable distance from the undisturbed vortex core location ($\varepsilon_{max} = 5$cm), and for both the flat-plate and cylindrical support $(\varepsilon/b)_{max} > (\varepsilon/b)_{CRIT}$.

B) A motion symmetric about the undisturbed vortex core location, so that $\varepsilon_0/b = 0$; $\varepsilon_1/b = 0.1$. This condition represents a small amplitude oscillation which does not move far from the vortex core and $|(\varepsilon/b)_{max}| < (\varepsilon/b)_{CRIT}$.

C) A small amplitude oscillation of amplitude $\varepsilon_1/b = 0.1$ offset from the vortex core by $\varepsilon_0/b = (\varepsilon/b)_{CRIT}$. For this waveform, the dummy support moves just outside and just inside $(\varepsilon/b)_{CRIT}$, where $(\varepsilon/b)_{CRIT} = 0.3$ for the 12mm cylindrical support and $(\varepsilon/b)_{CRIT} = 0.2$ for the 96mm flat-plate support. (The parameter $(\varepsilon/b)_{CRIT}$ was defined and discussed in Chapter 4).

To ensure that the oscillatory rather than transient response was measured, all data were recorded after at least 20 convective time scales ($20c/U_\infty$) following the start of the oscillating motion. Greenwell and Wood (1994) showed that the overall response time of vortex breakdown to a pitching disturbance is of the order of $10c/U_\infty$ and Gursul (2000) showed how the breakdown response was universal across a range of disturbing influences. The author was therefore satisfied that any transients had settled sufficiently by the start of each test.

5.2 Support Interference due to Oscillatory Support Motion

This section describes the vortex-support interactions in the absence of changes in vortex strength. First, the results of flow visualisations of the leading edge vortices are presented showing the location of the breakdown and its response to the oscillating motions considered. Analysis of these results in the form of cross spectra and phase averaging are then used to demonstrate the dependence of the breakdown location on the support oscillations over the range of oscillating frequencies. Following this, lift force measurements over a range of wings are used to expand understanding of the support interference effect.

5.2.1 Breakdown Location Response

The effect of an oscillating dummy support structure on the mean and instantaneous breakdown location was first studied using dye flow visualisation. All flow visualisation data were taken with a simple delta of $\Lambda = 80°$ at an incidence of $\alpha = 30°$. This wing configuration was shown to be particularly sensitive to support interference in static testing, and it therefore seemed natural to begin by considering support interference in oscillatory testing under these conditions also.

5.2.1.1 Breakdown location time history

Figure 5.2 - Figure 5.4 show the response of the breakdown to the 12mm cylindrical support at $x_{LE} = c/4$ for each of the oscillating motions considered. Figure 5.2 shows how a large amplitude oscillation (waveform A in Figure 5.1) affected the breakdown

location. Breakdown was observed throughout the support cycle at all of the frequencies considered, even when the support was at its greatest distance from the vortex and at the lowest frequency, $f_e c/U_\infty = 0.025$. To explain this observation, it is useful to recall the bifurcation analysis introduced in §4.3.1. It will be recalled that $(\varepsilon/b)_{CRIT}$ is the offset from the undisturbed vortex core location at which breakdown is first observed over the wing when stepping the support *towards* the vortex, while $(\varepsilon/b)_0$ is the offset at which breakdown dissipates when stepping *away* from the vortex. These parameters were explained figuratively in Figure 4.10. For the 12mm cylindrical support, $(\varepsilon/b)_{CRIT} = 0.32$ and $(\varepsilon/b)_0 = 0.65$. The largest distance from the undisturbed vortex core location that the cylinder achieved during the large amplitude oscillation was $(\varepsilon/b)_{max} = 0.57$, which lies in the range $(\varepsilon/b)_{CRIT} < (\varepsilon/b)_{max} < (\varepsilon/b)_0$. Thus even though the support moved out of its range of influence of the vortex, it did not move outside $(\varepsilon/b)_0$. The breakdown could not therefore propagate downstream between successive approaches of the support, even at low frequencies, and the breakdown location was constrained to $x'_{BD}/c < 1.0$.

Fluctuations of breakdown location were observed at all of the frequencies considered, but the magnitude of the fluctuations reduced with increasing forcing frequency. This showed that the vortex could not respond quickly enough at the highest forcing frequencies, and as such, the variations in the breakdown location were much less. The most upstream breakdown location during the support cycle was $(x'_{BD}/c)_{min} \approx 0.65$. This value appeared to be independent of forcing frequency, and was further upstream than was expected from the static case for $\varepsilon/b = 0$.

Figure 5.3 shows the effect of a small amplitude oscillation symmetric about the undisturbed vortex core location (waveform B). The magnitude of the breakdown fluctuations in this case was a lot smaller than for the previous case. Further, the effect of forcing frequency on the magnitude of the fluctuations was small. This might be expected considering that the support never moved outside of its range of influence, and it was therefore always directly affecting the vortex core. Breakdown was always observed forward of the trailing edge at a minimum value of $(x'_{BD}/c)_{min} \approx 0.68$, slightly upstream of static case at $\varepsilon = 0$. In this case $(x'_{BD}/c)_{min}$ was a function of forcing

frequency, with the breakdown moving slightly further downstream with increasing forcing frequency.

Figure 5.4 shows the breakdown response to waveform C for the cylindrical support. The response to this form of motion was similar to that observed for waveform A, with the magnitude of the breakdown location fluctuations reducing with increasing forcing frequency. However, it was noted that the breakdown did not propagate as far upstream in this case as for the large amplitude case. In this case $(x'_{BD}/c)_{min} \approx 0.78$, which was comparable with that observed at $\varepsilon = 0$ in the static case. Once again, consideration of the range of influence of the support may be used to explain these observations. For waveform C for the cylindrical support, the closest the support got to the undisturbed vortex core location was $(\varepsilon/b)_{min} = 0.2$, within the range of influence of the vortex and therefore close enough to induce breakdown. However, since the support did not reach the vortex core it had a reduced effect, and breakdown was not induced as far upstream. In this case $(x'_{BD}/c)_{min}$ was the same regardless of the forcing frequency.

Figure 5.5 - Figure 5.7 show the breakdown response to the 96mm flat-plate support for each of the oscillating waveforms. A large amplitude oscillation (waveform A), shown in Figure 5.5, induced large fluctuations in the breakdown location at low frequencies, and the amplitude of the fluctuations reduced with increasing frequency. It should be noted that in this case the magnitude of the fluctuations at $f_e c/U_\infty = 0.025$ were much larger than for the cylindrical support (note the scale of the plots differ), and the breakdown actually transits the trailing edge between each approach of the support. This may be explained by considering that for the plate $(\varepsilon/b)_0 = 0.52$, while for the cylinder $(\varepsilon/b)_0 = 0.65$. Thus at its greatest distance from the vortex core, $(\varepsilon/b)_{max} = 0.57$, the support was outside of its range of influence and the vortex was therefore able to begin its propagation downstream before the plate's next approach. Doubling the forcing frequency to $f_e c/U_\infty = 0.05$ significantly reduced the magnitude of the breakdown location fluctuations, as the breakdown no longer transited the trailing edge with each cycle. This was a result of the reduced time between each cycle during which the support was outside $(\varepsilon/b)_0$; the breakdown could not respond quickly enough to dissipate downstream, and was therefore constrained to the surface of the wing. In

contrast to the data presented for the cylindrical support, the value of $(x'_{BD}/c)_{min}$ was a weak function of the forcing frequency, with $(x'_{BD}/c)_{min} \approx 0.8$ and 0.9 at $f_e c/U_\infty = 0.025$ and 0.5 respectively. In addition, for all frequencies $(x'_{BD}/c)_{min}$ in the oscillating case was downstream of that observed in static tests; in-fact, it was considerably closer to the trailing edge, lying in the range $0.8 < (x'_{BD}/c)_{min} < 0.9$, compared with $(x'_{BD}/c)_{min} \approx 0.55$ for the static case.

Figure 5.6 shows the effect of waveform B. The most forward breakdown location was $(x'_{BD}/c)_{min} \approx 0.75$ at $f_e c/U_\infty = 0.025$, and was again weakly dependent on the forcing frequency. In contrast to the equivalent case for the cylindrical support, the amplitude of the breakdown location fluctuations reduced significantly with increasing forcing frequency.

Figure 5.7 shows that waveform C resulted in a further movement of the minimum breakdown location downstream to $(x'_{BD}/c)_{min} \approx 0.9$. For all the frequencies considered the mean breakdown location was close to the trailing edge, especially at higher frequencies where the magnitude of the fluctuations was small. In this case the mean breakdown location was in the region of the trailing edge for all the forcing frequencies considered, and was approximately 0.4c downstream of the static $\varepsilon = 0$ case.

Figure 5.8 summarises the variation of the mean and RMS breakdown location with forcing frequency for the support oscillations considered. Also shown on these plots is the value of x'_{BD}/c observed at $\varepsilon/b = 0$ in static testing. The mean breakdown location did not show a strong dependence on forcing frequency, with the only significant changes being seen between $f_e c/U_\infty = 0.025$ and 0.05. In most cases, a slight upstream movement of the mean breakdown location was observed with frequencies up to $f_e c/U_\infty = 0.25$. At the highest frequency this trend was reversed, with a slight downstream movement. It should be noted that although in some cases the mean breakdown location was downstream of the trailing edge, the most upstream breakdown location in these cases was always upstream of the trailing edge, and support interference was therefore still a factor.

While the mean breakdown locations for the small amplitude symmetric (B) oscillation of the plate and cylinder were similar, for the large amplitude (A) and small amplitude offset (C) oscillations the mean breakdown locations for the plate were much further downstream than those for the cylinder. Further, the mean breakdown locations for the cylinder were in the same region as was observed in static testing, with waveforms A and C being slightly upstream, and waveform B being slightly downstream. For the flat-plate support, the mean breakdown location was significantly further downstream for all the oscillating waveforms than was observed in static testing.

The RMS breakdown location was strongly influenced by forcing frequency, especially at low frequencies when the vortex had time to at least partially recover its natural state between successive approaches of the support. At high frequencies the RMS breakdown location tended to a value of $(x'_{BD}/c)_{RMS} \approx 0.035$, comparable with those found for breakdown induced by a static support under similar conditions (see Table 4.2), but was significantly increased at low frequencies for some support motions. At the lowest frequency $(x'_{BD}/c)_{RMS} \approx 0.06$ for the cylindrical support, double that observed in the static case, and $(x'_{BD}/c)_{RMS} > 0.25$ for the flat-plate support, more than seven times greater than the static case. So although large fluctuations of breakdown location were observed at low frequencies of support motion, at higher frequencies the breakdown response tended to that observed in the static case. This indicates that low frequency motions are of greater concern in terms of the magnitude of the support interference as not only is the mean breakdown location moved upstream, but there is a large fluctuating component that would affect spectral measurements of the flowfield.

5.2.1.2 Phase averaged breakdown location

Figure 5.9 shows the phase averaged breakdown location at each point through the support cycle for different frequencies of the large amplitude motion of the cylindrical support. The static response is also shown on these plots for comparison. At all frequencies the variation of breakdown location formed a hysteresis loop, with breakdown further downstream when the support was on its approach to the vortex than on its retreat. Note that the amplitude of the fluctuations of breakdown location in the dynamic case were not as large as those in the static case, as at no time did the phase

averaged breakdown location transit the trailing edge. Phase averaged breakdown locations were upstream of the static case at all points through the cycle, but the difference between the two cases was small, as was also shown in Figure 5.8.

The results show that the phase averaged $(x'_{BD}/c)_{min}$ for this case was independent of the forcing frequency, being approximately equal to 0.7. An increasing phase delay between the support motion and the breakdown location with increasing forcing frequency was observed as the movement of the location of $(x'_{BD}/c)_{min}$ in each of the plots. At $f_e c/U_\infty$ = 0.025, 0.05 and 0.125, $(x'_{BD}/c)_{min}$ occurs at ε/b = 0, 0.2 and 0.38 respectively. Further discussion of the phase delays is included in the following section. A further effect of increasing the frequency was to flatten the hysteresis loop. This was due to the vortex having less time to respond to the support motion as the speed of the support was increased, and is shown in Figure 5.2 - Figure 5.7 as a reduction in the magnitude of the breakdown fluctuations.

Figure 5.10 shows the phase averaged breakdown location for large amplitude motion of the flat-plate support. The hysteresis loop at the lowest frequency was much larger than that for the cylindrical support, which once more shows the effect of the smaller region of influence of this support. At all frequencies the breakdown was significantly further downstream in the dynamic case than in the static case. Not only this but the minimum phase averaged breakdown location moved further downstream with increasing forcing frequency. This indicates that the oscillation of the plate had a significant positive effect on the breakdown location, i.e. the mechanism by which the plate induced breakdown was actually alleviated by the oscillation of the plate. As the excitation frequency increased, the phase lag between the support location and the breakdown location also increased. This may be seen as the shift of the location of $(x'_{BD}/c)_{min}$ from $\varepsilon/b \approx 0.02$ to $\varepsilon/b \approx 0.2$ as the excitation frequency was increased.

Figure 5.11 shows the phase averaged breakdown location at the lowest forcing frequency, $f_e c/U_\infty$ = 0.025, for all three waveforms of the cylindrical support. Both small amplitude oscillations (B and C) of the cylindrical support induced breakdown locations comparable with those observed in the static case while the large amplitude oscillation induced breakdown only slightly further upstream. It may therefore be

concluded that the effect of oscillating the cylindrical support is small compared with the static case. Of course, in terms of the magnitude of the support interference effect, this means that the breakdown response is still severe. However, it also means that the breakdown response in oscillatory testing may be predicted by first studying the static response. The underlying conclusion here is that the mechanism that induces breakdown in the static and oscillatory cases is of equal magnitude, i.e. the process of oscillating the support neither worsens nor improves the vortex-support interaction process.

Figure 5.12 shows the similar comparison for the flat-plate support. All of the waveforms considered for the plate induced breakdown much further downstream than expected from the static case. In the case of the large amplitude and small amplitude offset motions (A and C), an explanation for this may lie in the fact that the phase averaged breakdown locations for these waveforms broached the trailing edge for part of their cycle. Since the fluctuations of the breakdown location were large, it is suggested that the breakdown did not have enough time to propagate upstream as far as expected. While this is a reasonable explanation, it does not explain why the small amplitude symmetric oscillation (B) also induced breakdown further downstream than expected. Since this oscillation results in the support never leaving its range of influence of the vortex it may be considered in many ways to be equivalent to the static case. Since in all the cases the breakdown was much further downstream than in the static case, it may be concluded that, in contrast to the effect of the cylindrical support, the mechanism resulting in breakdown of the vortices was in some way alleviated by the action of oscillating the flat-plate support.

5.2.1.3 Frequency domain analysis

The correlation between the relative motions of the breakdown location and the support are shown in Figure 5.13 and Figure 5.14. These plots show the variation of the cross-spectral density function over the frequency spectrum for the large amplitude oscillation (waveform A) of the cylindrical and flat-plate supports respectively. Note the change of scales between these figures. On each plot the location of the forcing frequency is indicated with an arrow, and it can be seen that in all the cases shown, the dominant

spectral peak occurred at the forcing frequency, indicating that a significant component of the frequency of the fluctuations of breakdown location was equal to the frequency at which the support was oscillated. This proves that the fluctuations of breakdown location were a result of the oscillation of the support, and were not just natural fluctuations. For both types of support, the correlation between the signals was largest at the lowest support frequencies, and the correlation fell as the excitation frequency increased, as would be expected from observations of the fluctuation magnitudes. The coherence between the signals fell to a background level at the highest frequencies, indicating only a very small dependence of the breakdown location on the motion of the support. This result confirms the previous observation that the RMS breakdown locations fall to a similar level to that found in static testing at high forcing frequencies (see §5.2.1.1).

The magnitudes of the dominant cross spectral peak as a function of forcing frequency for all the cases presented thus far are compared in Figure 5.15. At low forcing frequencies the breakdown location was dependent on the support motion to a large degree, but as the frequency increased this dependence dropped off. Between the two large amplitude motions, it was the plate that dominated more at low frequencies, while the cylinder had a greater effect at the higher frequencies, although the difference at higher frequencies was small. Of the small amplitude oscillations, it was waveform C that had the greatest effect at low frequencies. The inconsistency between some of the results shown at high frequencies may be explained by the reduced coherence between the signals resulting in a 'background' signal with a significant proportion of noise.

The results of previous investigations have shown a similar reduction in coherence between the breakdown location and a given forcing mechanism with increasing forcing frequency. Gursul and Xie (2001), for example, showed how the amplitude ratio comparing the motions of a vibrating fin with the response of the resultant breakdown, reduced with increasing forcing frequency. Further, the variation was observed within the same range of reduced frequencies as observed in the current tests, as Figure 1.14 shows. This is the first evidence that the results of Gursul (2000), who suggested the existence of a universal mechanism for forced breakdown of different types (see

§1.2.3.4), may be extended to include the current case of support interference, at least in the limited case of an oscillating dummy support.

Variation of the phase lag between the breakdown location and the support motion for the large amplitude oscillation of the cylinder and flat-plate is shown in Figure 5.16. This data was calculated from the cross-spectra presented above. Phase data is only shown at low frequencies, as for the higher frequencies, and in general for the other support cycles, the data were unsuitable for plotting due to the low resolution of data points (the breakdown location was only recorded at 10 points through each cycle), and the small amplitudes of motion considered which resulted in smaller coherence peaks. Also shown is the second order analysis of Greenwell and Wood (1994), who plotted a range of data published by other authors in an effort to determine the overall order of the breakdown response to a disturbance in the form of a pitching wing. They suggested that the breakdown response could be adequately modelled by a second order system with a gain, $K = 2$, and damping ratio, $\zeta = 1.67$. Finally, in order to compare the data with other experimental results, the data summarised by Gursul (2000) are also plotted.

The phase lags observed in the current results were much larger than would be expected from both the analysis of Greenwell and Wood, and from previous experimental results; the vortex takes longer to respond to the oscillation of the support structure than it does to the other forms of oscillating motion considered in literature. Qualitatively though, the data show similar trends, with the phase angle increasing with increasing forcing frequency. There may be a number of reasons why the phase angles observed in this case differ from those observed in other cases. Firstly, Greenwell and Wood only considered pitching motions that resulted in breakdown locations that were at all times forward of the trailing edge, as the discontinuity associated with the trailing edge "...only add[s] to the difficulty of interpretation of the results". In the current tests breakdown was observed to transit the trailing edge for the flat-plate at the lowest frequency, which may explain why the phase angle in this case is particularly high. Further, the forcing mechanism was fundamentally different from those considered in literature. The perturbation of the breakdown in this case is an imposed local pressure gradient at a point downstream of the trailing edge of the wing, whereas literature has

mostly considered the effect of forcing mechanisms that directly affect the formation of the vortices (oscillating pitch, leading edge flaps and sweep). Even in the case of an oscillating fin, which does not affect the formation of the vortex, the process occurs much further upstream than in this case. The effect of the local pressure gradient downstream will be reduced due to the much larger pressure gradient imposed by the trailing edge region. It has therefore been shown that the mechanism forcing the breakdown in the simplified oscillating support case is similar to those considered in literature, and that the presence of trailing edge effects in this case may explain the larger phase delays.

This section has documented the support-vortex interaction in the absence of time-dependent vortex strength effects by studying the time-history of breakdown location fluctuations induced by an oscillating dummy support structure. In terms of support interference, the current results have indicated that support interference in oscillatory testing is a particular problem. However, it should be remembered at this point that the simplified case of the moving support is being considered, and that a full understanding of the interference effect will not be elucidated until the more complex moving wing case is discussed. Before this case is considered, the moving support case is extended by investigating the effect of oscillating support structures on the lift force generated by the delta wing.

5.2.2 Lift Force Response

The range of cases considered in lift force experiments was widened due to the relative ease of analysis of the results compared to the flow visualisation data. Both the 70° and 80° wings were tested at two angles of attack each. For the 70° wing, incidences of α = 20° and 30° were chosen to represent the case where the breakdown is known to be sensitive to the dummy support, and an increased incidence when the breakdown will at all times occur forward of the trailing edge. For the 80° wing, incidences of α = 30° and 35° were chosen for the same reasons. For each of these model configurations the three oscillating waveforms were considered for each of the two dummy support configurations.

For brevity, only two examples of the lift force time-history are presented. Figure 5.17 and Figure 5.18 show how the lift force developed by the 80° wing varied due to the large amplitude oscillation (A) of the cylindrical and flat-plate supports respectively. In these plots the filtered lift force is shown to give an appreciation of the variation of lift force with time. The calculations that follow are all based on the unfiltered data. The lift force response was at first impression very similar to that of the breakdown location. For both supports considered, reducing the frequency of the support motion resulted in larger amplitude force oscillations. The time-history of lift force fluctuations due to the oscillation of the plate exhibited peak values which appeared to be 'capped', i.e. during the retreating phase of the support, the lift force increased to a certain level, at which it remained until the next approach of the support. This observation was attributed to the transition of breakdown over the trailing edge as illustrated by the time-history of breakdown location for the same case, shown in Figure 5.5. Since further movement of the breakdown downstream of the trailing edge does not affect the lift generated by the wing, the lift force appears to level off. This feature of the lift force response was not observed at any of the other frequencies, nor for the cylindrical support.

Figure 5.19 and Figure 5.20 show the results of cross-spectral analysis comparing the force and support motion signals for the same cases. These figures confirm that the greatest coherence was observed at the lowest frequencies, and the spectral peaks reduced in magnitude as the frequency of the motion was increased. At very high frequencies there was little coherence between the signals. The peak spectral magnitude for the cylinder and plates were similar in this case. Since fluctuations of breakdown location aft of the trailing edge do not influence the lift force generated by the wing, the large amplitude spectral peaks observed between the breakdown and support locations for the large amplitude oscillation of the plate (Figure 5.14) were significantly reduced when considering the coherence between lift force and support location.

The influence of support interference on lift force is summarised for all the cases considered in Figure 5.21 and Figure 5.22, which show the variation of the peak cross-spectral magnitude with excitation frequency for the 70° and 80° wings respectively. For all the configurations tested, a large amplitude oscillation (A) of either support resulted in a higher magnitude spectral peak at all frequencies than was observed for

either of the other cycles. The response to the small amplitude motions (B and C) was a little more complex, especially at higher frequencies when the peak spectral magnitudes dropped to a background level. For the 80° wing, at the lowest frequencies it was the small amplitude motion offset from the vortex core (C) that induced the strongest response. This result agrees with the response of the breakdown location spectra presented above, and is intuitively to be expected. However, for the 70° wing at both α = 20° and 30°, at some frequencies waveform B produced a more coherent response. As was observed for the breakdown location spectra, there was a degree of spread in the data for small amplitude oscillations (B and C) at high frequencies. This was due to the small coherence between the signals resulting in the signals becoming noisy – a further indication of the converging of static and oscillatory trends at high support frequencies.

The results show that the magnitude of the coherence between the signals is similar for equivalent angles of attack. For α = 30° for the 80° wing and α = 20° for the 70° wing, breakdown is not observed in the natural case, but is observed upstream of the trailing edge in static and oscillatory testing, and the results show that the magnitude of the coherence between the signals is similar for these cases. Likewise for α = 35° and 30° for the 80° and 70° wings respectively, breakdown is observed over the wing in all cases and spectral magnitudes between the cases are similar. This shows that provided the equivalent angles of attack are chosen, the breakdown response between different wings is similar.

Curiously, spectral magnitudes at the greater incidence were higher than at the lower incidence. This was unexpected as it was thought that the movement of the breakdown over the trailing edge at the lower incidence would induce larger magnitude oscillations of the breakdown location (take Figure 5.5 as an example: when the breakdown transits the trailing edge at the lowest frequency, the magnitude of the breakdown fluctuations is large, but when the breakdown remains over the wing at higher frequencies, the magnitude of the fluctuations is small). This may be a result of the fact that once the breakdown has moved downstream of the trailing edge, no further reduction in lift force will result so although the magnitude of breakdown fluctuations was large, the magnitude of the lift force fluctuations will be smaller. In addition, as the incidence of

the wing is increased and breakdown now remains over the wing at all times, the magnitude of the lift force fluctuations will therefore increase.

Figure 5.23 shows the variation of the phase lag between the support location and force balance signals for large amplitude oscillations, and compares these with the second order theoretical response suggested by Greenwell and Wood (1994). At low frequencies the data were qualitatively consistent, showing increasing phase lag with increasing forcing frequency, and were also similar to the calculated delays between the support motion and the breakdown location indicating that there is little phase delay between breakdown location and lift force developed by the wing. The majority of the points at low frequencies lay above the proposed analyses of Greenwell and Wood, indicating that the phase delay for this form of perturbation was greater than that for the pitching wing motions on which the analyses are based. Once again it is pointed out to the reader that the analysis of Greenwell and Wood considered only motions in which breakdown did at no time broach the trailing edge during each cycle of the pitching wing, and this may represent the difference between the data and the analysis. High frequency data were of poor quality due to the diminishing magnitude of the signals and increasing noise level, and are therefore not presented.

This section has extended flow visualisation results of the previous section to include the effect of the vortex-support interaction on the lift force generated by a wing. It has been shown that the effect of the premature breakdown is to induce a reduction of lift over the wing. The magnitude and frequency of the fluctuations of lift force are dependent on the oscillating frequency of the dummy support, as was also shown using flow visualisation data. Preliminary data show that increasing incidence results in lift force fluctuations of a greater magnitude, contrary to expectation. This implies that the effect of support interference is to significantly affect the spectral component of any lift force measurements, and that increasing incidence results in more affected results.

Vortex-support interactions in the simplified case of constant vortex strength have therefore been investigated, and the principal conclusion to be drawn from the data is that support interference is a significant factor throughout the range of forcing frequencies considered. At low frequencies, large fluctuations of breakdown location

are observed, altering not only the mean lift force, but the spectral characteristics of the flow. At high frequencies premature breakdown is induced over the wing, although the fluctuations of breakdown locations reduce to a magnitude expected from static testing at $\varepsilon = 0$.

5.3 Support Interference due to Oscillatory Model Motion

The closing sections of this chapter complete the investigation of oscillatory support interference by examining the moving wing case. In the following tests, flow visualisation is used to yield breakdown locations, which are correlated with the wing motion and support locations to give an indication of the extent of support interference in this case. Finally, PIV measurements are used to investigate the topology of the flow on the suction surface of the wing, and in particular the time-dependent nature of the development of the leading edge vortices during the movement of the wing, in order to study the mechanism of the vortex-support interaction.

All experiments were carried out with the $\Lambda = 80°$ wing at $\alpha = 30°$, with oscillating frequencies in the range $0.015 < f_e c/U_\infty < 0.5$ and a dummy support at $x_{LE} = c/4$, for direct comparison with the moving support case discussed above. Further, the same oscillating waveforms were considered, which are summarised in Figure 5.1. The complexities of combining the force balance with the oscillating mechanism prevented the measurement of unsteady lift force over the moving wing, and so dye flow visualisation and PIV were the main experimental tools used.

5.3.1 Breakdown Location Response

First, the effect of the oscillating wing in the absence of a dummy support was studied. Figure 5.24 shows the effect of a laterally oscillating wing on the breakdown location of one of the leading edge vortices in the absence of a dummy support for waveform A (see Figure 5.1). In this figure, the visualised vortex was on the windward side of the model during the decreasing ε/b phase of the cycle. At frequencies below $f_e c/U_\infty = 0.25$,

no breakdown was observed. However, at $f_e c/U_\infty = 0.25$ and 0.5, the motion of the wing alone was sufficient to induce premature breakdown of the vortex.

An interesting feature of the breakdown response was the discontinuity in the breakdown location at various points in the cycle. At approximately t/T = 0.4 in each cycle, the breakdown was seen to rapidly move upstream from a position 0.4c downstream of the trailing edge to 0.1c upstream, behaviour which will subsequently be referred to as *breakdown jumping*. Similar jumping of the vortex breakdown location in unsteady testing was observed by Gursul and Ho (1994) who were investigating the effect of an unsteady free-stream on the breakdown location. The phenomenon was observed to varying degrees over a range of delta wing models, regardless of the angles of sweep and incidence, indicating that it is a universal response of the breakdown to an unsteadiness of this form. While Gursul and Ho were investigating the effect of a sinusoidal oscillation of the free stream velocity, this study is effectively considering the effect of a sinusoidal variation of cross-flow velocity. Since the breakdown location is thought to be independent of Reynolds number (Erickson, 1982, for example), it is likely that the response observed by Gursul and Ho was due to the unsteadiness in the flow, rather than the magnitude of the velocity through the cycle. In the current tests, the variation of the cross-flow velocity results in a change in the effective sweep angles of the leading edges of the wing, which in turn affects the strength of the vortices generated by the wing. Additionally, the effects of the unsteadiness due to the oscillation of the wing will also have an effect on the response of the vortices. Vortex strength effects will be quantified in the subsequent section; attention will currently focus on the breakdown response to these unsteady effects.

Figure 5.24 shows that the effect of increasing the frequency of the oscillating motion was to move the mean breakdown location upstream. Additionally, at $f_e c/U_\infty = 0.25$ some breaks in the time-history were observed due to the breakdown being washed downstream. This did not occur at $f_e c/U_\infty = 0.5$, indicating that the amplitude of the breakdown response reduced with frequency, as would be expected from previous results. The data show that vortex strength effects dominated only at high forcing frequencies, since no breakdown was observed at frequencies below $f_e c/U_\infty = 0.25$.

Figure 5.25 and Figure 5.26 show how the breakdown responds to the cylindrical and flat-plate supports placed in the wake of the moving wing for the same case as shown in Figure 5.24. At low frequencies the breakdown responses were similar to that for the moving support case, with $(x'_{BD}/c)_{min} \approx 0.7$ for both supports. In contrast to the moving wing in the absence of a support, the breakdown was, with few exceptions, always upstream of the trailing edge. At the lowest frequency a degree of incoherence was observed in both cases, even though the overall response was clearly periodic with a period equal to that of the forcing frequency. As the forcing frequency was increased to $f_e c/U_\infty = 0.25$, the amplitude of the breakdown location fluctuations decreases. However, above this frequency, the amplitude of the fluctuations increases, and the breakdown fluctuations appear more coherent than at low frequencies. This shows that the mechanism forcing the breakdown location to fluctuate is different at high and low frequencies. Comparison of the data shown here with that presented for the moving support shows that at low frequencies it is the presence of the support in the wake of the wing that induces the breakdown, whereas at the higher frequencies it is the effect of time-dependent vortex strength that is dominating the breakdown process. The data shows that while in the unobstructed case (shown in Figure 5.24) vortex strength effects dominated at frequencies above $f_e c/U_\infty \geq 0.25$, when the cylindrical support was placed downstream vortex strength effects did not become apparent until $f_e c/U_\infty > 0.25$. This was because the vortex strength effects at anything but the highest frequency were hidden by the already fluctuating breakdown location, and the fact that the presence of the support was constraining the breakdown to $x'_{BD}/c < 1$.

In the case of the oscillating wing in the presence of a dummy support, even though vortex strength effects were clearly dominant at the highest frequency, similar jumping of the breakdown location was not observed. Comparison of Figure 5.25 and Figure 5.26 with Figure 5.24 shows that the dummy supports constrain the breakdown location to $x'_{BD}/c < 1.0$. It is suggested that since the magnitude of the fluctuations is much smaller, the variation in vortex strength (thought to be the cause of the breakdown jumping as will be shown below) would not have such a dramatic effect on the breakdown location. Therefore, the effect of the support is to shift the breakdown

location upstream at high frequencies, and support interference is therefore still a factor when time-dependent vortex strength effects dominate.

Variation of the magnitude of the dominant cross-spectral density of model motion and breakdown location with forcing frequency is shown in Figure 5.27; also shown for comparison are the results presented previously for the moving support (see Figure 5.15). This figure is particularly revealing, and highlights some of the fundamental differences between the moving support and moving wing cases. In the moving wing case, there is little difference between the response of the breakdown to either of the supports. The large amplitude oscillation (waveform A) induces the largest coherence between the signals, and the small amplitude oscillation (waveform B) the smallest. Coherence between the signals is greatest at low frequencies, and reduces with increasing forcing frequency until the effects of vortex strength begin to dominate the breakdown process above $f_e c/U_\infty = 0.25$, at which point the coherence between the signals increases once more. The small amplitude offset oscillation induces a very small coherence at low frequencies, and the signal only increases with increasing forcing frequency. There are therefore many differences between the moving wing and moving support cases. In the moving support case, for example, it is easy to see the differences between the breakdown response to the cylinder and flat-plate. In the moving wing case, the conclusions relating to the mechanism of breakdown in the moving support cases do not apply. It is easy to see from the preceding figures that the plate induces a very similar response to the cylinder, and no beneficial effect is observed when the wing is oscillated.

Note that the dominant spectral peak at higher frequencies was observed for the oscillating wing in the absence of a support structure. This may be explained by comparing the time-histories presented above. In the absence of a support the breakdown location is free to transit the trailing edge, whereas in the presence of a support the breakdown is constrained to $x'_{BD}/c < 1$. The larger magnitude breakdown location fluctuations in this case result in a greater spectral peak. In this sense, it may be concluded that it is in fact of benefit to have a dummy support structure, since the presence of the support reduces the magnitude of the breakdown fluctuations. However, this argument does not consider the fact that the fluctuations of breakdown location

generated in the moving wing case are the 'natural' case, and when testing a wing in this manner one would *expect* to observe fluctuations of this form. These results do, however, indicate a fundamental difference between the form of support interference in the moving support and moving wing cases: in the moving support case the support induces artificial fluctuations of the breakdown location; in the oscillating wing case, the natural fluctuations of the breakdown due to changing vortex strength are damped by the presence of the support at high frequencies, and exaggerated at low frequencies.

To summarise, the effect of support interference in oscillatory testing is to affect the mean breakdown location throughout the range of test frequencies. Although at high frequencies the breakdown location is more dependent on the strength of the vortices than on the support location, the effect of the support is still to promote breakdown. It must therefore be concluded that support interference is a factor throughout the range of oscillating frequencies considered. The point at which time-dependent vortex strength effects begin to dominate the breakdown process for the large amplitude motion is $(f_e c/U_\infty)_{CRIT} \approx 0.25$, which is high for realistic aircraft manoeuvres.

The remaining sections of this chapter focus on the changes in the flow structure observed in dynamic testing, and attempts to explain some of the observations made.

5.3.2 Observations of time-dependent vortex strength effects

Flow visualisation data have shown that time-dependent vortex strength effects dominate for cases where, for the current configuration, $f_e c/U_\infty \geq 0.25$. However, further observations relating to the unsteady nature of the vortex under these conditions have also been made. It has been noted that the trajectories of the leading edge vortices are altered by the cross-flow velocity imposed by the wing motion. Figure 5.28 shows visualisations of the lateral and vertical deflections of the vortex core resulting from the lateral movement of the wing, compared with the static case. The images were captured at t/T = 0.25 and 0.75, at which the velocity of the wing was greatest in both directions of the motion. When the visualised vortex was on the windward side of the wing (t/T = 0.25), the vortex moved slightly closer to the wing compared to the static case, and shifted towards the wing centre-line. When on the leeward side (t/T = 0.75), the vortex moved away from the wing surface and centre-line. Similar observations of the

deflections of vortex trajectories due to sideslip were made by Guglieri and Quagliotti (1997). In their tests, Guglieri and Quagliotti considered the effect of static sideslip on the leading edge vortices of a 65° wing, and showed that the vortices were deflected in a similar manner to that shown herein.

Figure 5.29 shows a sequence of flow visualisation images showing the large deflections of the vortex that were observed during the large amplitude motion of the wing at a high frequency, $f_e c/U_\infty = 0.5$. At the beginning of the sequence, the visualised vortex was in the lee of the model motion, and, as expected from the images presented in the previous figure, the vortex is lifted away from the suction surface of the wing. However, at $t/T = -0.2$, a small 'kink' in the trajectory of the vortex may be observed just aft of the apex of the wing, the position of which is indicated as an arrow in Figure 5.29. As the wing continued its motion, this kink moved downstream and, as it did so, seemed to grow significantly. At $t/T = 0$, the vortex was seen to bend through an angle of approximately 30°. By the time the wing had reached $t/T = 0.2$ into the next cycle, the kink in the vortex trajectory had been washed out. It is thought that this large instability of the vortex is a result of the change in direction of motion of the wing, due to which the leading edges changes their effective orientation to the flow. Due to the effective change in sweep resulting from the change in direction, the vortex moves from an elevated position above the wing to a position close to the wing surface. In the high frequency case, the change from one orientation to the next occurs rapidly, and the realignment of the vortex is therefore similarly rapid, and a kink is formed in the vortex.

As the time series shown in Figure 5.29 progresses, a rapid movement of the breakdown location in the upstream direction was observed at some point in the cycle. At $t/T = 0.2$, the vortex undergoes what may be described as a double breakdown as the breakdown undergoes a step change in its location. Upstream of the clearly defined breakdown at $x'_{BD}/c \approx 0.9$, at approximately 0.6c, there is a region of turbulence that will develop into the primary breakdown at $t/T = 0.3$. It almost appears as if two breakdowns exist in the vortex simultaneously. This 'double breakdown' phenomenon was also observed in transient tests, as will be seen in the subsequent chapter.

The only previous account of this phenomenon in literature is given by Sarpkaya (1971b). In carefully controlled vortex tube experiments, the existence of clearly defined trains of bubble breakdowns were observed as the swirl angle of the flow was rapidly increased. However, Sarpkaya makes it clear that a train of breakdowns of this form represents an unstable solution of the flow, and that the existence of multiple breakdowns was observed for only a short time before instabilities present downstream propagated upstream to destroy all but the primary breakdown. The observations of Sarpkaya may be compared directly to those presented here. In the current results, vortex jumping, and associated double breakdown, was only observed on the advancing side of the wing, the side on which circulation (and therefore swirl angle) were increasing. Additionally, the existence of the double breakdown as a transient phenomenon is recognised. Although the vivid visualisations of multiple breakdowns produced by Sarpkaya have not been reproduced in the current results, this may be accounted for by the differences between vortex tube and delta wing vortex experiments. It is possible that double breakdowns have also been observed in static testing over delta wings. Despite considering it worthy of only a brief mention, Lowson and Riley (1995) observed a region of double breakdown in static testing of a 70° delta with a 25° apex flap at high angles of attack, although few details of their observations are given.

The observations presented in this section may be summarised as follows. As the wing moves laterally through the fluid, the effective sweep angle on the leading side is reduced while that on the trailing side is increased. It may therefore be deduced that the circulation (and swirl angle) of the windward vortex is consequently increased, resulting in premature breakdown compared to the static case. Conversely, the leeward vortex experiences a reduction of circulation and breakdown on that side is therefore delayed. The variation of the effective sweep angle of the leading edges may also explain the vertical deflections of the vortices, since low sweep delta wings tend to develop vortices much closer to the wing surface than do higher swept wings (Gursul *et al*, 2002); the windward vortex (that has developed from a leading edge of reduced effective sweep angle) is therefore lowered towards the wing surface. The wandering of the vortices

observed during the wing motion is summarised and illustrated figuratively in Figure 5.30.

A mechanism based on the observations of Sarpkaya (1971b) has been proposed above to explain the jumping of the breakdown location during the motion of the wing. It has been suggested that as the frequency of the wing motion increases, the variations in vortex strength occur more rapidly, and that at a given point the increase in vortex strength is sufficient to induce a train of breakdowns that rapidly disappear, leaving only the most upstream breakdown as evidence of the jump. This may be explained physically by considering the response time of the breakdown. When the strength of the vortex increases rapidly, the breakdown will tend to move forward rapidly also. If the breakdown cannot respond quickly enough to move forward in a smooth manner, then a new breakdown is formed upstream of the original one. Since the original breakdown is in the wake of the new breakdown, it will soon become distorted and disappear.

An association of the double breakdown with the change in circulation has been hence hypothesised. The following section aims to qualify this hypothesis with quantitative measurements of vortex strength variations resulting from the oscillation of the wing, and discusses the topology of the flow in detail.

5.3.3 Flow topology

Particle Image Velocimetry (PIV) was used to document the time-dependency of the vortex strength and trajectory observed above. The cross-flow velocity field throughout the cyclic motion of the wing was studied at x/c = 0.8 at the highest forcing frequency, $f_e c/U_\infty = 0.5$, and at a free-stream velocity of $U_\infty = 0.1$m/s. Figure 5.31 shows velocity vectors plotted on contours of constant vorticity at eleven points during the cycle. The fields are phase-averaged over 10 frames.

Near the beginning of the cycle (t/T = 0.120) the size and strength of the leading edge vortices were approximately equal, with any differences being remnants of the previous cycle. As the wing continued its motion (in these images the wing moved to the left during the first half of the cycle, and to the right to complete the cycle), the windward vortex (on the left of the image) began to strengthen and move towards the model

centre-line. As it did so, the vortex was seen to flatten and shift slightly towards the surface of the wing. During this half of the cycle, the leeward vortex (on the right of the image) moved away from the model centre-line and lifted significantly from the surface of the wing. At t/T = 0.681 the vortices once again became approximately equal in strength and size, indicating the phase lag between the model motion and the response of the vortices. At this point in the cycle the vortices had swapped their orientations, with the former windward vortex now becoming the leeward vortex, and vice versa.

An analysis of vortex strength using vorticity, as plotted in Figure 5.31, is limited as it is a point measurement related to the angular velocity of a fluid element at that point. Most often when discussing the strength of a vortex one is referring to its circulation, which is the integral of vorticity within a closed curve. The relationship between vorticity and circulation, and methods for calculating them have been discussed fully in Chapter 3. The variation of circulation of the leading edge vortices during the motion of the wing was calculated in order to provide a more accurate understanding of how the strength of the vortices varied through the oscillating cycle. Plotted in Figure 5.32 is the variation of the normalised circulation of the left vortex with normalised time (t/T) and integration square size (h/b). As expected, the magnitude of circulation was strongly dependent on the size of the integration square for small values of h, but the value reached a plateau at around h/b = 0.227. For values of h greater than this, in some cases there was a drop in the calculated circulation. This reduction was due to the square boundary encroaching on vortical structures of the opposite sign, a feature that results from the relative movement of the vortices during the oscillation of the wing. For the purposes of this analysis, h/b will be taken to be 0.227, at which the highest values of circulation were observed.

For clarity, the value of circulation calculated for a constant h/b of 0.227 is plotted separately in Figure 5.33. Also plotted in this figure are the variation of breakdown location for the same case, and the variation of the position and velocity of the wing through the cycle. At the start of the cycle, the vortex was seen to strengthen, reaching its peak strength of $\Gamma/cU_\infty = 0.4$ at t/T = 0.49, almost exactly half way through the cycle. The strength of the vortex did not rise continuously though, and between t/T = 0.2 and 0.3 a slight reduction in circulation was observed, although the cause of this reduction is

not apparent. Following the peak in strength, the vortex rapidly loses strength, falling to $\Gamma/cU_\infty = 0.32$ at $t/T = 0.68$. The value of circulation then continues to reduce more slowly, reaching a minimum at $t/T = 0.96$, before rapidly rising once more at the beginning of the subsequent cycle

Comparing the data presented in Figure 5.33 with that presented in Figure 4.5, the values of circulation observed in the current tests were slightly below that expected from the static tests presented above. However, it should not be forgotten that the calculations of circulation were performed at the trailing edge in the static case, and at $x/c = 0.8$ in the oscillating case. Assuming a linear increase of vortex strength along the wing (similar assumptions have been made previously by Hemsch and Luckring, 1990, and Traub, 1997), one might therefore expect a circulation of $\Gamma/cU_\infty = 0.4 \times 0.8 = 0.32$ in the static case at $x/c = 0.8$. This value lies towards the lower range of values presented in Figure 5.33, indicating that the overall effect on the oscillation of the wing is to impart greater strength to the vortex; i.e. the vortex strengthens significantly from the static case when leading the motion, but the opposite motion does not lead to a drop in circulation of the same magnitude. Further testing would be required to draw more firm conclusions about the behaviour of the vortex strength in this manner.

Considering the variation of the velocity of the wing through the cycle, it is curious that the peak vortex strength was observed at $t/T = 0.49$, when the velocity of the wing was approaching zero. This indicates the presence of a phase delay between the wing motion and the response of the leading edge vortices. Previous flow visualisation results have indicated that the realignment of the vortex following a disturbance begins at the apex and continues downstream; this may be the origin of the phase delay between the motion of the wing, and the value of circulation measured at $x/c = 0.8$.

It was hypothesised in the previous section that it was a rapid infusion of vorticity from the leading edge on the advancing side of the wing that results in the breakdown jump phenomenon observed during flow visualisation experiments. Figure 5.33 shows that the advancing vortex does experience a rapid increase in vortex strength due to the increased effective sweep resulting from its lateral motion. It is also apparent from Figure 5.33 that the location of the vortex jump during the cycle coincides almost

exactly with this increase in vortex strength. These results therefore lend weight to the previous proposition, although further testing is required to fully explore the interaction between these phenomena.

5.4 Chapter Review

This chapter has documented the effect of support interference in oscillatory dynamic testing. This section reviews the conclusions and discussions pertinent to this chapter. First, the experimental approach to the investigation is reviewed, following which the effects of support interference in the case of the moving support and moving wing are summarised. Following this is a discussion of the combined effect of support interference in oscillatory testing. Finally, the observations relating to the variation of vortex strength in the moving wing case are reviewed.

The simplified condition of support interference in the case of constant vortex strength was first considered. This was achieved by oscillating the dummy support structures downstream of the delta wing models, and measuring the effect on both the breakdown location and lift force generated by the wing. Next, the more realistic oscillating wing case was considered. In most cases two dummy supports were considered, being the 12mm cylindrical and 96mm flat-plate supports placed at x_{LE} = c/4. A number of oscillatory waveforms were chosen to represent different dynamic cases, being one large amplitude oscillation, and two small amplitude oscillations with different mean locations. The 80° wing at 30° incidence was used for the majority of the tests.

The effect of an oscillating dummy support was to induce fluctuations of breakdown location with a frequency equal to that of the support oscillation. As the frequency of the support motion was increased, the magnitude of the breakdown fluctuations reduced, to the point where RMS breakdown fluctuations at very high frequencies were similar to those observed in static testing. Cross-spectral analysis of the breakdown location confirmed the reduction of the magnitude of the breakdown fluctuations with increasing forcing frequency.

The effect of the cylinder was to induce a response that was largely indifferent from that observed in static testing. Mean and phase-averaged breakdown locations have shown that the breakdown location was similar regardless of the oscillating frequency, although significant phase lags were observed as the forcing frequency was increased. The effect of oscillating the flat-plate support was to delay the onset of breakdown to a point much further downstream than observed in static testing. The action of oscillating the support actually improved the breakdown response.

Analysis of the peak cross-spectral magnitudes have shown that the amplitude of the breakdown oscillation falls with increasing forcing frequency, and that the reduction in amplitude occurs over the same range of reduced frequencies as observed for other forms of forced oscillation considered in literature, such as oscillating pitching, leading edge flaps and sweep angle. Phase calculations showed that the breakdown response in the moving support case was slower those observed in literature. The mechanism of this delay is suggested to be the trailing edge, so that despite the larger phase angles, the response is thought to be comparable with the group of forcing motions examined by Gursul (2000).

Lift force measurements confirmed the presence of fluctuations of lift force of a frequency equal to that of the support oscillation and the breakdown location fluctuations. Thus the effect of premature breakdown is to significantly affect the lift force generated by the wing. It was concluded that the effect of support interference in the simplified case of constant vortex strength is significant at all frequencies, although the effect on the breakdown response differs at high and low frequencies. At low frequencies a large amplitude fluctuating component is induced affecting spectral characteristics and magnitudes of the measured forces. At high frequencies the fluctuating components reduce significantly, but the time-averaged breakdown location is in all cases upstream of the trailing edge when in the natural case breakdown does not occur. At high frequencies the breakdown response tended to that observed in static testing.

A number of time-dependent vortex strength effects have been identified in this research which, whilst not directly relevant to the support interference problem, are interesting

none the less. At a sufficiently high forcing frequency, the breakdown location was observed to undergo a step change from a position downstream of the trailing edge, to one upstream of the trailing edge. This step change results in the formation of a double breakdown instantaneously in the flow. Similarities with the results of Sarpkaya (1971b), and subsequent experiments have shown that this response may be due to the rapid increase of circulation of the leading edge vortex due to the motion of the wing.

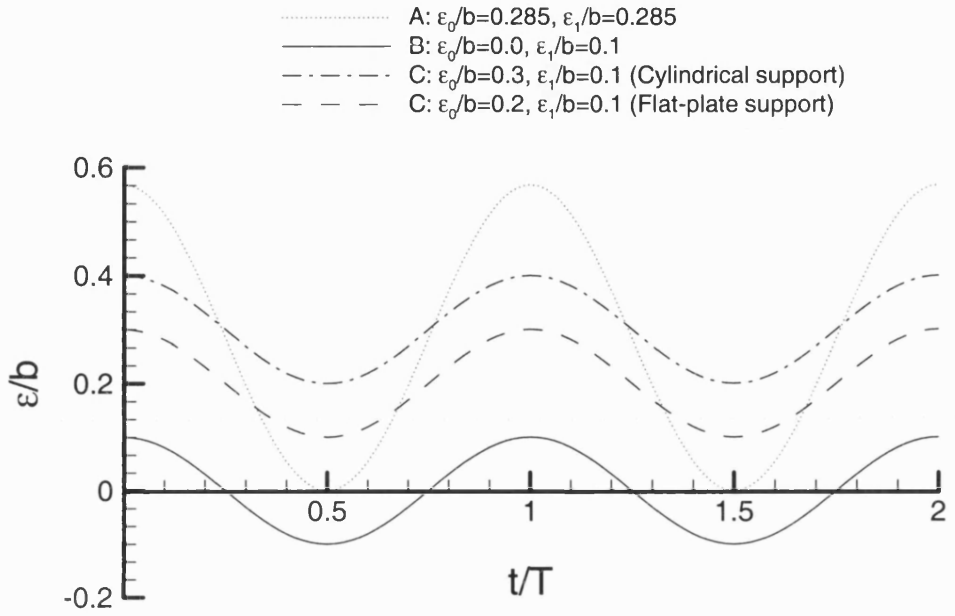

Figure 5.1: Time history of the oscillatory dummy support and wing motions.

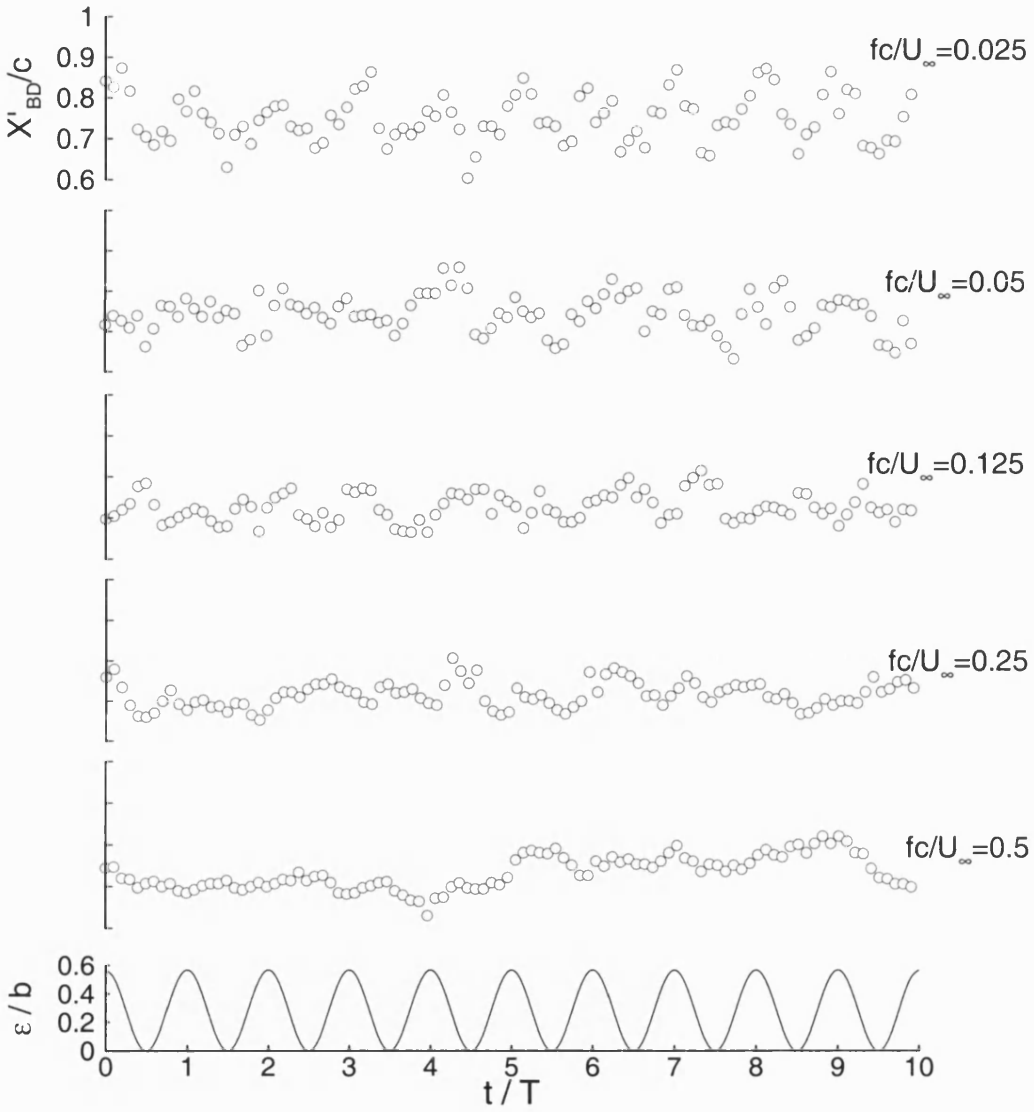

Figure 5.2: Breakdown response to oscillatory support motion; waveform A, cylindrical support.

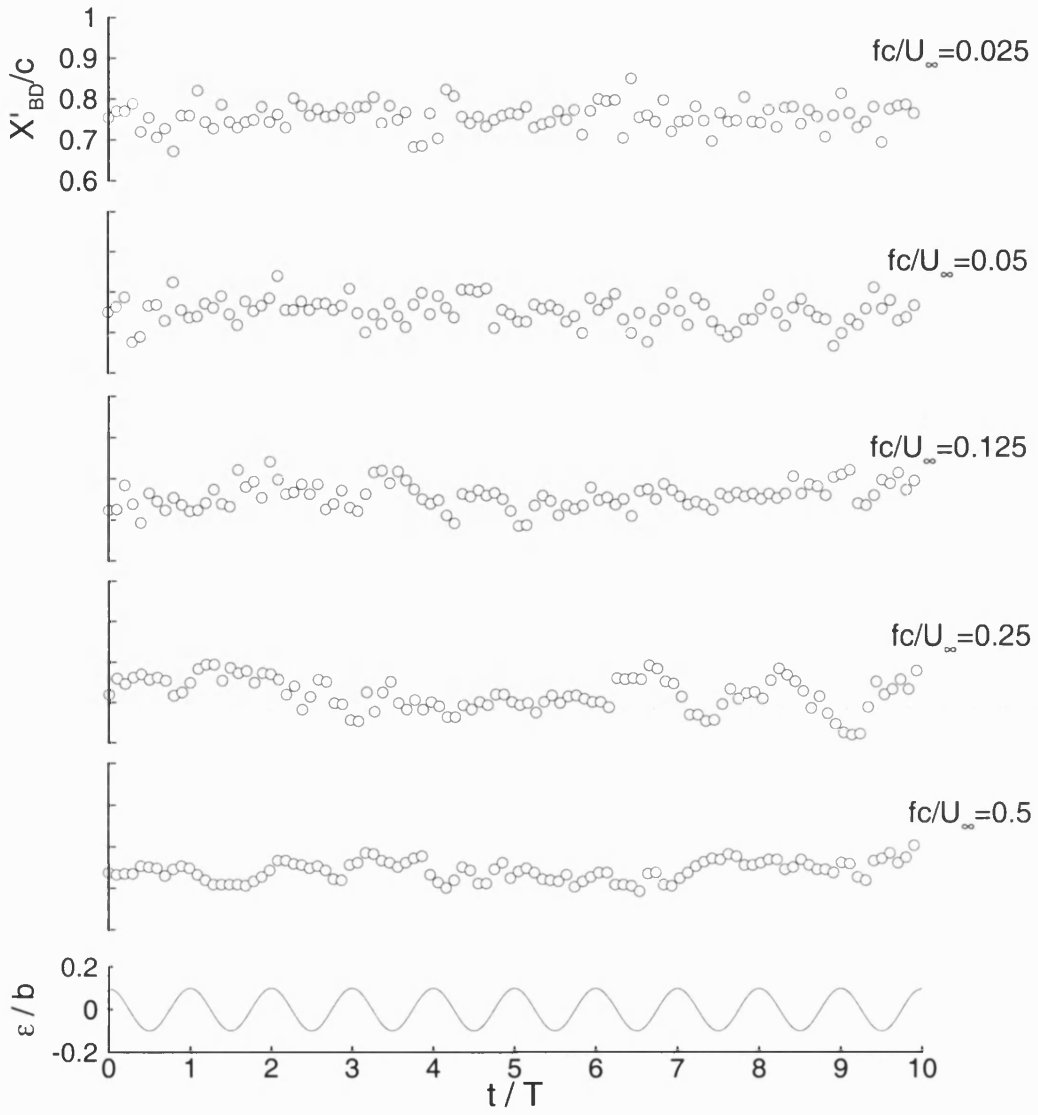

Figure 5.3: Breakdown response to oscillatory support motion; waveform B, cylindrical support.

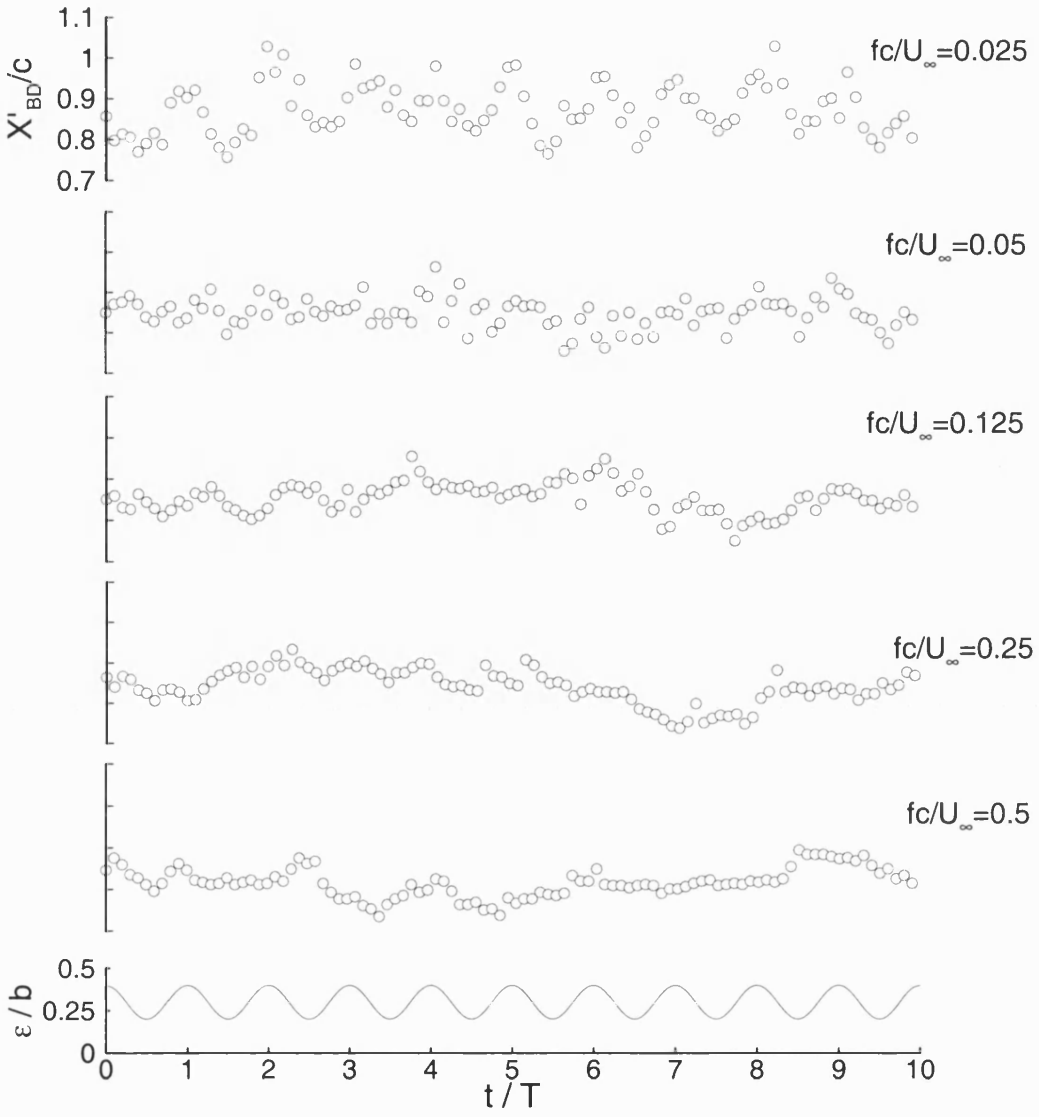

Figure 5.4: Breakdown response to oscillatory support motion; waveform C, cylindrical support.

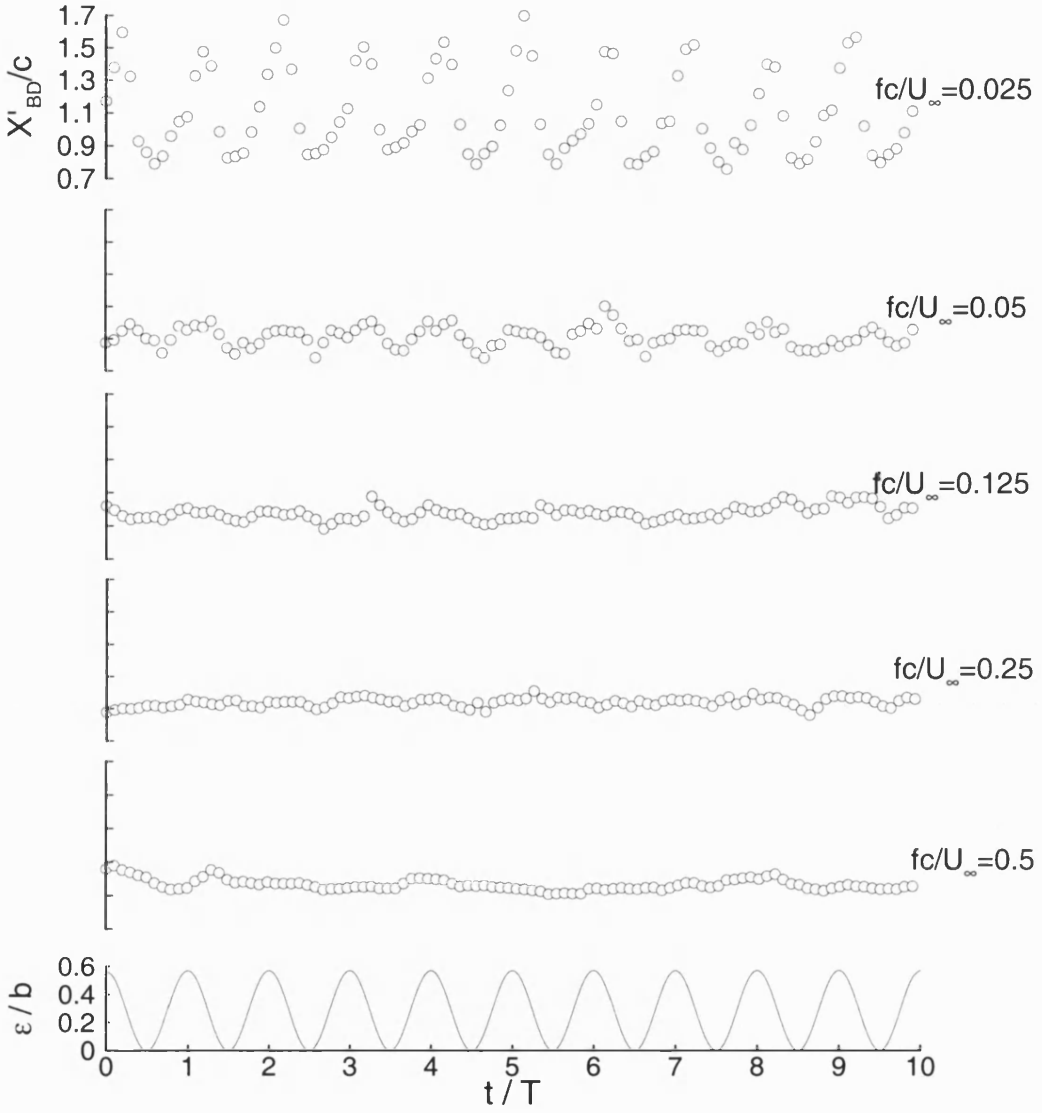

Figure 5.5: Breakdown response to oscillatory support motion; waveform A, flat-plate support.

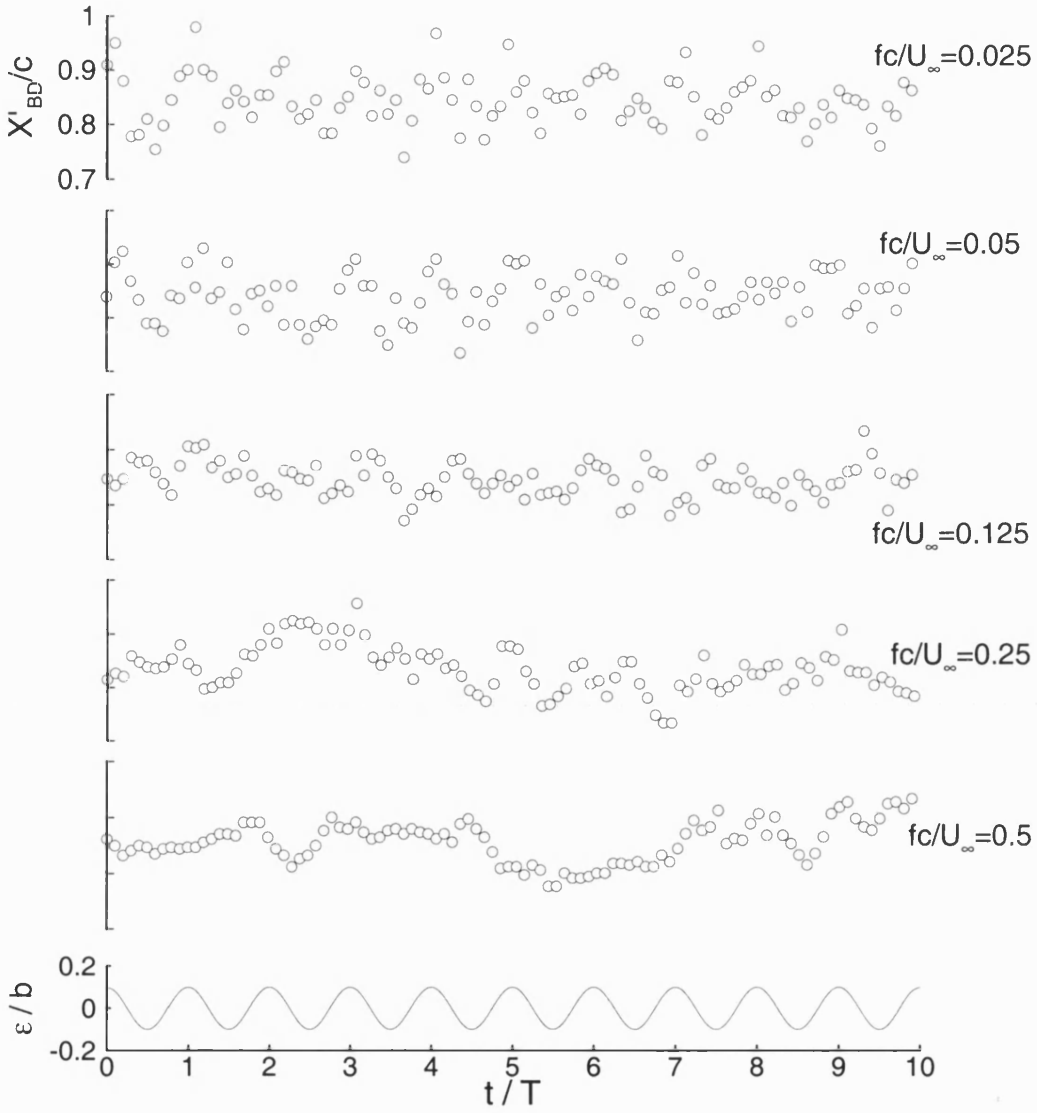

Figure 5.6: Breakdown response to oscillatory support motion; waveform B, flat-plate support.

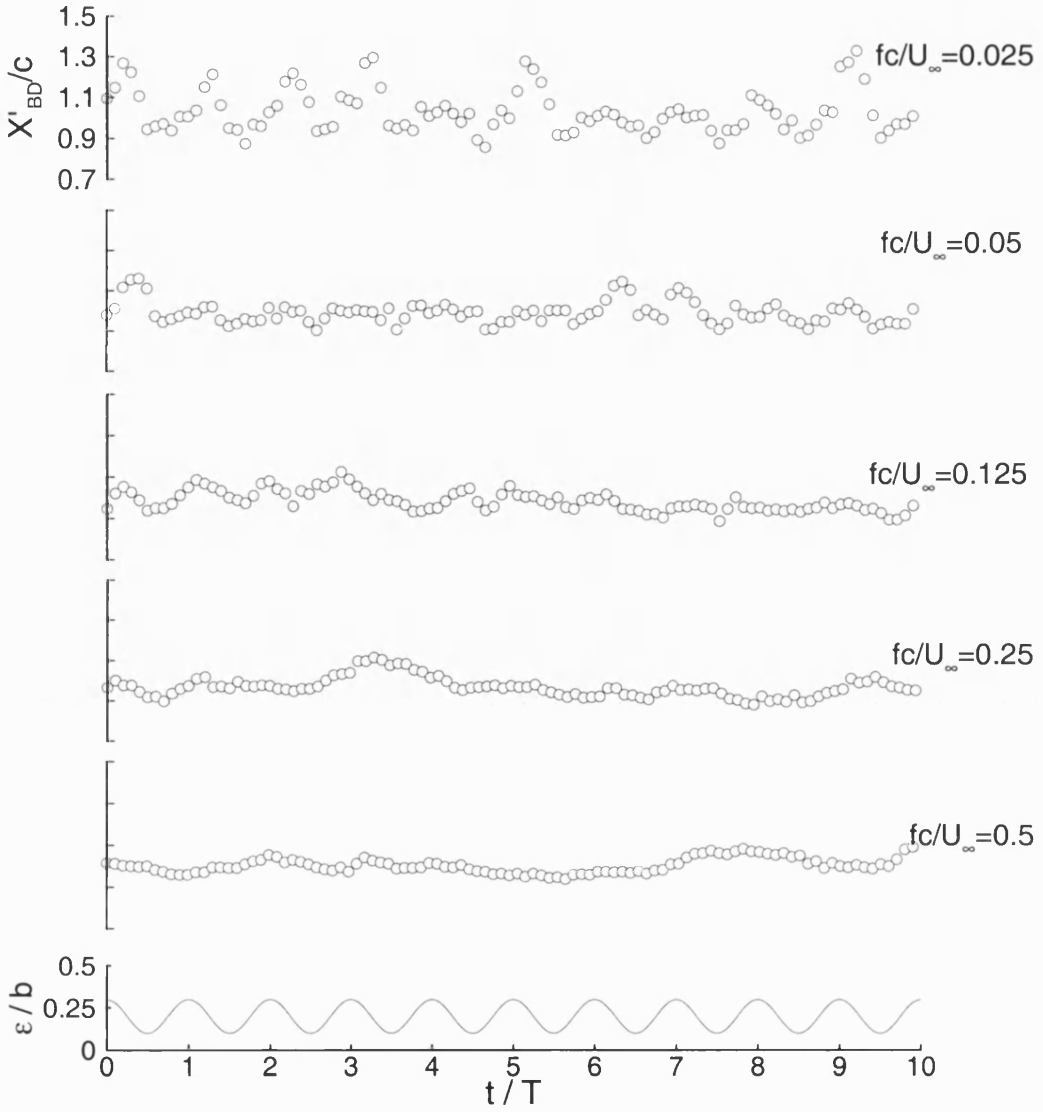

Figure 5.7: Breakdown response to oscillatory support motion; waveform C, flat-plate support.

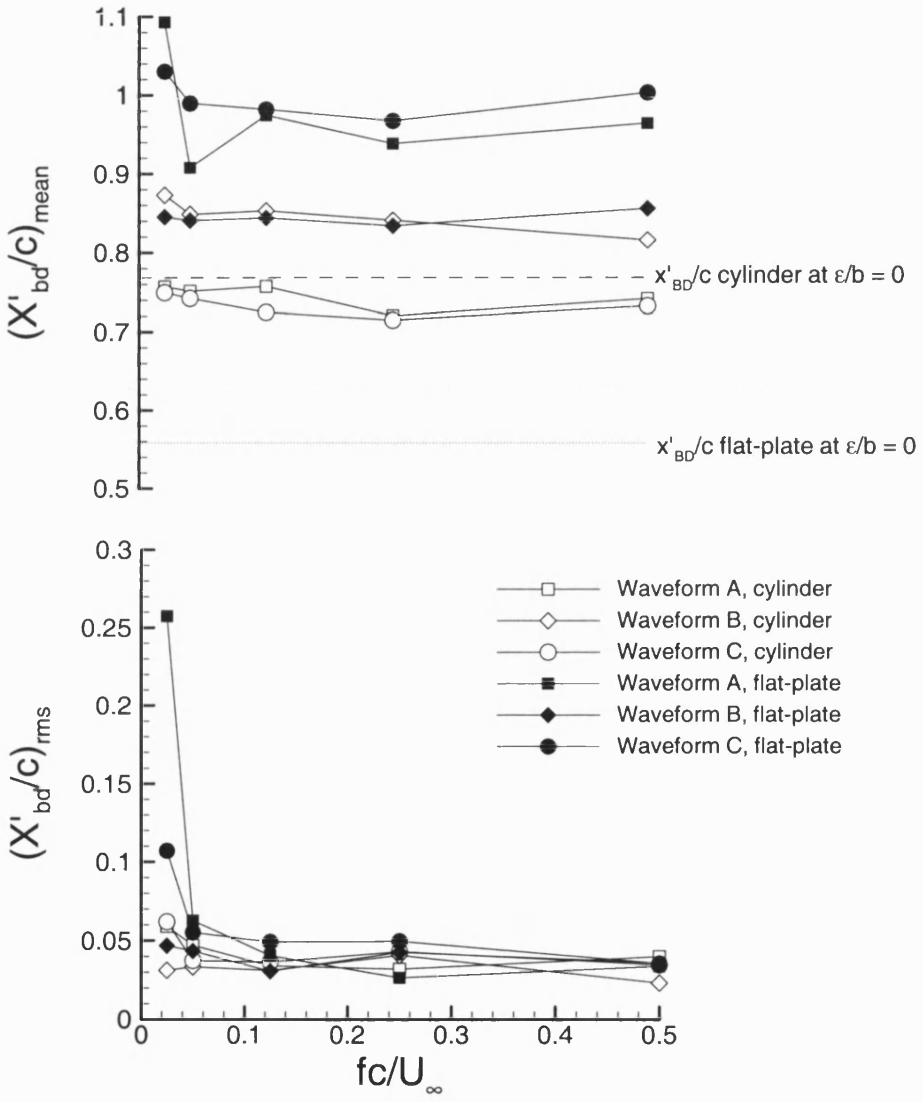

Figure 5.8: Mean and RMS breakdown location with frequency and waveform.

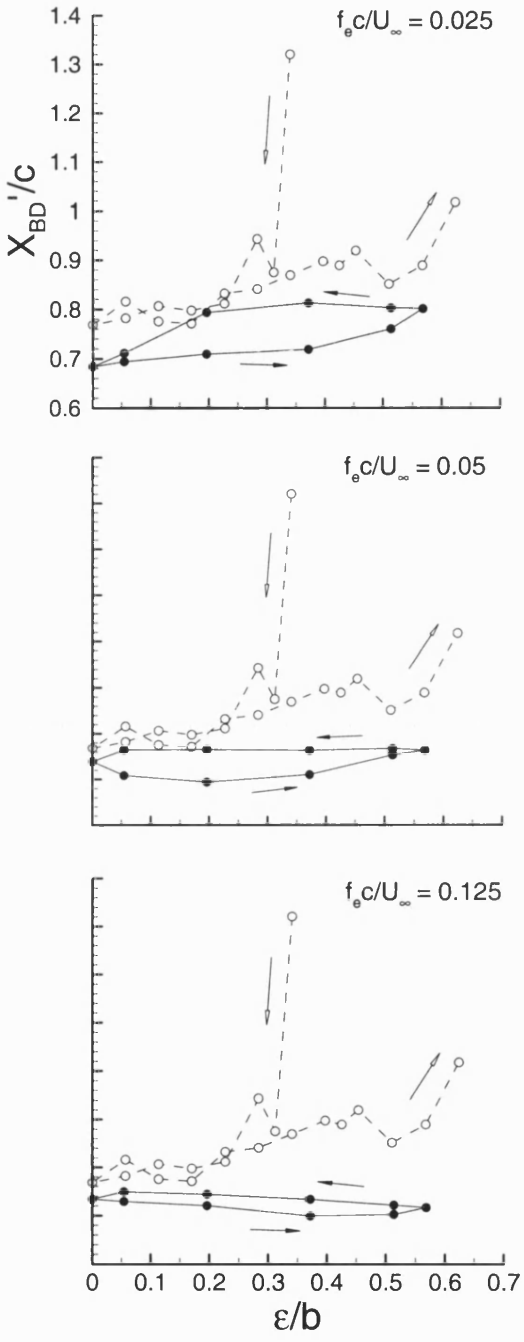

Figure 5.9: Variation of phase averaged breakdown location with ε and frequency; waveform A, cylindrical support.

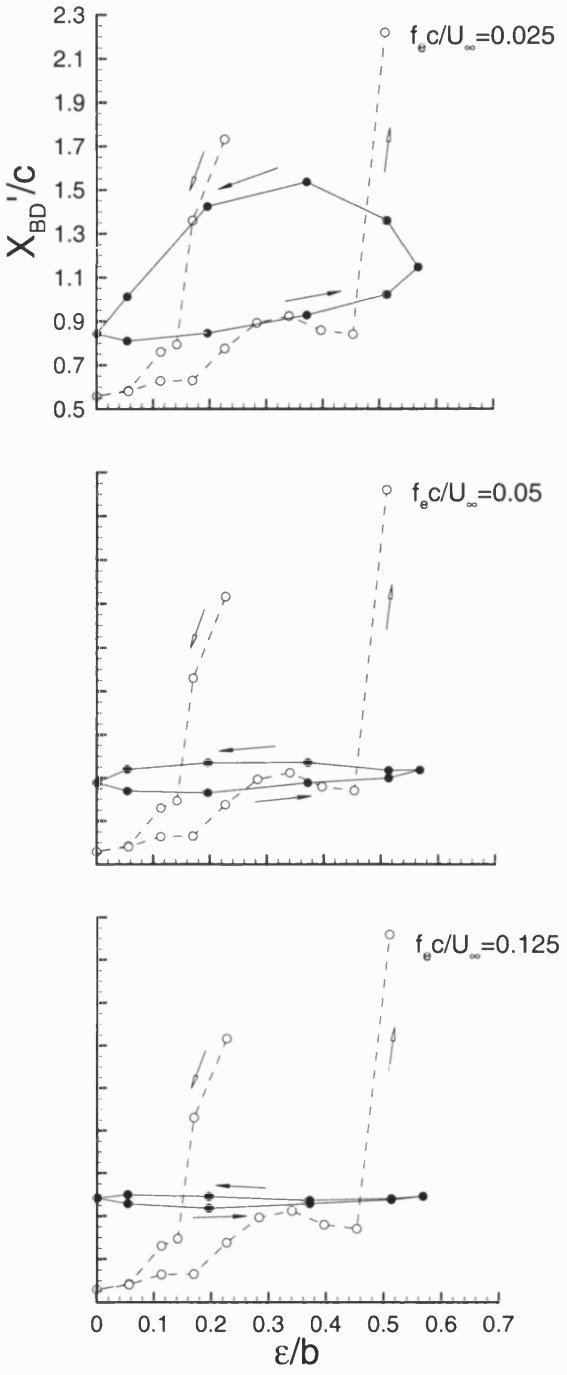

Figure 5.10: Variation of phase averaged breakdown location with ε and frequency; waveform A, flat-plate support.

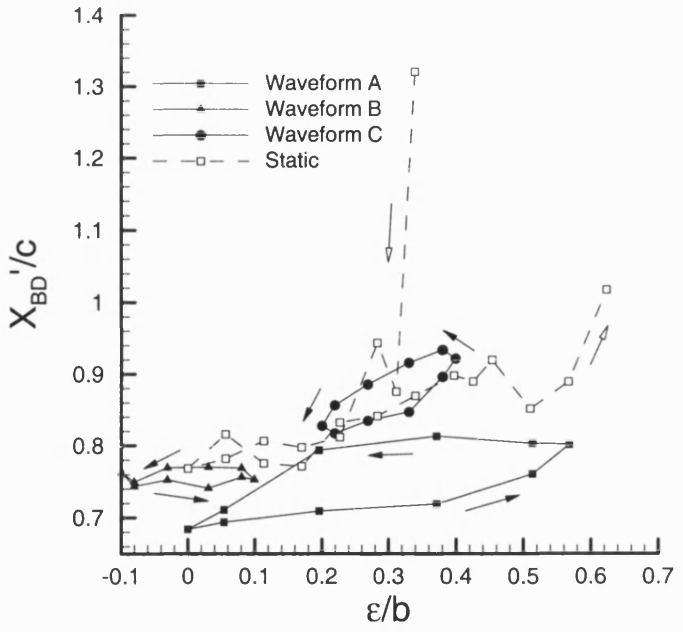

Figure 5.11: Variation of phase averaged breakdown location with ε and oscillatory motion; cylindrical support, $f_e c/U_\infty = 0.025$.

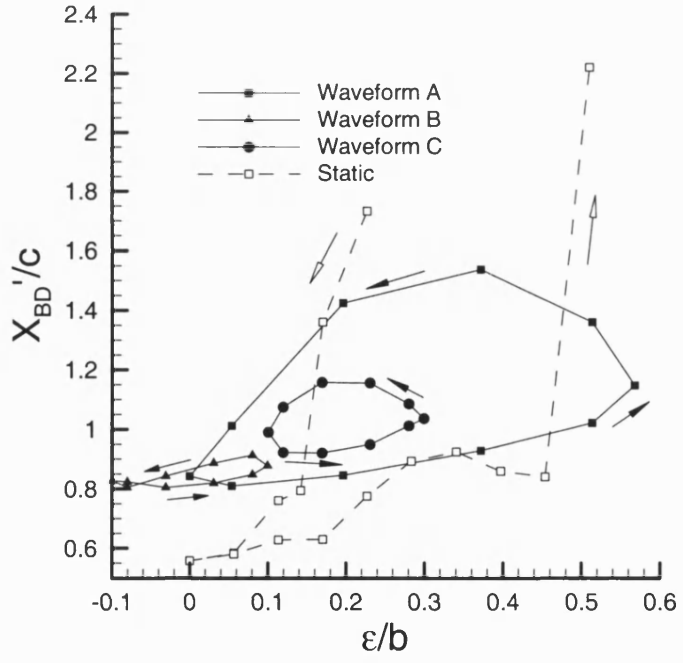

Figure 5.12: Variation of phase averaged breakdown location with ε and oscillatory motion; flat-plate support, $f_e c/U_\infty = 0.025$.

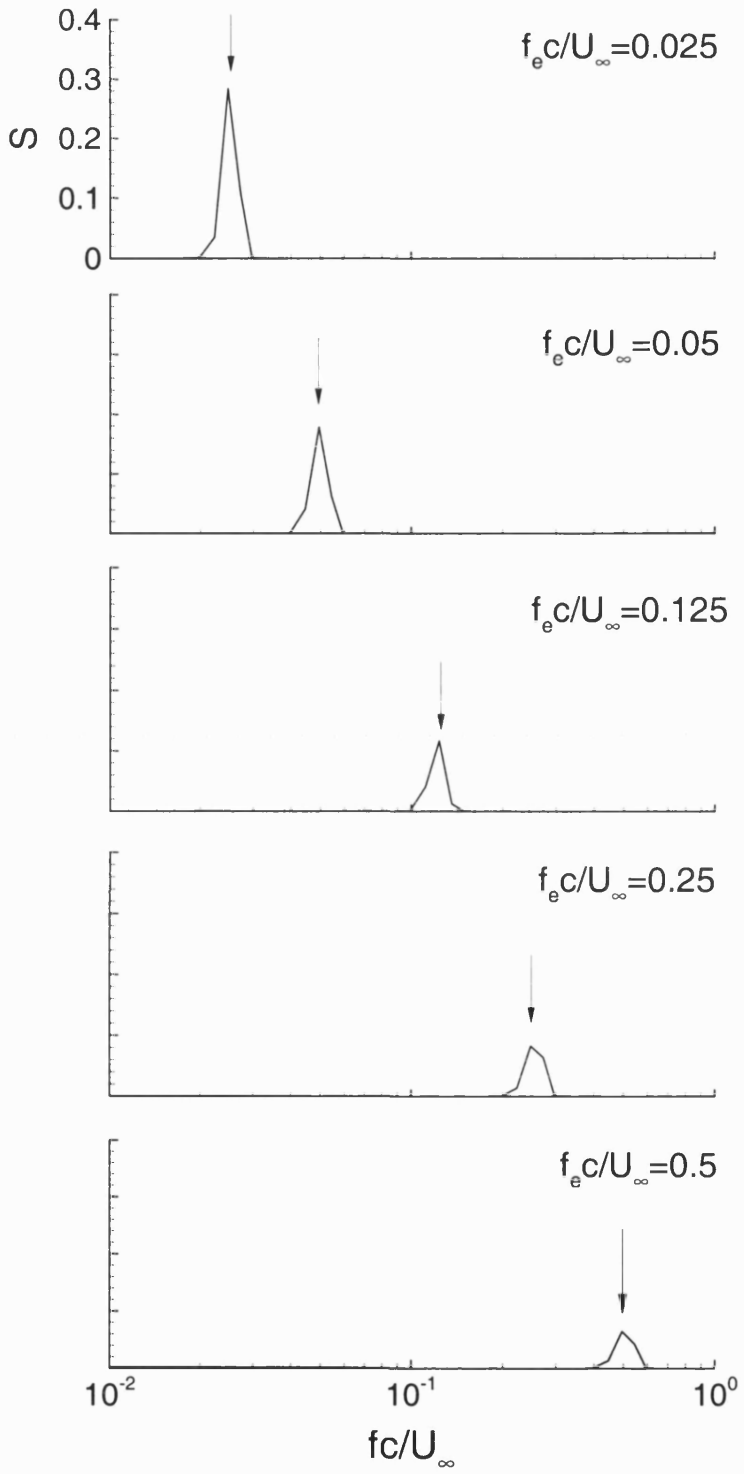

Figure 5.13: Cross spectral density of x'_{BD}/c and ε/b as a function of forcing frequency; waveform A, cylindrical support.

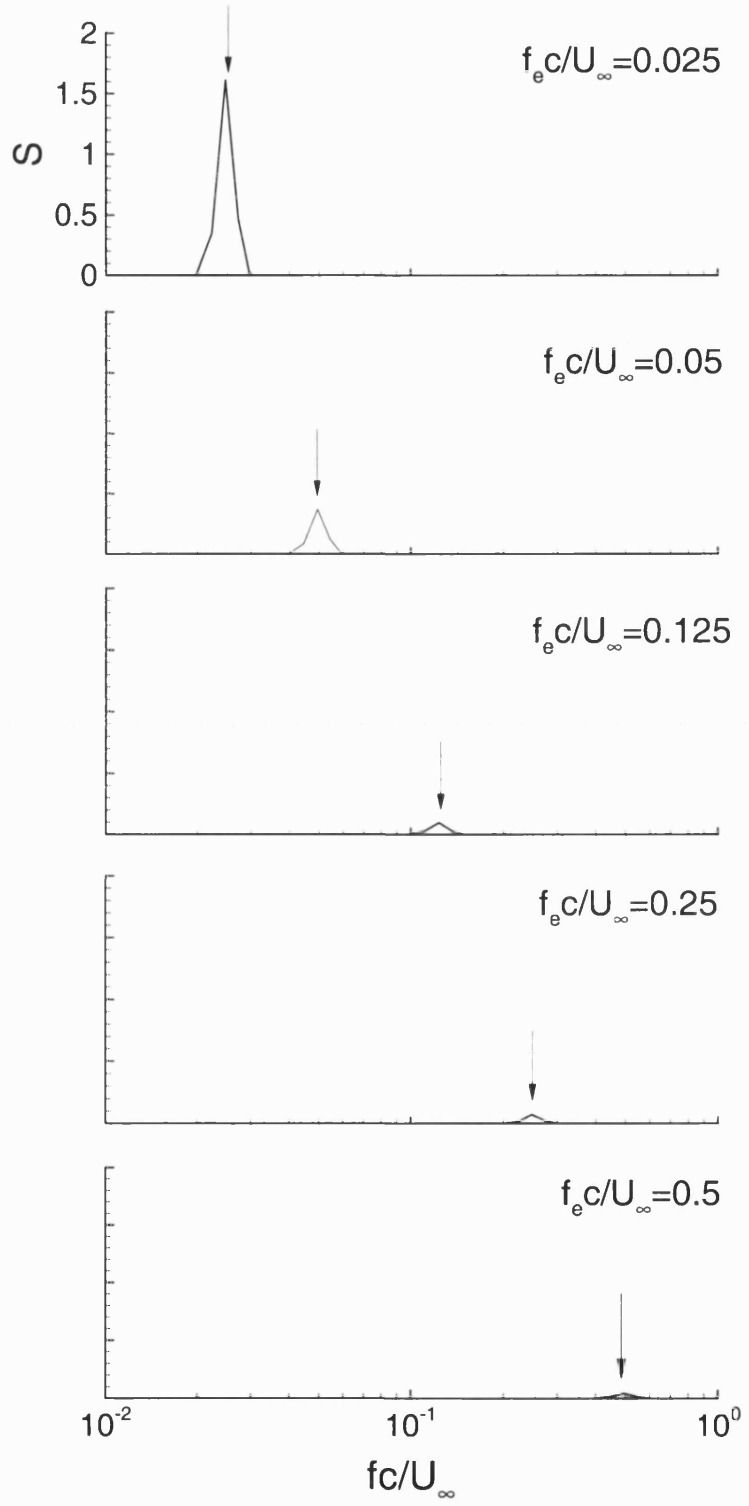

Figure 5.14: Cross spectral density of x'_{BD}/c and ε/b as a function of forcing frequency; waveform A, flat-plate support.

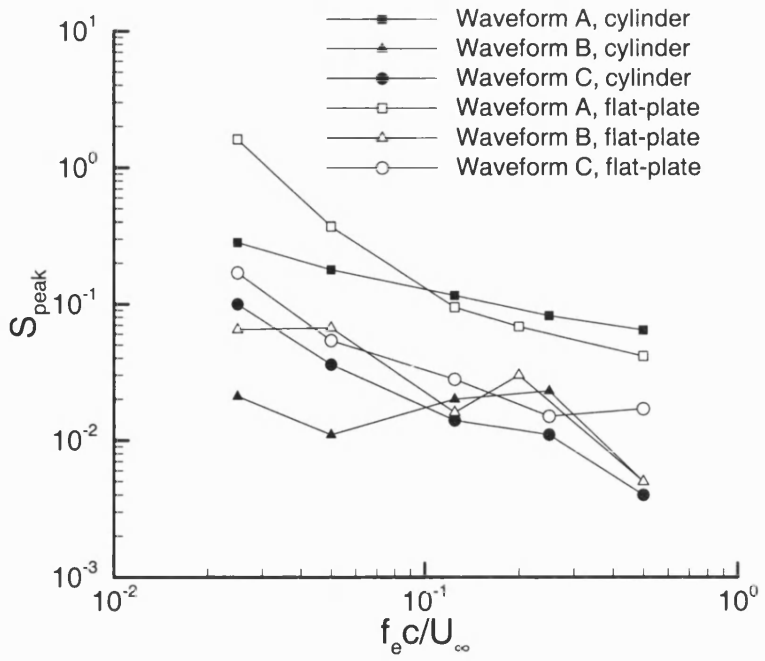

Figure 5.15: Variation of magnitude of dominant cross-spectral density of breakdown and support locations.

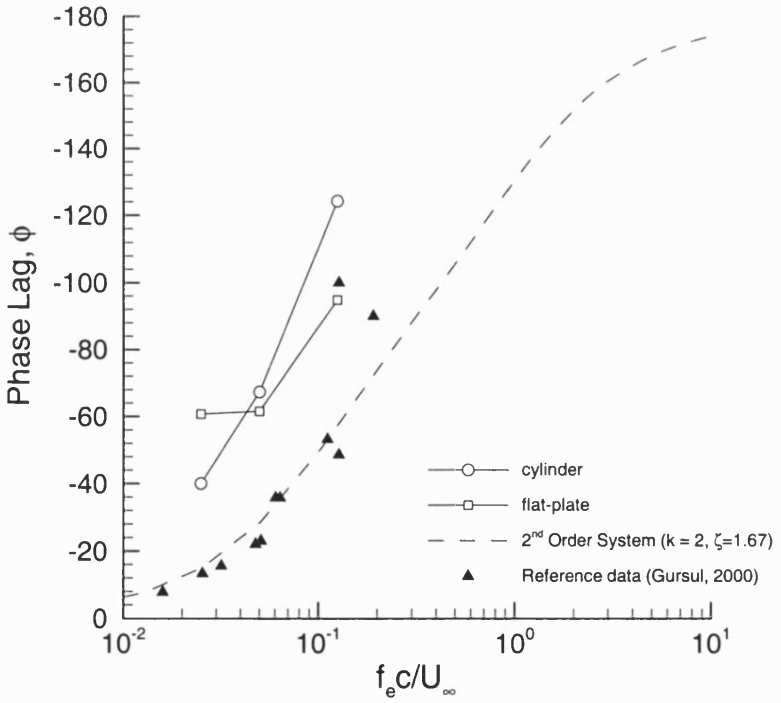

Figure 5.16: Variation of phase lag between support motion and breakdown location for cylindrical and flat-plate supports.

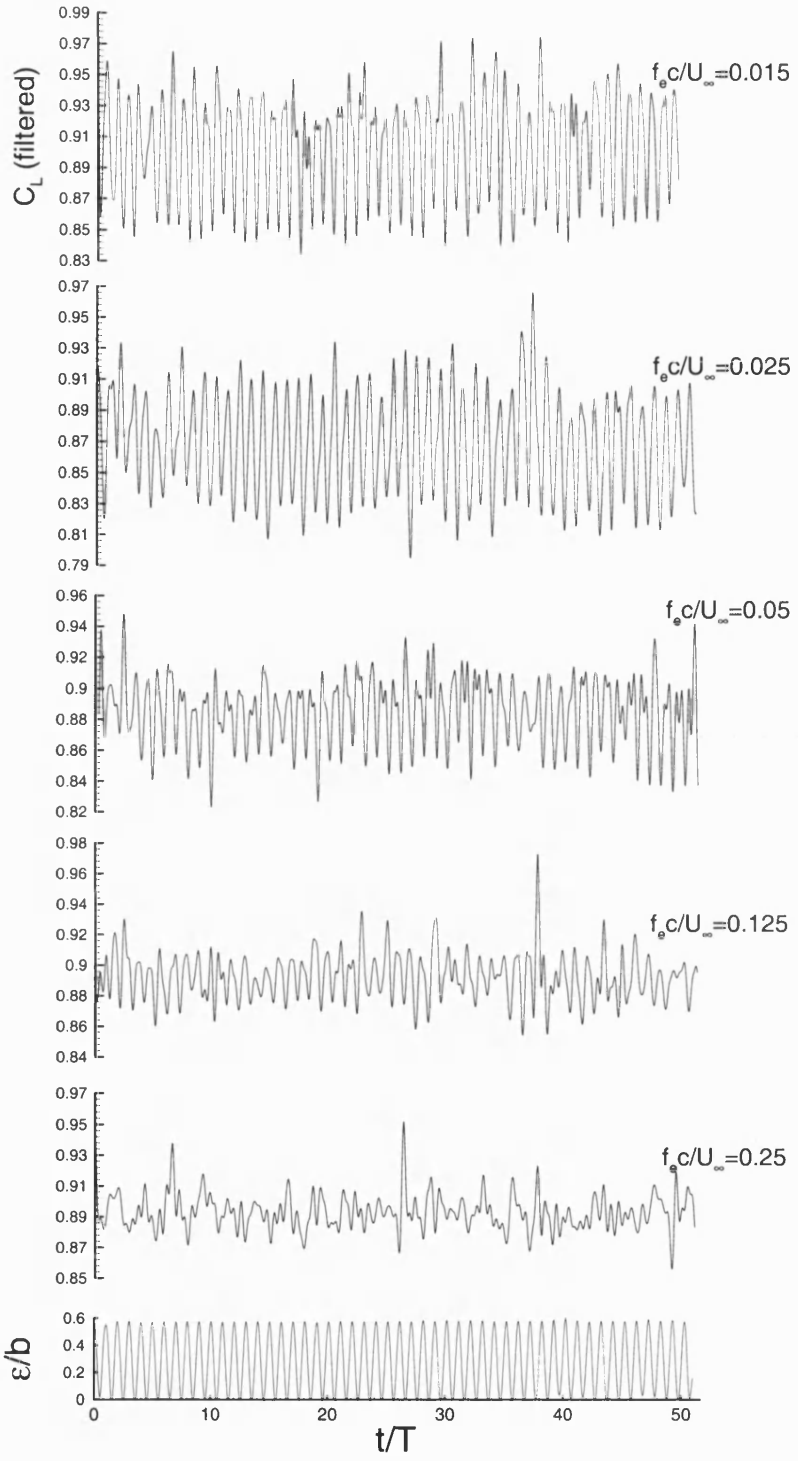

Figure 5.17: Lift force response; waveform A, cylindrical support.

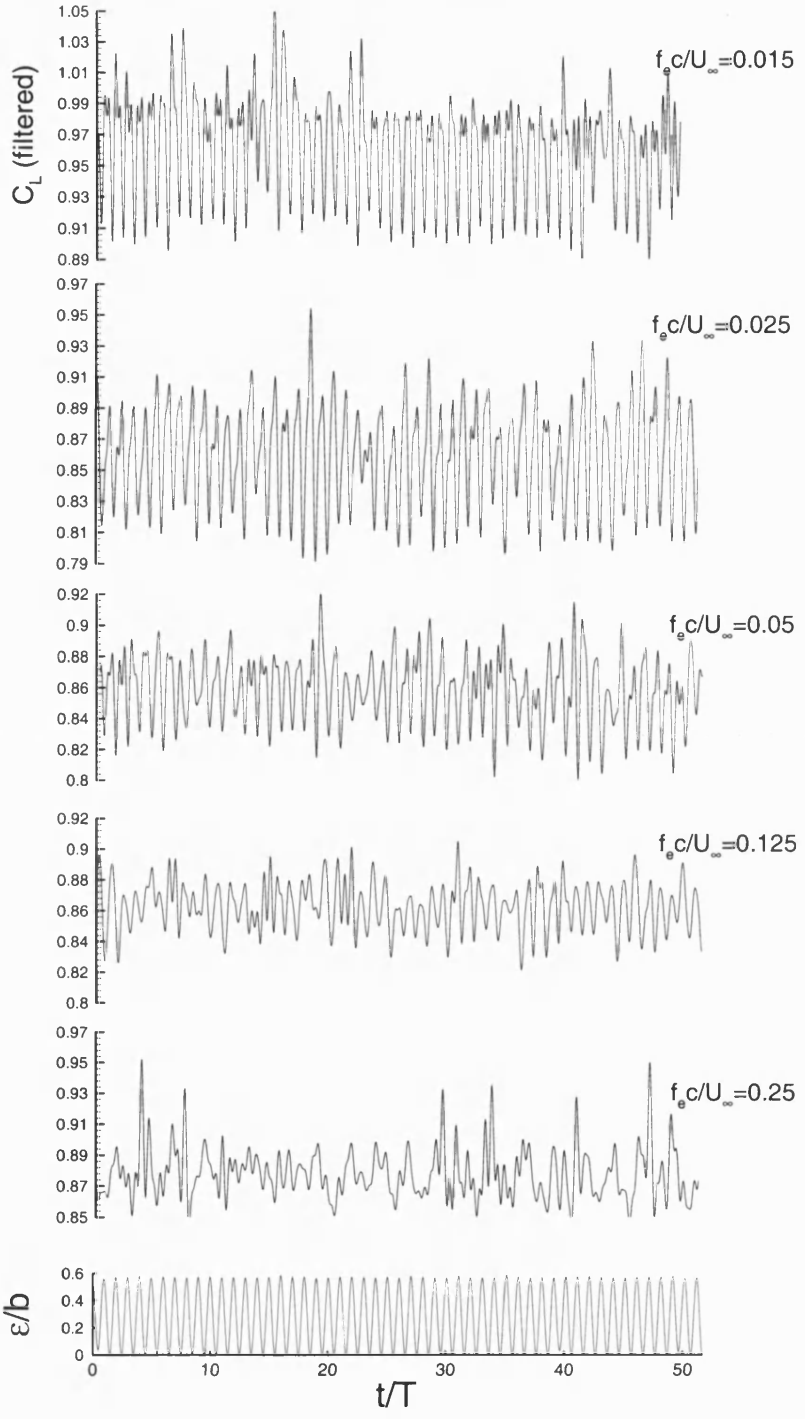

Figure 5.18: Lift force response; waveform A, flat-plate support.

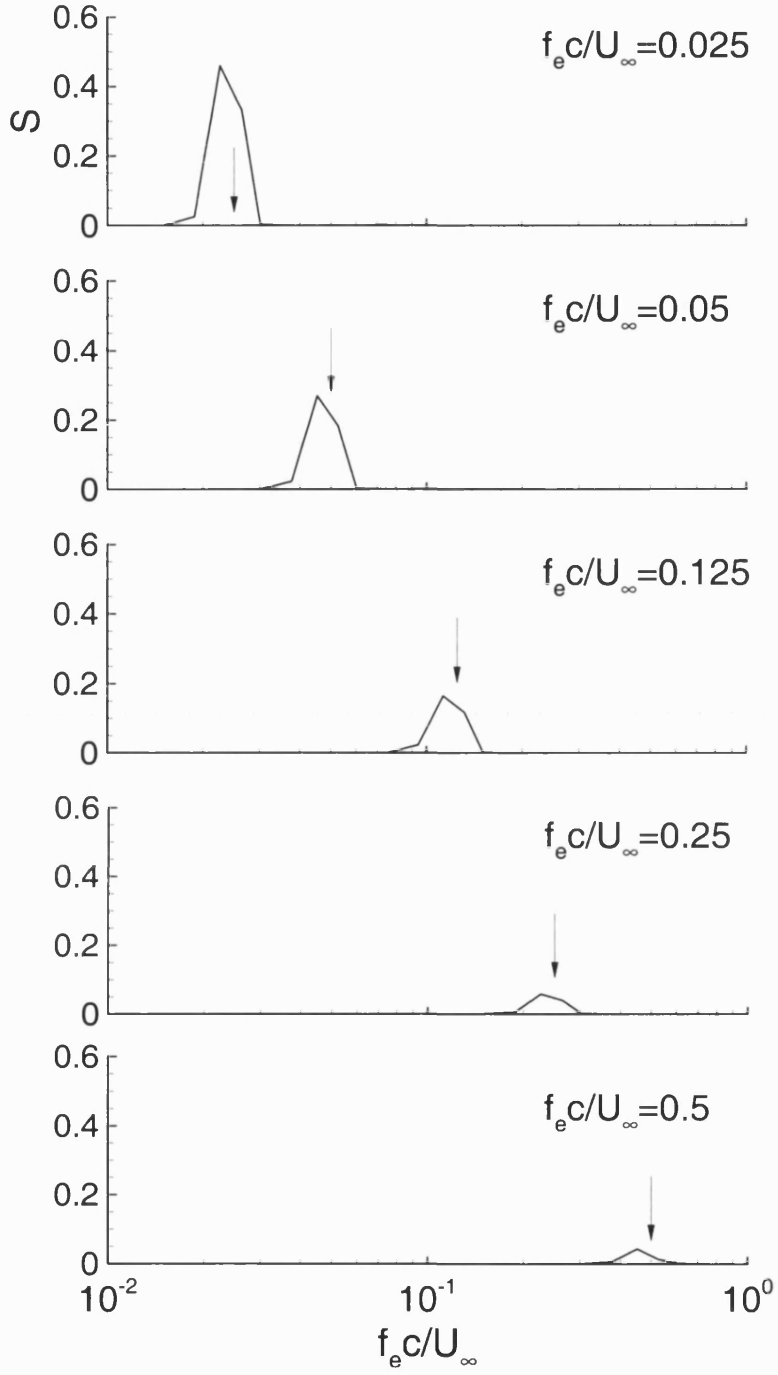

Figure 5.19: Variation of cross-spectral density of C_L and ε/b as a function of $f_e c/U_\infty$; waveform A, cylindrical support.

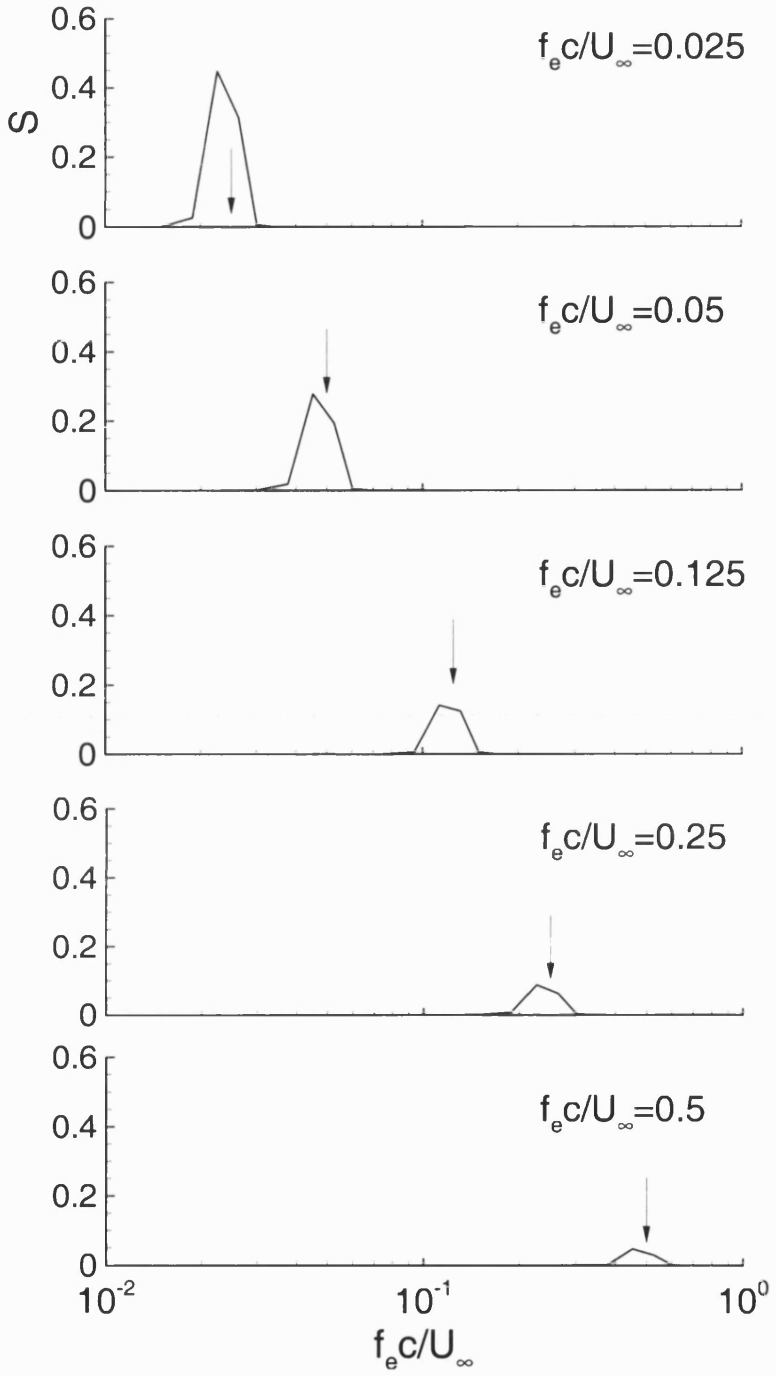

Figure 5.20: Variation of cross-spectral density of C_L and ε/b as a function of $f_e c/U_\infty$; waveform A, flat-plate support.

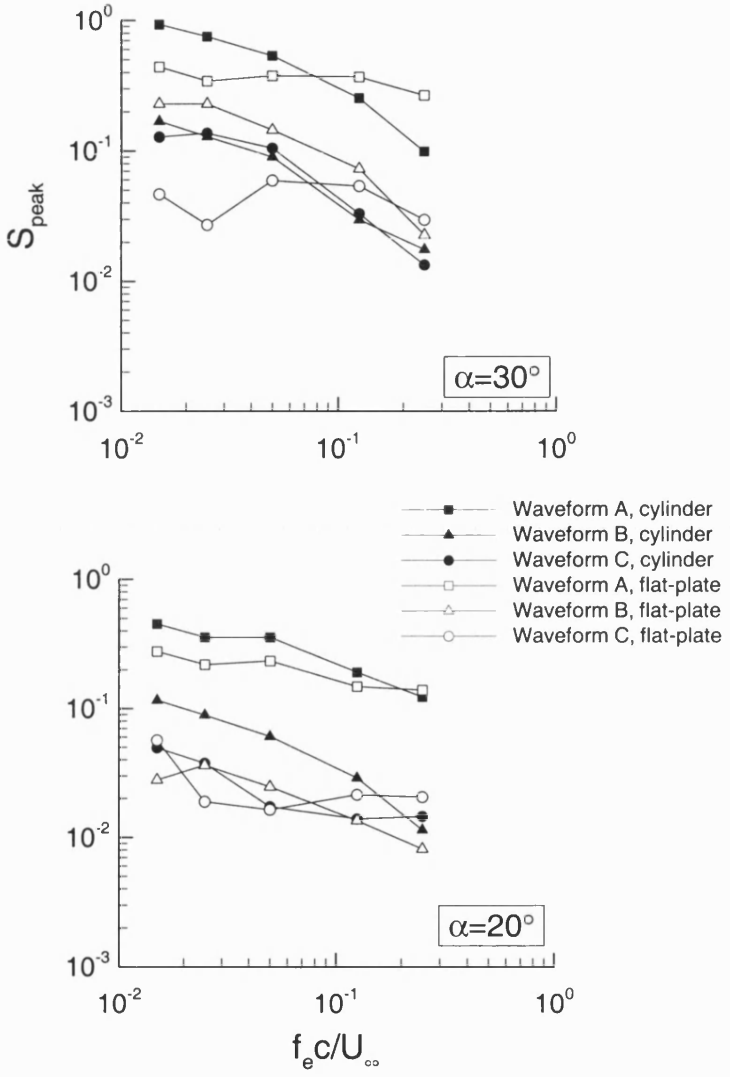

Figure 5.21: Variation of magnitude of dominant cross-spectral density of lift force and ε/b for the 70° wing.

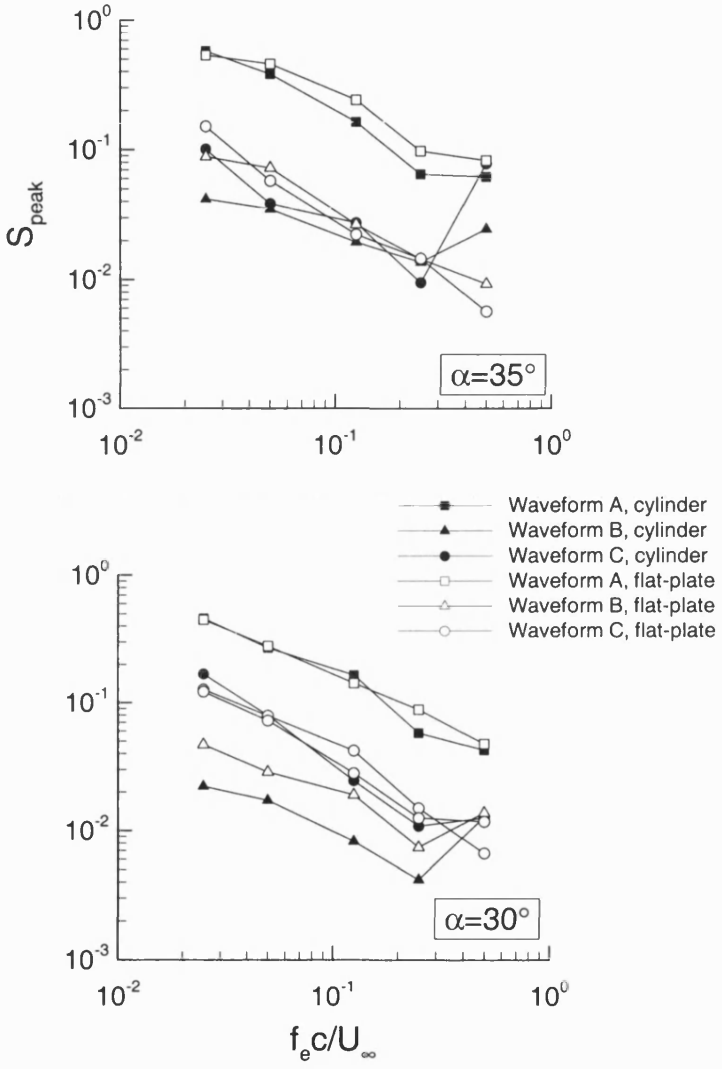

Figure 5.22: Variation of magnitude of dominant cross-spectral density of lift force and ε/b for the 80° wing.

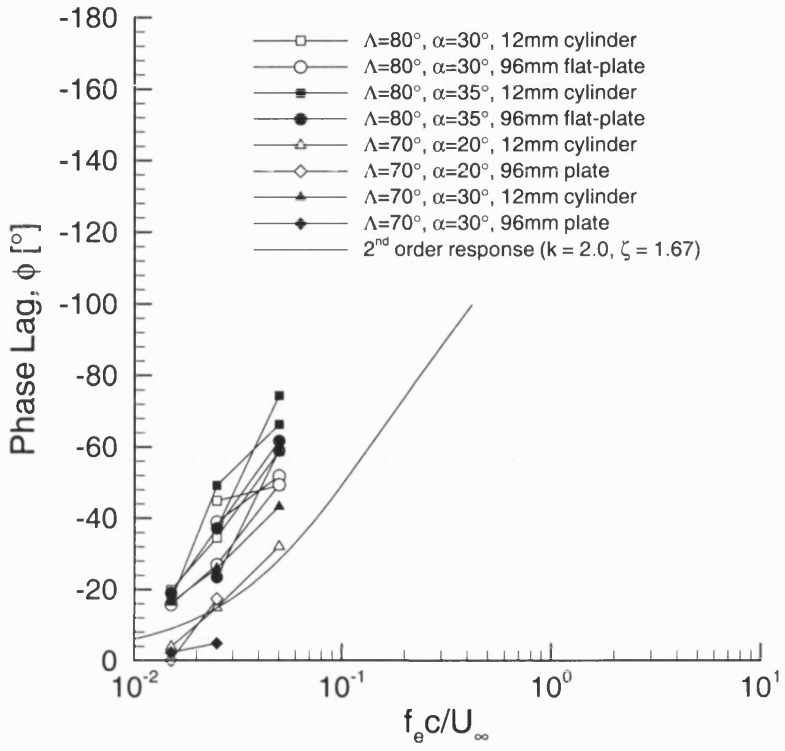

Figure 5.23: Phase lag between support motion and lift force compared to analysis of Greenwell and Wood (1994) for pitching wings; waveform A.

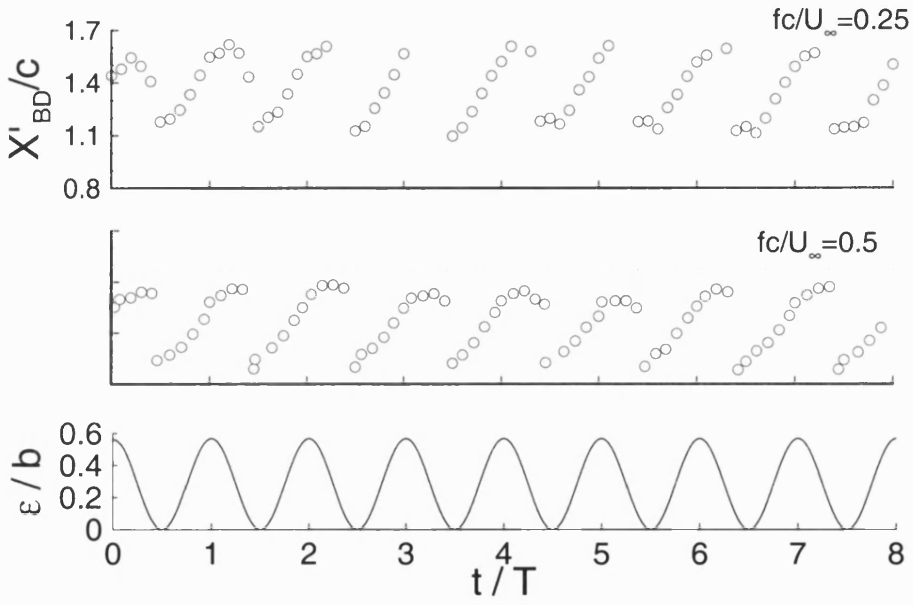

Figure 5.24: Vortex breakdown response to laterally oscillating wing motion in the absence of a dummy support.

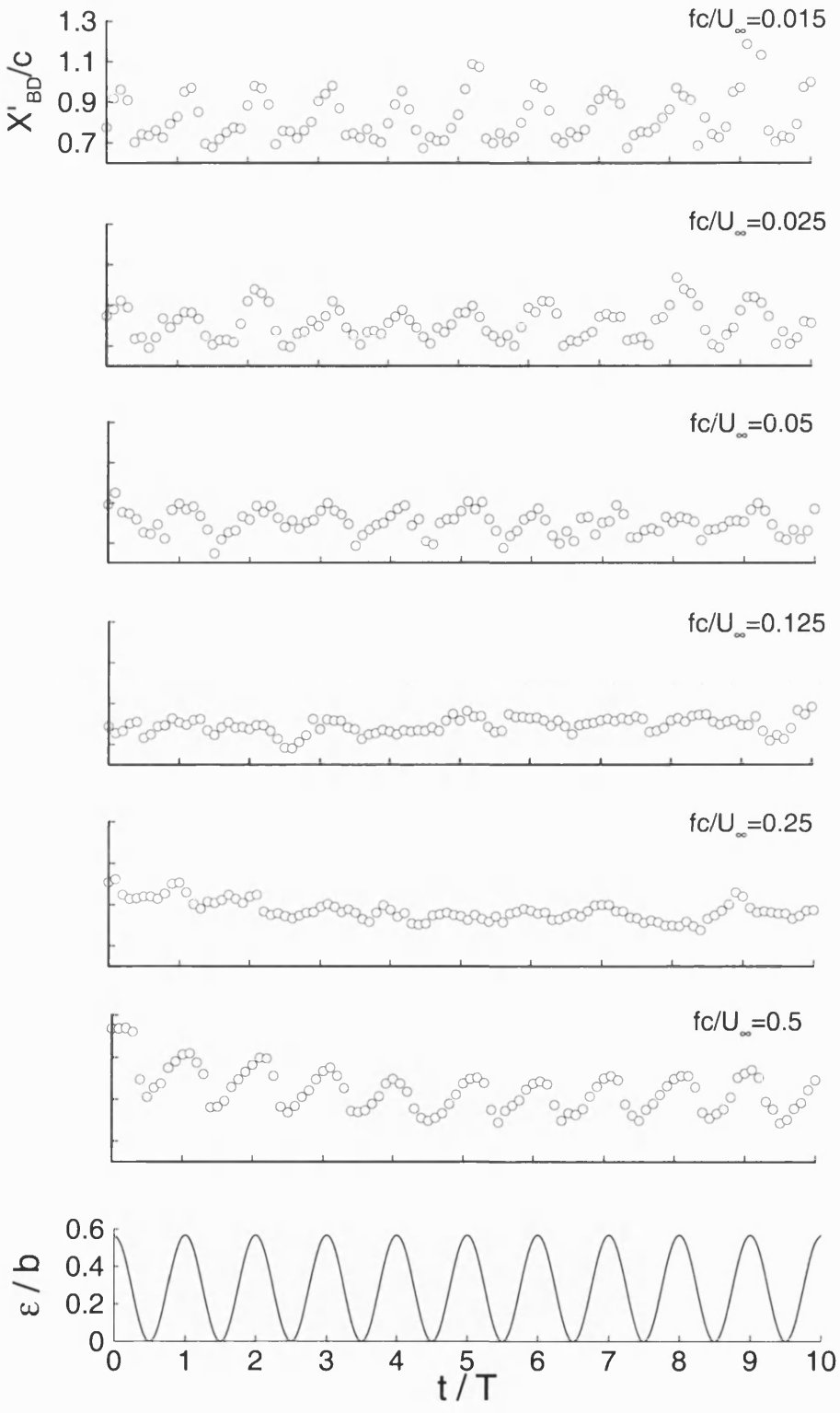

Figure 5.25: Breakdown response to oscillatory wing motion; waveform A, cylindrical support.

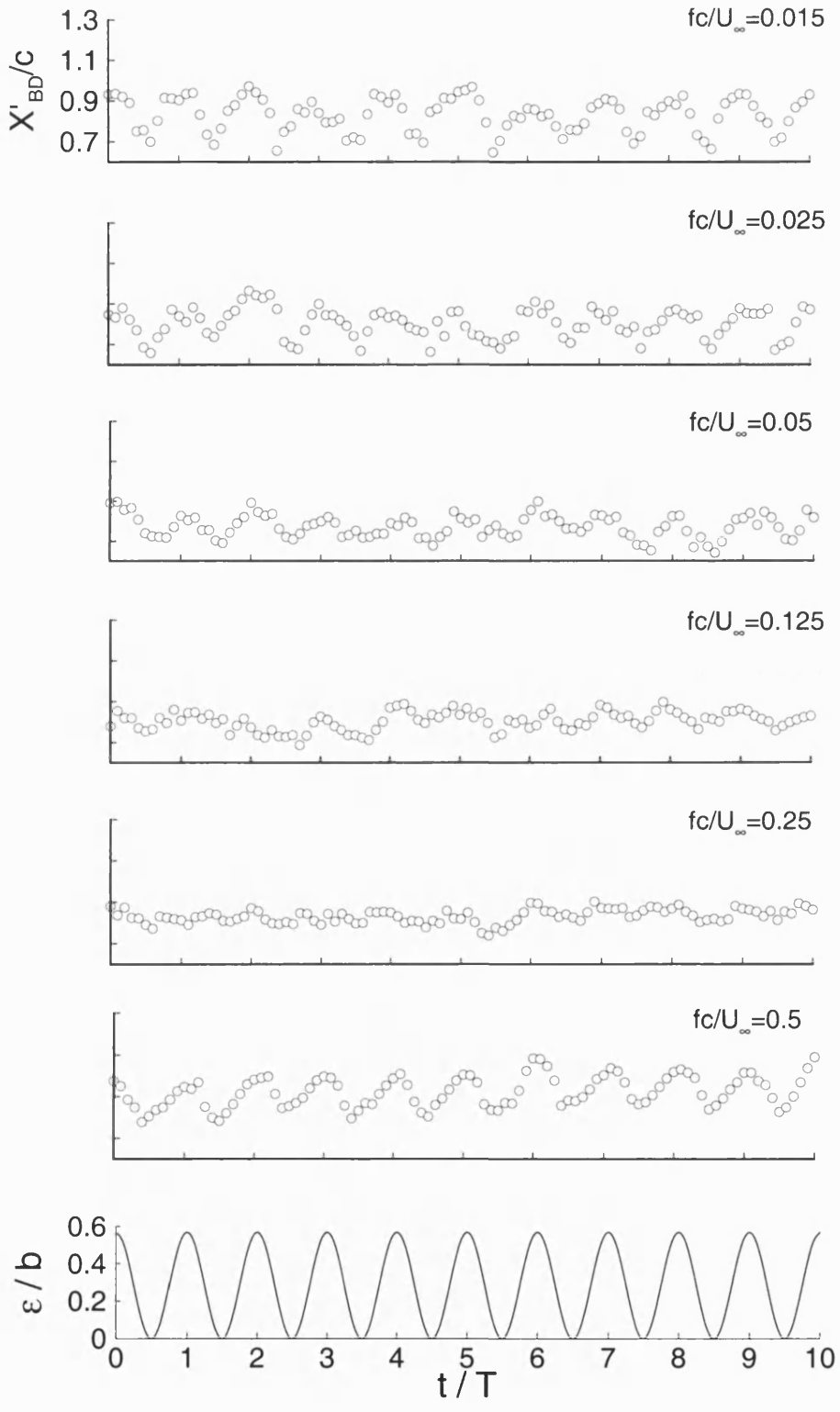

Figure 5.26: Breakdown response to oscillatory wing motion; waveform A, flat-plate support.

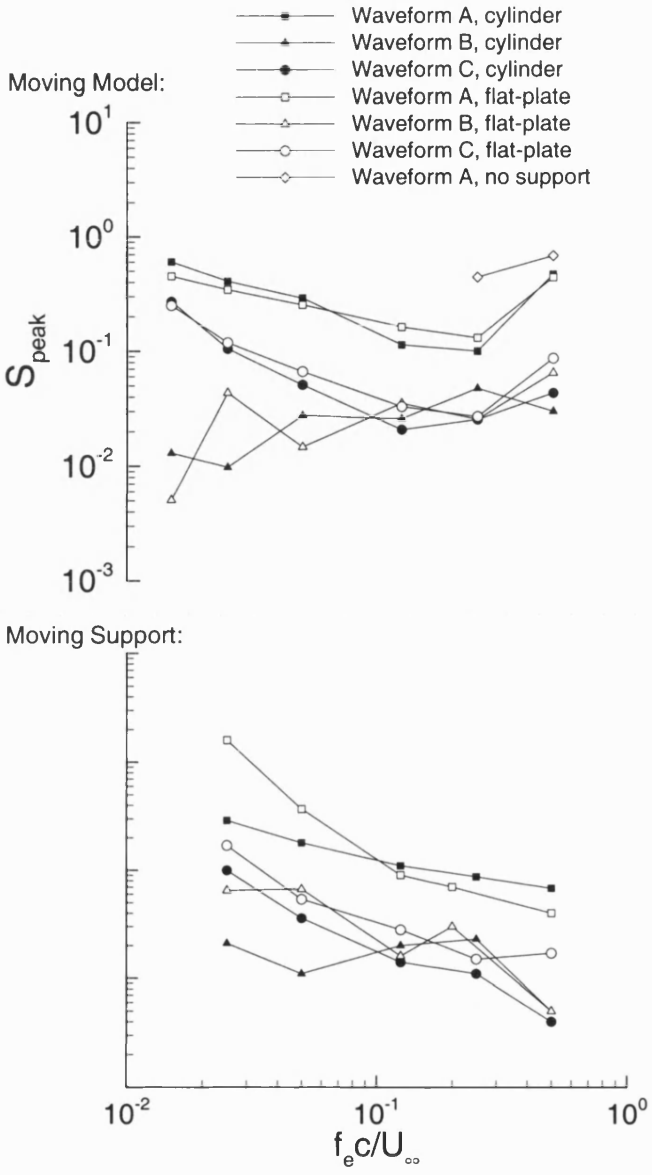

Figure 5.27: Variation of magnitude of dominant cross-spectral density of breakdown location with wing motion.

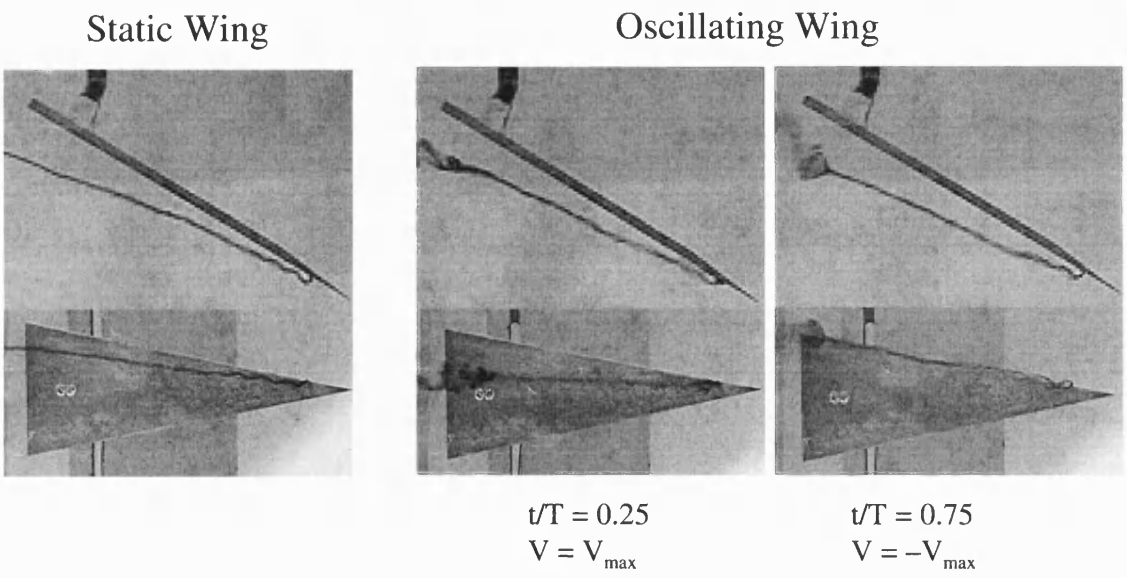

Figure 5.28: Vortex trajectories under static and oscillatory conditions.

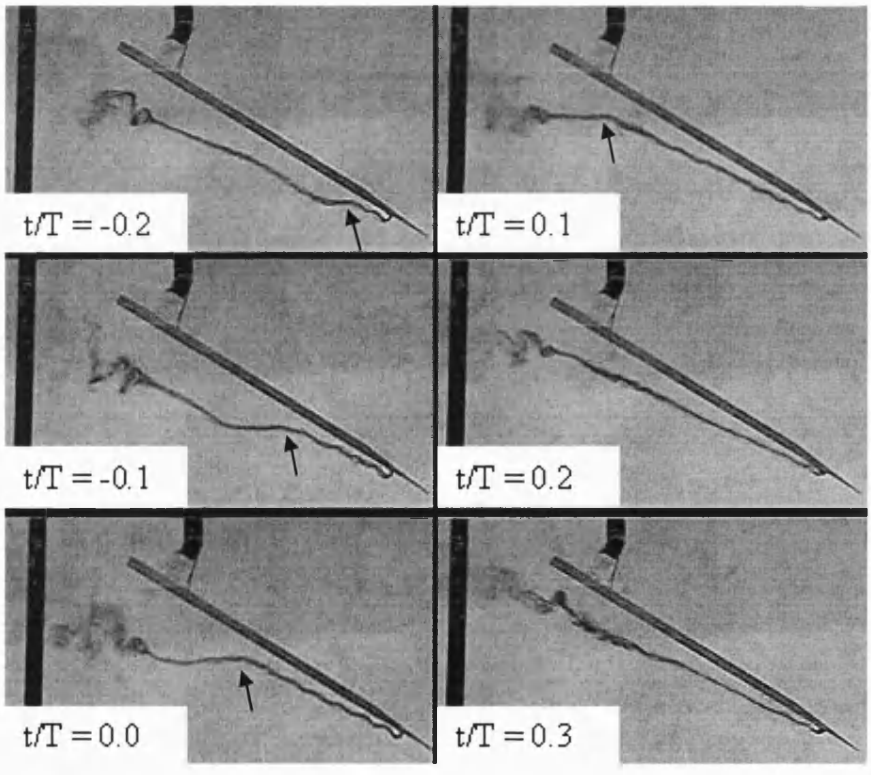

Figure 5.29: Time series showing deflection of a vortex during wing oscillation; waveform A, cylindrical support. Arrows show the downstream progression of the 'kink'.

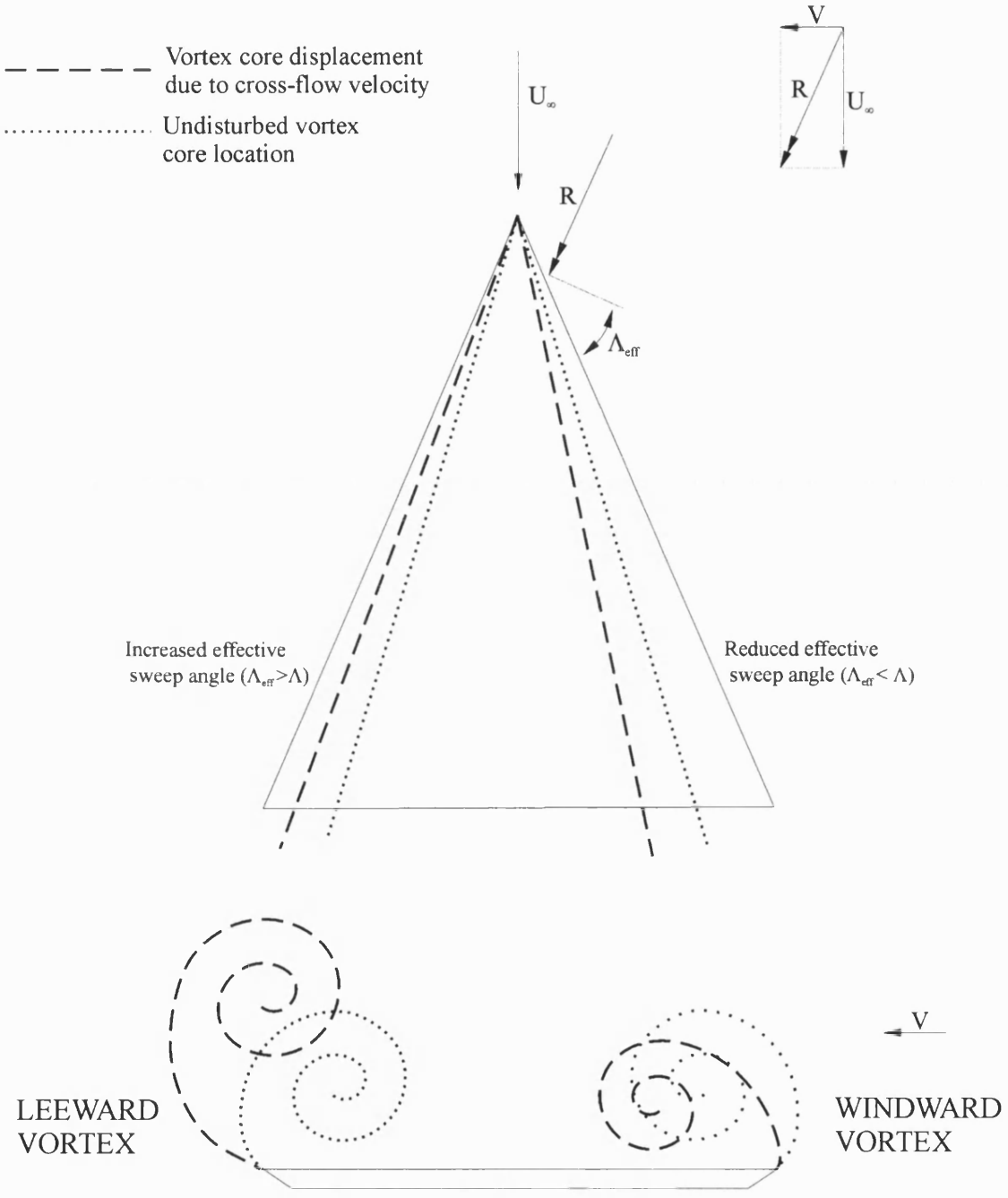

Figure 5.30: Displacement of vortex cores due to cross-flow velocity, V.

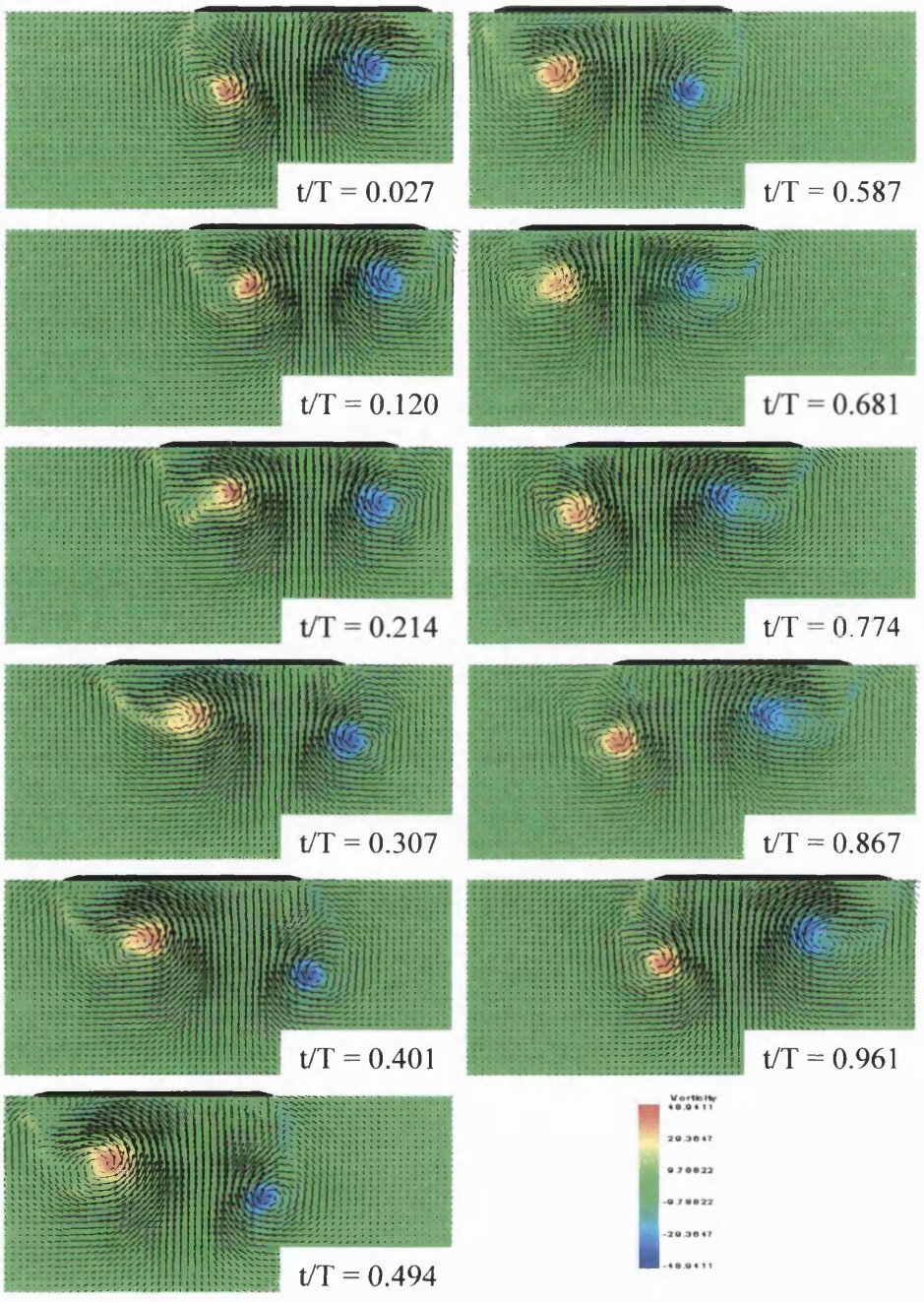

Figure 5.31: Response of vortices to oscillatory wing motion. Velocity vectors plotted on vorticity contours at x/c = 0.8, $f_e c/U_\infty = 0.5$, waveform A, no dummy support.

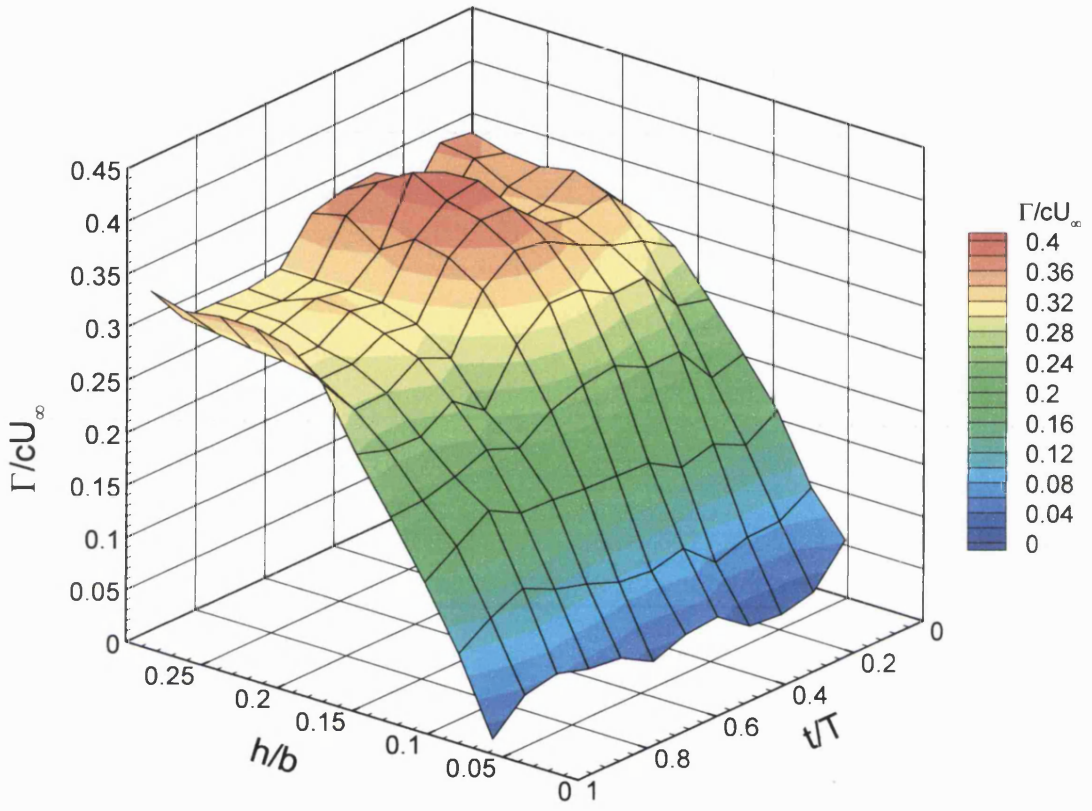

Figure 5.32: Variation of normalised circulation at x/c=0.8 with square size and time.

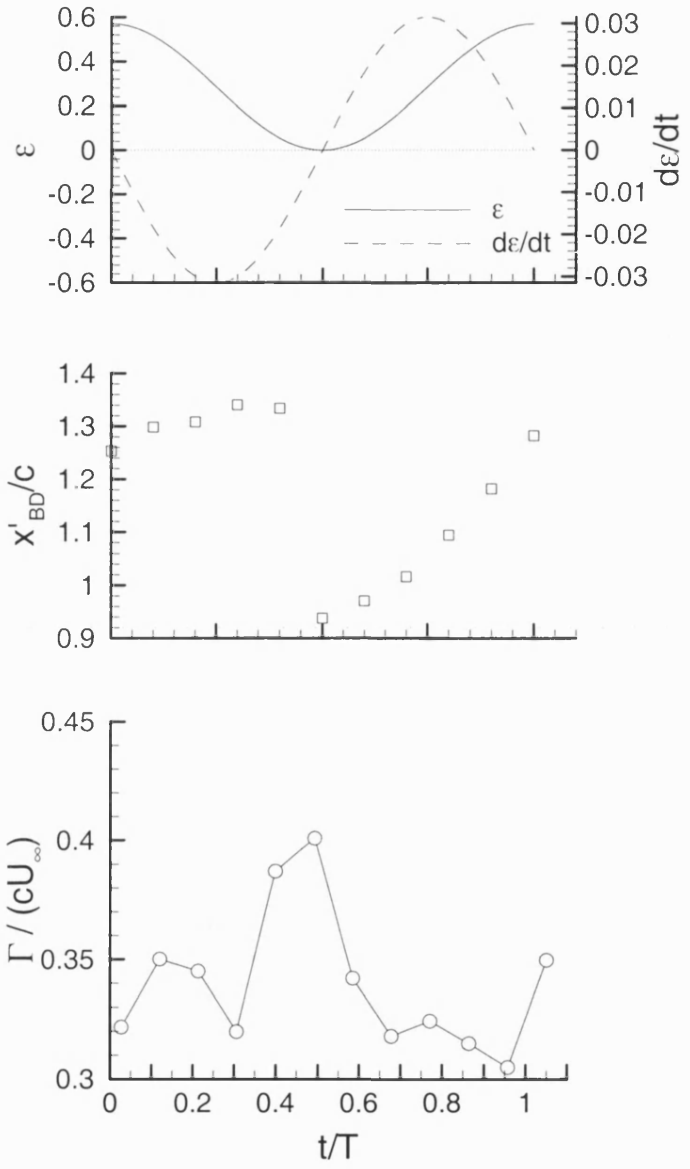

Figure 5.33: Variation of phase averaged circulation with time at h/b = 0.227, compared with phase averaged breakdown location (x'_{BD}/c) and location (ε) and velocity ($d\varepsilon/dt$) of wing through cycle.

Chapter 6 Support Interference in Transient Testing

6.1 Introduction

This chapter completes the investigation of support interference by documenting the breakdown response to transient support motions. The chapter begins with a review of the approach taken in transient testing, followed by a summary of the types of transient motion considered. Following this is a discussion of the results of the transient tests, and the chapter completes with a review of the principal conclusions drawn.

The approach taken in transient testing was similar to that taken for oscillatory testing. Initially, the effect of a transient support motion was considered with the wing remaining at a fixed location. The effect of a number of transient waveforms was analysed using dye flow and laser sheet visualisations. To complete the investigation the effect of a transient motion of the wing was considered, with the support remaining fixed. Dye flow visualisation and PIV measurements were used to document the flow in this case. The support and wing motions considered are shown in Figure 6.1, and in all cases form all or part of a sine wave. In most cases a single complete wave of different amplitudes was considered (cases A-D), although two motions of one half cycle were also taken into account; one motion symmetric about the vortex core (case E), the other completing its motion at $\varepsilon = 0$ (case F). In each case, the characteristic period (forcing frequency) of the wave was varied. For all of the experiments documented in this chapter, an 80° delta wing set at an incidence of 30° was used since this configuration was shown to be particularly sensitive to support interference in static testing. Only the effect of one type of support was considered, being the 12mm

cylindrical support. The amplitudes of waveforms A, E and F were chosen to represent transient cases similar to those considered in oscillatory testing.

6.2 Support Interference due to Transient Support Motion

In this section, the effect of waveforms that move into and out of the vortex core (waveforms A-E) are considered separately from the unique case of the half sinusoidal motion that completes at the $\varepsilon/b = 0$ (waveform F). This distinction has been made purely on the grounds of clarity.

6.2.1 The effect of waveforms A-E

Figure 6.2 shows the vortex response to a single complete wave of the cylindrical support, with $(\varepsilon/b)_{max} = 0.568$ and $(\varepsilon/b)_{min} = 0.0$ (waveform A in Figure 6.1). The most upstream breakdown location observed during each test moved downstream with increasing forcing frequency, i.e. $(x'_{BD}/c)_{min}$ increases with $f_e c/U_\infty$. This was expected since as the forcing frequency increases the support spends less time within its range of influence of the vortex.

The results also show that the point at which breakdown was first observed as the support approached the vortex was delayed as the forcing frequency was increased. In the static case breakdown was first observed at $\varepsilon/b = 0.32$ when stepping the support towards the vortex, but Figure 6.2 shows that for a moving support the support needs to be closer to the vortex to induce breakdown. At the higher frequencies, the onset of breakdown is delayed even further; at $fc/U_\infty = 0.5$, for example, breakdown is first observed at $t/T = 0.6$, at which point the support is retreating from the vortex. This feature of the flow is illustrated in Figure 6.3, which shows dye flow visualisation images at $t/T = 0.5$ (corresponding to $\varepsilon/b = 0$) for all the frequencies considered. At low frequencies the vortex has broken down at this point in the cycle, but the effect of increasing frequency is to delay the onset of breakdown. At the highest frequency the vortex maintains its form by deflecting around the incumbent object, thus delaying its breakdown.

These observations may be explained by considering that the response of the breakdown is known to be of the order of $10c/U_\infty$ (Greenwell and Wood, 1994), and may be independent of the disturbance applied to the vortex (Gursul, 2000). A simple calculation shows that the extremes of forcing frequencies considered, $f_e c/U_\infty = 0.05$ and 0.5, relate to a period of motion equivalent to $2c/U_\infty$ and $0.2c/U_\infty$ respectively. The response of the breakdown is therefore slow compared to the speed of the approaching support, and this explains the delay in the onset of breakdown at high frequencies. Extrapolation of this result suggests that at a sufficiently high frequency no breakdown would be observed, although it is unlikely that such unrealistically rapid motions would be considered in the testing of current aircraft configurations.

Returning to Figure 6.2, it is important to note that in terms of t/T, the breakdown appeared to take longer to propagate downstream with increasing forcing frequency. This was an illusion created by the fact that as the forcing frequency was increased, the normalising time, T, decreased. It therefore appeared that the breakdown was taking longer to dissipate, when in real-time the breakdown actually dissipated more rapidly.

Figure 6.4 shows the effect of a support motion symmetric about the vortex core centre-line, such that motion begins at $\varepsilon/b = 0.568$ and completes at $\varepsilon/b = -0.568$ (waveform E). Only one half cycle was completed so that a single pass through the vortex core was made. The trends observed in this case were similar to those observed for waveform A (Figure 6.2); $(x'_{BD}/c)_{min}$ moved further upstream with reducing frequency, and the onset of breakdown was delayed at higher frequencies. However, in contrast to the previous data none of the frequencies considered induced breakdown upstream of the trailing edge of the delta, although $(x'_{BD}/c)_{min}$ did begin to approach unity as the frequency was reduced. This shows that the breakdown was sensitive to this type of motion, and it was only because sufficiently low frequencies were not considered that a severe response was not observed. Comparison of the response to waveforms A and E show that E represented a less severe disturbance of the vortex, since for a given frequency the breakdown did not propagate as far upstream. As the amplitude of the motion was greater, the velocity of the support through the vortex for a given frequency was greater

in waveform E, and the support therefore spent less time in the range of influence of the vortex.

Figure 6.5 shows how varying the minimum distance between the vortex core and the support, $(\varepsilon/b)_{min}$, affected the breakdown location. Figure 6.5A is actually a duplicate of the results shown in Figure 6.2; Figure 6.5B, C and D (waveforms B–D in Figure 6.1) vary the motion by reducing the amplitude of the sinusoid whilst maintaining the same start and finish locations ($\varepsilon/b = 0.568$); in this way the parameter $(\varepsilon/b)_{min}$ was varied. As $(\varepsilon/b)_{min}$ was increased, the presence of the support had less influence, and a lower frequency was required to induce a severe response. In Figure 6.5A and B all but the highest frequency affected the vortex by inducing breakdown over the wing. However, in C only the lowest frequency induced breakdown over the wing, and in D no breakdown was observed forward of the trailing edge. A curious feature of the breakdown response was observed in Figure 6.5C at $f_e c/U_\infty = 0.05$, where the breakdown appeared to get 'trapped' in the trailing edge region of the wing for a considerable period of time before finally moving downstream and dissipating. This phenomenon was also observed in Figure 6.5B for $f_e c/U_\infty = 0.25$. Given previous discussions in this thesis, it is suggested that the mechanism for this trapping effect is the pressure recovery region at the trailing edge. Similar observations were made by Huang and Hanff (2000), who investigated the breakdown response over a 75° delta to an impulse disturbance. An unspecified obstruction placed instantaneously co-incident with the vortex core was found to move the breakdown location to a new time-averaged location. It was found that there exist three equilibrium breakdown locations in the region of the trailing edge, being just aft, just fore and incident with the trailing edge. The authors suggested a number of factors that influence the breakdown in this region, including the interaction of the vortices, the existence of a trailing edge vortex (vorticity shed from the trailing edge at incidence) and the pressure recovery region at the trailing edge.

To this point it has been shown how different transient support motions affect the location of breakdown of the leading edge vortices, but it is important that the effect of each support motion be quantified so that they can be compared. Reviewing the

analysis introduced in Chapter 4, the breakdown response may be broadly categorised into one of three types, each representing a different level of severity of the breakdown response:

(i) Natural and forced breakdown aft of the trailing edge;

(ii) Natural breakdown aft of trailing edge, forced breakdown over wing;

(iii) Natural and forced breakdown over wing.

In the current tests, the vortex did not break down in the natural case, so the analysis may be limited to considering only the first two types of response. One may therefore categorise the breakdown as severe when $(x'_{BD}/c)_{min} < 1$, or not severe when $(x'_{BD}/c)_{min} \geq 1$. Although it has been shown that the likelihood of a severe breakdown response is dependent upon the forcing frequency, it has also been shown that the form of transient motion is also a factor, and that forcing frequency alone is therefore not a sufficient criterion. The following paragraphs discuss the results above and attempt to correlate these with a parameter that it is hoped will provide future experimentalists with a method for determining those conditions under which a severe breakdown response may be expected.

To review the results of this chapter so far: Figure 6.2 showed that for waveform A, forcing frequencies below $f_e c/U_\infty = 0.25$ induced a severe response, while $f_e c/U_\infty = 0.5$ did not; Figure 6.4 showed that none of the frequencies considered were critical for waveform E; and Figure 6.5 showed that as $(\varepsilon/b)_{min} \rightarrow 0$, the forcing frequency required to avoid a severe response was increased. Consideration of these results has lead to the supposition that during a given cycle, it is the time during which the support is within its range of influence of the vortex core that defines the severity of the breakdown response. Thus for the cylindrical support, it is suggested that it is the time during which the support lies in the range $|\varepsilon/b| < 0.32$ during a given cycle that is important. This "time parameter" has been labelled τ_p, where $\tau_p = t_p U_\infty/c$, and is a function of the amplitude and frequency of the support motion.

The time parameter τ_p is plotted against $(x'_{BD}/c)_{min}$ for the transient motions considered herein in Figure 6.6. Although some scatter exists, there is a good correlation; the larger the time parameter the further upstream the breakdown is observed. This indicates that the likelihood of a severe breakdown response may be measured by considering this time parameter for a given type of motion. A trend line has been fitted to the data, which shows that the data are asymptotic to a given breakdown location as $\tau_p \rightarrow \infty$. It is assumed that the value of the asymptote is equal to the value of x'_{BD}/c observed in static testing. A critical value of this time parameter may be derived by noting the value required for breakdown to broach the trailing edge, and thus form a severe response. From Figure 6.6 it is seen that $(\tau_p)_{CRIT} \approx 1.8$, indicating that any support motion that spends longer than this within the critical region is likely to induce breakdown upstream of the trailing edge, and may therefore be categorised as severe.

A parameter has therefore been derived which gives the experimental investigator some idea of the likelihood of a severe breakdown response being induced as a result of support interference in transient testing. However, although the data correlate well with this parameter, it is acknowledged that it is somewhat less than ideal as a prediction tool due to the quantity of data required for its implementation. To be used successfully the investigator would require a knowledge of the critical value of the time parameter for a range of different support configurations. If, as expected, the critical value is uniform regardless of the type of support or motion considered, it is also expected that it will vary with the strength of the vortex, since a stronger vortex has been shown to be more sensitive to support interference than a weaker one. Further experimentation may yield a further correlation to account for these effects, and this would be the ideal.

6.2.2 The effect of waveform F

The transient motions considered thus far have all been of a form that spend a limited time in the region of influence of the vortex. To complete the current section, the effect of a support motion which begins outside the vortex, but which completes its motion coincident with the vortex core is considered. The motion of the support is shown as waveform F in Figure 6.1.

$f_e c/U_\infty$	$\frac{d(x'_{BD}/c)}{d(\log tU_\infty/c)}$
0.025	-0.817
0.05	-1.071
0.125	-1.370
0.25	-2.010
0.5	-2.063

Table 6.1: Gradient of transient response to support motion.

Figure 6.7 shows how the breakdown responded to this form of motion. As observed in previous transient tests, the higher the forcing frequency the closer the support was to the vortex at the point at which breakdown was first observed. While the data plotted in Figure 6.7 are useful in visualising the form of the response, the breakdown response to transient pitching motions considered in literature have tended to measure the speed of the response in terms of the characteristic time scale, c/U_∞ (Thompson *et al*, 1991, and Greenwell and Wood, 1994, for example). Figure 6.8 shows the breakdown location plotted against tc/U_∞ for the forcing frequencies considered. Colour has been used in this figure for clarity, and the abscissa uses a log scale due to the length of the data series. In terms of the number of characteristic time units taken to reach equilibrium, the lowest frequency motion obviously results in the slowest response as the length of the perturbation is greater. As the figure shows, the time taken for the support to induce breakdown lengthens with reducing forcing frequency; as a result of the slower motion the support takes longer to reach its range of influence of the vortex. Figure 6.8 also shows that the slower the motion of the support, the slower the breakdown response, as measured by the gradient of the transient part of the response curves. These gradients are tabulated in Table 6.1, and it can be seen that at high frequencies, the gradients of the curves are similar, but as the frequency is reduced, the gradient of the curves reduce significantly due to the slower encroachment of the support on the vortex.

Finally, a different approach to visualising the flow was taken to determine the cross-flow characteristics of the vortex-support interaction. The flow was seeded using the

seeding particles described in §2.5.4, and the cross-flow plane was illuminated using a laser sheet. The results were recorded using a digital video camera, and in this way the response of both leading edge vortices was measured. Figure 6.9 shows how the encroachment of the 12mm cylindrical support affects the formation of the left-hand vortex of the vortex pair. On this plot, the support location is shown as a black band, and the laser sheet and support are situated at x_{LE} = c/4. As the support begins to interfere with the vortex, the vortex first appeared to reduce in diameter, then began to lose some coherency and distorts, before finally losing all structure entirely. Although significant interactions between the vortex breakdown locations of leading edge vortex pairs have been observed in literature (Huang and Hanff, 2000, for example), these results show that at the cross-plane considered no interaction between the vortices was observed, i.e. the obstruction of the left-hand vortex due to the presence of the cylindrical support did not affect the coherence or structure of the right-hand vortex. A similar result is shown in Figure 6.10 which shows a similar experiment conducted for the 96mm flat-plate. In this case, although the overall form of the interaction was the same, the vortex appeared be able to sustain a much greater distortion in the presence of this support. As the vortex approached breakdown, the vortex became elongated so that the particles did not seem to be rotating around a circular path.

6.3 Support Interference due to Transient Wing Motion

To complete the study of transient vortex-support interactions, the breakdown response to transient model motions was considered. All of the motions considered were similar to those considered previously, and are therefore described in Figure 6.1. Only two waveforms were considered for the moving wing case, being waveforms A and F. The effects of these waveforms are considered separately below. Initially, though, it was considered important to document the response of the vortices to a moving wing in the absence of a dummy support.

This case is shown in Figure 6.11. At $f_e c/U_\infty = 0.5$ the transient motion of the wing artificially induced breakdown at $t/T \approx 0.5$. Following this, the breakdown propagated

downstream until $t/T \approx 1.3$, at which point the location of the burst was seen to move rapidly upstream, from $x'_{BD}/c \approx 1.52$ to $x'_{BD}/c \approx 1.1$. The breakdown was then seen to move downstream. The effect of reducing the forcing frequency was to reduce the magnitude of the jump of breakdown location. No breakdown was induced below $f_e c/U_\infty = 0.25$. It is interesting to note that the onset of breakdown occurred at around $t/T = 0.5$, rather than at $t/T = 0.25$, the point at which the lateral velocity of the wing was at its greatest, and at which the circulation of the vortex would be assumed to be at its greatest. A further interesting feature of the breakdown response was the time at which the breakdown jump occurred. The jumping of the vortex breakdown location was also observed in oscillatory testing, and a discussion of the phenomenon has been provided in §5.3.1. However, the current data show that the jumping of the breakdown occurred following the *completion* of the model motion, which was unexpected from the oscillatory results.

The mechanism responsible for both of these observations is thought to be related to the delay between the change in lateral velocity and the resulting increase in circulation of the leading edge vortex. This hypothesis will be discussed in detail shortly, following a discussion of the response of the breakdown to a moving wing in the presence of a dummy support.

6.3.1 The Effect of Waveform A

Figure 6.12 shows the breakdown response to waveform A. At all but the highest forcing frequency the trends observed in these results were similar to those observed in the moving support case. The effect of increasing forcing frequency was to move the most upstream breakdown location, $(x'_{BD}/c)_{min}$, downstream, and to delay the number of cycles taken for the breakdown to dissipate. Further, the delayed onset of the breakdown at higher frequencies was observed, and a comparison with the moving support case (Figure 6.2) showed that the effect was more pronounced in the current case. This is caused by the phase delay resulting from the lateral deflection of the vortex away from the oncoming cross-flow, essentially meaning that the vortex takes longer to reach the support in the moving wing case. Deflections of the leading edge

vortices undergone in lateral dynamic testing have been described and discussed in Chapter 5. Further discussion is omitted here to avoid repetition.

At the highest forcing frequency ($f_e c/U_\infty = 0.5$), the effects of time-dependent vortex strength began to become apparent. Figure 6.12 shows that at approximately $t/T = 1.0$, the breakdown was moving downstream having previously attained its most upstream position at $x'_{BD}/c \approx 1.08$, aft of the trailing edge. The progression of the breakdown downstream did not continue; first its motion slowed and inflected, and then at $t/T \approx 1.3$ suddenly jumped from $x'_{BD}/c \approx 1.22$ to $x'_{BD}/c \approx 1.02$. Following this, the breakdown once again progressed downstream, taking until $t/T \approx 4.0$ to attain its previous most downstream location of $x'_{BD}/c \approx 1.22$. Jumping of the breakdown location was only observed at the highest forcing frequency, contrary to the results shown in Figure 6.11. A similar result was observed in oscillatory testing, which shows that the presence of the support in some way reduces the effect of the time-dependent vortex strength effect. This is further seen in Figure 6.12, as the reduced magnitude of the breakdown jump at $f_e c/U_\infty = 0.5$ is small compared to that observed in the absence of a support.

The discontinuity associated with the breakdown location at high frequencies affects the classification of the severity of the response. As has been used previously, the minimum breakdown location, $(x'_{BD}/c)_{min}$ is used here as a measure of the severity of the breakdown response. While in moving support tests $(x'_{BD}/c)_{min}$ increases with forcing frequency, the current tests show that the time dependency of the vortices reverses this trend at higher forcing frequencies. Although high enough frequencies have not been tested, it is considered likely that further increasing the forcing frequency would result in $(x'_{BD}/c)_{min}$ reducing further. The response of the breakdown may therefore be summarised as follows. At low frequencies the vortex spends a large amount of time within the range of influence of the support, and therefore induces a severe breakdown response. At high frequencies the time-dependent nature of the leading edge vortices results in large oscillations of the breakdown locations and breakdown jumping, resulting in a severe response. At first glance, these trends would indicate the existence of an optimum test frequency at which the effect of support interference would be minimised. However, the time-dependent nature of the

breakdown at high frequencies is not a result of the presence of the support structure; rather, as has been previously shown for oscillatory testing, a result of the oscillation of the wing. Further, the effect of the support was to alter the mean breakdown location throughout the range of frequencies tested.

6.3.2 Observations of Time-Dependent Vortex Strength Effects

Focus is now moved to discussion of the vortex breakdown jumping observations in transient testing. This feature is clearly illustrated in Figure 6.13, which shows a time-sequence of images recording the breakdown location over the moving wing in the presence of the support. Clearly shown is the existence of a breakdown jump between t/T = 1.4 and 1.5. At t/T = 1.35, the vortex appears slender, with the breakdown being observed to the right of the frame. However, by t/T = 1.45, the region of the vortex ahead of the breakdown has enlarged, and the definition of the point of breakdown is lost. At t/T = 1.50, it is possible to identify two breakdown locations, the most upstream being a result of the instability observed in the previous frames.

It was suggested in the previous chapter that it was the variation of circulation of the leading edge vortices due to the wing motion that was responsible for the breakdown jumping phenomenon observed in oscillatory testing. It was therefore hypothesised that a similar mechanism was responsible for the same phenomenon observed in transient testing. Although in the current case the jumping of the breakdown is not observed until completion of the model motion, it was hypothesised that the vortex takes an amount of time to regain its steady state structure, and that it was during this period of readjustment that the jumping of the breakdown was observed. The phase delay between model motion and vortex strength has already been observed in oscillatory tests, where the peak vortex strength occurs almost a quarter of a cycle (90°) after the peak velocity of the wing.

PIV data was therefore used to elucidate the cross-flow velocity field, allowing the strength of the vortices to be calculated at different stages through the transient motion. The velocities were measured in a plane at which it was known from visualisation experiments that breakdown did not reach under the conditions considered, being at x/c = 1 in this case (the same data for the oscillatory case was taken at x/c = 0.8). Figure

6.14 shows velocity vectors plotted on contours of constant vorticity through the entire period of motion for waveform A at $f_e c/U_\infty = 0.5$. As the wing began its motion, the windward vortex strengthened and moved a small distance towards the wing, while the leeward vortex weakened and moved a greater distance away from the wing surface. During the second half of the motion, the vortices reversed their roles. At inflection of motion, the core of the vortex that became the windward one (the right-hand vortex in this case) became slightly larger and elliptical, taking a few frames to reform its compactness. On termination of the wing motion, the vortex that trailed during the second half of the cycle (the left-hand vortex) was the one in which vortex jumping was observed, and from Figure 6.12 and Figure 6.13, one can see that the jumping was observed at $t/T = 1.4$. Comparing the frames at $t/T = 1.334$ and 1.521, little difference between the strength of the left-hand vortex in each case was seen.

However, as discussed previously, the circulation of the vortex provides a more accurate representation of the strength of the vortex than does the vorticity. As such, the variation of circulation with integration square size and time through the cycle was calculated and is plotted for the transient case in Figure 6.15. This figure shows the normalised circulation of the left-hand vortex from $t/T \approx -0.5$ to +2.0, where the motion of the wing begins at $t/T = 0.0$. The value of circulation increased rapidly as the size of the integration square was increased, until reaching a plateau at around $h/b = 0.227$, similar to that chosen in the oscillating wing case. Once more, a slice through the data for a constant h is plotted in Figure 6.16 for clarity, together with the time-history of the breakdown location at $f_e c/U_\infty = 0.5$, and the position and velocity of the wing through the transient cycle. At this streamwise location the steady-state value of normalised circulation (i.e. the value at $t/T < 0$), $\Gamma/cU_\infty \approx 0.42$, which is similar to the value observed in static testing. Almost immediately following the start of the model motion, the strength of the vortex started to increase, reaching a maximum at $t/T = 0.31$. This result shows that the time lag between the motion of the model and the response of the vortex is actually reduced in the transient case in the first half of the cycle, since the peak circulation coincides almost exactly with the maximum velocity of the wing. Following this peak in circulation, the vortex then weakens, reaching a minimum of $\Gamma/cU_\infty = 0.3234$ at $t/T = 0.962$. Thus the delay in the second half of the motion was

greater, reaching a similar value to that observed in oscillatory testing, being around 90°. It is only after the model has completed its motion that the strength of the vortex begins to increase once more. The increase in circulation during this period is rapid and regains its starting value by t/T = 1.36.

Analysis of the vortex strength through the transient cycle has shown the existence of a lag between the model motion and the resulting increase in vortex strength. Although in the first half of the cycle this phase lag was small, by the end of the motion the time lag was approaching 90°. It has also been shown that the vortex takes a while to settle following completion of the motion, which may account for the delay in the appearance of the breakdown jump that was observed at t/T = 1.4.

The results presented herein also lend further viability to the hypothesis stated in the previous chapter that the vortex jump is a phenomenon resulting from a rapid increase in vortex strength. In the current set of tests, the vortex rapidly gains strength between t/T = 0.962 and 1.36, and the vortex jump is observed just after this, at t/T = 1.4. The delay between these observations, if they are indeed linked, is a result of the relative streamwise stations at which they were measured (the circulation was measured at the trailing edge; the breakdown is observed much further downstream than this prior to the jump). Clearly although the results presented here have indicated a possible relationship between the increase in vortex strength, and the vortex jumping phenomenon, more investigation of this relationship is required before firm conclusions may be drawn. It is possible that there are a number of other factors involved in the jumping process that have not been considered here.

6.3.3 The Effect of Waveform F

Figure 6.17 shows the breakdown response to a half wave model motion. The motion is the equivalent of waveform F in Figure 6.1. Once again the delay in the onset of breakdown with increasing frequency was observed, and compared to the moving support case, breakdown is observed earlier. In these results though, since the vortex completes its motion at ε/b = 0, breakdown does not dissipate downstream following completion of the motion.

Comparing Figure 6.17 with Figure 6.7, the response of the breakdown in the moving wing and moving support cases appears similar. However, significant differences between the responses may be seen by comparing Figure 6.18, which shows the breakdown response to the moving wing in terms of the characteristic time scale, with the similar plot for the moving support, Figure 6.8. The gradients of the transient portions of these curves are tabulated in Table 6.2.

$f_e c/U_\infty$	$\frac{d(x'_{BD}/c)}{d(\log tc/U_\infty)}$	
	Moving support	**Moving wing**
0.015		-0.412
0.025	-0.817	-0.701
0.05	-1.071	-1.805
0.125	-1.370	-2.965
0.25	-2.010	-3.360
0.5	-2.063	-3.480

Table 6.2: Gradient of transient response to support and wing motions.

As Table 6.2 shows, the response of the breakdown to the moving support and moving wing shows similar trends. In both cases, increasing the frequency of the motion resulted in a quicker breakdown response. However, there are some important differences between the two cases. At high frequencies, the moving wing induces a far more rapid response than does the moving support. However, at low frequencies, the gradient of the slopes are approximately equal, indicating that in the limit $f_e c/U_\infty \rightarrow 0$, both forms of motion induce a similar response. The more rapid response at high frequencies is probably due to the premature breakdown of the vortex due to the increased circulation created as a result of the wings motion.

6.4 Chapter Review

This chapter has addressed the problem of support interference in transient dynamic testing. Transient oscillations of both the dummy support and wing model have been considered separately, and have been shown to induce similar breakdown responses at low forcing frequencies. At high forcing frequencies, time-dependent vortex strength effects lead to large oscillations of breakdown location, and the breakdown jumping phenomenon in the moving wing case.

The principal characteristics of the interaction include the delay of the onset of breakdown due to the approaching support with increasing forcing frequency, i.e. the support needs to be closer to the vortex as the forcing frequency of either the support or the wing is increased before breakdown is observed. The vortex maintains its structure at the higher frequencies by deflecting around the support. Further, with increasing frequency the most upstream breakdown location moves downstream. This relationship continues indefinitely for the moving support case, but in the moving wing case where time-dependent vorticity effects begin to dominate, the trend is reversed at high forcing frequencies. The effect of the support is to move the breakdown location upstream in all cases compared to the natural case, so that support interference is a factor throughout the range of frequencies tested.

Using the method of measuring the most upstream breakdown location to determine the severity of the breakdown response, it was shown that the likelihood of a severe breakdown response to a given support motion may be estimated using a time parameter. This time parameter was a non-dimensional parameter defining the length of time within which a support spends within the range of influence of a vortex core. It was shown that plotting this parameter against $(x'_{BD}/c)_{min}$ provides a good correlation, and the parameter may therefore be used as a predictive tool. However, this method has a number of limitations; principally the amount of knowledge of a particular configuration required to provide an estimate of the support interference effect.

A particularly interesting feature of the flow was the presence of breakdown jumping following cessation of model motion. PIV measurements have shown that this may be attributed to the rapid infusion of vorticity from the leading edge as the vortex returns

from a state of reduced vorticity to regain its steady state structure. A delay between the rapid increase of circulation and the vortex jump was observed, although this has been accounted for by attributing it to the fact that PIV measurements were taken upstream of the breakdown location.

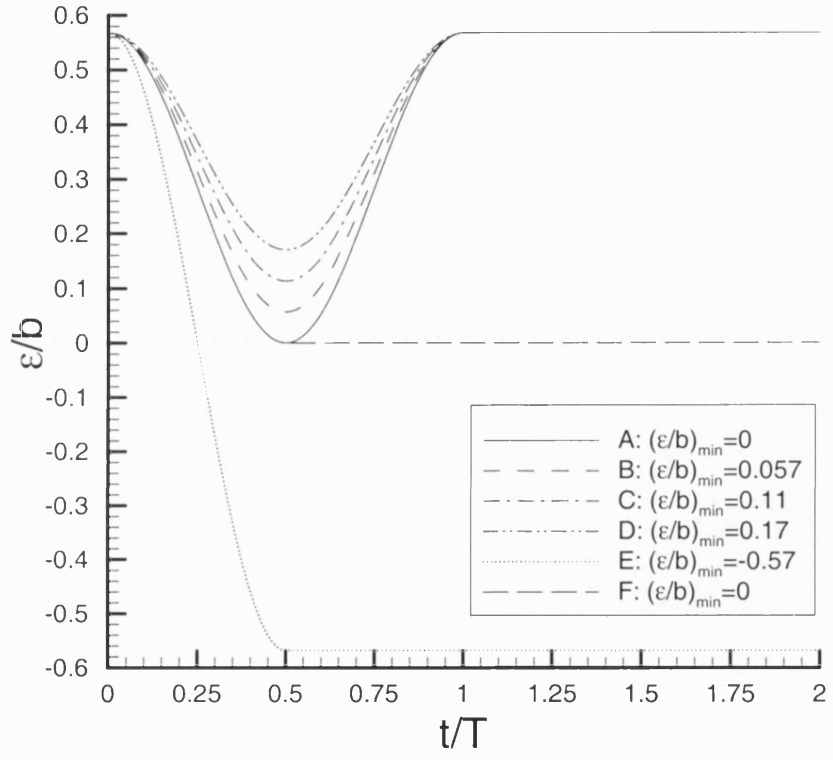

Figure 6.1: Time history of support and wing motion for transient cases studied.

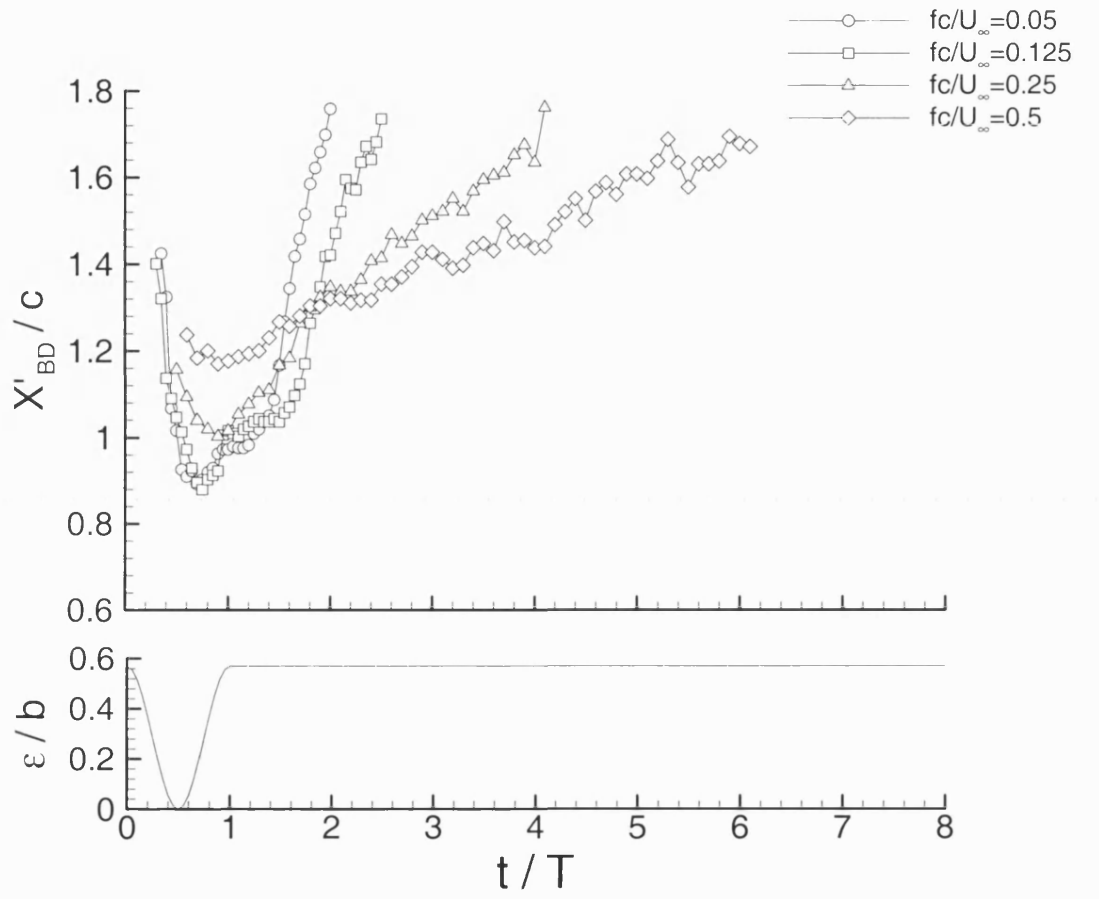

Figure 6.2: Transient response of vortex breakdown location to a single sinusoidal movement of 12mm cylindrical support (waveform A in Figure 6.1).

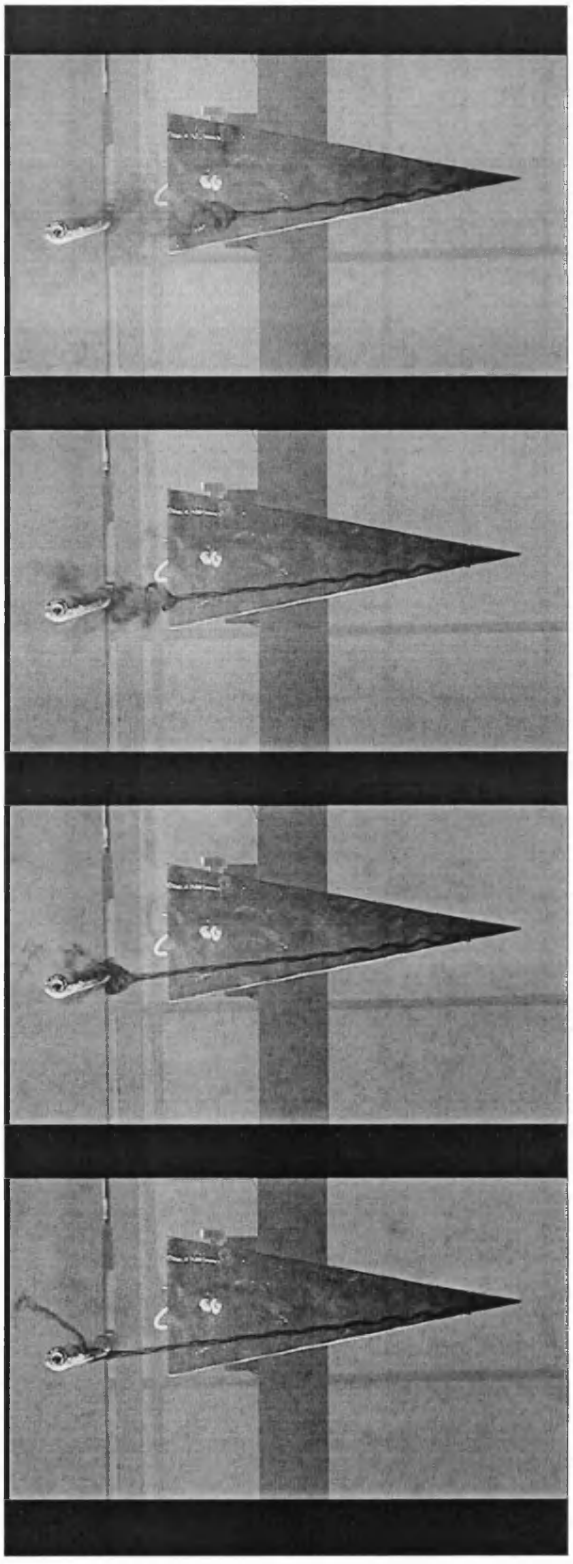

Figure 6.3: Flow visualisation of the interaction of leading-edge vortex with the dummy support at t/T = 0.5.

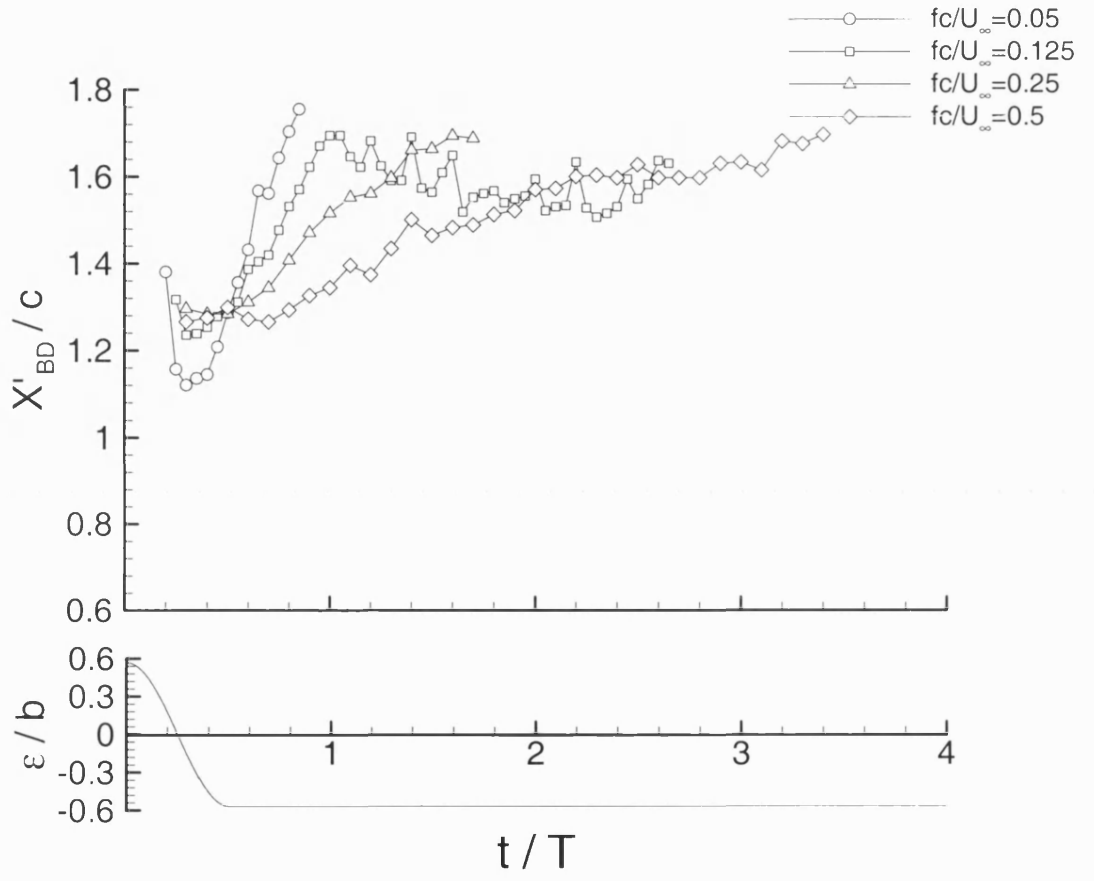

Figure 6.4: Transient response of vortex breakdown location to a half sinusoidal movement of 12mm cylindrical support (waveform E in Figure 6.1).

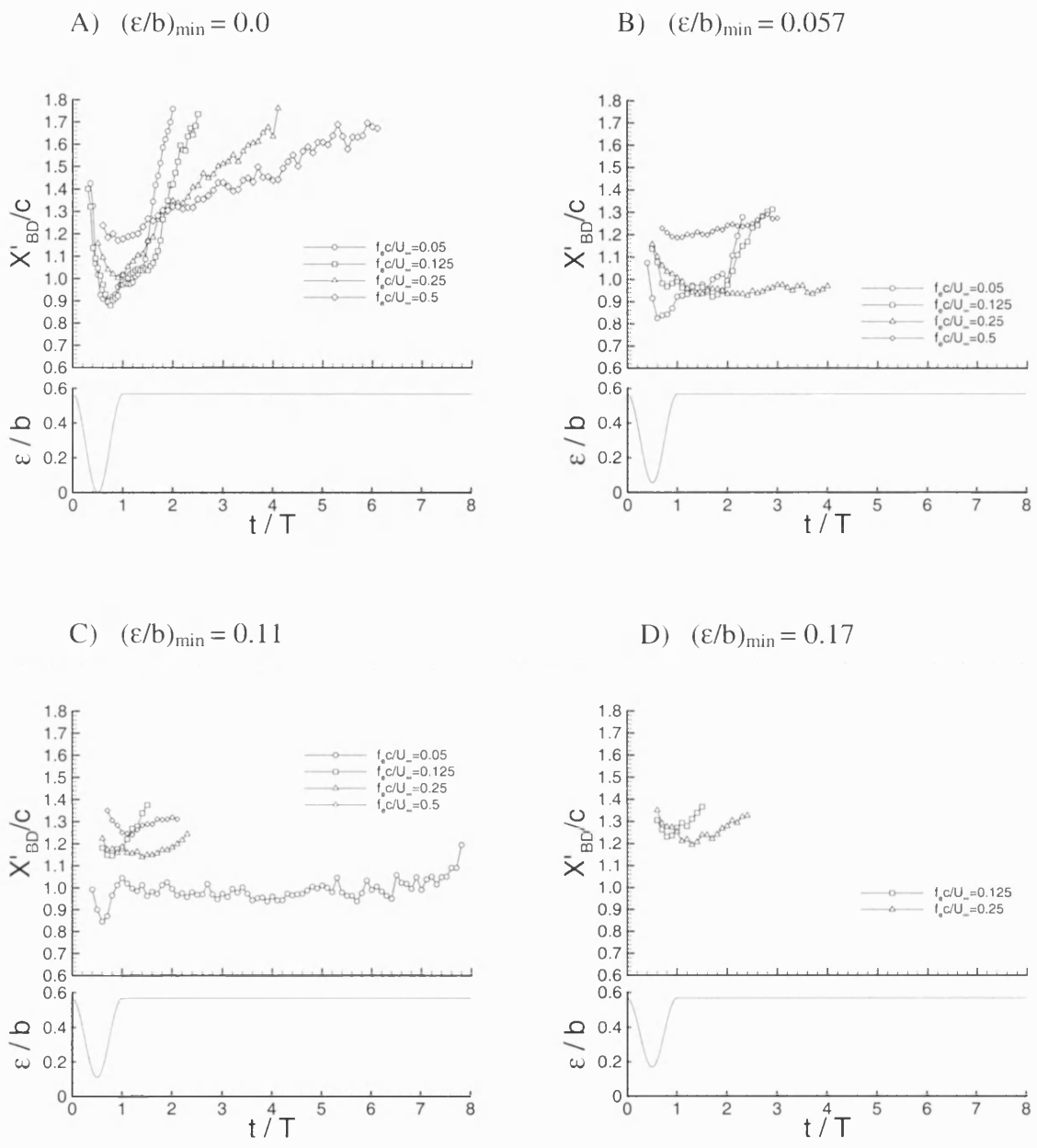

Figure 6.5: Transient response of vortex breakdown to a single sinusoidal movement of 12mm cylindrical support (waveforms A to D in Figure 6.1).

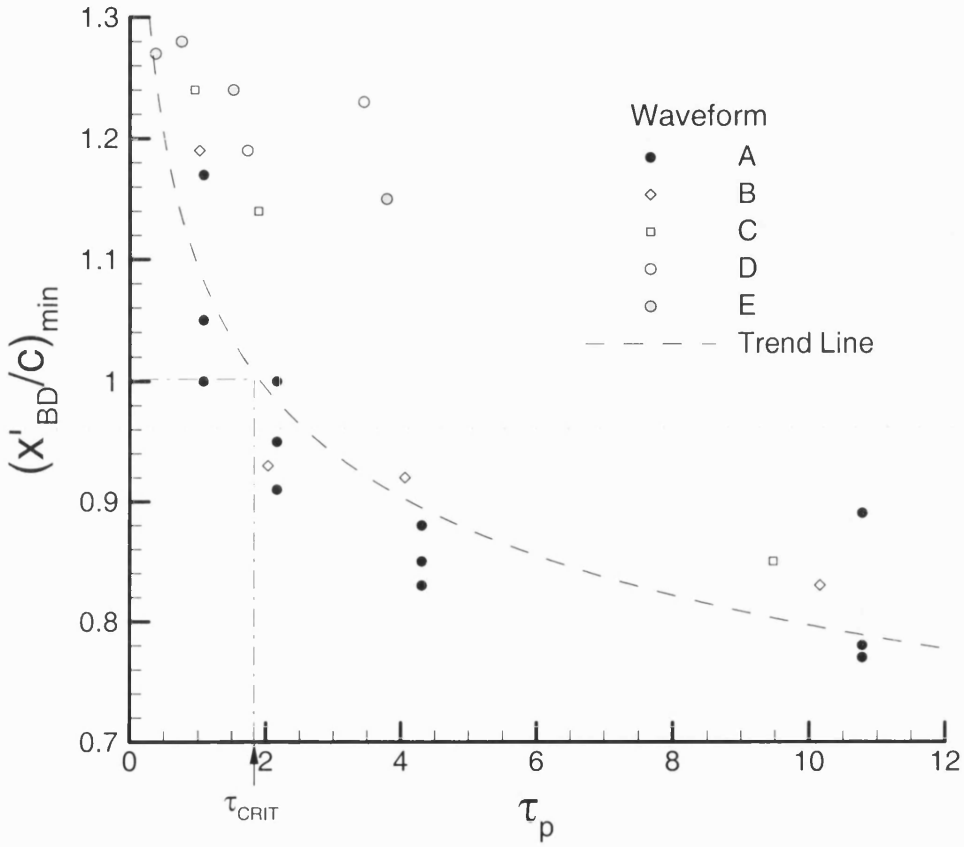

Figure 6.6: Variation of $(x'_{BD}/c)_{min}$ with τ_p for various transient motions and 12mm cylindrical support.

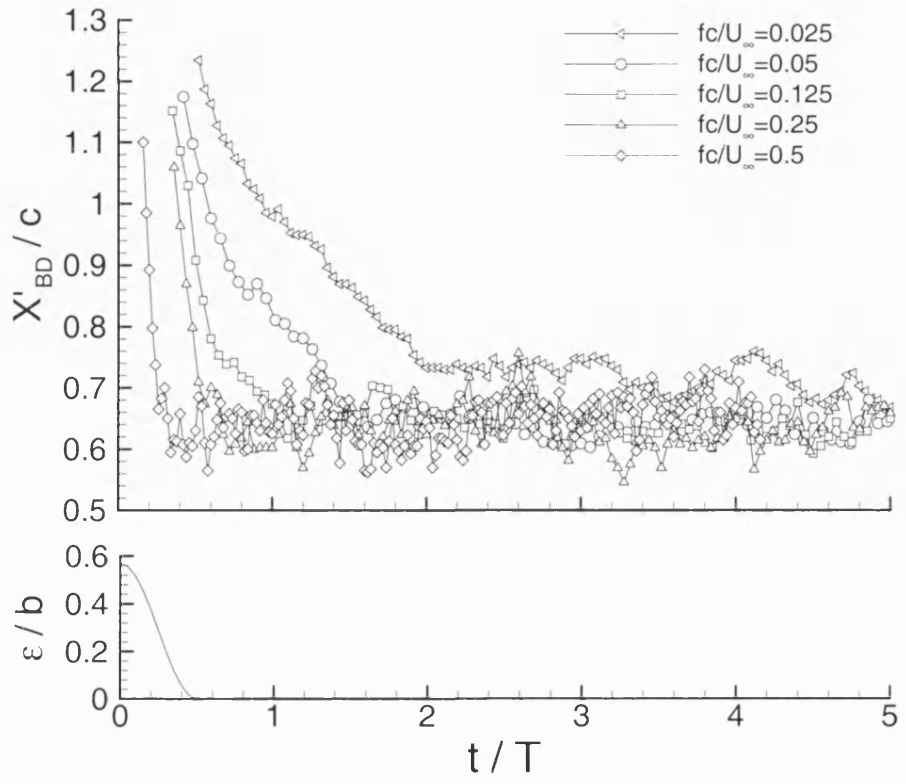

Figure 6.7: Transient response of vortex breakdown to transient movement of 12mm cylindrical support (waveform F in Figure 6.1).

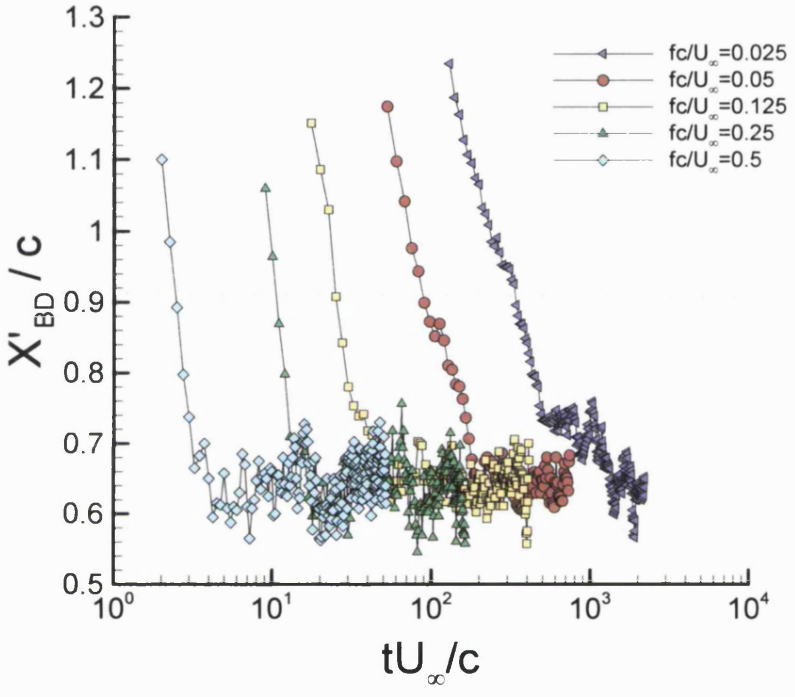

Figure 6.8: Transient response of vortex breakdown to transient movement of 12mm cylindrical support.

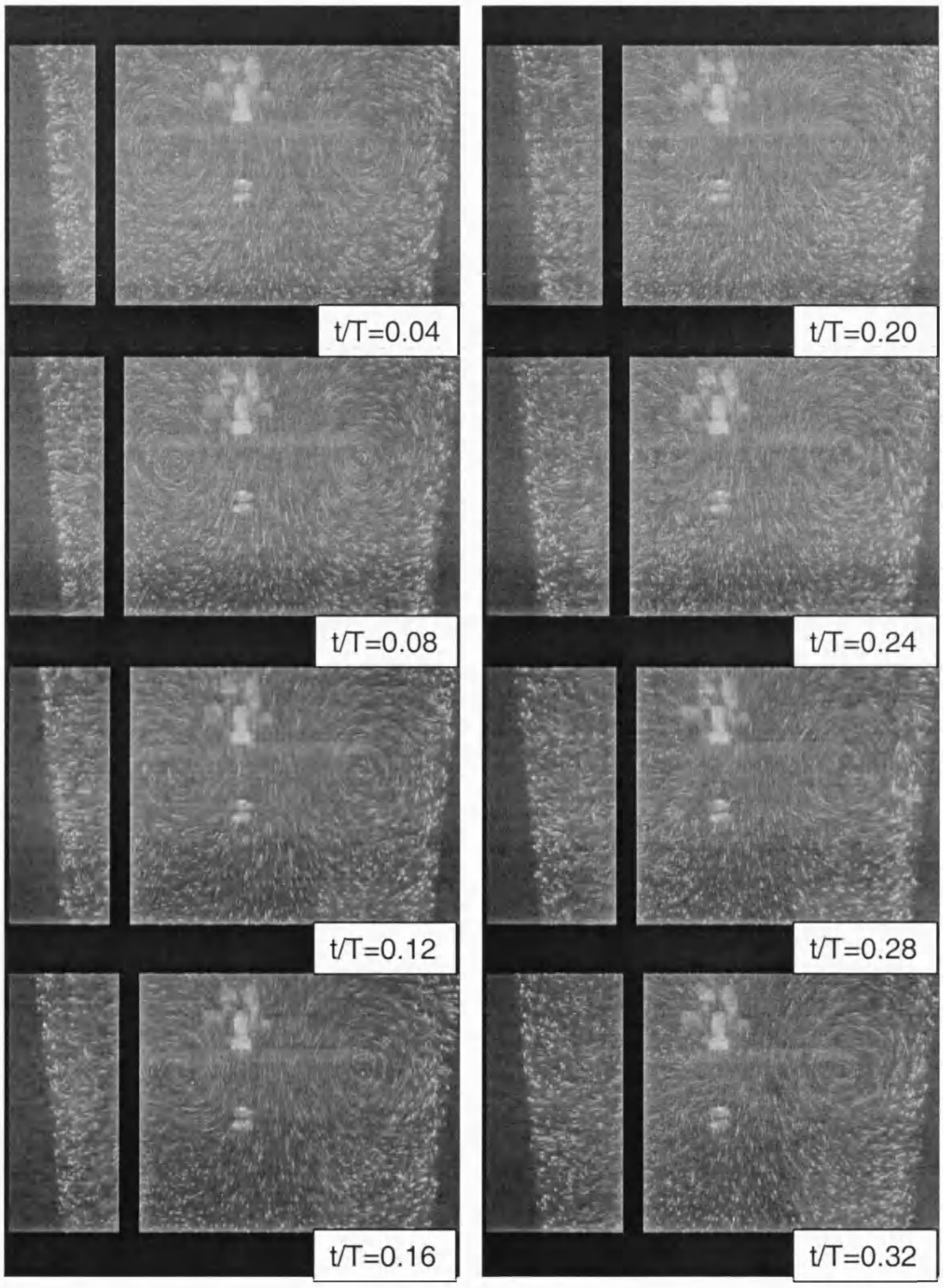

Figure 6.9: Laser sheet visualisation of the cross-flow plane at x_{LE} = c/4, showing interaction of 12mm cylindrical support with left-hand vortex.

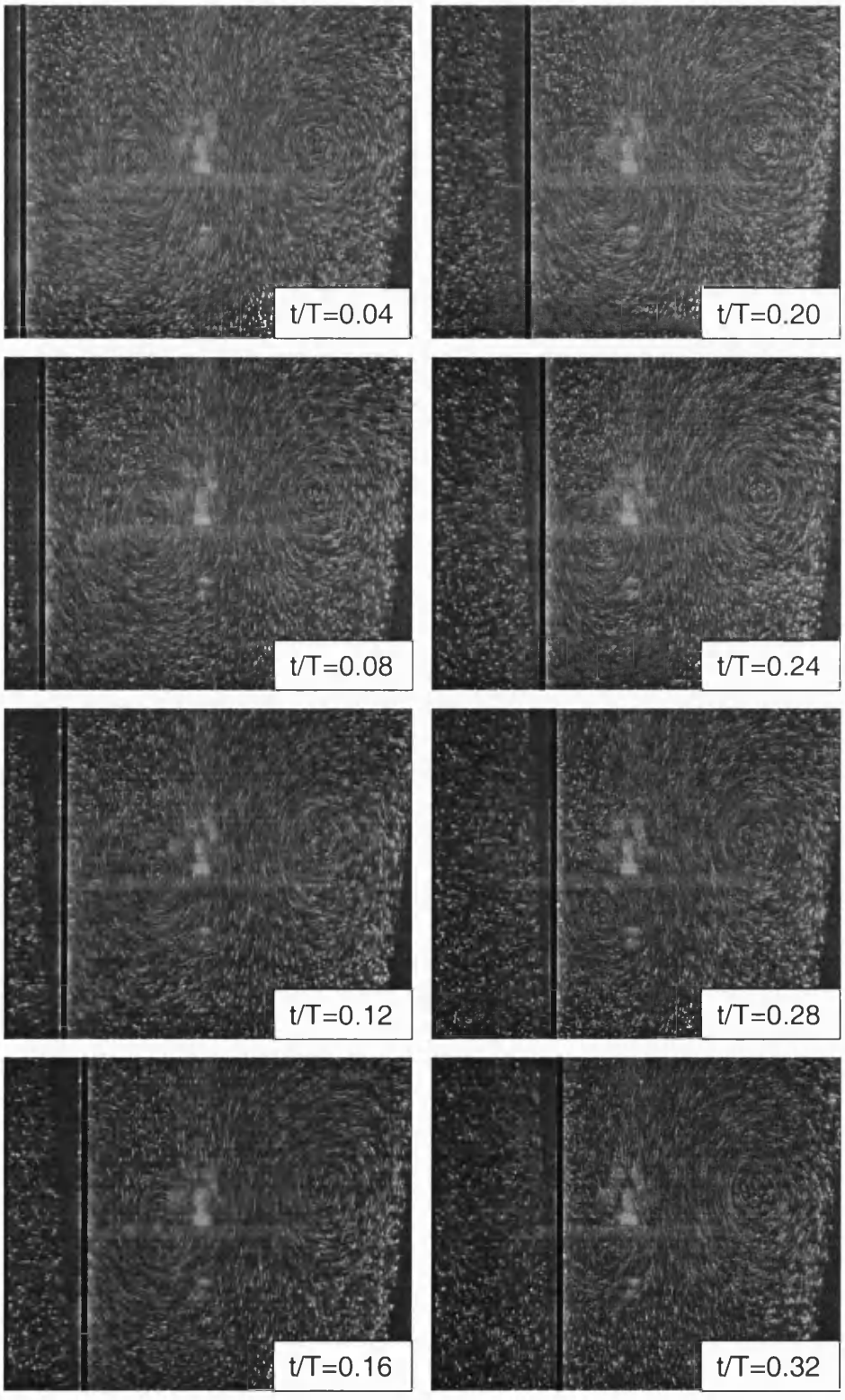

Figure 6.10: Laser sheet visualisation of the cross-flow plane at x_{LE} = c/4, showing interaction of 96mm flat-plate support with left-hand vortex.

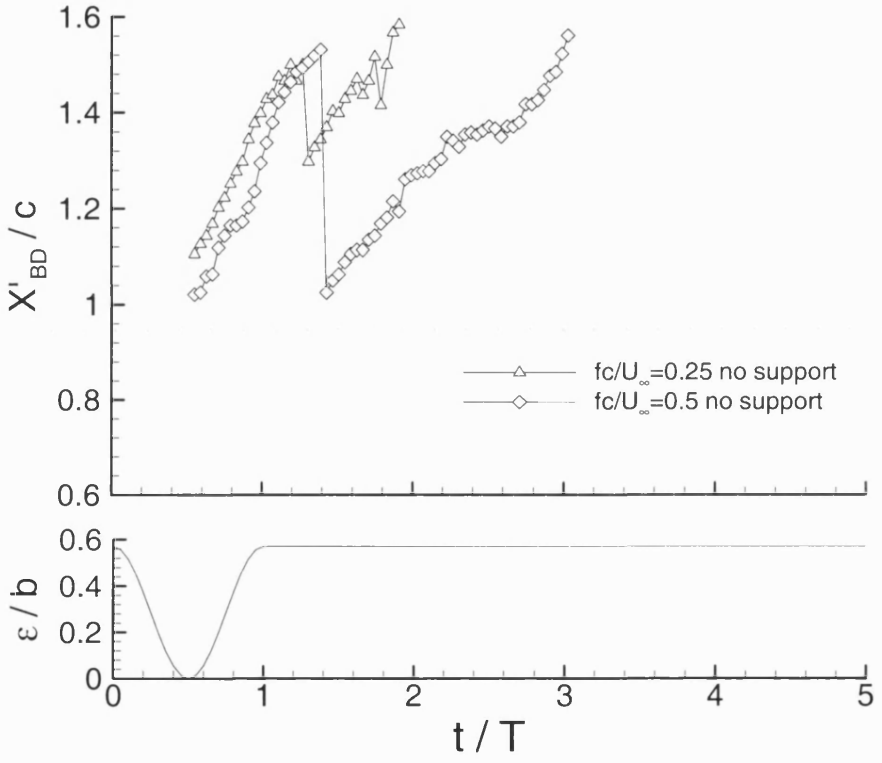

Figure 6.11: Transient response of breakdown to single sinusoidal movement of the wing (waveform A) with no dummy support.

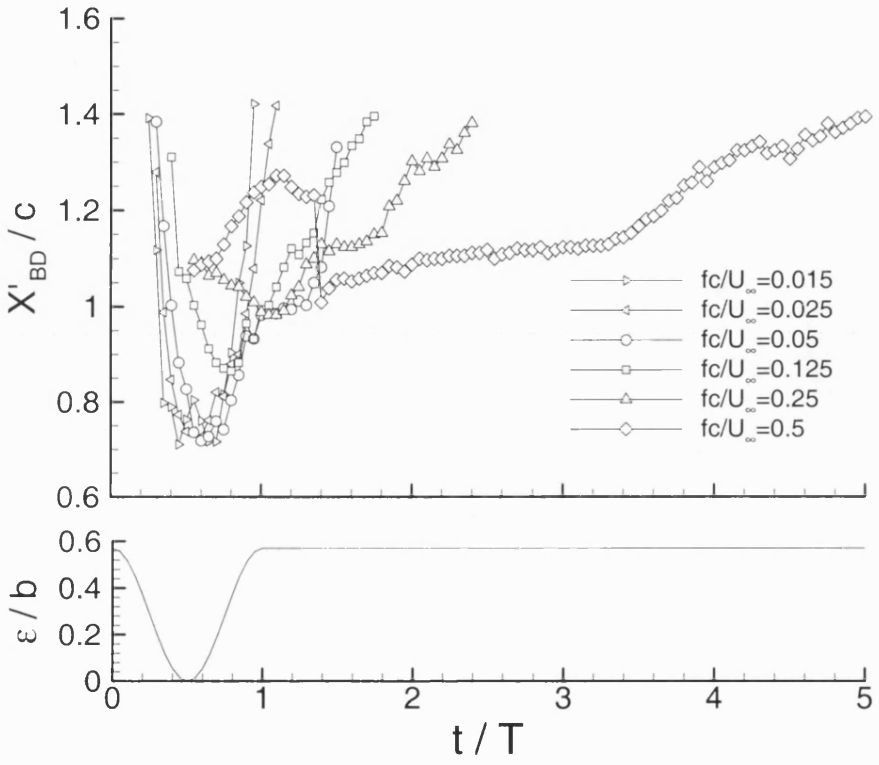

Figure 6.12: Transient response of breakdown to single sinusoidal movement of the wing (waveform A), with 12mm cylindrical support.

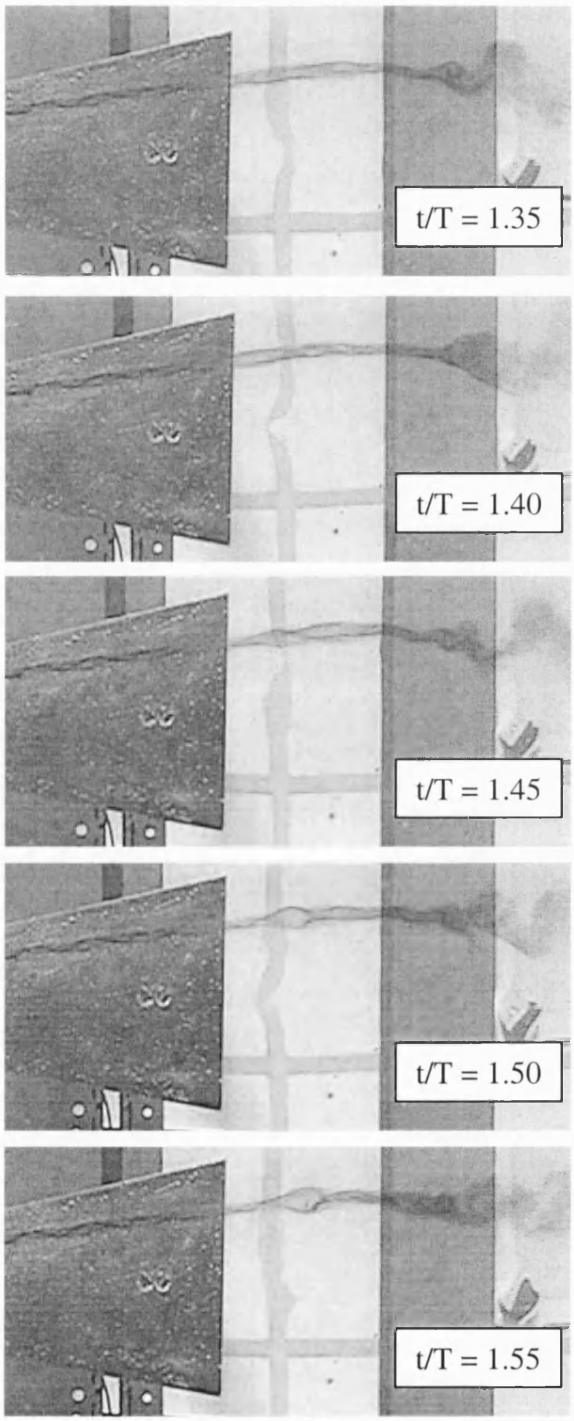

Figure 6.13: Development of a breakdown jump observed following cessation of a large amplitude transient model motion.

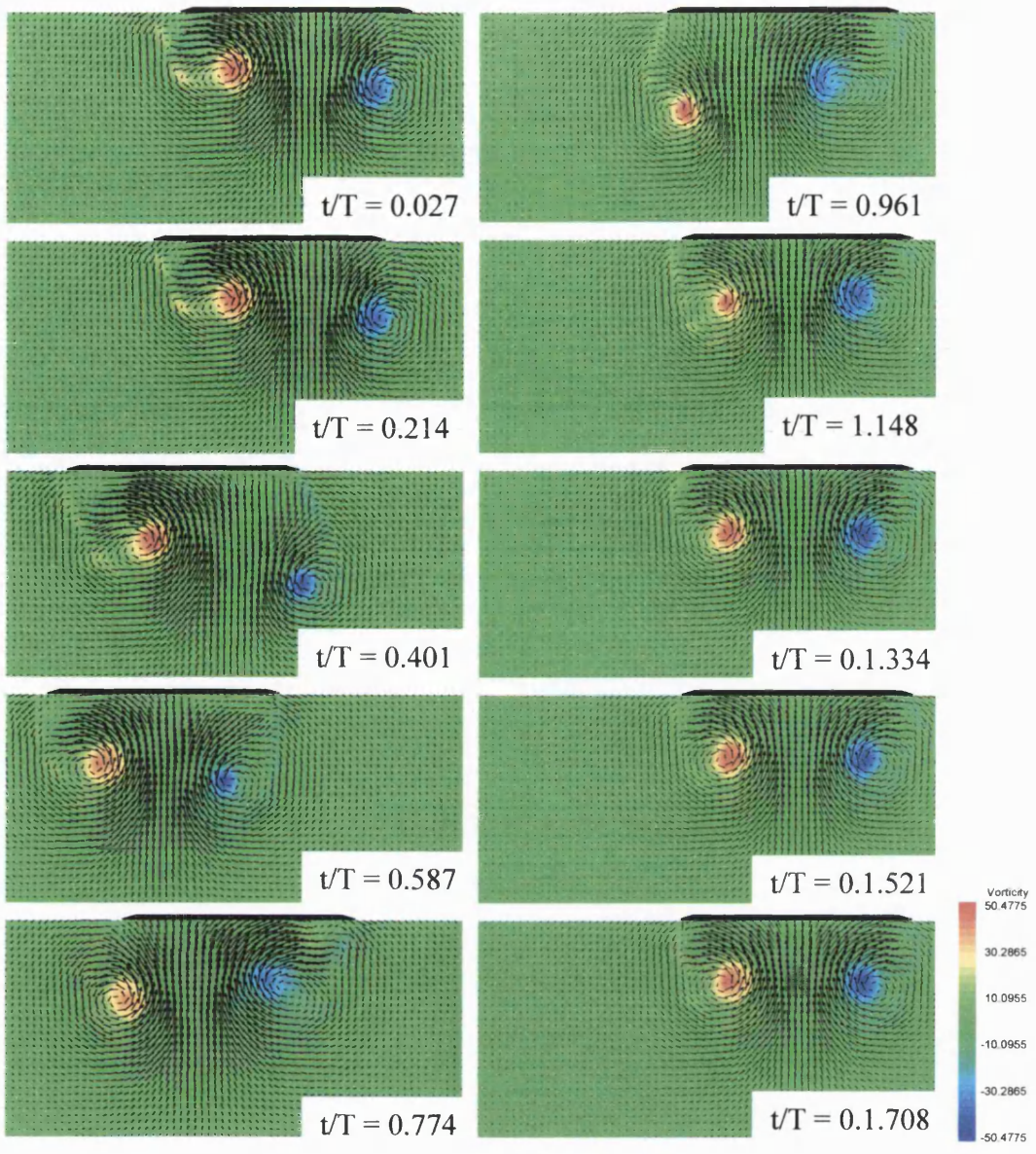

Figure 6.14: Velocity vectors plotted on contours of vorticity at x/c = 1.0, $f_e c/U_\infty = 0.5$ with no dummy support.

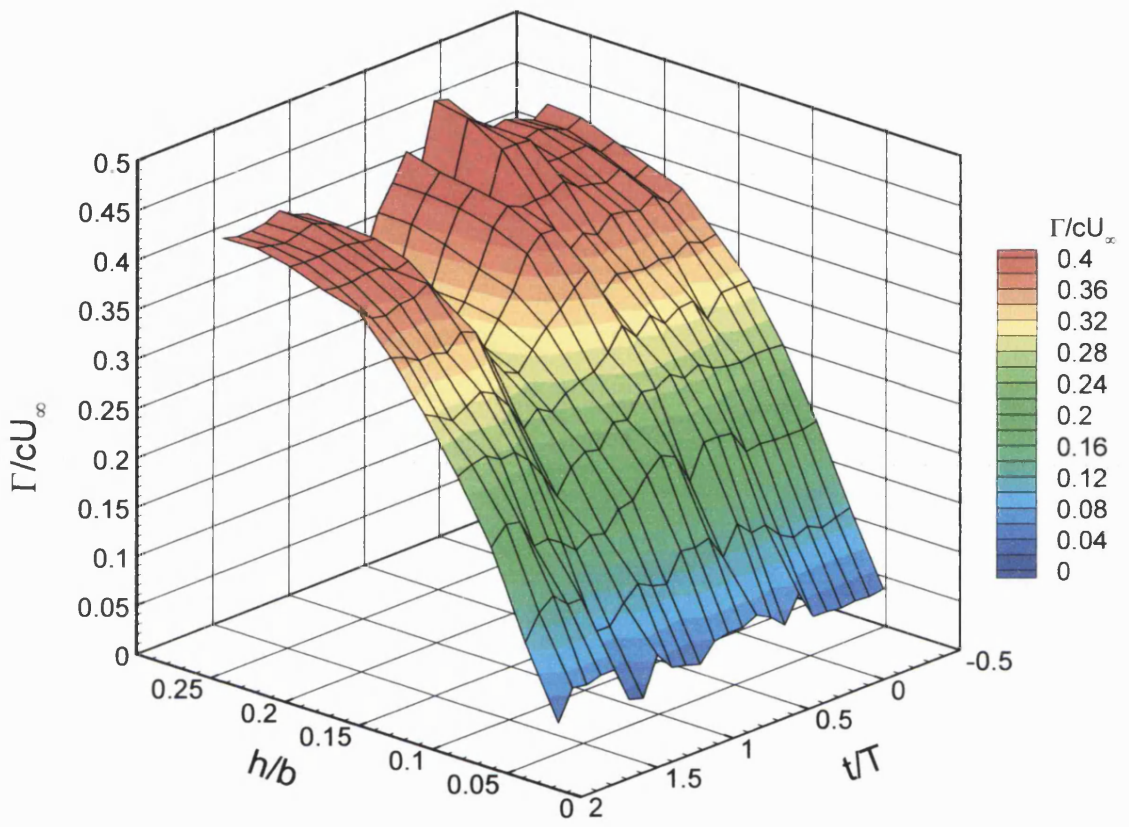

Figure 6.15: Variation of normalised circulation with square size and time.

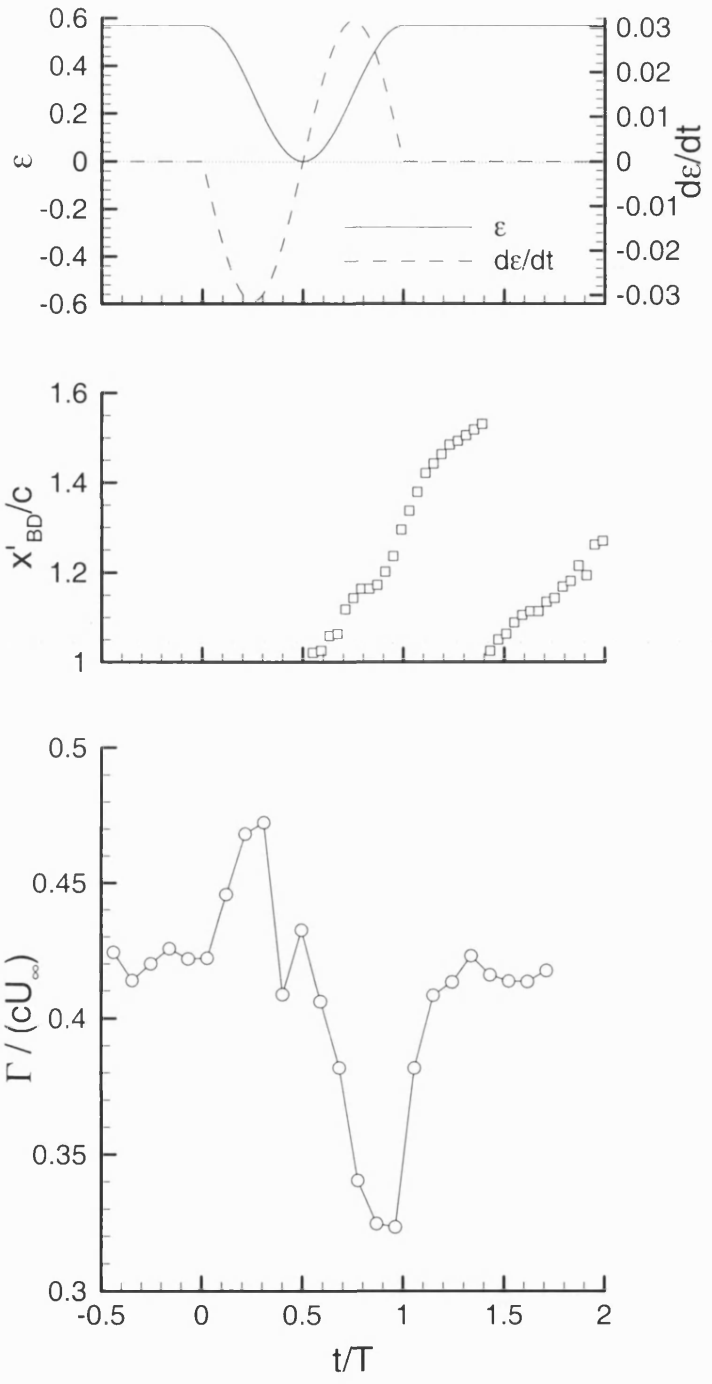

Figure 6.16: Variation of phase averaged circulation with time at h/b = 0.227, compared with phase averaged breakdown location (x'_{BD}/c) and location (ε) and velocity ($d\varepsilon/dt$) of wing through the transient cycle.

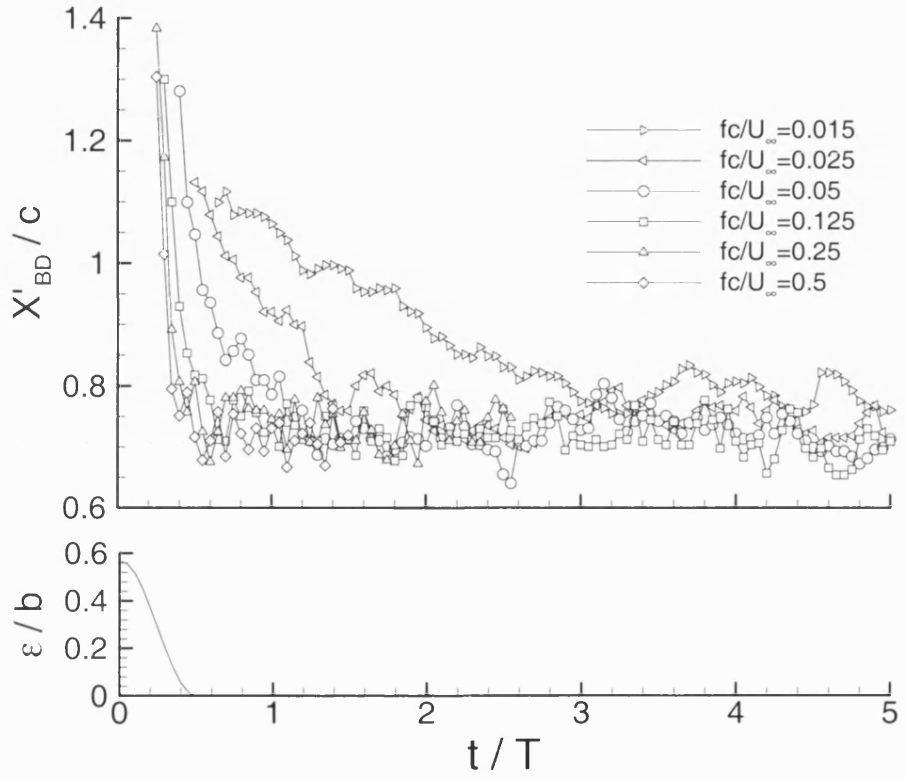

Figure 6.17: Transient response of breakdown to half sinusoidal movement of the wing (waveform F).

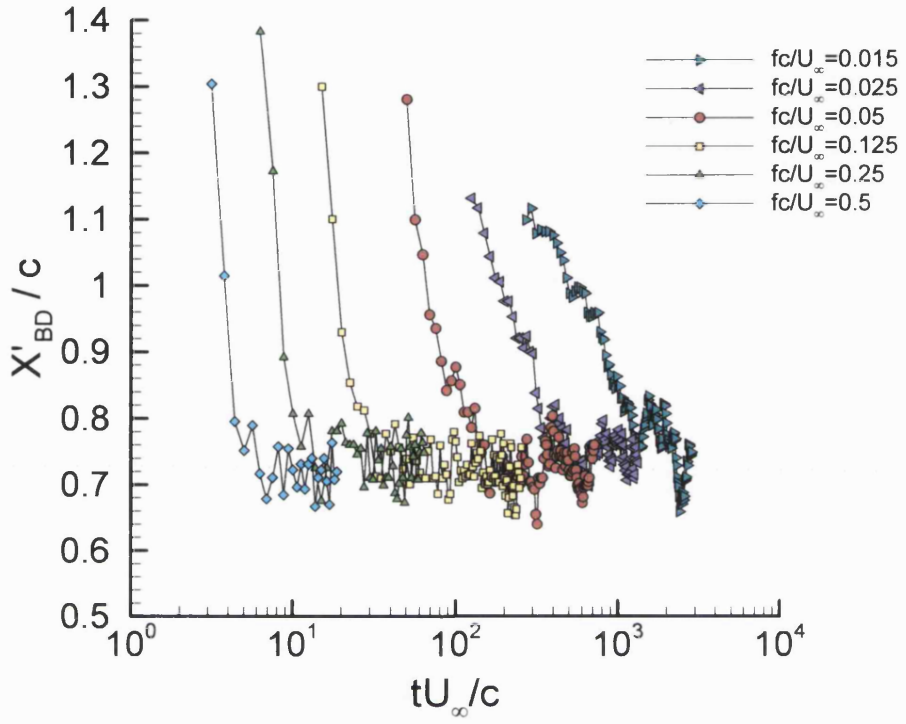

Figure 6.18: Transient response of breakdown to half sinusoidal movement of the wing.

Chapter 7 Review, Conclusions and Scope

7.1 Introduction

It is not the aim of this chapter to repeat the conclusions drawn in the previous chapters, but to review them in terms of the objectives of the research programme in order to give the reader an understanding of what answers to the support interference problem have been addressed. The chapter begins with a review of the objectives of the research programme, followed by a brief summary of the methodology employed. Following this is a discussion of support interference under each of the cases considered, and then a statement of the areas in which the author feels further attention is merited. Finally, some concluding remarks are made.

7.2 A Discussion of Support Interference

It was the aim of this investigation to study the effect of support interference in static, oscillatory and transient testing, with specific emphasis on the interaction with vortices generated by models at high incidence. More specifically it was hoped to investigate those conditions under which support interference may be a particular problem, and to use these results to formulate prediction tools where possible. With these aims in mind, the conclusions of the preceding chapters are reviewed.

The methodology employed was simple. In order to simplify the flow structure, simple delta wing models were used to represent a test model; a simplified 'dummy' support structure was then used to simulate a c-strut type support. The investigation was then

divided into three parts: support interference in static, oscillatory and transient testing. It is also useful here to review the classification of support interference. The use of the term 'severe' in terms of the breakdown response has been common in this report, and has been used in cases where breakdown of the vortices has been induced forward of the trailing edge where it does not occur in the natural case. In those cases where the interference induced breakdown aft of the trailing edge, the interference effect is not considered severe since no detriment to the lift force occurs.

7.2.1 Support Interference in Static Testing

A parametric study of a number of variables that affect the sensitivity of vortex breakdown to support interference was conducted. Since it is known from literature that the propensity of a vortex to break down is related to the strength of the vortex and the adverse pressure gradient acting on it, the parameters studied were classified accordingly. It was found that those parameters that affected the strength of the vortices (α, β, Λ) had a significant effect on the sensitivity of the vortex to support interference. In static testing there was a limited range of conditions under which support interference was considered to be severe. At low incidences the vortices were weak, and breakdown was only induced downstream of the trailing edge; increasing incidence resulted in a more significant breakdown response. However, consideration of the results leads to the conclusion that geometry is also a factor, since more slender wings were found to be more sensitive to support interference than non-slender wings. Therefore, the formation of the vortices is also a factor, and more careful study of these parameters, including the measurement of vortex strength for each case considered, would be advantageous.

It must be concluded, then, that the greatest factor in determining the sensitivity of an aircraft configuration to support interference is the strength of vortices shed from the model. If the vortices are of insufficient strength, there is no need to consider support interference effects, but conversely models that shed very strong vortical structures would be particularly prone to interference of this type.

Also studied was the effect of support geometry and location. Most significantly, under none of the conditions studied in this investigation was breakdown induced forward of the trailing edge when the dummy support structure was placed a distance of one chord

length downstream of the trailing edge of the delta wing. This shows that no matter what the strength of the vortices, interference may be avoided by increasing the distance between the model and the support. The effect of lateral support location was similar in that a vortex that impinged directly on the support was most affected, while moving the support to one side would reduce the interference effect.

Thus the two main parameters that affect the magnitude of the interference effect have been identified, being the strength of the vortices, and the distance between the model and the support. Another significant finding has been the observation of static hysteresis of vortex breakdown location when the lateral distance between the vortex core and the support was varied. This is the first time that hysteresis not involving changes to vortex strength has been reported, and represents another important consideration for the experimental researcher. Should a model be adjusted 'in-situ' and under 'wind-on' conditions (in an open-jet wind-tunnel, for example), it is possible that accidental obstruction of the vortices may induce a breakdown that will persist following removal of the obstruction; further, it may be the case that breakdown would not be apparent in this case under natural conditions. Although this particular scenario is unlikely, it does demonstrate the importance of understanding the hysteretic behaviour of the breakdown. It has been suggested that the pressure gradient associated with the trailing edge is the mechanism responsible for this form of hysteresis, and therefore the presence of similar behaviour over a realistic aircraft model will depend entirely on the geometry being considered.

Also studied was the effect of support geometry on the magnitude of interference. Five geometries were considered, and it was found that a cylindrical support performed significantly better than a thin flat plate support with a large streamwise dimension. The latter support was representative of a streamlined support structure, and it was therefore surprising that it had a greater effect on the vortex than did a cylindrical support that acted as a bluff body. A mechanism for this response was proposed based on the extent of separation over the leading edges of the plate.

Finally, lift force measurements were made to determine the relationship between premature breakdown of the leading edge vortices, and the reduction in lift generated by

the wing. It was found that, particularly for lower sweep angles, the lift detriment was lower than expected, and the peak detriment occurred at a greater incidence. For the 80° wing the maximum reduction in lift occurred at the incidence at which breakdown occurred at the trailing edge in the natural case, as was predicted from flow visualisation experiments. However, this relationship did not hold for lower sweep angles, where the maximum lift detriment occurred at the stall angle. For all the sweep angles considered, the incidence at which breakdown occurred at the trailing edge in the forced case was that at which the lift generated in the forced case began to differ from that observed in the natural case. This confirms the suspicion that support interference is only a problem when the breakdown is induced upstream of the trailing edge in the forced case; under other conditions the lift generated by the wing is not affected. The experimentalist need not, therefore, concern himself with any condition at which breakdown is induced artificially if it occurs downstream of the trailing edge of the wing. In the case of an aircraft model, premature breakdown of wing-tip or flap-edge vortices may affect the forces acting on the fuselage, and may also affect the dynamics of a multiple vortex flow. These are specific areas where further investigation would be required to draw further conclusions.

7.2.2 Support Interference in Oscillatory Testing

To simplify the consideration of vortex-support interactions in oscillatory testing, a moving support was first considered to remove the effects of time-dependent vortex strength. Following this, the moving wing case was considered. The type of motion considered consisted of a sinusoidal lateral movement, selected due to its ease of generation and analysis.

In the case of the moving support, for a case identified as being particularly sensitive in static testing, both the 12mm cylindrical and 96mm flat-plate supports were studied for three types of lateral motion. It was found that at low frequencies, both supports induced large fluctuations of breakdown location, of a frequency equal to the oscillating frequency. This indicates that the fluctuations observed were a result of the oscillation, rather than natural oscillations of the breakdown location. As the frequency of the support motion was increased, the magnitude of the breakdown fluctuations reduced,

the phase lag between the oscillation and the breakdown increased, and the RMS value of breakdown location tended to that observed in static testing. For the cylindrical support, the mean breakdown location observed in oscillatory testing was similar to that observed in static testing for all the amplitudes and frequencies of motion considered. However, it was noted that for the flat-plate support the mean breakdown locations were significantly further downstream in the oscillating case, and it was therefore concluded that the action of oscillating this support had a beneficial effect on the magnitude of support interference.

Analysis of the peak spectral magnitudes comparing the support motion with the breakdown fluctuations showed a similar trend to that observed by a previous investigator for a range of different forcing mechanisms. Phase calculations, however, were only qualitatively similar, showing greater phase angles than expected. The mechanism for this observation is expected to be the barrier between the support and the breakdown caused by the pressure gradient associated with the trailing edge, and this may explain the differences between the current observations and those presented in literature. However, despite the lack of quantitative similarity between the current results and those presented in literature, the fact that qualitatively the data show similar trends suggests that the mechanism of the breakdown response may be similar, and further investigation of this issue would be of benefit. Ultimately, if the mechanism controlling the breakdown response under dynamic conditions can be understood, one may be able to predict the breakdown response in a range of situations, such as fin buffeting and dynamic wing motions in addition to the support interference case studied here.

Lift force measurements were then made to understand the effect of the breakdown fluctuations on the lift generated by the wing. It was shown that the transit of the breakdown over the trailing edge resulted in a capped peak in some tests, once more confirming that breakdown aft of the trailing edge does not affect the lift force. For the conditions tested, it was also shown that lift force fluctuations were of a greater magnitude at an incidence greater than that at which the largest magnitude breakdown fluctuations were observed. This has again been attributed to the existence of the

trailing edge, and the possible transit of the breakdown over the trailing edge at the lower incidences.

Next, the breakdown response to a moving wing was considered. It was found that the breakdown response at low frequencies was similar to that observed in the moving support tests, with large amplitude breakdown fluctuations being observed with a frequency equal to that of the wing motion. As the frequency was increased, the magnitude of these fluctuations began to fall until, at a critical frequency, the fluctuations began to increase due to the effects of the time-dependent vortex strength. In the absence of a support, the critical frequency was in the range $0.125 < f_e c/U_\infty < 0.25$, but in the presence of a support, time-dependent vortex strength effects only began to dominate in the range $0.25 < f_e c/U_\infty < 0.5$. While this frequency is high compared to traditional aircraft manoeuvres, the effect of the support compared to the natural case was to move the mean breakdown location upstream at all frequencies, indicating that even at those frequencies at which time-dependent vortex-strength effects dominate, support interference is still a factor. Further, it is noted that there has recently been significant interest in the design and manufacture of Unmanned Air Vehicles (UAVs) that would not necessarily need to adhere to traditional low-g manoeuvres. As such, it is important to recognise the need to consider a wide range of manoeuvre rates in order for these results to apply over the range of traditional, modern and future aircraft configurations.

At low frequencies the moving support approximation is a valid technique to understand the effects of support interference, but the removal of time-dependent vortex strength effects limits its validity at high frequencies. In moving support tests, it was shown that the breakdown response tended to that observed in static testing, at least in terms of the magnitude of the breakdown fluctuations, while in the moving wing case, a much more severe response is observed.

A number of important observations have been made relating to the behaviour of the vortices at high forcing frequencies. It was noted that the trajectories of the vortices were altered by the movement of the wing through the fluid, with the vortex on the windward side of the model moving towards the wing surface and the wing centreline,

while the opposite motion occurred on the leeward side. Significant 'kinking' of the vortex was seen under some conditions, which was related to the change in direction of the wing at the limits of its motion. Most curious was the observation of a jumping of the breakdown location on the windward side of the model at high frequencies. In this case the breakdown was seen to rapidly progress upstream, to the point where in some cases, two breakdowns were observed in the flow simultaneously. PIV measurements of the cross-flow plane, and subsequent circulation calculations, have shown that a rapid increase in vortex strength may be the cause of this phenomenon, and parallels have been drawn with a similar result found in vortex tube experiments presented in literature. The effect of the support was to reduce the magnitude of the breakdown jump, but jumping was nevertheless observed in all the cases considered at high enough forcing frequencies.

Thus the overall response of vortex breakdown to an oscillatory lateral motion has been elucidated, but it is felt that further investigation is merited to expand the database of results. Too few cases were investigated in this research to enable a prediction methodology to be formulated, although it can be stated that a wing that is sensitive to breakdown in static testing will be similarly sensitive in oscillatory testing. As was the case for static tests, the overall response will be a function of the mean strength of the vortices and the location of the support. It is recommended that future investigations focus on alternative motions, such as pitching, rolling and yawing, and that comparisons be drawn with the current case.

7.2.3 Support Interference in Transient Testing

In transient testing two principal transient motions were considered: a single sinusoidal motion that moves into, and then out of the vortex core; and a half sinusoidal motion that starts outside the vortex, and completes inline with the vortex core. Both of these types of motion were tested for the moving support and moving wing cases. For both types of motion, it was found that the point at which breakdown was first observed was delayed as the forcing frequency was increased, and flow visualisations indicated that the cause of this was the deflection of the vortex around the incumbent object at high frequencies. In some cases the support had passed its closest point to the vortex before

a clear breakdown was observed. This implies that if, during a transient test, a support were to move through a vortex core at a high enough speed, it would not severely affect the breakdown location.

In the case of the former type of motion, for the moving support a correlation between a time parameter and the most upstream breakdown location induced by each motion was found. The time parameter is a value based on the amount of time during each cycle that the support spends in the "range of influence" of the vortex, as defined in static testing. It was also possible, for the cases considered, to identify a critical value of the time parameter, at which greater values would induce a severe breakdown response. Theoretically, this technique should allow the prediction of the magnitude of the support interference effect quite simply. However, although a good correlation was found between these variables, a large database of experimental information would be required to employ this method as a reliable prediction tool, and its limitations are recognised. It may be possible to use a limited dataset to formulate a semi-empirical prediction tool, and to then test this on further datasets, and in this way it may be possible to reduce the number of datasets that need to be considered.

In the case of the latter form of motion, the speed of the breakdown response was measured by calculating the slope of the linear portion of the response curve, and it was found that the breakdown responded quicker to a higher frequency support motion, which may be expected due to the speed at which the support approaches the vortex.

In the moving wing case, similar observations of vortex strength time-dependency were observed as in oscillatory testing. In particular, the jumping of the breakdown location at high frequencies was still apparent, although in the cases considered the jump did not occur until completion of the motion of the wing. PIV measurements and circulation calculations showed, as before, that the breakdown jump coincided with a rapid increase in vortex strength, and that this may be the origin of the observations. However, the need for further investigation is recognised, as the phenomenon may be more complex than the analysis employed herein. There is no doubt though that these observations are important for consideration of future aircraft designs. With the advent of greater

manoeuvring speeds, the behaviour of the breakdown in this manner at high frequencies may be of particular interest.

Returning to the support interference case, the effect of the moving wing was to induce breakdown further upstream than in the moving support case. Further, the existence of breakdown jumping resulted in the breakdown persisting for longer in this case. Although no attempt has been made, it is possible that the time parameter used to predict breakdown response in the moving support case, may be adapted to incorporate the effect of vortex jumping at high frequencies, although it is expected that resolution of this may be difficult. In the case of the motion that completed its motion in line with the vortex core, the effect of the moving wing was to increase the gradient of the response at high frequencies, indicating that the breakdown responded quicker in this case.

Overall, it has been shown that the breakdown response to support interference in transient testing is more complex than in oscillatory testing. Despite this, and in the absence of vortex-strength effects, a prediction methodology has been suggested that may prove to be a useful starting point for further investigation.

7.3 Scope for Future Work

It was concluded during static testing that the extent of support interference is a function of the strength of the leading edge vortices. A number of conditions under which support interference is of particular concern have been identified, and in particular the importance of vortex strength has been demonstrated. It was therefore felt that, given further time and resources, it would be beneficial to quantify the strengths of the vortices for a range of sweep angles and incidences, and to correlate this data with the regions of sensitivity that have been identified. It is expected that a study of this type would elucidate those conditions under which a vortex is sensitive, data which could then be extrapolated not only to simple deltas of different sweep angles to those studied here, but to alternative wing planforms. In dynamic testing, more waveforms need to be considered, and perhaps different forms of motion (such as roll, pitch and yaw, for

example). It would also be useful to consider the effect of premature breakdown on the pitching and rolling moments generated by the wing, in addition to the effect on lift force along. Further, studying the forces generated by the wing in the moving wing case would provide further understanding of the influence of premature breakdown.

An area of particular interest, and one in which the author is particularly keen to see more progress, is that of vortex breakdown jumping. More work on understanding the role that varying circulation plays in the process is important, in addition to trying to determine what other factors may play a role. The hypothesis relating to the rapid increase of vortex strength agrees well with the results presented, but further experimentation is required to fully understand the relationship, particularly since this phenomenon may have wider interest in the study of dynamic aircraft motions in general.

In static testing, it was hypothesised that the extent of separation over the leading edge of the plate was the cause of the large effect on the breakdown location. Although literature has been cited that tends to confirm this hypothesis, more investigation of this area is required before firm conclusions may be drawn. Particularly in this area the use of computational techniques would be of benefit in understanding the interaction between the support structure and the vortex.

7.4 Concluding Remarks

Support interference in static, oscillatory and transient testing has been investigated. Although a number of advances have been made, only a limited number of cases were tested making formulation of prediction tools difficult. However, the form of the response in each of these cases has been elucidated both in the simplified case of constant vortex strength, and the more complex moving wing case. In the latter case, interesting observations have been made regarding the changes in vortex trajectory during the motions, and in particular a breakdown jumping phenomenon has been identified.

Chapter 8 References

Allan, M. R. (2002), 'A CFD investigation of wind tunnel interference on delta wing aerodynamics', Ph.D. Thesis, Dept. of Aerospace Engineering, University of Glasgow, Scotland, UK.

Anderson, J. D. (2001), 'Fundamentals of aerodynamics', *McGraw-Hill*, 3rd Ed., ISBN 0-07-118146-6.

Bartlett, G. E. and Vidal, R. J. (1955), 'Experimental investigation of influence of edge shape on the aerodynamic characteristics of low aspect ratio wings at low speeds', *J. Aero. Sci.*, Vol. 22, No. 8, pp. 517-533.

Benjamin, T. B. (1962), 'Theory of the vortex breakdown phenomenon', *J. Fluid Mech.*, Vol. 14, pp. 593-629.

Benjamin, T. B. (1967), 'Some developments in the theory of vortex breakdown', *J. Fluid Mech.*, Vol. 28, part 1, pp. 65-84.

Beran, P. S. and Culick, F. E. C. (1992), 'The role of non-uniqueness in the development of vortex breakdown in tubes', *J. Fluid Mech.*, Vol. 242, pp. 491-527

Beyers, M. E. (1992), 'Unsteady wind-tunnel interference in aircraft dynamic experiments', *J. Aircraft*, Vol. 29, No. 6, pp. 1122-1129

Beyers, M. E. and Ericsson, L. E. (1993), 'Ground facility interference on aircraft configurations with separated flow', *J. Aircraft*, Vol. 30, No. 5, pp. 682-688

Beyers, M. E. and Ericsson, L. E. (2000), 'Implications of recent rotary rig results for flight prediction', *J. Aircraft*, Vol. 37, No. 4, pp. 545-553.

Canbazoglu, S., Lin, L. -C., Wolfe, S., and Rockwell, D. (1995), 'Buffeting of fin: Distortion of incident vortex', *AIAA Journal*, Vol. 33, No. 11, pp. 2144-2150.

Délery, J. M. (1992), 'Physics of vortical flows', *J. Aircraft*, Vol. 29, No.5, pp. 856-876.

Délery, J. M. (1994), 'Aspects of vortex breakdown', *Prog. Aero. Sci.*, Vol. 30, pp. 1-59.

Deng, Q. and Gursul, I. (1997), 'Vortex breakdown over a delta wing with oscillating leading edge flaps', *Exp. Fluids*, Vol. 23, pp. 347-352.

Earnshaw, P. B. and Lawford, J. A. (1964), 'Low-speed wind-tunnel experiments on a series of sharp-edged delta wings', *ARC R&M 3424.*

Elle, B. J. (1958), 'An investigation at low speed of the flow near the apex of thin delta wings with sharp leading edges', *ARC R&M 3176.*

Elle, B.L. (1960), 'On the breakdown at high incidences of the leading edge vortices on delta wings', *J. Royal Aero. Soc.*, Vol. 64.

Erickson, G. E. (1982), 'Water-Tunnel studies of leading-edge vortices', *J. Aircraft*, Vol. 19, No. 6, pp. 442-448.

Ericsson, L. E. (1991), 'Another look at high-alpha support interference in rotary tests', *J. Aircraft*, Vol. 28, No. 5, pp. 584-591.

Ericsson, L. E. and Beyers, M. (2000), 'Aspects of ground facility interference on leading-edge vortex breakdown', AIAA Paper 2000-0978, *38th Aerospace Sciences Meeting and Exhibit*, 10-13 Jan 2000, Reno NV.

Ericsson, L. E. and Reding, J. P. (1983), 'Review of support interference in dynamic tests', *AIAA Journal*, Vol. 21, No. 12, pp. 1652-1666.

Ericsson, L. E. and Reding, J. P. (1986), 'Dynamic support interference in high-alpha testing', *J. Aircraft*, Vol. 23, No. 12, pp. 889-896.

Escudier, M. (1988), 'Vortex Breakdown: Observations and explanations', *Prog. Aero. Sci.*, Vol. 25, pp. 189-229.

EDSU (1980), 'Blockage correction for bluff bodies in confined flows', *Engineering and Sciences Data Unit*, Item 80024.

Faler, J. H. and Leibovich, S. (1977), 'Disrupted states of vortex flow and vortex breakdown', *Phys. Fluids*, Vol. 20, pp. 1385-1400.

Frink, N. T. (1987), 'Computational study of wind-tunnel wall effects on the flow field around delta wings', AIAA-87-2420, 1987.

Gad-el-Hak, M. and Blackwelder, R., F. (1985), 'The discrete vortices from a delta wing', *AIAA Journal*, Vol. 23, No. 6, pp. 961-962.

Garg, A. K. and Leibovich, S. (1979), 'Spectral characteristics of vortex breakdown flowfields', *Phys. Fluids*, Vol.22, No. 11, pp. 2053-2064.

Goldstein, R. J. (1983), 'Fluid mechanic measurements', 2nd Ed., Taylor and Francis Pub., ISBN 1-56032-306-X.

Gordnier, R. E. and Visbal, M. R. (1994), 'Unsteady vortex structure over a delta wing', *J. Aircraft*, Vol. 31, No. 1, pp. 243-248.

Gordnier, R. E. and Visbal, M. R. (1999), 'Numerical simulation of the impingement of a streamwise vortex on a plate', *IJCFD*, Vol. 12, pp. 49-66.

Greenwell, D. I. (1998), 'A review of low-speed maneuvering aerodynamics of slender configurations', *DERA/MSS4/CR980592/1*.

Greenwell, D. I. and Wood, N. J. (1982), 'Determination of vortex burst location on delta wings from surface pressure measurements', *AIAA J.*, Nov. 1982, pp. 2736-2739.

Greenwell, D. I. and Wood, N. J. (1994), 'Some observations on the dynamic response to wing motion of the vortex burst phenomenon', *Aero. J.*, Feb. 1994, pp. 49-59.

Guglieri, G. and Quagliotti, F. B. (1997), 'Experimental investigation of vortex dynamics on a 65° delta wing in sidesip', *Aero. J.*, March 1997, pp. 111-120

Gursul, I. (1994), 'Unsteady flow phenomena over delta wings at high angles of attack', *AIAA Journal*, Vol. 32, No. 2, pp. 225-231.

Gursul, I. (1995), 'Criteria for location of vortex breakdown over delta wings', *Aero. J.*, pp. 194-196.

Gursul, I. (2000), 'A proposed mechanism for the time lag of vortex breakdown location in unsteady flows', AIAA Paper 2000-0787, *38th Aerospace Sciences Meeting and Exhibit*, 10-13 Jan 2000, Reno, NV.

Gursul, I. and Ho, C. (1994), 'Vortex breakdown over delta wings in unsteady freestream', *AIAA Journal*, Vol. 32, No. 2, pp. 433-436.

Gursul, I., Taylor, G. S., and Wooding, C. (2002), 'Vortex flows over fixed-wing micro air vehicles', AIAA Paper 2002-0698, 40th AIAA Aerospace Sciences Meeting and Exhibit, 14-17 January 2002, Reno, NV.

Gursul, I. and Xie, W. (1999), 'Buffeting flows over delta wings', *AIAA Journal*, Vol. 37, No. 1, pp. 58-65.

Gursul, I. and Xie, W. (2001), 'Interaction of vortex breakdown with an oscillating fin', *AIAA Journal*, Vol. 39, No. 3, pp. 438-446.

Gursul, I. and Yang, H. (1995), 'On fluctuations of vortex breakdown location', *Phys. Fluids*, Vol. 7, No. 1, pp. 229-231.

Hall, M. G. (1961), 'A theory for the core of a leading-edge vortex', *J. Fluid Mech.*, Vol. 11, pp. 209-228.

Hall, M. G. (1966), 'The structure of concentrated vortex cores', *Prog. Aero. Sci.*, Vol. 7, pp. 53-110.

Hall, M. G. (1972), 'Vortex breakdown', *Ann. Rev. Fluid Mech.*, Vol. 4, pp. 195-217.

Hart, D. P. (1998), 'The elimination of correlation errors in PIV processing', *9th International Symposium on Applications of Laser Techniques to Fluid Mechanics*, Lisbon, Portugal, July 1998.

Hemsch, M. J. and Luckring, J. M. (1990), 'Connection between leading edge sweep, vortex lift, and vortex strength for delta wings', *J. Aircraft*, Vol. 27, No. 5, pp.473-475.

Hsing, C-C. A. and Lan, C. E. (1997), 'Low-speed wall interference assessment / correction with vortex flow effect', J. Aircraft, Vol. 34, No. 2, pp. 220-227.

Huang, X. Z. and Hanff, E. S. (2000), 'Visualisation of Bifurcating vortex breakdown location over slender delta wings', *9th International Symposium on Flow Visualisation*, Heriot-Watt University, Edinburgh.

Hummel, D. (1965), 'Untersuchungen über das Aufplatzen der Wirbel an schlanken Delta Flügeln', *Zeitschrift für Flugwissenschaften*, Vol. 5, No. 3, pp.158-168.

Hummel, D. and Srinivasan, P. S. (1967), 'Vortex breakdown effects on the low-speed aerodynamic characteristics of slender delta wings in symmetric flow', *J. Royal Aero. Soc.*, Vol. 71, pp. 319-322.

Johnson, J. L., Grafton, S. B., and Yip, L. P. (1980), 'Exploratory investigation of vortex bursting on the high angle of attack lateral directional stability characteristics of highly swept wings', AIAA Paper 80-0463.

Jumper, E. J., Nelson, R. C., and Cheung, K. (1993), 'A simple criterion for vortex breakdown', AIAA-93-0866, *31st Aerospace Sciences Meeting and Exhibit*, 11th-14th Jan, Reno NV.

Kline, S. J. and McClintock, F. A. (1953), 'Describing uncertainties in single-sample experiments', *Mechanical Engineering*, Vol. 75, No. 1, 1953, pp. 3-8.

Lambourne, N. C. and Bryer, D.W. (1961), 'The bursting of leading edge vortices – some observations and discussion of the phenomenon', *ARC R&M 3282*.

Lee, B. H. K. and Tang, F. C. (1994), 'Characteristics of the surface pressures on a F/A-18 vertical fin due to buffet', *J. Aircraft*, Vol. 31, No. 1, pp. 228-235.

Lee, M. and Ho, C. (1990), 'Lift force of delta wings', *App. Mech. Rev.*, Vol. 43, No. 9, pp. 209-221.

Leibovich, S. (1978), 'The structure of vortex breakdown', *Ann. Rev. Fluid Mech*, Vol. 10, pp. 221-246.

Leibovich, S. (1984), 'Vortex stability and breakdown: survey and extension', *AIAA Journal*, Vol. 22, No. 9, pp. 1192-1206.

Lopez, J. M. (1994), 'On bifurcating structure of axisymmetric vortex breakdown in a constricted pipe', *Phys. Fluids*, Vol. 6, No. 11, pp. 3683-3693.

Lowson, M. V. (1964), 'Some experiments with vortex breakdown', *J. Royal Aero. Soc.*, Vol. 68, pp. 343-346.

Lowson, M. V, (1988), 'The three-dimensional vortex sheet structure on delta wings', *Fluid Dynamics of Three-Dimensional Turbulent Shear Flows and Transition*, October 1988, AGARD-CP-438.

Lowson, M. V. (1991), 'Visualisation methods of vortex flows', *J. Aircraft*, Vol. 28, No. 5, pp. 320-327.

Lowson, M. V. and Riley, A. J. (1995), 'Vortex breakdown control by delta wing geometry', *J. Aircraft*, Vol. 32, No. 4, pp. 832-838.

Mayori, A. and Rockwell, D. (1994), 'Interaction of a streamwise vortex with a thin plate: A source of turbulent buffeting', *AIAA Journal*, Vol. 32, No. 10, pp. 2022-2029.

Menke, M., Yang, H., and Gursul, I. (1999), 'Experiments on the unsteady nature of vortex breakdown over delta wings', *Exp. Fluids*, Vol. 27, pp. 262-272.

Mitchell, A. M. and Molton, P. (2002), 'Vortical substructures in the shear layers forming leading-edge vortices', *AIAA J.*, Vol. 40, No. 8, pp. 1689-1692.

Mitchell, A. M., Molton, P., Barberis, D., and Délery, J. M. (2001), 'Vortical substructures in the shear layers forming leading-edge vortices', *19th AIAA Applied Aerodynamics Conference*, 11-14th June 2001, Anaheim, CA

Nelson, R.C. and Visser, K.D. (1990), 'Breaking down the delta wing vortex: The role of vorticity in the process', *AGARD-CP-494 Symposium of the Fluid Dynamics Panel*, Scheveningen, Netherlands (1-4 October 1990).

Pankhurst, R. C. and Holder, D. W. (1965), 'Wind-tunnel technique', First printed 1952, 1965 reprint, Sir Isaac Pitman & Sons Ltd. Pub.

Payne, F. M., Ng, T. T., and Nelson, R. C. (1988), 'Visualization and wake surveys of vortical flow over a delta wing', *AIAA Journal*, Vol. 26, No. 2, pp. 137-143.

Peckham, D. H. and Atkinson, S. A. (1957), 'Preliminary results of low speed wind-tunnel tests on a Gothic wing of aspect ratio 1.0', *ARC CP 508.*

Perkins, E. W. (1951), 'Experimental investigations of the effects of support interference on the drag of bodies of revolution at a Mach Number of 1.5', *NACA TN 2292.*

Polhamus, E. C. (1971), 'Predictions of vortex lift characteristics by a leading edge suction analogy', *J. Aircraft*, Vol. 8, No. 4, pp. 193-199.

Redinoitis, O. K., Stapountzis, H., and Telionis, D. P. (1993), 'Periodic vortex shedding over delta wings', *AIAA Journal*, Vol. 31, No. 9, pp. 1555-1561.

Robinson, B. A., Barnett, R. M., and Agrawal, S. (1994), 'Simple numerical criterion for vortex breakdown', *AIAA Journal*, Vol. 32, No. 1, pp. 116-122.

Rockwell, D., (1998), 'Vortex-body interactions', *Ann. Rev. Fluid Mech.*, Vol. 30, pp. 199-229.

Roos, F. W. and Kegelman, J. T. (1990), 'An experimental investigation of sweep-angle influence on delta-wing flows', AIAA-90-0383, *28th Aerospace Sciences Meeting and Exhibit*, Jan 8-11, Reno NV.

Sarpkaya, T. (1971a), 'On stationary and travelling vortex breakdown', *J. Fluid Mech.*, Vol. 45, No. 3, pp. 545-599.

Sarpkaya, T. (1971b), 'Vortex breakdown in swirling conical flows', *AIAA Journal*, Vol. 9, No. 8, pp. 1792-1799.

Sarpkaya, T. (1974), 'Effect of adverse pressure gradient on vortex breakdown', *AIAA Journal*, Vol. 12, No. 5.

Squire, H. B. (1960), 'Analysis of the vortex breakdown phenomenon, part 1', Aero. Dept., Imperial College London, Report 102.

Srinivas, S., Gursul, I., and Batta, G. (1994), 'Active control of vortex breakdown over delta wings', AIAA 94-2215, *25th AIAA Fluid Dynamics Conference*, 20-23 June, Colorado Springs CO.

Thomas, J. P. And Lan, C. E. (1991), 'The simulation and correction of wind tuennel wall interference on delta wing lift using Navier-Stokes and Euler solutions', AIAA-91-3300-CP, 1991.

Thompson, S. A., Bathill, S. M., and Nelson, R. C. (1991), 'Separated flowfield on a slender wing undergoing transient pitching motions', *J. Aircraft*, Vol. 28, No. 8, pp. 489 – 495.

Thompson, S. A. and Nelson, R. C. (1992), 'Wind tunnel blockage effects on slender wings undergoing large amplitude motions', AIAA-92-3926, 1992.

Tobak, M. and Peake, D. J. (1982), 'Topology of three-dimensional separated flows', *Ann. Rev. Fluid Mech.*, Vol. 14, pp. 61-85.

Traub, L. W. (1996), 'Simple prediction method for location of vortex breakdown on delta wings', *J. Aircraft*, Vol. 33, No. 2, pp. 452-454.

Traub, L. W. (1997), 'Prediction of delta wing leading-edge vortex circulation and lift-curve slope', *J. Aircraft*, Vol. 34, No. 3, pp. 450-452.

Traub, L. W., Moeller, B., and Rediniotis, O. (1998), 'Low-Reynolds-number effects on delta-wing aerodynamics', *J. Aircraft*, Vol. 35, No. 4, pp. 653-656.

Tsai, C. and Widnall, S. E. (1980), 'Examination of group-velocity criterion for vortex breakdown of vortex flow in a divergent duct', *Phys. Fluids*, Vol. 23, No. 5, pp. 864-870.

Visbal, M. R. (1995), 'Computational and physical aspects of vortex breakdown on delta wings', AIAA Paper 95-0585, *33rd Aerospace Sciences Meeting and Exhibit*, 9-12 Jan, Reno, NV

Visser, K. D. and Nelson, R. C. (1993), 'Measurements of circulation and vorticity in the leading-edge vortex of a delta wing', *AIAA Journal*, Vol. 31, No. 1, pp. 104-111.

Wéntz, W. H. and Kholman, D. L. (1971), 'Vortex breakdown on slender sharp-edged wings', *J. Aircraft*, Vol. 8, No. 3, pp. 156-161.

White, F. M. (1991), 'Viscous Fluid Flow', 2nd Ed., McGraw-Hill Inc. Pub., ISBN 0-07-100995-7.

Weinburg, Z. (1992), 'Effect of tunnel walls on vortex breakdown over delta wings', *AIAA Journal*, Vol. 30, No. 6, pp. 1584-1587.

Willert, C.E and Garib, M. (1991), 'Digital particle image velocimetry', *Exp. Fluids*, Vol. 10, pp. 181-193.

Wolfe, S., Lin, J.-C., and Rockwell, D (1995), 'Buffeting at the leading-edge of a flat-plate due to a streamwise vortex: Flow structure and surface pressure loading', *J. Fluids Struct.*, Vol. 9, pp. 359-370.

Xie, W. (1998), 'An experimental investigation of buffeting flows over delta wings', MSc Thesis, University of Cincinnati, USA.